

UC Davis

UC Davis Electronic Theses and Dissertations

Title

A multi-species investigation of neural fate specification

Permalink

<https://escholarship.org/uc/item/90s1d3tw>

Author

Williams, Elizabeth Fishman

Publication Date

2024

Peer reviewed|Thesis/dissertation

A Multi-Species Investigation of Neural Fate Specification

By

ELIZABETH FISHMAN WILLIAMS

DISSERTATION

Submitted in partial satisfaction of the requirements for the degree of

DOCTOR OF PHILOSOPHY

in

BIOCHEMISTRY, MOLECULAR, CELLULAR, AND DEVELOPMENTAL BIOLOGY

in the

OFFICE OF GRADUATE STUDIES

of the

UNIVERSITY OF CALIFORNIA

DAVIS

Approved:

Anna La Torre, Chair

Nadean Brown

Crystal Rogers

Committee in Charge

2024

Abstract

Sight relies on the integrity of the photoreceptor cells of the retina (rods and cones), and damage to these cells results in irreversible vision loss. Several degenerative diseases affect cones specifically, including age-related macular degeneration (AMD), one of the leading causes of blindness worldwide. A promising therapeutic strategy to restore vision in these patients is photoreceptor replacement, but our ability to produce cones *in vitro* is limited. Humans and other primates have a specialized region of the central retina called the fovea—the region affected by AMD—that contains the highest density of cones. This cone dominance is a sharp contrast to the majority of the retina, where rods outnumber cones 20:1. All the neurons of the retina (including rods and cones) are born from a single population of multipotent progenitors. However, the molecular mechanisms that dictate why the foveal progenitors differentiate into high yields of cones and not rods are unknown. A more complete understanding of these factors can be used to optimize existing stem cell protocols and increase cone production *in vitro*.

In my collection of published work, I explored various molecular mechanisms that contribute to neural fate specification, including molecules of the retinoic acid pathway and microRNAs (miRNAs). My research focused primarily in the retina. I began by reviewing foveal development and curating the current knowledge of the steps towards its specification and maturation. The mechanisms driving foveal development are widely unknown, so I sought to study the fovea in the human and nonhuman primate. The La Torre lab is just three miles down the road from the California National Primate Research Center, priming us for access to nonhuman primate tissue across gestation. With these rhesus macaque tissues, I characterized retinal development and identified key stages of

neurogenesis. I also showed that the expression patterns of molecules in and associated with the retinoic acid pathway, including CPY26A and FGF8, are not conserved between chicken and primate. Whereas in the chicken retina, these molecules contribute to the specification of the high acuity area, they are not fovea-specific in the primate retina. I continued to explore the role of miRNAs in fate specification through analyzing of the miRNA landscape across the developing nonhuman primate retina. I further validated those miRNAs found to be highly differentially expressed in the human retina. I reviewed oscillation patterns of miRNAs and the role in retinal development. Given that the cortex shares a similar developmental pattern with the retina, also having a progenitor population that all the neurons descend from in a stereotypic sequence, I explored how the Notch pathway and miRNAs influence fate specification in the mouse brain. Together, these studies identify a subset of the molecular mechanisms that drive neural differentiation and will inform future research on increasing the cone production in stem cell protocols with an ultimate goal of restoring vision in patients affected by optic neuropathies.

*For Eric, I miss you every day.
And for Joseph and Charlotte, my sunshines.*

Acknowledgments

First, I would like to thank my thesis advisor and mentor, Dr. Anna La Torre. Joining your lab was *b'shert*. I leave every conversation with you even more excited about science and inspired that I can do anything and everything. Thank you for your guidance, both in and out of the lab.

My decision to pursue my doctoral degree at UC Davis is one of the best I've ever made. Thank you to the scientific community of UC Davis, especially the Biochemistry Molecular, Cellular, and Development Biology Graduate Group, Vision Science Community, and weekly Retinal Meeting Group. It has been a pleasure learning from such curious, creative, and intelligent minds. Thank you to my dissertation committee, Dr. Nadean Brown and Dr. Crystal Rogers, for your excitement and feedback on my projects. I have thoroughly enjoyed learning from and collaborating with both of you.

I am so appreciative of the current and former members of the La Torre and Simó labs: Dr. Simran Cheema, Steven Decker, Dr. Corrine Fairchild, Dr. Jisoo Han, Keiko Hino, Miranda Krueger, Dr. Mikaela Louie, Dr. Adam Miltner, Raenier Reyes, and Daniela Santamaría Muñoz. Working with such kind, motivated, and entertaining scientists has been a joy. Adam and Mikaela, thank you for sticking by me during my interview weekend and convincing me to come to Davis. Miranda, thank you for joining me on so many projects and always being ready for a Trader Joe's run and extended lunch. Keiko and Raenier, thank you for keeping the lab running.

I can attribute my interest and foundation in science to my wonderful mentors and teachers during my undergraduate and postbaccalaureate training. Thank you to my scientific mentors from Haverford College, Dr. Roshan Jain, Dr. Rachel Hoang, and Dr.

Jonathan Wilson, and from the National Institutes of Health, Dr. Judith Kassis and Dr. Karl Pfeifer. I am so grateful to each of you for taking a chance on me. Your contagious scientific curiosities have changed my life.

To the new family I gained through marriage, the Williams: Kevin, Virginia, Jacqueline, Desi, and James, thank you for being there for me in Sacramento. It is a treat living close to family and being surrounded by so much love. I love our game nights, family dinners, and Mexico travels.

Thank you to my loving family for being with me every step of the way. To my parents, James and Linda, thank you for always making me a priority. I love our late night calls, last minute photo book editing, and long car rides talking about science. I am grateful to follow in your footsteps. To my brother, Adam, and sister-in-law, Allie, thank you for being my best friends. Our daily calls (sometimes twice daily when you forget we had already talked earlier that day) are something I always look forward to. I love raising our children together. To my younger brother, Eric, thank you for being you. I know that you would be proud of me.

Finally, I have so much gratitude to the family that I have created. I could have never predicted that I would meet my person just one month into starting graduate school (thank you to the MCB T32 retreat at Fallen Leaf Lake). To my dear husband, Joseph, what an adventure! I am forever inspired by your infinite curiosity and thirst for knowledge. I love that you always have a new topic to share with me—you are the best storyteller and teacher. Thank you for being so patient. You help me become the best version of myself, and I hope that I can always do the same for you. Thank you for the greatest gifts of sharing your life with me and making me a mother. You are the best father to our sweet

girl. I love you dearly. As you tell me every morning, you are my dream. Endless love to my daughter, Charlotte Jane. I could not have asked for better company and distraction while writing my dissertation. You are my greatest pride and joy.

Table of Contents

Abstract	ii
Acknowledgments	v
List of Abbreviations	xiv
List of graduate school publications	xix
1. Introduction	1
1.1 General introduction	1
1.2 The retina	2
1.3 Retinal cell types	3
1.3.1 Photoreceptors.....	3
1.3.1.1 Phototransduction.....	4
1.3.1.2 Opsins.....	5
1.3.2 Bipolar cells.....	5
1.3.3 Horizontal cells.....	6
1.3.4 Amacrine cells.....	6
1.3.5 Retinal ganglion cells.....	7
1.3.6 Müller glia.....	8
1.3.7 Retinal pigment epithelium.....	8
1.4 The developing vertebrate retina	9
1.4.1 Eye field specification.....	9
1.4.2 Early retinal development.....	10
1.4.2.1 Retinal progenitor cell proliferation.....	11
1.4.2.2 Neurogenesis in the retina.....	13
1.4.3 Specification and differentiation of photoreceptors.....	15
1.4.3.1 Photoreceptor or non-photoreceptor fate.....	15
1.4.3.2 Rod vs. cone fate.....	17
1.5 MicroRNAs	19
1.5.1 MicroRNA biogenesis.....	19
1.5.2 MicroRNAs in retina development.....	20
1.6 Summary	22
1.7 Figures	23
2. Accepted encyclopedia chapter: Development of the primate fovea	31
2.1 Abstract	32
2.2 Key points	32
2.3 Introduction	33

2.4 Patterning and differential growth	37
2.4.1 FOXD1 and FOXC1.....	37
2.4.2 SHH and FGF.....	38
2.4.3 Ventropin and BMP-2.....	38
2.4.4 EphrinA2/A5 and EphrinB1.....	39
2.4.5 Retinoic acid signaling.....	39
2.5 Differential neurogenesis timing	41
2.5.1 Retinal layering.....	42
2.5.2 Neurogenesis begins in the fovea first.....	43
2.5.2.1 Early cell types.....	44
2.5.2.2 Late cell types.....	45
2.5.3 Neurogenesis completes in the fovea first.....	46
2.6 Differential cell fate acquisition	46
2.6.1 Cone photoreceptor mosaic.....	47
2.6.2 Rod photoreceptor mosaic.....	48
2.6.3 RGCs.....	49
2.6.4 Inner nuclear layer cells.....	49
2.6.5 Could cell cycle exit play a role in the differential neurogenesis in the fovea?	49
2.6.6 Post-transcriptional mechanisms in foveal development.....	50
2.7 Differential vascularization	51
2.8 Pit formation	56
2.8.1 The Albinism Riddle.....	57
2.8.2 SLC38A8.....	58
2.8.3 PAX6.....	59
2.9 Conclusions	59
2.10 Acknowledgements	60
2.11 Figures	61
3. Published results: Expression patterns of CYP26A1, FGF8, CDKN1A, and NPVF in the developing rhesus monkey retina	64
3.1 Keywords	66
3.2 Abstract	66
3.3 Introduction	67
3.4 Materials and methods	70
3.4.1 Sample collection.....	70
3.4.2 RNAscope <i>in situ</i> hybridization and immunohistochemistry.....	71
3.4.3 Hematoxylin and eosin (H&E) staining.....	73
3.4.4 Edu Click-iT.....	73

3.4.5 Statistical methods.....	73
3.5 Results	74
3.5.1 Neurogenesis in the developing rhesus retina follows a fovea-to-periphery gradient.....	74
3.5.2 A switch from early to late progenitor competence takes place in the late first trimester at 50 days gestational age in the center of the fovea	75
3.5.3 CYP26A1 is highly expressed in the developing rhesus monkey fovea at different stages of development.....	78
3.5.4 FGF8 is expressed in retinal progenitors in a ONH-to-periphery gradient.....	79
3.5.5 CDKN1A is expressed by the Müller glia and ONH cells.....	79
3.5.6 The neuropeptide NPVF is expressed by the Müller glia.....	80
3.6 Discussion	81
3.7 Acknowledgements.....	86
3.8 Figures	87
3.9 Tables	97
3.10 Supplementary figures	101
4. Published results: MicroRNA signatures of the developing primate fovea	106
4.1 Abstract.....	107
4.2 Introduction	108
4.3 Results	111
4.3.1 Transcriptomic characterization of the developing rhesus monkey retina	111
4.3.2 miRNA-sequencing and differential expression profiles between temporal and nasal fetal rhesus monkey retina	114
4.3.3 miRNA expression in the developing mouse retina	116
4.3.4 Expression in the developing human retina.....	117
4.4 Discussion	119
4.5 Materials and methods	123
4.5.1 Experimental models and subject details	123
4.5.1.1 Rhesus monkeys	123
4.5.1.2 Mice.....	124
4.5.1.3 Human fetal samples	124
4.5.2 RNA and miRNA sequencing.....	125
4.5.2.1 Library preparation and next generation sequencing.....	125
4.5.2.2 Sequence analyses.....	126
4.5.2.3 miRNA-sequencing: library preparation and next generation sequencing	126
4.5.3 Analyses of RNA-seq and miRNA-seq data	127
4.5.4 <i>In situ</i> hybridization (ISH).....	128

4.5.5 Immunofluorescence	129
4.5.6 Hematoxylin and eosin staining	130
4.5.7 Microscopy.....	130
4.6 Data availability statement	130
4.7 Ethics statement	130
4.8 Author contributions.....	131
4.9 Conflict of interest	131
4.10 Funding	131
4.11 Acknowledgements.....	132
4.12 Figures	133
4.13 Supplementary figures	140
4.14 Supplementary Tables	148
<i>5. Published literature review: Oscillatory behavior of microRNA networks: emerging roles in retinal development.....</i>	<i>149</i>
5.1 Abstract.....	150
5.2 Key words	150
5.3 Introduction	151
5.4 miRNAs in the developing retina.....	152
5.5 miR-183, -96, and -182 and the circadian clock.....	154
5.6 Let-7 levels oscillate with the cell cycle in the embryonic retina	158
5.7 miR-9 is part of the Notch ultradian oscillator	161
5.8 Conclusions and perspectives	165
5.9 Author contributions.....	166
5.10 Conflict of interest	166
5.11 Funding	166
5.12 Acknowledgements.....	167
5.13 Figures	168
5.14 Tables	175
<i>6. Published results: Notch directs telencephalic development and controls neocortical neuron fate determination by regulating microRNA levels.....</i>	<i>178</i>
6.1 Introduction to cortical development (unpublished).....	179
6.2 Abstract.....	180
6.3 Key words	181

6.4 Introduction	181
6.5 Results	184
6.5.1 Notch signaling regulates corpus callosum and hippocampal development	184
6.5.2 Notch signaling is not a main mediator of dorsal telencephalic patterning but regulates Cajal-Retzius cell production	186
6.5.3 Early-born projection neuron production is limited by Notch signaling during neocortical development.....	188
6.5.4 Notch signaling regulates radial glia cell cycle dynamics	191
6.5.5 Overactivation of Notch signaling results in transcriptomic changes of Notch effectors, bHLH transcription factors, and miRNAs let-7, miR-99a/100, and miR-125b	193
6.5.6 Let-7, miR-125b, and miR-99/100 are required downstream of Notch to restrict early-born projection neuron fates	195
6.6 Discussion	196
6.6.1 Multifaceted functions of Notch during telencephalic morphogenesis	196
6.6.2 Balanced Notch signaling is essential for the development of the corpus callosum.....	197
6.6.3 Notch regulates radial glia cell cycle length and cortical neurogenesis.....	198
6.6.4 miRNAs downstream of Notch are required for upper-layer neuron fate acquisition.....	200
6.7 Acknowledgments.....	202
6.8 Experimental models and subject details.....	202
6.8.1 Animals	202
6.8.2 Constructs.....	203
6.8.3 Histology and immunohistochemistry	203
6.8.4 In utero electroporation.....	205
6.8.5 FlashTag NSC labelling and FACS	206
6.8.6 RNA and miRNA sequencing.....	206
6.8.7 Data availability.....	207
6.8.8 Edu and BrdU labeling.....	207
6.8.9 Statistical methods.....	208
6.9 Figures	209
6.10 Supplementary figures	222
6.11 Supplementary tables	234
7. Concluding remarks.....	235
7.1 Summary.....	235
7.2 Utilizing microRNAs to advance stem cell protocols	237
7.2.1 Organoid protocols	237
7.2.2 microRNAs and the cell cycle	239

7.3 Alternative models	242
7.2.1 Primate model.....	243
7.2.2 Avian model	244
7.2.3 Interpreting results with additional models.....	246
8. References	249

List of Abbreviations

αRGC	alpha retinal ganglion cell	CC	Corpus callosum
Ago	Argonaute	CDK	Cyclin-dependent kinase
AC	Amacrine cell	CFSE	Carboxyfluorescein esters
AMD	Age-related macular degeneration	cGMP	Cyclic guanosine monophosphate
ANP	Anterior neural plate	Ch	Choroid
Ascl1	Acheate-scute homolog 1	CH	Cortical hem
Atoh7	Atonal bHLH transcription factor 7	ChP	Choroid plexus
ATRA	All-trans retinoic acid	CNS	Central nervous system
BCIP	5-bromo-4-chloro-3- indolyl phosphate	CPM	Counter per million
bHLH	basic helix-loop- helix	Crx	Cone-rod homeobox
BMP	Bone morphogenic protein	CRY	Cryptochrome
BP	Bipolar cell	CYP26	Cytochrome P450
BrdU	5-bromo-2'- deoxyuridine	DAPI	4',6-diamidino-2- phenylindole
CA1-3	Comu ammonis hippocampal regions	(#)DG	Days gestational age
		DG	Dentate gyrus
		DGCR8	DiGeorge syndrome critical region 8
		DIO2	Iodothyronine Deiodinase 2

DL	Delta-like	GPCR	G protein-coupled
DN	Dominant negative		receptors
DNA	Deoxyribonucleic acid	GS	Glutamine synthetase
E(#)	Embryonic day of development	H&E	Hematoxylin and eosin
EdU	5-ethynyl-2'-deoxyuridine	hESC	Human embryonic stem cell
EFTF	Eye field transcription factor	HAA	High acuity area
EGF	Epidermal growth factor	HC	Horizontal cell
ESC	Embryonic stem cell	HER10	Human embryonic retina cell
FAZ	Foveal avascular zone	HES	Hairy and enhancer of split
FBS	Fetal bovine serum	HEY	Hairy ears, Y-linked
FDR	False discovery rate	HFL	Henle's fiber layer
FGF	Fibroblast Growth Factor	HIF-a	Hypoxia Inducible Factor
G1	Gap 1 phase of cell cycle	Hip	Hippocampal primordia
G2	Gap 2 phase of cell cycle	IACUC	Institutional Animal Care and Use Committee
GCL	Ganglion cell layer	IF	Insulin-derived growth factor
GMP	Guanosine monophosphate	IHC	Immunohistochemistry
GO	Gene ontology		
GOF	Gain-of-function	INL	Inner nuclear layer

INM	Interkinetic nuclear migration	MDS	Multidimensional scaling analysis
IP	Intermediate progenitors	Mfng	Manic Fringe
IPL	Inner plexiform layer	MG	Müller glia
IS	Inner segment	MIENTURN	microRNA
ISH	<i>In situ</i> hybridization	ET	Enrichment
IUE	<i>In utero</i> electroporation	miR	Short for miRNA when denoting specific miRNAs
Jag	Jagged	miRNA	microRNA
L	Lens	mRNA	messenger RNA
L-cones	Long wavelength cones	MZ	Marginal zone
LGN	Lateral geniculate nucleus	N	Nasal
LHON	Leber's hereditary optic neuropathy	Na⁺	Sodium
LP-miRNA	Late progenitor microRNA	NbL	Neuroblastic layer
LV	Lateral ventricle	NBT	Nitroblue tetrazolium
M	Mitosis	NFL	Neural fiber layer
M-cones	Medium wavelength cones	NRL	Neural retinal leucine zipper protein
Maml2	Mastermind-like transcriptional co-activator 1	Ngn	Neurogenin
		NICD	Notch intracellular domain
		NIH	National Institutes of Health

NPPB	Natriuretic peptide precursor B	PFA	Paraformaldehyde
		PH3	Phospho-Histone3
NPVF	Neuropeptide VF precursor	PL	Photoreceptor layer
		PR	Photoreceptor
nt	Nucleotide	pre-miRNA	Precursor miRNA
OCT	Optimum cutting temperature	pri-miRNA	Primary miRNA
		RA	Retinoic acid
ON	Optic nerve	RALDH	Retinaldehyde dehydrogenase
ONH	Optic nerve head		
ONL	Outer nuclear layer	Rax	Retina and anterior neural fold homeobox
OPL	Outer plexiform layer		
OS	Outer segment	Rb	Retinoblastoma
Otx2	Orthodenticle homeobox protein	Rbpj	Recombination signal-binding protein for immunoglobulin kappa J region
OV	Optic vesicle		
P(#)	Postnatal day of development		
Pax2	Paired box gene 2	RFZ	Rod free zone
Pax6	Paired box gene 6	RG	Radial glia cells
PCNA	Proliferating cell nuclear antigen	RGC	Retinal ganglion cell
		RISC	RNA-induced silencing complex
PCA	Principal component analysis	RNA	Ribonucleic acid
PDE	Phosphodiesterase	RNAseq	RNA sequencing
PEDF	Pigment epithelium derived factor	ROP	Retinopathy of prematurity
PER	Period	RP	Retinitis pigmentosa

RPC	Retinal progenitor cell	T3	Thyroid hormone
		T4	Prohormone thyroxine
RPE	Retinal pigment epithelium	Tc	Total cell cycle time
Rx	Retinal homeobox protein	Ts	Time of S-phase
		TvN	Temporal vs. nasal
S-cones	Short wavelength cones	TYR	Tyrosinase
		UTR	Untranslated region
S-phase	Synthesis phase of cell cycle	VEGF	Vascular endothelial growth factor
SCN	Suprachiasmatic nuclei	Vsx2	Visual system homeobox 2, also known as Chx10
Shh	Sonic hedgehog		
Sox2	SRY-box transcription factor 2	VZ	Ventricular zone
		Wnt	Wingless-related integration site
SVZ	Subventricular zone	ZT	Zeitgeber time
T	Temporal		
T	Transducin		

List of graduate school publications

Krueger MR, **Fishman-Williams E***, Simó S, Tarantal AF, La Torre A. (2024) Expression patterns of *CYP26A1*, *FGF8*, *CDKN1A*, and *NPVF* in the developing rhesus monkey retina. *Differentiation*, 135: 100743. doi: 10.1016/j.diff.2023.100743. ***co-first authors**

Fishman-Williams E*, Krueger MR*, La Torre A. (2024) Development of the fovea. *Encyclopedia of the Eye, Second Edition*. Pending publication. ***co-first authors**

Han JS*, **Fishman-Williams E***, Decker SC*, Hino K, Reyes RV, Brown NL, Simó S, La Torre A. (2023) Notch direct telencephalic development and controls neocortical neuron fate determination by regulating microRNA levels. *Development*, 150: 201408. doi: 10.1242/dev.201408. ***co-first authors**

Fishman ES, Han JS, La Torre A. (2022) Oscillatory behaviors of microRNA networks: Emerging roles in retinal development. *Frontiers in Cell and Developmental Biology*, 10: 831750. doi: 10.3389/fcell.2022.831750.

Fishman ES*, Louie M*, Miltner AM, Cheema SK, Wong J, Schlaeger NM, Moshiri A, Simó S, Tarantal AF, La Torre A. (2021) MicroRNA signatures of the developing primate fovea. *Frontiers in Cell and Developmental Biology*, 9: 654385. doi: 10.3389/fcell.2021.654385. ***co-first authors**

1. Introduction

1.1 General introduction

Vision begins, and may end, in the photoreceptor cells. The ability to see relies on the integrity of the photoreceptor cells in the retina (rods and cones) to receive light and convert this information into biochemical messages. The electrical signal is transported through a circuit of cells in the retina and sent to the brain for interpretation. All the neurons of the retina that participate in this transmission of signal, including rods and cones, are born from a single population of multipotent progenitors ¹. These progenitors are primed by both intrinsic and extrinsic factors to differentiate into the appropriate populations of neurons or glia at any given stage of development. This ensures that the developed retina has the appropriate composition of cells for the animal's vision needs. Rods are low light sensing cells responsible for night vision, and cones are color sensing cells that mediate most daylight vision ². In the primate eye, rods are the dominant photoreceptor population throughout the retina, outnumbering cones 20:1 ³. There is one region in the central retina, the fovea, that contains the highest density of cones and no rods ⁴. The fovea is especially vulnerable to several degenerative diseases, including age-related macular degeneration (AMD). As the leading cause of non-inherited blindness, AMD affects over 6% of the world population ⁵. The retina is part of the central nervous system (CNS) and cannot regenerate. Current treatments only slow down the progression of these neurodegeneration diseases; degenerated photoreceptors are unsalvageable, so any therapeutic strategy to restore vision will require prosthetics or cone replacement. Consequently, there is strong interest in developing neuron replacement therapies for

degenerative eye diseases. Pluripotent stem cells hold great potential as an unlimited donor source for photoreceptor replacement therapies, as embryonic stem cells (ESCs) and induced pluripotent stem cells (iPSCs) may be differentiated into several retinal cell fates⁶⁻¹⁵. However, there is no method for making cone-enriched retinal organoids, as the current protocols closely replicate endogenous developmental mechanisms¹⁶⁻¹⁸. Thus, cone production *in vitro* is expensive, inefficient, and difficult to scale up. A more complete understanding of the molecular mechanisms that dictate cone photoreceptor specification is critical to translate stem cell technologies into novel cone transplantation approaches.

1.2 The retina

Visual perception is a multi-step process that transpires in the eyes and brain. A photon of light is converted into an electrical signal that is further refined, and then the signal is interpreted as a visual image. This orchestrated process commences in the retina. The retina is a highly organized, laminar tissue that lines the posterior of the eye (Figure 1.1). All the cells that participate in the retinal circuitry are born from a single population of multipotent stem cells, called retinal progenitor cells (RPCs). RPCs differentiate into six types of neurons—rod and cone photoreceptors (PRs), bipolar cells (BPs), horizontal cells (HCs), amacrine cells (ACs), and retinal ganglion cells (RGCs)—and one glia—Müller glia (MG)¹⁹⁻²¹. These neurons and glia are positioned across the layers of the retina, each residing within their appropriate neuronal layer and synapsing with their respective targets in the appropriate plexiform layer. There are three neuronal layers—the outer nuclear layer (ONL), inner nuclear layer (INL), and ganglion cell layer (GCL)—and two plexiform layers—the outer plexiform layer (OPL) and inner plexiform

layer (IPL). The retina is part of the central nervous system (CNS) and directly connects to the brain via the optic nerve (ON)²². RGCs project long axons that shape the nerve fiber layer (NFL) within the retina, and bundle together to form the ON. Outside of the eye, the ON is myelinated to efficiently send signals over a long distance towards the vision processing centers of the brain²³. Retinal signal travels from the retina to the lateral geniculate nucleus (LGN) in the thalamus and superior colliculus in the midbrain (among other regions in the brain), and finally to the primary visual cortex in the occipital lobe to be synthesized and interpreted²⁴⁻²⁶. Overall, a healthy retina with functioning photoreceptors is vital for proper vision.

1.3 Retinal cell types

1.3.1 Photoreceptors

Photoreceptors (PRs) are the primary light-sensing neurons in the retina. There are two types of PRs: rods and cones. Rods are acutely sensitive to light and are thus responsible for vision in low-light conditions; cones are less responsive to light and are adapted for bright light and color perception^{27,28}. To perform their function, PRs are highly compartmentalized. They consist of an outer segment (OS), inner segment (IS), soma, and synaptic terminal. The OS and IS reside in the photoreceptor layer (PL), the soma lies in the outer nuclear layer (ONL), and the synaptic terminal synapses to second-order neurons in the outer plexiform layer (OPL).

A photon of light must pass through the entire retinal thickness before it reaches the PRs in the apical retina, farthest from where light enters the eye. The OS is most

apical and the outermost part of the retina. Rods and cones have distinguishing OS morphologies that give rise to their nomenclature: rod OSs are long, thin, and rod-like, while cone OSs are shorter, stockier, and conical ²⁹. It is here where phototransduction occurs. The IS is connected to the basal side of the OS. Here, the PR's metabolic machinery resides. Proteins synthesized in the IS are transported to the OS through the connecting cilium. The synaptic terminal is the most basal part of the PR. Although the synaptic terminal in rods is called a spherule and in cones a pedicle, both types of PRs participate in "ribbon synapses" via the synaptic ribbons ²⁹.

1.3.1.1 Phototransduction

Phototransduction is the process where a photon of light is converted into an electrical signal (Figure 1.2) ³⁰. Within the OSs are stacks of discs that house Opsins (rhodopsin in rods and cone opsins in cones) and retinal molecules. When retinal absorbs light, its consequent configuration change prompts Opsins to activate transducin ³¹. Transducin activates phosphodiesterase to break down cyclin guanosine monophosphate (cGMP) ³². As cGMP levels decrease, the ion channels that they mediate close. The decreased sodium influx and continued potassium outflux cause the PR to hyperpolarize. Whereas an unstimulated PR constantly releases the neurotransmitter glutamate to the postsynaptic BPs and HCs, a light stimulated, hyperpolarized PR decreases the release of glutamate ^{33,34}. Thus, decreased neurotransmitter release signals that a light stimulus is present. After responding to a light stimulus, the PR must arrest the phototransduction cascade and repolarize. The appropriately named Arrestin proteins (arrestin-1 in rods and arrestin-1 and -4 in cones) support this process by

arresting the activity of G protein-coupled receptors (GPCRs), which includes Opsins^{35,36}. Finally, when retinal is restored to its original configuration, the PR is ready to respond to the next light stimulus³¹.

1.3.1.2 Opsins

In primates, each PR contains one type of Opsin, either Rhodopsin in rods or one of three types of cone opsin in cones. These Opsins vary in their sensitivity to light. Rhodopsin has peak sensitivity to wavelengths of light at 500 nanometers (nm). Cone opsins are sensitive to 420 nm (short wavelength, S-opsin), 530 nm (medium wavelength, M-opsin), or 560 nm (long wavelength, L-opsin) wavelengths³⁷⁻³⁹. Together, these blue, green, and red cone subtypes allow for perception of the visual spectrum. It is worth noting that the visual system of each organism has evolved to fit its needs. While diurnal primates have three types of cone PRs, each with a distinct cone opsin, nocturnal mice have only two cone opsins that are co-expressed in a single cone PR. Without L-opsin, mice cannot perceive red light^{40,41}.

1.3.2 Bipolar cells

Bipolar cells (BPs) are the second-order neurons that receive the signal from PRs. These interneurons reside in the INL, receive input from PRs and HCs in the OPL, and relay signal to RGCs and ACs in the IPL. BPs are characterized as ON or OFF, depending on their response to light. ON BPs respond to light stimulus by depolarizing, and OFF BPs respond by hyperpolarizing⁴². In addition to receiving input from PRs, BPs receive

lateral input from HCs ^{19,43}. This lateral inhibition of the PRs' signal enhances image contrast ⁴⁴.

1.3.3 Horizontal cells

Horizontal cells (HCs) are laterally connecting interneurons that moderate signaling across the OPL. Their cell bodies reside on the apical side of the INL, and they synapse to PRs and BPs in the OPL. HCs are GABAergic and provide inhibitory feedback to PRs and feedforward signaling to BPs ⁴⁵. This lateral inhibition enhances contrast and improves color opponency ⁴⁶. HCs are characterized by their dendritic structure and synaptic terminal organization ⁴⁷. In humans, three types of HCs have been identified ^{47,48}.

1.3.4 Amacrine cells

Amacrine cells (ACs) are a diverse group of interneurons that also modulate the transmission of visual signal within the retina. There are over 60 subtypes, each with distinct morphologies ^{49,50}. AC bodies reside on the basal side of the INL, with some displaced in the GCL, and they synapse in the IPL ⁵¹. They primarily receive input from BPs and output signal to other ACs and RGCs ⁵². Most ACs are GABAergic or glycinergic, serving as inhibitors to their synapsing neurons ⁴⁹. Such regulation influences the temporal and spatial aspect of visual processing, including direction selectivity and motion detection ^{19,52,53}.

1.3.5 Retinal ganglion cells

Retinal ganglion cells (RGCs) are the output neurons of the retina that send the visual signal to the brain. These third-order neurons are the sole connection between the retina and the brain. RGCs reside in the most basal retina; the cell bodies lie in the GCL, they receive input from BPs and ACs in the IPL, and their axons form the NFL. RGC axons converge at the optic nerve head (ONH, also known as the optic disc), where they bundle together to form the ON. Consequently, the NFL is thinnest towards the *ora serrata* and thickest closest to the ONH⁵⁴. Action potentials are transmitted down the long axons, which are myelinated outside of the retina, towards the brain. In this final location of the visual pathway, RGCs synapse to visual processing centers, including the Lateral Geniculate Nucleus (LGN) and Superior Colliculus^{24,25}. There is a large diversity of retinal ganglion cell subtypes, based off distinct morphologies, physiologies, and molecular classifications—17 subtypes have been identified in primates⁵⁵. One subtype of note in the mouse retina is the alpha retinal ganglion cell (α RGC), which is especially resilient to degeneration in glaucoma models. Glaucoma causes blindness through retinal ganglion cells death, prematurely suspending the transmission of visual signal before it reaches the brain⁵⁶.

The density of RGCs serves as a useful tool for understanding visual acuity in various organisms. Retinal regions responsible for high visual acuity, such as the fovea in primates, birds of prey, and lizards or a high acuity area in some birds, have unique circuitry. In primates, the majority of the retina contains parasol circuitry (or magnocellular pathways), where the signals from many PRs converge onto an interneuron, and many interneurons converge on a RGC. In high acuity regions, midget circuitry (or parvocellular

pathways) dominates, where a PR synapses with two BPs (ON and OFF), which synapse onto two RGCs^{57,58}. As a result, there is a much higher density of RGCs in high acuity areas compared to the rest of the retina. Identifying regions of high RGC density in flat mount retinas has been useful to compare visual acuity across species.

1.3.6 Müller glia

Müller glia (MG) are the primary glia of the retina. They are the only cells that extend over every retinal layer, from the apical ONL to the basal NFL. Their ubiquitous presence is appropriate for their many roles. Beyond maintaining tensile strength within the retina, MG are involved in neurotransmitter uptake and recycling, especially of glutamate^{59,60}. They respond to retinal damage by removing cell debris and secreting neurotrophins^{61,62}. Perhaps most important and exciting for this research field is that MG are born from the same population of progenitor cells as the retinal neurons. In some species, MG may dedifferentiate into a RPC-like state and then differentiate into new retinal neurons⁶²⁻⁶⁴. There is ongoing research into reprogramming MG to treat PR degeneration models.

1.3.7 Retinal pigment epithelium

Although originating from the optic vesicle (OV), the retinal pigment epithelium (RPE) diverges away from the neuroepithelial developmental program and is thus distinct from the neural retina^{22,65}. This monolayer of cells contains a high concentration of melanin, making them pigmented. They line the apical retina and interact with the PR OSs. A normal functioning retina is vulnerable to toxic photooxidative product build up

from light exposure and the energy-intensive process of phototransduction⁶⁶. PRs are continuously producing new discs and pushing the existing ones apically. Consequently, PRs shed up to 10% of their volume daily for the RPE to phagocytose and clear away⁶⁷. Their proximity to the PRs also primes the RPE for a key role in phototransduction. Specifically, they participate in the initiating event of converting all-*trans*-retinal into 11-*cis*-retinal^{68,69}. When the RPE degenerates, as in the Age-Related Macular Degeneration (AMD) model, the retina cannot properly function, leading to blindness^{70,71}.

1.4 The developing vertebrate retina

1.4.1 Eye field specification

The central nervous system (CNS), including the retina and the brain, is derived from the neuroectoderm. When the neural plate forms into the neural tube, a group of cells positioned at the center of the anterior neural plate (ANP) are specified as eye field progenitors. A gene regulatory network, the eye field transcription factors (EFTFs) *Rax*, *Pax6*, *Six3*, and *Lhx2*, are responsible for the specification^{22,65,72-75}. Additionally, a combination of four key morphogenic molecules—Bone Morphogenetic Protein (BMP), Sonic hedgehog (Shh), Wingless/Integrated (Wnt), and Insulin-derived Growth Factor (IGF)—establish the eye field domain. When most of the cells are converging into the neural plate, these eye field progenitors bilaterally evaginate to form the optic vesicles (OVs) (Figure 1.3)^{65,73,75}. The pseudostratified OVs continue to outwardly displace until the tissues contact the surface ectoderm. This event cues the ectoderm and OVs to invaginate, thus establishing the lens placodes and optic cups, respectively^{22,73}. Within the bilayered optic cup, the proximal tissue becomes the RPE and the distal tissue

becomes the neural retina. A group of transcription factors specify the distinct regions of the developing eye. *Mitf* appears in the OV and is selectively restricted to the future RPE across time. *Pax2* is initially expressed by all RPCs and progressively restricts to the optic stalk and ONH. *Vsx2* (*Chx10*) labels the RPCs^{22,65,75-79}. Proper eye development requires the proper patterning of these developmental transcription factors.

1.4.2 Early retinal development

All the cells of the retina are derived from a single population of multipotent stem cells, called retinal progenitor cells (RPCs). Lineage tracing studies, where fluorescent tags or retroviruses label a RPC and allow for its future progeny to be identify, showed that a single RPC is capable to differentiating into all six types of neurons and one glia in the retina⁸⁰⁻⁸³. As a RPC is dividing, it undergoes interkinetic nuclear migration (INM) (Figure 1.4)⁸⁴⁻⁸⁶. During this process, the nucleus travels the width of the retina, ensuring that it is in the basal retina during S-phase (synthesis phase, when DNA is being synthesized) and in the apical retina during M-phase (mitosis, when the cell is dividing)⁸⁴. A cycling RPC has one of three paths to follow during mitosis: symmetric division into two RPCs, asymmetric division into one RPC and one neuron, or symmetric post-mitotic division into two neurons (of the same or different types) (Figure 1.5). Retinogenesis, and organogenesis in general, requires the balance between progenitor proliferation and differentiation. Early in retina development, RPCs symmetrically divide into more RPCs to maintain the progenitor pool and grow the tissue. As development progresses, asymmetric divisions and symmetric post-mitotic divisions become more prevalent.

1.4.2.1 Retinal progenitor cell proliferation

The proliferative state of RPCs is maintained by both intrinsic and extrinsic factors. Intrinsically, a group of transcription factors, including *Rax*, *Six6*, *Pax6* and *Sox2*, regulates RPC proliferation⁸⁷.

1.4.2.1.1 Cell Cycle

Of course, RPC proliferation relies on the ability to advance through the cell cycle. Briefly, the cell cycle involves four phases and three major checkpoints (Figure 1.6)⁸⁸. After a cell divides, the new daughter cells begin the cell cycle in Gap 1 (G1) phase, that is simply the gap between cell division and DNA synthesis. The G1/S checkpoint ensures the integrity of DNA before the genome is replicated in S-phase (synthesis phase). The cell can either remedy a problem at this checkpoint to continue in the cell cycle or advance to G0 phase, which is a resting phase. When replication is complete, the cell continues to grow during Gap 2 (G2) phase. The G2/M checkpoint ensures proper chromosome duplication before cell division occurs in mitosis (M-phase). Within mitosis is prophase, metaphase, anaphase, telophase, and cytokinesis. A checkpoint between metaphase and anaphase ensures that each kinetochore attaches to a spindle fiber. The resulting daughter cells begin a new cell cycle or exit the cell cycle and differentiate⁸⁹.

Progression through the cell cycle is driven by cyclin-dependent kinases (CDKs) binding to their cognate cyclin partners. Whereas cyclins are variably expressed through the cell cycle, with specific cyclins produced at specific stages, CDKs are always present. A CDK is only active when bound to its appropriate cyclin partner. During G1, cyclins D and E are produced, facilitating the creation of CDK4/6-cyclin D and CDK2-cyclin E

complexes. Importantly, the CDK4-cyclin D complex phosphorylates retinoblastoma (Rb) to render the protein inactive and unable to inhibit DNA replication. Such an event allows for progression from G1 to S-phase. S-phase coincides with cyclin A production, which complexes with CDK1/2 to activate DNA replication. During G2, cyclin B is produced and activates cell division with CDK1. The timely production of cyclins and consequent activation of the appropriate CDKs are necessary to inhibit proteins blocking cell cycle progression or promote proteins needed for cell cycle progression.

Specifically, the expression of *CyclinD1* (*Ccnd1*) is key for RPC proliferation⁹⁰. CyclinD1 interacts with kinases to promote progression through G1 and inhibit activity of *p27^{Kip1}* (*Cdkn1b*), a cyclin-kinase inhibitor (CKI) that causes cell cycle arrest⁹¹⁻⁹³.

1.4.2.1.2 Notch pathway

The Notch pathway is one of the most well-studied extrinsic pathways responsible for regulating the balance between RPC proliferation and differentiation¹. Activated by cell-to-cell contacts, the intercellular pathway perpetuates RPC maintenance (See Figure 5.5, page 173). When the transmembrane Notch receptor of one cell interacts with the Notch ligands (Delta and Jagged) on a neighboring cell, the Notch receptors' intracellular domain (NICD) is cleaved and translocates to the nucleus. There, it complexes with the Rbpj/Maml1 transcriptional coactivator protein complex and activates the expression of target genes. Two well-known targets, *Hes1* and *Hes5*, encode antiproneural basic helix-loop-helix (bHLH) proteins that block neurogenesis⁹⁴. Studies show that increasing Notch pathway activity prolongs the period of progenitor maintenance and consequently delays differentiation. Conversely, disrupting or inhibiting the Notch pathway signaling causes

premature neuronal differentiation⁹⁴⁻⁹⁷. There are other signaling pathways that also control the expression of Hes family proteins, including Sonic hedgehog (Shh) and fibroblast growth factor (FGF)⁹⁸. Therefore, RPC proliferation is regulated by a variety of intrinsic and extrinsic factors in concert.

1.4.2.2 Neurogenesis in the retina

The retina is built by the consecutive addition of different classes of cells in a stereotypic sequence that is conserved in all vertebrates: RGCs, cone PRs, HCs, and starburst ACs are the first populations born, and the remaining subtypes of ACs, rod PRs, BPs, and MG are born later^{1,99,100}. With that, some cell populations are made only at early stages of development (early-born cells), while others are generated at later ontogenic stages (late-born cells). Such findings were observed in birth dating studies, where radiolabeled thymidine (and more recently, 5-ethynyl-2'-deoxyuridine, EdU, and 5-bromo-2'-deoxyuridine, BrdU) marked cells during S-phase of the cell cycle and followed the fate of their progeny¹⁰¹. These experiments discovered the temporal patterning of retinogenesis and showed that multiple retinal cell types are born concomitantly at any given developmental time^{99,102,103}. Specification of RPCs to different neuron types and glia is internally regulated by transcription factors that belong to the basic helix-loop-helix (bHLH), homeodomain, and forkhead families^{20,104}.

There are several theories regarding what regulates the order of neurogenesis in the retina. The competence model suggests that RPCs pass through waves of competence to make specific cell types as development proceeds¹⁰⁰. Early RPCs are capable of making early-born cells, and then the RPCs undergo a shift of competence to

both lose the ability to make early-born cells and acquire the ability to make late-born cells. MicroRNAs (miRNAs) are necessary for the RPC competence shift (See “microRNAs in retina development” section, page 20). This intrinsic change is irreversible. Heterochronic transplantation studies, where RPCs of one developmental age were transplanted into tissue of a different age, revealed that early RPCs cannot be induced to make late-born cells prematurely and late RPCs cannot reacquire the ability to make early-born cells after already undergoing the competence switch ^{1,105-107}. Additionally, competence is intrinsically restricted. To complement the findings of the heterochronic transplantation studies, experiments on retinal explants revealed that late RPCs differentiate into the appropriate ratios of cell types regardless of their environment ¹⁰⁸⁻¹¹⁰. A model of stochasticity explains how early or late RPCs then make different cell types ¹¹¹. RPCs experience fluctuations of gene expression that cause the stochastic nature of cell fate decisions. For example, a study using single cell RNA sequencing (RNAseq) of human retinas found the NFI transcription factors selectively expressed in late RPCs and implicated in controlling BP and MG cell fate specification ¹¹². Similarly, only late RPCs express some transcription factors, such as Sox9 and Ascl1, and respond to epidermal growth factor (EGF) ¹¹³⁻¹¹⁷. *In vivo* lineage tracing of individual RPCs in the zebrafish and rat retinas showed that the size and cellular composition of retinal clones are highly variable ^{109,118}. Such variability allows for the concurrent generation of different cell types from the single population of RPCs and the lineage progression observed.

Although RPC competence is minimally impacted by the retinal environment, that is not to say that there are no extrinsic factors that regulate proper retina development. Feedback inhibition is important for ensuring the proper ratio of different cell types. The

presence of differentiated neurons of a specific type negatively regulates further production of that neuron type. One example of this is RGCs producing Shh and Vascular endothelial growth factor (VEGF), both of which inhibit RPCs from differentiating into more RGCs^{119,120}. One compelling hypothesis is that intrinsic factors regulate cell fate specification before external factors regulate the volume of production of different cell types, and intrinsic factors respond by modifying RPC competence and cell fate specification²⁰. Recent studies support this, as the period of RPC competence to produce RGCs is slightly longer in *in vitro* models compared to *in vivo*. This delayed end to RGC neurogenesis suggests that extrinsic factors, in addition to intrinsic factors, do indeed contribute to cell fate specification neurogenesis in the retina.

1.4.3 Specification and differentiation of photoreceptors

While the gene regulatory networks controlling PR specification are well characterized in mice, zebrafish, and flies, there are efforts (beyond this dissertation) to better understand these networks in human and non-human primates. Although cones are an early-born cell type and rods are a late-born cell type, there is substantial overlap in the windows of cone and rod genesis. There are two key “decisions” that RPCs make for cone or rod specification. First, to become a PR or adopt a non-PR fate. Second, the choice between a cone or rod fate.

1.4.3.1 Photoreceptor or non-photoreceptor fate

A group of transcription factors, Cone-rod homeobox (Crx), Orthodenticle homeobox protein (Otx2), and Retinal homeobox proteins (Rx and Rax), facilitate PR

differentiation in vertebrates. *Otx2* is upregulated as RPCs exit the cell cycle to differentiate¹²¹. Cells expressing *Otx2* will differentiate into PR or BPs¹²²⁻¹²⁴. Downstream of *Otx2*, *Prdm1* (Blimp1) restricts *Otx2*-expressing cells to PR fates and *Vsx2* (*Chx10*) restricts to BP fates¹²⁴⁻¹²⁷. While knocking out *Otx2* prevents the development of PRs¹²³, *Prdm1* mutants create BPs at the expense of PRs^{127,128}.

Some groups hypothesize that *Otx2* activation is the “default” program in all RPCs, and those RPCs that will become cells other than PRs and BPs must repress *Otx2*¹²⁹. To this end, studies in cultured chick retinas suggest that all RPCs are able to express *Otx2*¹³⁰. Additionally, studies in cultured mouse retinas show that blocking Notch signaling drives *Otx2* expression, and consequently PR genesis⁹⁷. However, *Otx2*-expressing precursors do not make RGCs. In accordance with this hypothesis, a subpopulation of RPCs express *Atoh7* (*Math5*) and go on to become RGCs, while the rest of the RPCs will express *Ascl1* and eventually *Otx2* when they exit the cell cycle^{129,131-134}. Both *Ascl1*- and *Olig2*-expressing RPCs have the potential to differentiate into PRs, among all retinal cell types other than RGCs (*Ascl1* and *Olig2*) and MGs (*Olig2*)^{115,135,136}.

Transcription factor	Loss-of-function effect on mouse PR development
<i>Ascl1 (Mash1)</i>	Reduction in late-born fate ^{115,137}
<i>Atoh7 (Math5)</i>	More cones ¹³¹
<i>Crx</i>	PRs present but unfunctional ¹³⁸⁻¹⁴⁰
<i>Foxn4</i>	More PRs ¹⁴¹
<i>Neurod1</i>	Loss of M-cones, more S-opsin expression ^{142,143}
<i>Notch1</i>	Early loss causes more cones, late loss causes more rods ^{96,144}
<i>Nr2e3</i>	Many PRs co-express cone and rod genes, more S-opsin cones, rod functional deficits ^{145,146}
<i>Nrl</i>	Rods become S-opsin cones ¹⁴⁷
<i>Onecut1 (Oc1)</i>	Fewer cones in total, loss of M-cones, more S-opsin expression ¹⁴⁸
<i>Otx2</i>	No PRs ^{122,149}
<i>Pax6</i>	No PRs ¹⁵⁰
<i>Prdm1 (Blimp1)</i>	More BPs at the expense of PRs ^{126,127}
<i>Rorb</i>	More cones at the expense of rods, PRs unfunctional ¹⁵¹
<i>Rxrg</i>	More S-opsin cones ¹⁵²
<i>Thrb2 (Thrb)</i>	Loss of M-cones, more S-opsin expression ^{153,154}
<i>Vsx2 (Chx10)</i>	More rods at the expense of BPs ¹⁵⁵

Table 1. Transcription factors expressed in RPCs and loss-of-function effects on mouse photoreceptor development. Table modified from Brzezinski & Reh, 2015 ¹²⁹.

1.4.3.2 Rod vs. cone fate

The distinction between rod and cone gene expression occurs downstream of *Otx2* and *Crx*, both of which are necessary for the expression of most PR genes ¹²⁹. Rod specification requires the combined efforts of rod activators and cone repressors. In rod-fated cells, *Rorb* is also needed to initiate the expression of the transcription factor Neural

retina leucine zipper protein (*Nrl*)¹⁵⁶. *Nrl* is necessary to activate rod-specific genes¹²⁹. One such gene, *Nr2e3*, both activates other rod genes and silences cone genes, including *Opn1sw* (S-opsin)¹⁵⁷⁻¹⁶¹. This direct regulation of *Opn1sw* by *Nr2e3* could explain why aberrations to rod-associated genes generally result in the increase of S-opsin-expressing cones. As such, overexpressing *Nrl* results in cones reprogramming into rods¹⁶², and *Nr2e3* mutants show increased S-opsin expression at the expense of rod gene expression^{145,146,162}.

Cone specification is not as well understood as rod specification is. A smaller cohort of cone-specific markers have been identified, including the thyroid hormone receptor 2 (*Thrβ2*)¹²⁹. *Thrβ2* is neither necessary nor sufficient for cone development, as null mice still generate cones, and replacing *Nrl* with *Thrβ2* does not induce cone development at the expense of rods¹⁵³. However, *Thrβ2* manipulations in mice modulate the ratio between M-opsin- and S-opsin-expressing cones^{154,163,164}. Similar results were found in human retinal organoid experiments¹⁶. *NeuroD1* is necessary for sustained expression of *Thrβ2*¹⁴³. Additionally, *Onecut1* (*OC1*) and *Otx2* work in concert to activate *Thrβ2* expression¹²⁹. Although *OC1* mutant mice show similar phenotypes to *Thrβ2* mutant mice, with no substantial reduction in total number of cones and an increase in S-opsin-expressing cones¹⁶⁵, *OC1* could be part of the group of factors not lineage restricted to PR fates that regulate cone specification.

In zebrafish and chicken, retinoic acid (RA) signaling is also implicated in photoreceptor development. Specifically, rod specification through the *RARαb* and possibly the *RXR-γa* receptors^{166,167}, and cone specification through the *Rxγ* receptor^{152,168-170}. Loss of *Rxγ* does not modulate total cone number, just subtype¹⁴⁸. In Chapter

3, I explore the expression patterns of molecules associated with the RA pathway in the developing non-human primate retina.

A few hypotheses have emerged for what regulates cone specification¹²⁹. Perhaps the cone pathway is the default for all PRs, and negative regulators, such as Nr2e3, allow for rod specification. Alternatively, there could be a cone-activator, like Nrl is for rod specification, that has yet to be identified. Beyond the efforts in this dissertation, single-cell sequencing experiments will be valuable for identifying such genes. However, obtaining age-appropriate samples to study RPCs before cone specification is paramount.

1.5 MicroRNAs

1.5.1 MicroRNA biogenesis

MicroRNAs (miRNAs) are high-conserved, small, non-coding RNAs that regulate gene expression. A series of cleavage events process the initial RNA transcripts into mature miRNAs, which are typically 19-25 nucleotides long (See Figure 5.1, page 168). MiRNAs are first transcribed from DNA sequences by RNA polymerases II and III. These primary miRNAs (pri-miRNAs) are double-stranded transcripts that fold into hairpin-like structures. Depending on the miRNA being intergenic or intragenic, biogenesis follows a canonical or non-canonical pathway, respectively¹⁷¹. Intergenic miRNAs are processed *via* the canonical pathway, where the hairpin-like structures are cleaved by the Drosha/DiGeorge critical region 8 (DGCR8) Microprocessor protein complex. Intragenic miRNAs are processed *via* the non-canonical pathway by the splicing machinery. The resultant precursor miRNA (pre-miRNA) from both pathways is an individual hairpin-like

structure of about 70 nucleotides. Pre-miRNAs are exported from the nucleus into the cytoplasm, where they are further processed by Dicer into mature miRNA duplexes. One miRNA strand is loaded into Argonaute (Ago) to form a miRNA-Ago complex, called the RNA-induced Silencing Complex (RISC) ¹⁷¹⁻¹⁷³. Mature miRNAs bind to the antisense sequences in the 3' untranslated region (UTR) of target messenger RNA (mRNA) transcripts. They are implicated in influencing translation by inhibiting mRNA translation and inducing mRNA decay ¹⁷⁴⁻¹⁷⁶.

1.5.2 MicroRNAs in retina development

The first miRNA was discovered in *Caenorhabditis elegans* in 1984. In the 40 years since, over 2,000 miRNAs have been reported in the miRbase from over 200 species ¹⁷⁷. Computation and experimental analyses indicate that over 60% of the human transcriptome is regulated by one or more miRNA, with each miRNA predicted to regulate the mRNA transcripts of about 200 genes ¹⁷⁸. miRNAs have been implicated in slowing translating ribosomes and influencing mRNA stability, among other roles ^{179,180}. Given their broad ability to influence translation, miRNAs are likely involved in most biological processes.

To discern the role of miRNAs in retinal development, various research groups have targeted the enzymes necessary for miRNA processing. The most targeted enzyme is Dicer ¹⁸¹. Dicer plays a pivotal role in processing mature miRNAs, specifically by cleaving pre-miRNAs into miRNA duplexes. Except for one miRNA that is processed by Ago catalysis instead of Dicer, all miRNAs are processed in a Dicer-dependent manner ¹⁸²⁻¹⁸⁴. Bernstein *et al.* found in Dicer null mice that miRNAs are necessary for proper

development beyond gastrulation, and they observed embryonic lethality in their absence¹⁸⁵. This lethal phenotype when *Dicer* is removed in every tissue impedes studies on the role of miRNAs in late stages of development. Subsequent studies circumvented this roadblock by removing *Dicer* in specific tissues. The discrete expression patterns of various Cre lines gave way to strikingly different phenotypes. Damiani *et al.* used a floxed conditional *Dicer* allele with the *Chx10cre* allele to remove *Dicer* from retinal progenitor cells¹⁸⁶. *Chx10cre* causes mosaic recombination throughout the retina, resulting in interspersed *Dicer*-deficient and wildtype cells. They observed all cell types and proper lamination in these *Dicer*-deficient retinas, concluding that miRNAs are not necessary for cell fate specification. Georgi *et al.* used the α Pax6cre transgene with a conditional *Dicer* mutant mouse¹¹⁶. α Pax6cre mediates recombination in large blocks in the peripheral retina, as it is expressed in RPCs at E10.5. Their ROSA26-YFP reporter identified cells once *Dicer* activity was removed, showing developmental delay. Instead of following the stereotypic sequence of neurogenesis, these progenitors produced only early-born neurons at the expense of late-born neurons. Such findings suggest that miRNAs are indeed necessary for proper retinal neurogenesis.

La Torre *et al.* continued on to identify three specific miRNAs that mediate proper retinal development¹⁸⁷. In mice, the competence switch, when RPCs transition from making early-born neurons to making late-born neurons, occurs between E14 and birth (postnatal day P0). This study used miRNA microarray analysis of wildtype retinas during this key developmental window and found three miRNAs—let-7, miR-9, and miR-125b—that increased in expression. These miRNAs, termed Late Progenitor or LP-miRNAs, proved to be important for neuronal fate specification. When the LP-miRNAs are inhibited,

RPCs are restricted to making early-born neurons, even during the normal period of late-born neuron specification; when the LP-miRNAs are overexpressed before they are endogenously expressed, RPCs prematurely differentiate into late-born neurons. These LP-miRNAs are both necessary and sufficient for the RPC competence switch (Figure 1.7). Two of the three LP-miRNAs—let-7 and miR-9—have been shown to also mediate proper timing of fate specification during cortical development ¹⁸⁸. Overall, miRNAs are proven mediators of the temporal sequence of neurogenesis throughout the CNS.

1.6 Summary

In this dissertation, I explore the mechanisms that drive cell fate specification in the CNS, primarily focusing on how foveal progenitor cells preferentially differentiate into cone photoreceptors. I present an overview of the retina, fovea, and relevant concepts within the context of fate specification. Given that much of our understanding of retinal development is derived from rodent models, which are afoveated, I sought to investigate the mechanisms driving foveal development in the human and nonhuman primate. In primates, I characterized retinal development, identified expression patterns of retinoic acid pathway molecules, and presented novel miRNAs that are upregulated in the fovea. I reviewed oscillation patterns of miRNAs and the consequent role in retinal development, and explored how the Notch pathway and miRNAs influence fate specification in the mouse brain.

1.7 Figures

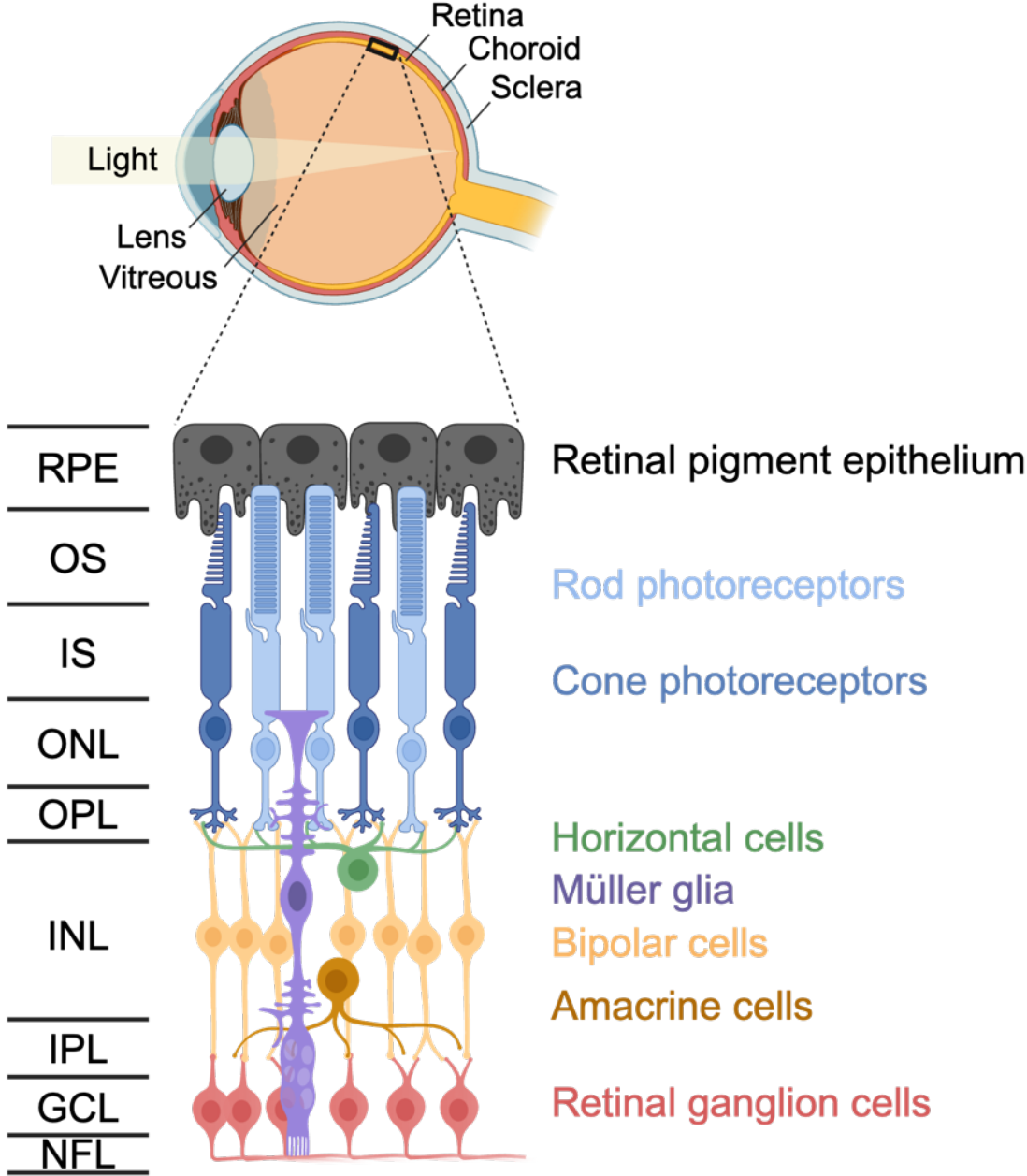


Figure 1.1 Eye and retina anatomy

(Top) Cross section of a human eye. Light passes through the lens to be focused on the retina (yellow) in the back of the eye. The vitreous (orange) is an optically transparent gel that maintains the shape of the eye. Behind the neural retina, the choroid (red) contains vasculature, and the sclera (blue) provides structural support. **(Bottom)** Inset is expanded to show retinal anatomy. Rod and cone photoreceptors receive photons of light and convert it into electrical signal. This signal is passed to bipolar cells and retinal ganglion cells, to be sent to the brain through the optic nerve, which are RGC axons bundled together. Horizontal and amacrine cells are interneurons that modulate the signal transmission. Müller glia are the non-neural cells of the retina. Sitting just behind the retina, apically in the eye, is a layer of pigmented cells, the retinal pigment epithelium. RPE: retinal pigment epithelium; OS: outer segment; IS: inner segment; ONL: outer nuclear layer; OPL: outer plexiform layer; INL: inner nuclear layer; IPL: inner plexiform layer; GCL: ganglion cell layer; NFL: nerve fiber layer. This figure was created with BioRender.com.

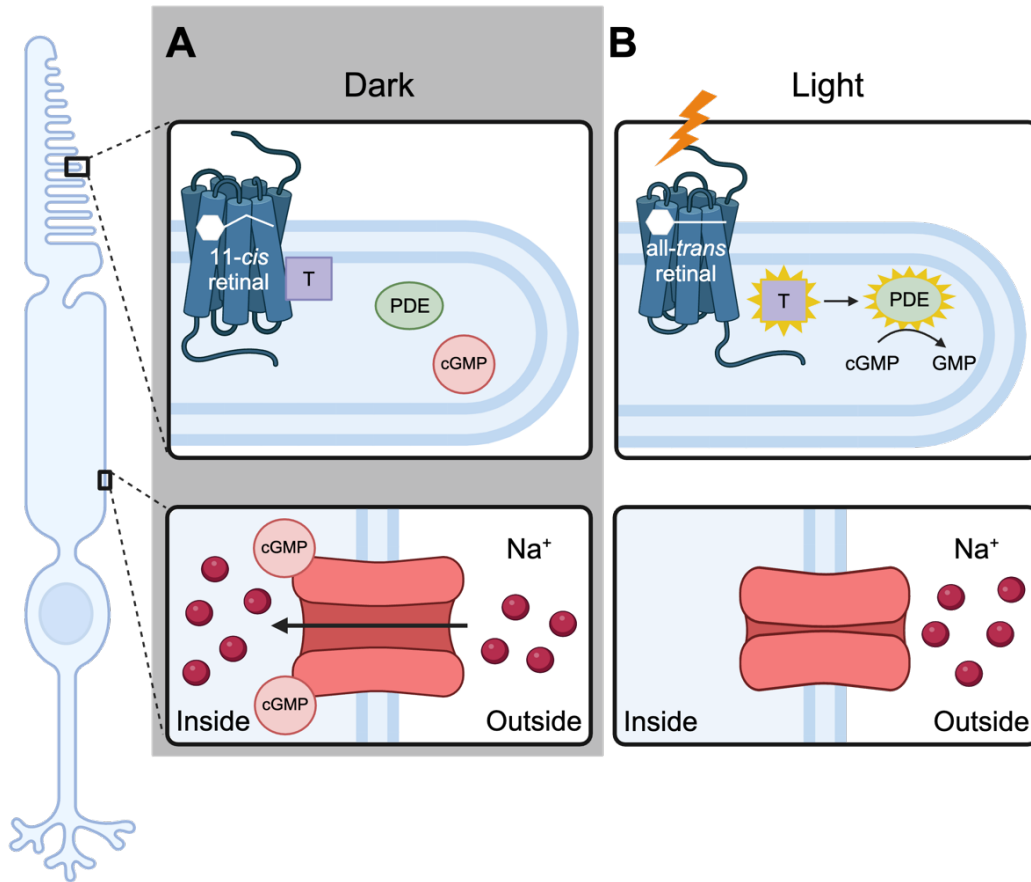


Figure 1.2 Phototransduction

Phototransduction begins in the outer segment of photoreceptors, where stacks of retinal- and Opsin-containing discs reside. Exposing PRs to dark (A) or light (B) yields different responses. **(A)** Unstimulated, retinal is in the 11-*cis* configuration. Transducin and phosphodiesterase are inactive (top), and cGMP is present to open ion channel and facilitate the influx of sodium ions into the cell (bottom). This allows for the PR to constantly release neurotransmitters. **(B)** In the presence of a light stimulus, the retinal undergoes a configuration change to all-*trans*. Transducin is activated, which prompts phosphodiesterase to convert cGMP to GMP. Without cGMP, the ion channels are closed, and sodium does not enter the cell. The consequent hyperpolarization causes the PR to decrease neurotransmitter release. T: transducin; PDE: phosphodiesterase; cGMP: cyclic guanosine monophosphate; GMP: guanosine monophosphate; Na⁺: sodium. Figure adapted from Kappler *et. al.*, 2016¹⁸⁹. This figure was created with BioRender.com.

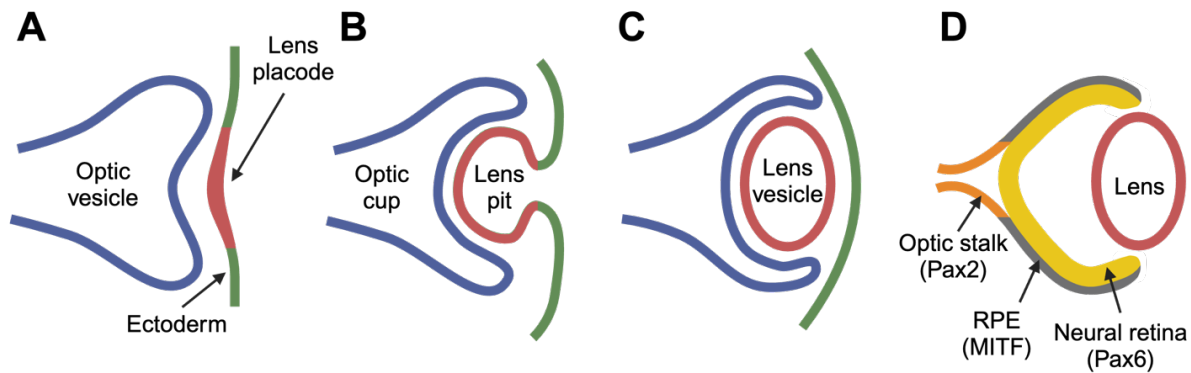


Figure 1.3 Early eye development

(A) The optic vesicles (blue) evaginate from the anterior neural plate towards the surface ectoderm (green), establishing the lens placode (red). **(B)** The optic vesicle and lens placode invaginate, forming the optic cup (blue) and lens pit (red), respectively. **(C)** After separating from the surface ectoderm (green), the lens vesicle (red) will become the lens. **(D)** The bilayered cup will become the neural retina (yellow; inner, proximal tissue) and retinal pigment epithelium (grey; distal, outer tissue). Gene expression domains distinguish the parts of the developing eye: optic stalk cells express Pax2, retinal pigment epithelium expresses MITF, and neural retina expresses Pax6. This figure was created with BioRender.com.

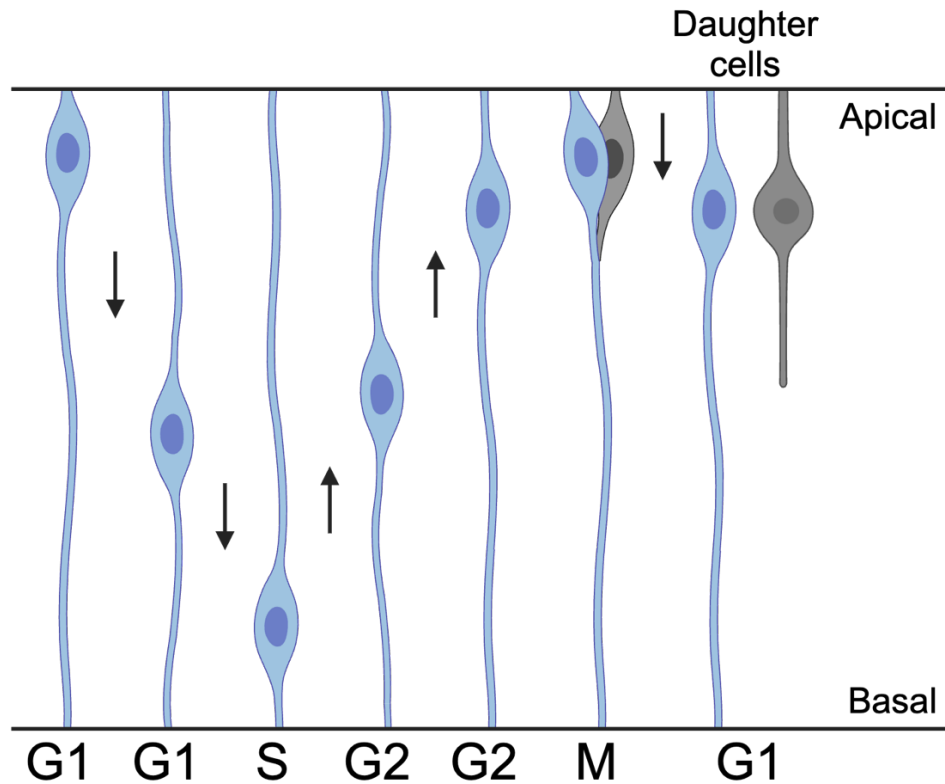


Figure 1.4 RPCs undergo interkinetic nuclear migration

Throughout the cell cycle, a RPC participates in interkinetic nuclear migration. The nucleus travel from the apical to the basal surface and then back to the apical surface during each cycle. A newly-born cell begins with its nucleus in the apical retina, and the nucleus will travel basally during G1. The nucleus is in the basal retina during S-phase, before travelling apically during G2. Mitosis occurs when the nucleus is most apical. This figure was created with BioRender.com.

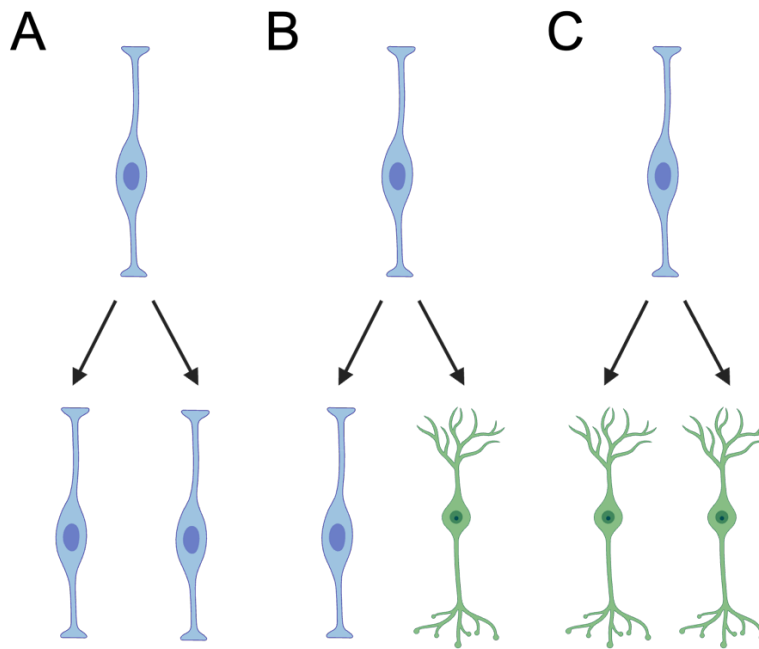


Figure 1.5 RPCs undergo symmetric or asymmetric divisions

During mitosis, a RPC will make one of three possible combinations of daughter cells: **(A)** symmetric division making two RPCs, **(B)** asymmetric division making one RPC and one post-mitotic cell, or **(C)** symmetric division making two post-mitotic cells of the same or different type.

This figure was created with BioRender.com.

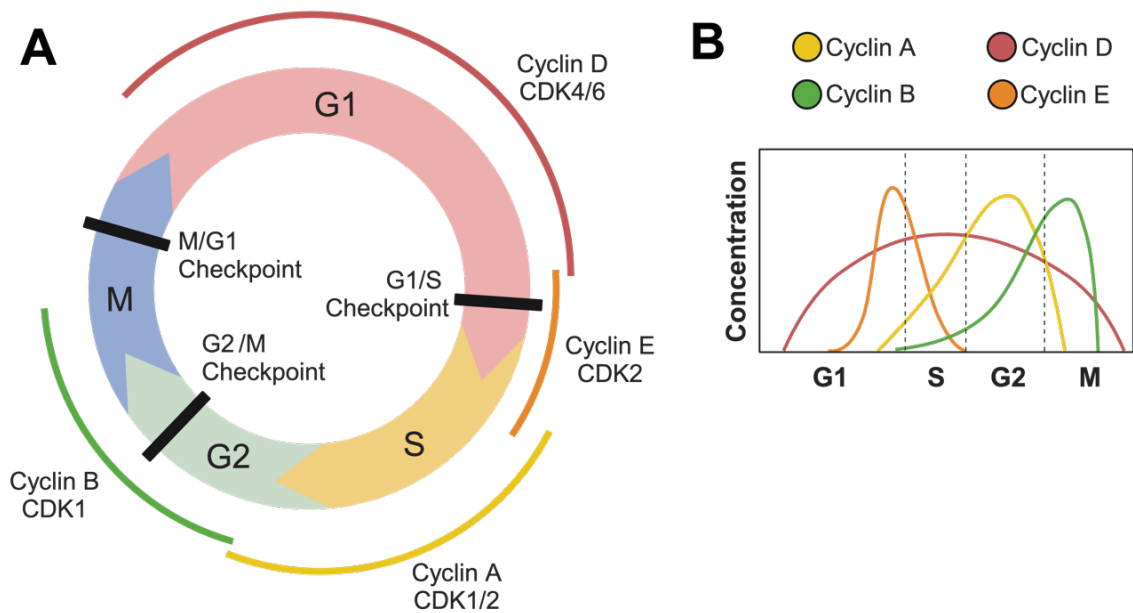


Figure 1.6 Cell cycle

(A) The cell cycle consists of four phases: Gap 1, synthesis phase, Gap 2, and mitosis. Three checkpoints ensure that one phase is appropriately completed before progressing to the next phase. Groups of cyclin and cyclin dependent kinases facilitate cell cycle progression. (B) Cyclin expression is variable throughout the cell cycle. Cyclin D is needed for most of the cell cycle. Cyclin E expression peaks at the transition from G1 to S-phase. Cyclin A is most highly expressed in G2. Cyclin B expression peaks at the transition from G2 to M-phase. CDK: cyclin-dependent kinase; G1: Gap 1 phase; S: synthesis phase; G2: Gap 2 phase; M: mitosis. This figure was created with BioRender.com.

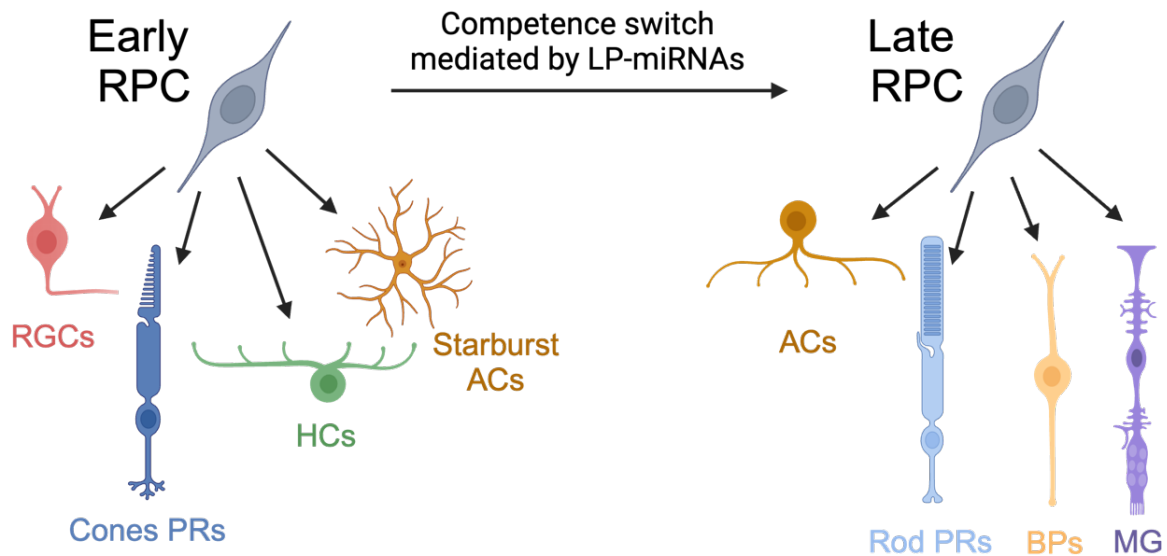


Figure 1.7 miRNAs control RPC competence

Neurogenesis in the retina occurs in a stereotypic sequence. RPCs can differentiate into early cell fates (retinal ganglion cells, cone photoreceptors, horizontal cells, and a subtype of amacrine cells) before shifting competence, where they lose the ability to make early-born fates and acquire the ability to make late-born fates (all the other subtypes of amacrine cells, rod photoreceptors, bipolar cells, and Müller glia). This competence switch is mediated by miRNAs, specifically the late progenitor miRNAs, Let-7, miR-9, and miR-125b. Expression of the LP-miRNAs increases as development continues. RPC: retinal progenitor cell; RGC: retinal ganglion cell; PR: photoreceptor; HC: horizontal cell; AC: amacrine cell; BP: bipolar cell; MG: Müller glia; LP-miRNA: late progenitor miRNA. This figure was created with BioRender.com.

2. Accepted encyclopedia chapter: Development of the primate fovea

Elizabeth Fishman-Williams^{1*}, Miranda R. Krueger^{1*}, and Anna La Torre¹

¹ Department of Cell Biology and Human Anatomy

School of Medicine, University of California Davis

* These authors contributed equally

The following chapter was submitted as a chapter to the *Encyclopedia of the Eye, Second Edition* and accepted on January 16, 2024. The accepted version of this manuscript has been reformatted for this dissertation. The authors of the manuscript were Elizabeth Fishman-Williams, Miranda R. Krueger, and Anna La Torre, with myself and Miranda contributing equally.

2.1 Abstract

The *fovea centralis* (fovea) is the region of the primate retina specialized for high visual acuity. It consists of a small pitted invagination located a few millimeters temporal to the optic nerve disc. The fovea contains a high density of cone photoreceptors and a large number of inner neurons that have been displaced peripherally to reduce light scattering and facilitate the direct illumination of the photoreceptors. The development of the fovea has been the subject of study for over a century, yet many of the molecular, cellular and mechanical factors that contribute to foveal development are not well understood. Here, we have identified five different developmental events that distinguish the fovea from the rest of the retina, including (1) differential retinal progenitor cell growth, (2) neurogenesis timing, (3) fate acquisition, (4) vascularization, and (5) pit formation. We discuss all these processes in detail, highlighting the current knowledge as well as normal versus pathological features.

2.2 Key points

- The development of the foveal region can be distinguished from the rest of the retina by a series of events that span from early embryonic development to postnatal stages.
- The first recognizable difference is a differential growth of the retinal progenitors of the fovea.
- In primates, neurogenesis follows a fovea-to-peripheral pattern.
- The center of the fovea contains an extraordinary number of cones photoreceptors while rods are not present at any developmental time-point.

- Anti-angiogenic factors, guidance cues, and an absence of astrocytes in the foveal center contribute to the development of the foveal avascular zone.
- Centrifugal and centripetal cell movements result in the development of the foveal pit.

2.3 Introduction

The vertebrate retina has evolved to fit the visual necessities required of animals' behaviors and habitats ^{190,191}. Different visual features can provide advantages for foraging, mate selection, predator avoidance, and navigation. One such adaptation is a specialized region in the primate central retina called the *macula lutea* ('yellow spot', macula), named because of the presence of yellow pigment. This region allows for high visual acuity to resolve spatial details and color, and has provided primates with extensive evolutionary advantages ¹⁹².

The macula resides in the posterior pole of the retina on the temporal side of the optic disc, spanning the central 3 mm of the visual field (or 10° of visual angle). Within the central 1 mm of the macula resides the *fovea centralis* (fovea), which is responsible for maximal visual acuity. The fovea lies on the visual axis of the eye, such that the light passing perpendicularly through the center of the lens will impact this region. The fovea is defined by a depression, or small pit as it is named after (*fovea* means 'pit' in Latin), where the inner retinal layers have migrated peripherally to leave only the outer nuclear layer (Figure 2.1). Thus, the macula is divided into four concentric areas: the foveola, the fovea, the parafovea, and the perifovea. The **foveola**, the innermost region of the foveal pit, is about 250 µm in diameter, and represents the central 1° 20' of the visual field. This

area is the thinnest part of the retina, as it contains only glial cells and cone photoreceptor inner and outer segments and their nuclei. The axons from these cones extend radially to synapse with cells that have been displaced away from the pit and form the Henle's fiber layer. The average length of these fibers is 558 μm and the first synapses occur approximately 350 μm from the foveal center ¹⁹³. Given the large number of foveal photoreceptors and the considerable displacement, the Henle's fiber layer constitutes a significant fraction of the thickness of the retina ¹⁹⁴ (Figure 2.1B). Next, the **fovea** encompasses the adjacent 750 μm around the foveola. The fovea contains all the layers of the retina, including the widest part of the retina and the foveal slope. This region has very wide ganglion cell and Henle's fiber/outer plexiform layers. In addition to the inner retina layers displaced laterally, blood vessels are also absent in the foveola and foveal slope, defining the **foveal avascular zone (FAZ)**, which is about 500 μm in diameter. The region adjacent to the fovea is the **parafovea**, a region 500 μm wide. In the parafovea, the ganglion cell layer is about 8 cells thick, but decreases to 4 cells thick at the peripheral edge. The rest of the macula is the **perifovea**, which is 1.5 mm wide, and its periphery lies near to the optic disk. In the peripheral edge of this region, the ganglion cell layer decreases to 1 cell thick.

While retina development has been well studied, the mechanisms governing fovea development remain largely unknown. This substantial gap in knowledge may be partially attributed to the lack of fovea in typical small model organisms and the limited number of foveated species that have been used for research. It is thought that the fovea first appeared in the temporal retina of teleost fish ¹⁹⁵. Then, birds developed a nasal fovea and bifoveated retinas emerged with foveas in both the central and temporal regions in

some avian species ^{196,197}. The fovea disappeared in primitive mammals before reappearing in diurnal primates. Other species, including chickens, pigeons, and zebrafish, have retinal specializations with the features of a high-acuity area (HAA) that have been the focus of ongoing research. This chapter will focus on fovea development in the human and non-human primate retina.

Primate fovea development has been the topic of research for more than two hundred years. In fact, several anatomists already documented some of the foveal specializations in the eighteenth century. In 1782, Francesco Buzzi described the macula in the dissected eyes of a 35-year-old man as a yellow-colored region in the retina posterior pole ¹⁹⁸. In 1799, Samuel Thomas Soemmerring was the first to use the term “*macula lutea*” ¹⁹⁹ and he also described the fovea but at the time, he thought the fovea was a hole in the central retina. The first studies of the developing primate retina were carried out by Johan Henrik Chievitz (1888) ²⁰⁰ and others ^{201,202}. These early anatomical characterizations were greatly expanded on by Ida Mann in 1928 ²⁰³. These classic studies already recognized that foveal specialization begins early in embryonic time and continues well into the neonatal period. After Ida Mann’s work, not many studies addressed the topic of foveal development until 1976, when Anita Hendrickson and Carl Kupfer published a paper entitled “The histogenesis of the fovea in the macaque monkey” ²⁰⁴. The subsequent legacy of Anita Hendrickson cannot be overstated. Using human samples and both Old World and New World primates, her work encompasses comprehensive studies of the photoreceptor topography, mechanics of the foveal pit formation, and development of the vasculature (see below). Her beautiful and extensive histological studies showed that key events of fovea development occur in a well-

established sequence that is comparable between human and non-human primates. More recently, advancements in molecular analyses, imaging technologies, and theoretical modeling have provided further clarity on the different ontogenic stages and events. Five key features have emerged that distinguish the development of the fovea from that of the rest of the retina: (1) **Differential progenitor growth.** The first indication of the incipient fovea, even before neurogenesis, is a swelling or enlargement in the temporal retina that will lead to the “foveal bulge”. (2) **Neurogenesis timing.** Neurogenesis begins in the temporal retina, at the center of the fovea, and continues in a wave that extends peripherally. (3) **Differential cell fate acquisition.** The fovea has the highest density of cone photoreceptors in the entire retina, about 200-fold higher than the most eccentric retinal regions. This peak of cone density parallels a peak in retinal ganglion cell density. Furthermore, the foveola contains only highly packed cones and no rods, defining a rod-free zone (RFZ). (4) **Differential vascularization.** Anti-angiogenic factors and axon guidance cues prevent the growth of capillaries into the incipient fovea. The foveal avascular zone (FAZ) is further defined postnatally when the vasculature further recedes away from the macula. (5) **Pit formation.** Late in gestation and into postnatal development, centrifugal migration of the inner retinal neurons results in the reduction of the ganglion and bipolar cell layers to establish a pitted invagination. The resultant foveal pit contains only cone cell bodies and glia in the depression floor.

Here, we will review the current knowledge regarding the mechanisms that orchestrate the coordinated progression of all these events.

2.4 Patterning and differential growth

The first morphological indication of the development of the incipient fovea is an asymmetric growth of the temporal retina, right after the formation of the optic cup. The location of this “foveal bulge” is constant; despite a widespread variation in eye and retinal sizes²⁰⁵⁻²⁰⁸ among all the foveal primates, the dimensions and relative position within the temporal retina are conserved.

During the optic cup stage, patterning processes are extremely important to define the various tissues (neuroretina, retinal pigment epithelium, ciliary marginal zone, etc.^{22,209}) as well as axial orientations. Nasal-temporal patterning refers to the organization along the nasal (toward the nose) to temporal (toward the temple) axis of the eye. The exact mechanisms by which nasal-temporal patterning is determined in the primate retina are not fully understood, but it is thought to be influenced by opposing combinations of gene expression, morphogenetic gradients, and cell interactions.

2.4.1 FOXD1 and FOXG1

The winged-helix transcription factors FOXD1 and FOXG1 are some of the earliest known determinants of the nasal-temporal axis. These proteins are expressed on either the temporal (FOXD1) or nasal (FOXG1) side of the optic vesicle in a complementary, restrictive pattern^{210,211}. The fovea, as well as the HAA of different species, is generally located in the temporal retina, suggesting that the specification of these regions may depend on temporal identity. In this direction, studies using zebrafish have shown that the establishment of a *foxd1* domain in the retina is linked to the

formation of the HAA. Thus, zebrafish larvae lacking *foxd1* showed absence of HAA markers, reduced numbers of UV cones, and expanded nasal identities²¹².

2.4.2 SHH and FGF

During retinal development, gradients of signaling morphogens also play a role in establishing positional information along the nasal-temporal axis. Gradients of Sonic Hedgehog (SHH) and Fibroblast Growth Factor (FGF) are known to be required in the establishment of nasal and temporal identities, respectively. Elegant experiments using zebrafish and chick models have shown that *Shh*, which is expressed by the ventral midline, is required for the expression of *foxd1*²¹³. This expression begins in the ventral half of the optic cup that will then become the temporal side. Similarly, *Fgf8* from the dorsal forebrain induces *foxf1* expression in the dorsal (future nasal) optic cup²¹³⁻²¹⁵. Cross-repression between *Foxg1* and *Foxd1* further refines this patterning^{213,216-218}.

2.4.3 Ventropin and BMP-2

In chickens, the BMP2/4 antagonist Ventropin is expressed in both a ventral-high dorsal-low pattern of expression as well as a nasal-high temporal-low pattern, reinforcing that this molecule is particularly enriched in the nasal-ventral quadrant²¹⁹. Conversely, BMP-2 is expressed in a pattern complimentary to that of Ventropin, with a double gradient along the temporal-nasal and dorso-ventral axes^{217,220}. Gain of function experiments of either Ventropin or BMP-2 shifted the retina axes. Interestingly, these experiments showed that *FoxG1* alterations were sufficient to modulate BMP signaling

²¹⁷, suggesting that the gradients of BMP and Ventropin take place downstream of FoxD1/FoxG1.

2.4.4 EphrinA2/A5 and EphrinB1

Eph receptors and their transmembrane ligands, Ephrins, are some of the classic molecules known to be expressed in complementary gradients in the developing retina. The Eph receptor EphA3 and its two ligands, Ephrin A2, and Ephrin A5, are enriched in the nasal retina ²²¹⁻²²³ and regulate the topographic targeting of axons on the optic tectum ^{217,224}. Similarly, two homeobox genes, SOHo1 and GH6 are expressed in a nasal-high, temporal-low pattern and misexpression of either of these genes represses EphA3 and leads to axon routing mistakes ²²⁵. In contrast, EphB1 is expressed in the peripheral ventro-temporal crescent of the retina and is sufficient to drive ipsilateral projections in mice ²²⁶. In humans, EPHB1 is expressed in the temporal half of the retina at 10 gestation weeks ²²⁷. However, all these Eph receptors and Ephrins are mostly expressed by retinal ganglion cells. Ablation of *Foxd1* in mice led to an expansion of EphrinA expression domains while proteins involved in ipsilateral projections, such as EphrinB1 were downregulated ²¹⁸. Similarly, FoxG1 induced the expression of EphrinA2, suggesting that the expression of these molecules is also dependent on the previous acquisition of temporal or nasal identities and remain downstream of FoxD1/FoxG1.

2.4.5 Retinoic acid signaling

An important study by da Silva and Cepko ²²⁸ discovered a key role for retinoic acid (RA), the active form of vitamin A, in the development of the avian HAA. This study

describes that the RA catabolizing enzymes *CYP26A1* and *CYP26C1* are enriched in the HAA, and RA reporters showed high RA activity across the retina with the exception of the HAA. Similarly, *FGF8* expression is also confined to the HAA. When the levels of RA were experimentally increased, the expression of *FGF8* was affected and rods were now present in the HAA. Together this evidence suggests that *FGF8* expression driven by low levels of RA in the presumptive HAA is required for the patterning of the avian rod-free area. Notably, *CYP26A1* has also been detected in the zebrafish HAA^{229,230}. In primates, different approaches have identified *CYP26A1* enrichment in both human and rhesus monkey foveal cells from early stages of development^{231,232}. Later in development, *CYP26A1* is exclusively expressed by the Müller glia cells of the macula (including the foveola, fovea, and parafovea)²³³. None of these experiments have detected enriched expression of *FGF8* in the primate fovea, suggesting that perhaps only some aspects of the avian HAA development are conserved. RA is important for some of the eye morphogenetic movements that shape the optic cup²³⁴, rod photoreceptor differentiation²³⁵, and for cone photoreceptor survival²³⁶ in mice. In humans, a microdeletion containing both *CYP26A1* and *CYP26C1* genes led to optic nerve aplasia and microphthalmia²³⁷. Thus, while it is clear the RA plays multiple and significant roles in eye development, how RA signaling and/or *FGF8* specifically contribute to the regulation of foveal development as well as what mechanism(s) restrict the expression of CYP26 enzymes in the developing eye remain unresolved. It is also important to note that *Cyp26A1* and *Cyp26C1* also establish a stripe of lower RA levels within the equatorial rodent retina^{238,239}. In mice, alterations in *Cyp26* expression led to perturbations in the ratios of cone opsins and RGC projection patterns²³⁹. However, given that mice do not have foveal

specialization or rod-free regions, and thus, neither *CYP26A1* expression nor lower levels of RA are sufficient to drive foveal development.

Besides the expression of different molecular markers, the nasal-temporal axis exhibits differential tissue growth beginning at early stages of development. The exact mechanisms of how this differential growth occurs still remains elusive. In rhesus monkey, the retina remains symmetrical across the temporal-nasal axis at 30 days gestational age (18% gestation), but less than a week later (36 days gestational age, 22% gestation), the temporal half is substantially larger at the foveal anlage, and more invaginated in comparison to its nasal counterpart²⁴⁰. Recent quantifications have shown that at these early stages, the temporal retina almost double the length (1.9 folds) of the nasal side²⁴¹. Similarly, the “foveal bulge” is apparent in human fetal week 8 samples and more marked by fetal week 12²⁴² (Figure 2.2). Thus, this asymmetry across the nasal-temporal axis appears to be established very early on in primate development, which indicates that the temporal progenitor cells must exhibit different growth dynamics relative to their nasal counterparts.

2.5 Differential neurogenesis timing

Neurogenesis in the developing human and non-human primate retina follows a fovea-to-periphery gradient. Studies using hematoxylin and eosin (H&E) staining, 3H-thymidine labeling, immunohistochemistry (IHC), *in situ* hybridization (ISH), and more recently, RNA-sequencing have described this wave of neurogenesis. While there are minor discrepancies between the ages of differentiation events, there is a strong

consensus in the literature about neurogenesis both beginning and finishing first in the center of the fovea.

All the cells of the retina are born from a single population of multipotent progenitor cells (RPCs) in a well-known sequence that is conserved across species: retinal ganglion cells (RGCs), cone photoreceptors, horizontal cells, and starburst amacrine cells are the first cell populations born, while other amacrine cells, rod photoreceptors, bipolar cells, and Müller glia are born later in development. This stereotypic sequence of neuronal differentiation and retinal layering has allowed for various studies aimed at comparing the rate of development within the fovea and peripheral retina.

2.5.1 Retinal layering

General staining methods such as methylene blue-azure II and H&E are valuable to compare the rate of laminar development across the developing primate retina. Before neurogenesis commences, the entire retina is comprised of progenitor cells that undergo interkinetic nuclear migration movements within the neuroblastic layer (NbL). Ganglion cell layer (GCL) differentiation is the first observable lamination event. By 20% gestation in humans and 25% gestation in rhesus monkey, RGCs are already distinguishable from retinal progenitors in both the temporal and nasal retina. However, both the GCL and the nerve fiber layer (NFL) of axons are thicker in the temporal retina. The emergence of the inner plexiform layer (IPL) clearly demarcates the GCL from the NbL (Figure 2.2). Older studies defined an “outer neuroblastic layer” and an “inner neuroblastic layer”; however, now it is clear that what was thought to be the “inner neuroblastic layer” is composed of RGCs and postmitotic RGC precursors migrating

inward and not mitotic neuroblasts. Thus, we propose that the correct nomenclature for this layer is GCL and that there is only one NbL.

In humans, the presence of the IPL has been recorded in the temporal retina at approximately embryonic day 56 (20% gestation) but it is not observed in the nasal retina until 45% gestation²⁴². In rhesus monkey, the IPL is first observable in the temporal retina at day 50 (30% gestation), and it is distinct by 36% gestation, but the IPL is not observed in the nasal retina until 42% gestation, and it is distinct by 48% gestation. Finally, the outer plexiform layer (OPL) first emerges in the temporal retina at 28% gestation, the nasal retina by 50% gestation, and the entire peripheral retina by 75% gestation. In the rhesus monkey retina, initiation of the OPL is noticeable in the temporal retina at 48% gestation, before it is observed in the nasal retina at 66% gestation. The discrepancy between developmental milestones in the human and non-human primate retina may be due to the inexact aging of human samples and sampling differences for each species.

2.5.2 Neurogenesis begins in the fovea first

There is overwhelming evidence that neurogenesis in the developing human and non-human primate begins in the fovea. In a hallmark study by La Vail, Rapaport, and Rakic¹⁰², 3H-thymidine labeling of non-human primate retinas *in utero* demonstrated that all retinal neurons and Müller glia are generated first in the fovea and neurogenesis gradually moves more peripherally as development continues. Labeling experiments in developing human retinas using specific cell type and synaptic markers showed that the peripheral retina is delayed from the central retina by almost 20%²⁴³. This developmental delay has been further validated in transcriptomic studies, where the temporal and nasal

samples of non-human primate retinas displayed differential expression of cell markers across gestation ²³².

2.5.2.1 Early cell types

In rhesus monkeys, 96% of all cells are generated between 36 and 120-days gestational age (22-73% gestation), with the peak in cell production at 85 days (52% gestation). Neurogenesis begins in the fovea at 30-33 days (18-20% gestation), when the first RGCs are generated ¹⁰². By day 40 (24% gestation), RGCs are observed in both the temporal and nasal central retina. Using human samples, Hoshino and collaborators already observed RGCs in both temporal and peripheral retinas by embryonic day 59 (21% gestation), but at this stage, the central retina contained about 10-15 rows of RGCs, while the peripheral retina had about half as many ²⁴³. Similarly, cones and horizontal cells are born before day 40 gestational period in rhesus monkeys ¹⁰². Early studies proposed that cones were first specified during week 11 of human development ²⁴⁴ but these observations were based on the expression of opsins. It is now clear that there is a substantial lag between cone genesis and cone opsin expression. In mice for instance, cone genesis begins around embryonic day 12, while M-opsin is not expressed until postnatal day 7 ^{129,245}. In this direction, subsequent analyses using early photoreceptor markers such as OTX2, RECOVERIN, and PDE6B already detected expression of these photoreceptor markers by embryonic day 59 ²⁴³.

ATOH7 is a basic helix-loop-helix (bHLH) transcription factor required for the generation of RGCs ^{131,246}. In mice and other vertebrates, ablation of *Atoh7* leads to an almost total loss of RGCs ^{131,247,248} and human mutations in *ATOH7* or its cis-regulatory

elements have been associated with optic nerve agenesis ²⁴⁹⁻²⁵¹. In mice, *Atoh7* is expressed between E11.5 and P0, corresponding with the early period of neurogenesis ^{132,252}, even though the *Atoh7* lineage give rise to all the different cell types ¹³². In rhesus monkeys, *ATOH7* is downregulated at the foveal center at 40 days gestation period (24% gestation) and absent in the central temporal retina by 30% gestation ²⁴¹. Similarly, *in situ* hybridization experiments have shown downregulation of *ATOH7* in the temporal retina by day 89 in human samples (32% gestation) ²⁴³.

2.5.2.2 Late cell types

Retinal progenitors undergo changes of competence to both lose the ability to generate early cell types (e.g., RGCs and cones) and acquire the ability to generate late cell types (e.g., bipolars, and Müller glia) ^{112,232}. In rhesus monkey, La Vail and collaborators identified the onset of rod photoreceptor, bipolar cells, and Müller glia genesis at around 45 days gestational period (27% gestation) ¹⁰². Similarly, bipolar cells and Müller glia have been observed only in the foveal center at embryonic day 50 (30% gestation) ²⁴¹, indicating that the shift between early and late competence states takes place during this time window in the non-human primate retina, well before this shift occurs in the nasal and rest of the peripheral retina. Consistent with this, upregulation of markers of bipolar cells and Müller glia markers have been detected in the temporal retina using transcriptomic approaches ^{231,232,243}. For instance, the bipolar markers *VSX1*, *GSG1*, and *TMEM215* ²⁵³ showed several folds enrichment in the rhesus temporal retina at 50 days gestational period compared to its nasal counterpart ²³². Similarly, *VSX1*, *GRM6*, *CABP5*, and *LHX4* were present in the human retina from embryonic day 67 ²⁴³

(24% gestation) and Müller glia genes such as *RLBP1*, *SLC1A3*, *CA2*, and *SOX9* were enriched in the temporal retina from 50 day gestation (30% gestation) in rhesus. The first Müller glia cells (RLBP1+ SOX9+) have been recently identified in the human fovea at day 54 (19% gestation), earlier than previously suspected ²⁵⁴.

2.5.3 Neurogenesis completes in the fovea first

In addition to neurogenesis beginning in the incipient fovea, neurogenesis is also completed first in the fovea. It was originally reported that mitotic figures were absent from the fovea of human retinas at 35% gestation, indicating that neurogenesis was complete in the central retina, while still ongoing past 60% gestation in the peripheral retina. More recent studies using the mitotic PH3 in both human and non-human primate retinas have shown even more precocious loss of mitotic progenitor cells in the fovea compared to the nasal retina—at 29% gestation in humans ²³² and 36% gestation in non-human primates²⁴¹.

2.6 Differential cell fate acquisition

Recently, comprehensive single-cell RNA-sequencing cell atlases have characterized at the cellular composition and gene expression patterns of the adult primate retina ^{233,255}. These experiments showed that both the macula region and the rest of the retina contain mostly the same cell types, and only a population of OFF bipolar cells seems to be fovea specific ²³³. Instead, the dramatic specialization of the fovea arises mostly from changes in cell ratios rather than region-specific cell types ²³³.

Cell movements are an essential part of foveal development (see the Pit Formation Section, page 56); these cellular rearrangements participate in the mechanisms that shift the ratios of cells detected in the adult fovea. However, some evidence indicate that the foveal progenitors yield different proportions of postmitotic cells from early stages of development. However, the mechanisms that regulate the differences in foveal progenitor competence and/or cell differentiation patterns are still not known and remain a fundamental question in the field of retinal developmental biology.

2.6.1 Cone photoreceptor mosaic

Whereas throughout the retina rods outnumber cones 20:1, within the foveola, the photoreceptor population is 100% cones. In the fovea, cones are in a tightly packed conformation and are at their maximum concentration in the foveal center (up to 200,000/mm², Figure 2.3) ^{4,256}.

The mature human fovea consists of 3 types of cones: L-cones (red or long wavelength), M-cones (green or medium wavelength), and S-cones (blue or short wavelength). S-cones are relatively infrequent in the foveal pit (2-3% of all cones in the region) ²⁵⁷, and some publications have suggested that the fovea is a “blue cone blind spot” ²⁵⁸. S-cone concentration is the highest at the foveal slope (15% of all cones) and on average, S-cones constitute 8-12% of all cones in the rest of the retina ^{257,259,260}. Distinguishing M- and L-cones is challenging given that these two molecules are very similar; in fact, the opsin genes *OPN1MW* and *OPN1LW* have 98% identical coding sequences ²⁶¹. Measurements using adaptive optics to quantify spectral sensitivities in

the living human eye ²⁶² have shown that humans varied greatly in the proportions of L-cones to M-cones, and their distribution seems random in the foveal center ²⁶³.

Work from different model systems and *in vitro* studies has proposed a role for thyroid hormone in the regulation of cone subtype specification. Mouse retinas treated with T3 (thyroid hormone) exhibited fewer S-cones and more M-cones ¹⁵⁴ while hypothyroid mice showed increased ratios of S-cones at the expense of M-cones ^{163,164}. More recently, similar effects were shown using a very elegant approach in human retinal organoids ¹⁶. Clinical evidence also supports these data as premature infants with low ratios of T3 to T4 experience impaired visual abilities ²⁶⁴. DIO2 (Iodothyronine Deiodinase 2), the enzyme that catalyzes the conversion of the prohormone thyroxine (T4) to the bioactive thyroid hormone (T3), has been found to be enriched in the human developing macula ²³¹. Thus, a differential expression of DIO2 could be a factor regulating the lower ratio of S-cones in the fovea.

2.6.2 Rod photoreceptor mosaic

Rods are not present in the foveal pit, and first appear in the central retina halfway into the foveal slope ^{4,205,265}. Notably, early markers of rod photoreceptor identity, such as NRL and NR2E3, are not detected in the foveal region even at early stages of development. For example, NRL and NR2E3 were detected from embryonic day 80 in human samples (30% gestation) in the foveal edge but not in the foveal center ²⁴³. This stage of development is prior to the cell rearrangements that lead to the pit formation and thus, this evidence indicates that the progenitor cells of the fovea do not produce rod photoreceptors.

2.6.3 RGCs

Many photoreceptors converge onto a RGC across the retina, but the ratio of cone photoreceptor to RGC in the fovea can be as low as 1:3^{57,266}. The macula is consequently home to 25% of all RGCs, while only occupying 0.02% of the total retinal area²⁶⁷. The RGCs of the macula resemble their peripheral counterparts, but generally they have much smaller dendritic fields. Morphological studies have distinguished about 18 RGC subtypes in the primate retina^{268,269}. This evidence has been recently confirmed by single-cell sequencing approaches²³³. In the fovea, midget (45%) and parasol (24%) RGCs are the majority of the RGCs. In the periphery these proportions decrease and instead show a higher ratio of broad thorny and other widefield RGCs²⁶⁹. Whether these differences are achieved through cell movements or differential cell production is currently not known.

2.6.4 Inner nuclear layer cells

In general, the makeup of the INL remains relatively constant throughout the retina. One notable exception is the increasing proportion of cone bipolar cells in the fovea from 37% to 52%, at the expense of rod bipolar cells²⁷⁰. The proportion of Müller glia cells near the fovea (17%) is relatively lower than in the peripheral retina (27%)²⁷⁰.

2.6.5 Could cell cycle exit play a role in the differential neurogenesis in the fovea?

A growing body of literature indicates that the progenitors of the fovea produce different ratios of cell types, including different subtypes of cones, an absence of rods, and perhaps different ratios of RGCs. Since all the cells of the retina are generated

following a conserved order, such that neurons that exit the cell cycle early assume early cell fates (e.g., RGCs and cones), could the timing of cell cycle exit account for some of the different cell ratios observed? The RPCs of the fovea exit the cell cycle before their nasal and peripheral counterparts and thus, it has been proposed that an early provision and ending of neurogenic RPCs in the central retina could produce an abundance of RGCs and cones along with fewer rods, with the opposite case in the peripheral retina^{271,272}. Heterochrony, a change in the timing of developmental events, is known to be an important mechanism of many evolutionary changes. Supporting this hypothesis, a comparison between the foveated diurnal New World monkey *Cebus apella* and the afoveated nocturnal owl monkey (*Aotus azarae*) have shown changes in cell ratios, as *Aotus* exhibits a higher proportion of rod photoreceptors and a reduction in cones and RGCs^{273,274}. Cell proliferation is extended in *Aotus*²⁷³ and thus, it has been proposed that an heterochronic change that shifts the timing of RPCs cell cycle exit with respect to the general timetable of retinal cell specification could be part of the molecular mechanism that controls these changes in cell population ratios²⁷¹. However, this model does not explain the complete lack of rods in the center of the fovea while other late born cells such as Müller glia and bipolar cells are produced in this region.

2.6.6 Post-transcriptional mechanisms in foveal development

MicroRNAs (miRNAs) are small post-transcriptional regulators known to regulate developmental transitions and cell fate decisions across the CNS^{188,275-278}, and in the retina in particular^{187,279}. Similarly, miRNAs regulate cell cycle kinetics in retinal cells²⁷⁶. Experiments looking at the miRNA landscape in the developing primate and human

retinas have identified several families of miRNAs differentially expressed in the foveal region ²³². As expected, miRNAs known to be enriched in photoreceptors, such as the miR-182/96/183 cluster ²⁸⁰⁻²⁸², are significantly enriched in the foveal region on in early development. MiR-15b-5p, miR-30b-5p, miR-103-3p and miR-369-3p are also enriched in the fovea, while other miRNAs, including miR-342-5p, miR-505-5p and miR-423-5p are expressed at lower levels in the fovea. The differential expressions noted could be attributed to three different factors: (1) the different cell composition of the fovea at the time analyzed, (2) the differences in timing as the foveal region is developmentally advanced, or (3) some of these miRNAs could be fovea specific or contribute to the molecular events that lead to the development of the primate fovea. Future studies aimed at the identification of the miRNA-mediated networks in conjunction with primate expression datasets may shed light on the roles of these post-transcriptional regulators in different ontogenic periods of foveal development.

2.7 Differential vascularization

Before photons of light reach the light-sensitive photoreceptors, they must first pass through the cornea, lens, vitreous, intra-retinal vasculature, and inner retinal layers. While many of these structures are clear and unobstructive, the presence of inner retina layers and blood vessels between the light source and the photoreceptors may pose challenges. In the majority of the retina where the photoreceptor population is dominated by rods, blood vessels have a minimal impact on visual perception as the circuitry is simplified through convergence. On the other hand, foveal cones participate in midget circuits, where a single cone synapses onto two bipolar cells (ON and OFF), which in turn

synapse onto two retinal ganglion cells ^{57,58}. In the context of this “private line”, blood vessels could create shadows on the retina and obstruct the visual field. Evolution of the mammalian retina has revealed a solution to this problem: the foveal avascular zone (FAZ). Studies in both rhesus monkeys and humans have revealed that the center of the fovea is not vascularized during any stage of development ²⁸³⁻²⁸⁶. At the same time, given the high density of cones in the fovea, this is a region of very high metabolic demand ^{287,288}. In avascular retinas found in many nocturnal mammals, the entire retina is oxygenated from the choroidal vasculature that abuts the retinal pigment epithelium. In diurnal species, the choroidal circulation serves the ONL, and the retinal circulation oxygenates the INL and GCL through a network of capillary plexuses within the inner retina, that reach as deep as the interface between the INL and OPL ^{289,290}. The OPL of foveated primates also receives oxygenation from the choroidal circulation and thus, the foveal center can spare the retinal circulation. While adaptations of the choriocapillaris underlying the fovea may suffice for the high oxygen and nutrient demands, these adaptations could also make the fovea more vulnerable to age-related changes, including accumulation of material in the Bruch’s membrane ²⁹¹.

Understanding how retinal vasculature develops is important to understand the mechanisms that establish the FAZ. Briefly, the primary vasculature sits at the NFL-GCL interface. In the human eye, blood vessels of the primary vasculature enter the developing retina at 14-weeks gestation (10-weeks gestation in macaque) ^{283,285}. Vasculogenesis begins as endothelial cells enter the retina through the optic disc, forming vessels in a lobular arrangement with lobes for each quadrant artery (nasal superior, nasal inferior, temporal superior, and temporal inferior). A combination of an astrocytic scaffold and

angiogenic factors further develop the vasculature towards the periphery in a stereotypical pattern. Astrocyte precursors across the retina are stimulated by the invading endothelial cells to differentiate into mature GFAP-expressing astrocytes^{292,293}. These astrocytes are broadly distributed ahead of the development of the vascular endothelium²⁹² and express vascular endothelial growth factor (VEGF) to further induce endothelial cell migration, proliferation, and maintenance. According to the hypoxia-mediated model of retinal vascularization, astrocytes are sensitive to hypoxia and respond to the lack of vasculature ahead by upregulating *VEGF* mRNA, thus stimulating endothelial cell migration to increase capillary formation and reduce the unfavorable hypoxic conditions. *VEGF* is now known to be one of the primary target genes of HIF- α (Hypoxia Inducible Factor)²⁹⁴ and some of these hypotheses have been recently confirmed in mouse models²⁹⁵.

Given that the fovea is the most developmentally advanced retinal region and has the highest density of cells, it is the most hypoxic region of the still-avascular retina. Thus, it would be expected that astrocytes and blood vessels are quick to vascularize the fovea. Instead, the opposite is observed. Many studies have shown that after initiation of the primary vasculature, the nasal lobes quickly merge along the horizontal axis (merged by 22 weeks in human, 95 days in rhesus monkey), while the temporal lobes are slower to meet along the horizontal meridian temporal to the incipient fovea (25 weeks in human, 105 days in rhesus monkey)²⁹⁶. The vasculature then proceeds to develop across the retina towards the *ora serrata*, skirting around the developing fovea, forming a ring around an avascular center. Formation of the deeper layers of retinal vessels is similarly delayed

in the region around the fovea; for example in rhesus monkey, the deep layers of capillaries only assemble around the foveal depression in the perinatal period ²⁹¹.

Studies looking at genes differentially expressed across the developing human retina at 20-weeks of gestation (50% gestation) observed anti-angiogenic factors differentially expressed in the macula compared to the nasal and peripheral retina ²⁹⁷. Thus, negative regulators of angiogenesis such as pigment epithelium derived factor (PEDF) and natriuretic peptide precursor B (NPPB) are highly upregulated in the fovea ²⁹⁸. Both PEDF and NPPB inhibit *VEGF*-induced angiogenesis and are localized in RGCs, among other cell types, where the primary vasculature develops.

The same study identified axon guidance genes differentially expressed in the macula, including 12 members of families known to regulate vascular development (Ephrin, Semaphorin, Slit, and Netrin). These expression patterns were sustained well after macular RGCs axons enter the optic disc, suggesting a possible role in vascular patterning of the macula. One axon guidance factor in particular, EphA6, has been well-studied for its role in patterning retinal blood vessels. EphA6 is expressed by RGCs in a gradient across the retina, centered at the developing fovea ²⁹⁹. Two ligands of EphA6, Ephrin-A1 and Ephrin-A4, are expressed by astrocytes. As the signaling between EphAs and their receptors is repellent, the presence of EphA6 in the macula could inhibit astrocytes from migrating into the fovea. This absence of astrocytes in the developing fovea has been proposed to both delay the migration of the temporal lobes of vasculature towards the fovea and inhibit vasculature from ever entering the fovea.

Between 37-40 weeks of gestation in humans (100% gestation), the FAZ diameter remains at 150-170 μm . Soon after birth, remodeling will shape the FAZ to its adult

dimensions (500 μm). These remodeling changes involve vessel retraction and occur at least up to 15 months of age ²⁹⁶. Similar findings have been found in marmoset monkeys (*Callithrix jacchus*), where the FAZ retracts quickly after birth from a central region of about 200 μm to a final 400 μm ³⁰⁰.

One clear paradox from these data is that while the fovea is the first region of the retina to differentiate and is developmentally advanced, it is the very last region of the retina to develop a blood supply. It has been proposed that the late arrival of the blood supply could cause metabolic stress that will be later ameliorated by the development of the foveal depression ²⁹¹. Both astrocytes and blood vessels form a ring that is spatially coincident with the rim of the early foveal pit ²⁹³, and notably, absence of FAZ has been associated with foveal hypoplasia in patients with different conditions ^{301,302}. Twenty-four to 27-weeks post-conception is a critical period for the development of the fovea, as it corresponds to the development of the perifoveal vascular plexus and the formation of the foveal pit. Preterm birth, and the accompanying change in oxygen supply, can alter the expression of the factors that guide the vessels around the FAZ, leading to defects in the formation of the foveal depression and retinopathy of prematurity (ROP) ³⁰³⁻³⁰⁵.

Springer and Hendrickson suggested that the absence of blood vessels makes the FAZ more flexible and malleable compared to the surrounding vascularized retina, and that the intraocular pressure is the stimulus that initiates the pit formation ³⁰⁶. While most current models support that the FAZ is a prerequisite for the formation of the pit, it is also important to note that some subjects with congenital achromotopsia can exhibit foveal hypoplasia but have a FAZ ³⁰⁷ and thus, the presence of FAZ may be a requirement but is not sufficient for complete pit formation.

2.8 Pit formation

The process of developing the foveal pit is a slow process that is not completed until after birth. In fact, the adult cone density at the center of the foveola is not reached until four years of age in humans^{286,308} and one year in monkeys²⁰⁵.

The development of the pit begins with a centrifugal migration of RGCs first, followed later by the neurons of the INL. In humans, the foveal pit is first evident at fetal week 25 (63% gestation)³⁰⁹ and 110 days gestational age (65% gestation) in macaques³¹⁰. As the process advances, the pit becomes wider and shallower, and appears mature by 12 weeks postnatal in rhesus monkeys but not until 15 months in humans. The photoreceptor layer also changes such that cones increase in density, elongate, and become thinner, and some rods get progressively closer to the foveola. Between week 25 and birth in humans, all photoreceptors develop distinct inner and outer segments, but these are shorter in foveal cones compared to peripheral cones. After birth, the foveal ONL becomes thicker as cone packing (centripetal migration) occurs. This process changes the OPL from a thin sheet of pedicles into one of the thickest layer in the central retina as the Henle's fiber layer develops. Foveal cone inner and outer segments length are comparable to that of peripheral cones by 15 months postnatal, and they are 4 times longer by 13 years³⁰⁹.

It has been proposed that adhesive interactions between photoreceptors may be part of the molecular mechanism that regulates foveal photoreceptor packing²⁸⁴. As the foveal cones become more elongated, neighboring photoreceptors anchored to those are drawn towards the center. Evidence indicates that cone packing takes place independently of their relationship to retinal pigment epithelium cells, since the ratio of

foveal cones increases 5-fold during development ³¹¹, but the initial trigger of cone elongation is still unknown.

While the data clearly show that differentiated photoreceptors (with complex morphologies and synaptic contacts) migrate towards the foveal center, the retinal area increases by a factor of 2.4 from two weeks before birth to adulthood in macaques (measurements made in pigtail macaques, *Macaca nemestrina*) as the central part of the temporal retina where the fovea resides remains stable throughout the same period. This growth results in a net decrease in peripheral rod and cone density ²⁰⁵.

2.8.1 The Albinism Riddle

Oculocutaneous albinism refers to a group of conditions that affect pigmentation of skin, hair, and eyes and are frequently caused by mutations in OCA2, TYR (Tyrosinase), TYRP1, or SLC45A2, which are enzymes that participate in the production of melanin. In contrast, ocular albinism presents hypopigmentation only in the eyes and is caused by mutations in the GPR143 gene or hypomorphic TYR variants ³¹²⁻³¹⁴. People affected by either type of albinism can exhibit a range of ocular features but some degree of foveal hypoplasia is systematically observed. Elschmig was the first to identify an absent fovea and underdeveloped macula in a human eye affected with albinism ³¹⁵. More recently, albino animal models have shown delays in neurogenesis ³¹⁶, and abnormal ipsilateral RGC projections ^{317,318}, but the cone population seems unaffected. However, the retina does not normally produce melanin and thus, how pigment can affect the development of the fovea has been dubbed “the albino riddle” ³¹⁹. One hypothesis is that the retinal pigment epithelium, a monolayer of highly pigmented cells adjacent to the

retina, influences retinal development through the regulation of calcium homeostasis via L-DOPA, a byproduct of melanin synthesis³¹⁹⁻³²¹. Recently, data from mice have shown that calcium signaling also regulates the expression of CyclinD2, changing the cell cycle dynamics at the ciliary marginal zone, a region that produces ipsilateral RGCs in mice. However, the riddle persists and the role(s) of pigmentation in foveal morphogenesis and pit formation have not yet been solved. One important piece of evidence comes from optical coherence tomography imaging datasets that indicates that individuals with albinism can have normal cone packing in the absence of foveal pit, suggesting that the pit formation is not a requirement for the cone displacement to occur³²². Also, the fovea remains located in its proper position in these patients, indicating that some of the early molecular events that regulate foveal development remain unaffected.

2.8.2 SLC38A8

Missense, nonsense, and frameshift mutations of *SLC38A8*, a putative glutamine transporter gene, result in foveal hypoplasia, nystagmus and optic nerve decussation defects, and anterior segment dysgenesis (FHONDA syndrome). These disorders share many phenotypical characteristics with albinism, but these patients exhibit no features of cutaneous or ocular hypopigmentation³²³. Thus, it is hypothesized that *SLC38A8* participates in a melanin-independent component of foveal development. *SLC38A8* patients also show reduced outer segment cone thickness that has been interpreted as a reduction in foveal cone photoreceptor packing³²⁴.

2.8.3 PAX6

PAX6 mutations are associated with many ocular phenotypes and display significant heterogeneity, including aniridia, microphthalmia, coloboma, and foveal hypoplasia³²⁵⁻³²⁸. *PAX6* is considered a master regulator of the eye. During early development, *PAX6* is expressed in the optic vesicle and optic cup but also in the anterior segment structures including the surface ectoderm and lens. Later in development, *PAX6* is expressed by RGCs, amacrine and horizontal cells within the retina, and in lens, cornea, iris and ciliary body³²⁹.

Hingorani *et al.*³³⁰ and Sannan *et al.*³³¹ described that 72-86% of patients (from a total of 43 and 33 patients, respectively) with *PAX6* mutations exhibited some degree of foveal hypoplasia. The *PAX6(5a)* isoform seems to be the isoform responsible for some of these phenotypes and it is known to have different binding properties and to be highly expressed in the fovea³³². However, the specific roles of *PAX6* in foveal development remain undetermined.

2.9 Conclusions

It is apparent that the development of the fovea is not a single developmental event but instead a beautifully orchestrated sequence of changes that affect progenitor cell growth, developmental timing, cell fate acquisition, vasculature development, and lateral cell migration. While all these steps are required for the proper development of the fovea, almost none of them is yet understood in any molecular or functional detail. The advent of novel technologies, including human stem cell-derived organoids, high-throughput “omics”, and imaging capabilities in combination with the use of a growing number of

foveated species for research may open new avenues for a better understanding of the processes that control foveal developmental dynamics. A better grasp of these events and their molecular underpinnings may shed light onto the changes that take place in the aging retina and lead to macular degeneration.

2.10 Acknowledgements

The authors wish to thank all the members of the Simo and La Torre laboratories for comments. We also wish to thank Drs. Sergi Simó, Nadean Brown, Tom Glaser, and Rob Hufnagel for valuable discussions.

2.11 Figures

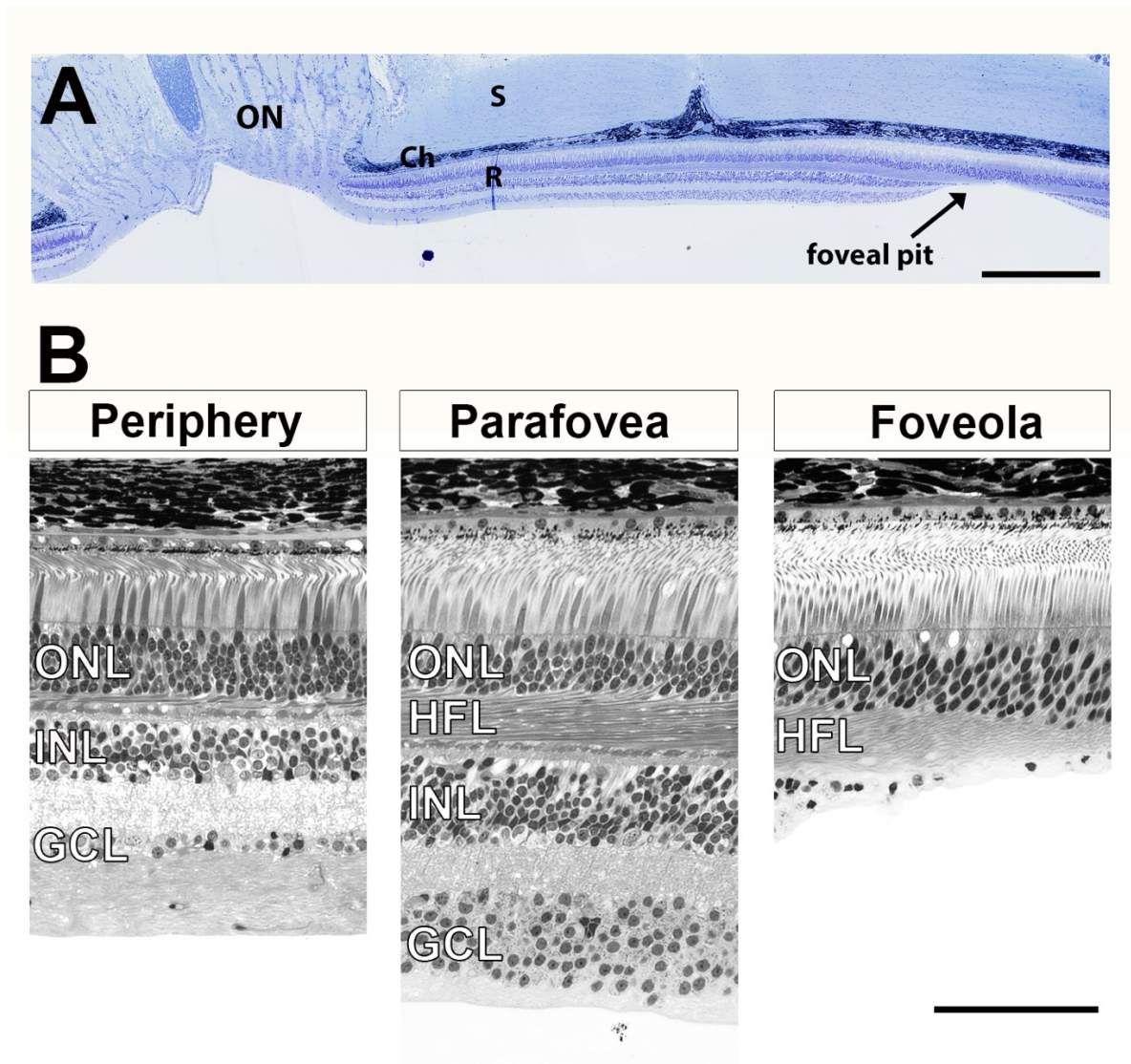


Figure 2.1

(A) Central temporal retina of an adult rhesus monkey retina stained with toluidine blue. (B) Periphery, parafovea, and foveolar regions of the rhesus monkey retina. Note the different widths of the GCL and INL, as well as the different size of the cone photoreceptor outer segments in the different areas. The displacement of the inner neurons is evident in the foveola. This displacement leads to the formation of the HFL. ON: optic nerve, S: sclera, Ch: choroid, R: retina, ONL: outer nuclear layer, INL: inner nuclear layer, GCL: ganglion cell layer, HFL: Henle's fiber layer. Scale bars: 500 microns in A, 150 microns in B.

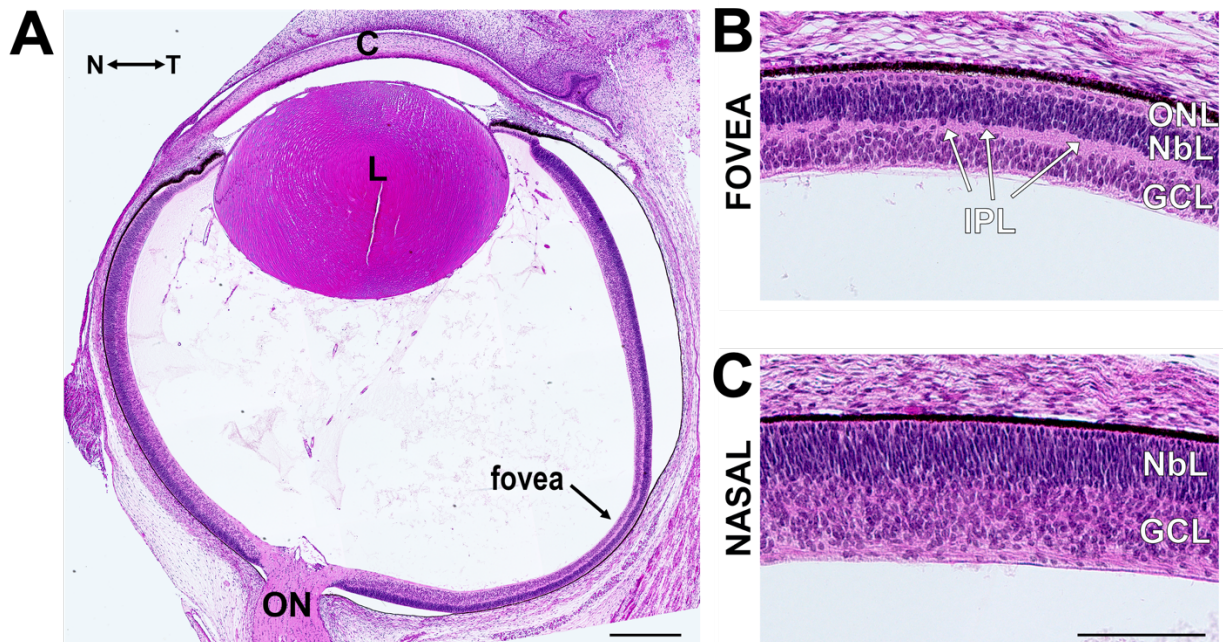


Figure 2.2

(A) Hematoxylin and eosin (H&E) staining of a 12-week human fetal retina shows a clear enlargement of the temporal side where the foveal anlage resides (arrow). **(B)** The temporal side of the retina exhibits a well-defined INL that separates the GCL from the NbL, and a row of cones form the ONL. **(C)** Contrarily, the ILM is not yet evident in the nasal side of the retina. N: nasal, T: temporal, C: cornea, L: lens, ON: optic nerve, ONL: outer nuclear layer, NbL: neuroblastic layer, INL: inner nuclear layer, GCL: ganglion cell layer. Scale bar: 250 microns in A and 100 microns in B-C.

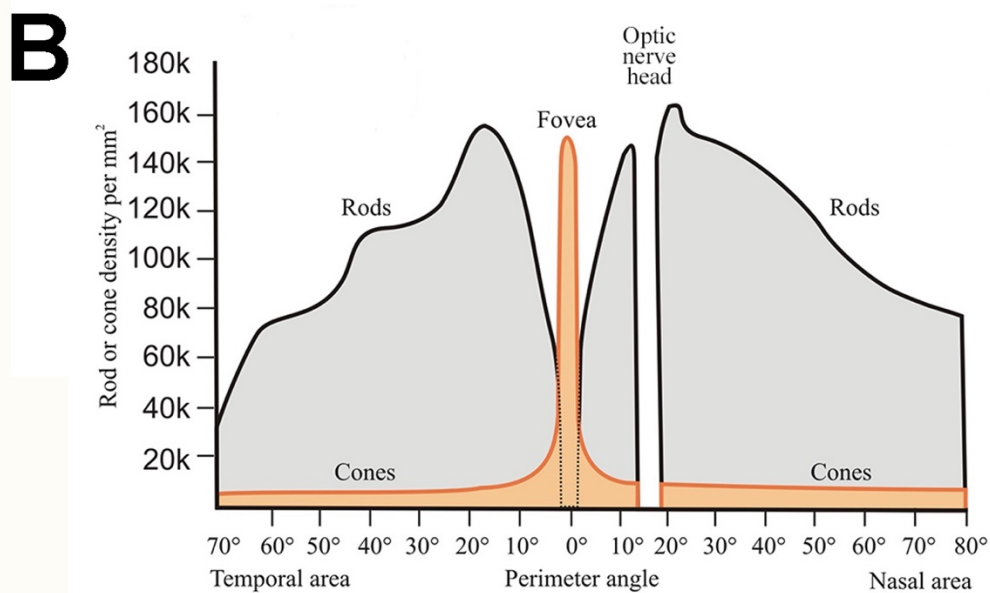
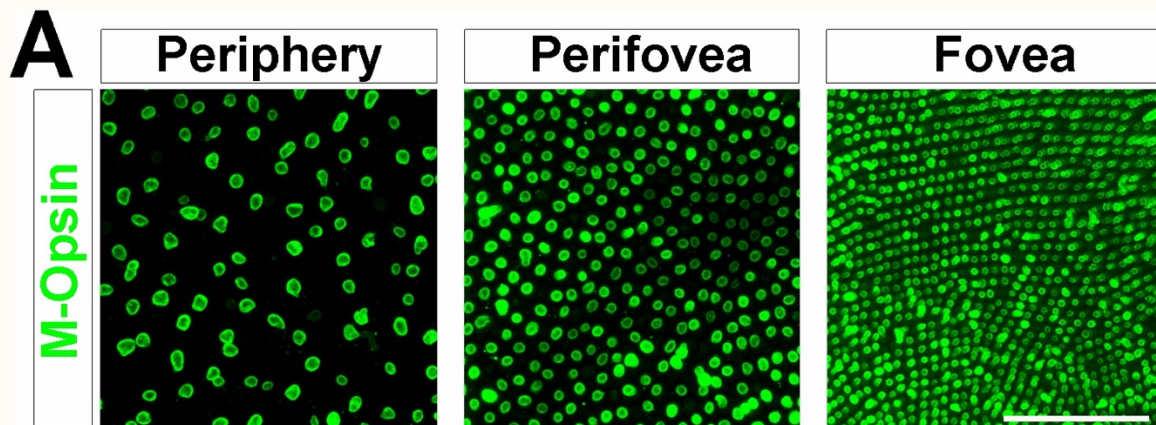


Figure 2.3

(A) Rhesus monkey flat-mounted retina at 140 gestational age labeled with L/M-Opsin (Sigma, AB5405). Note the diverse size and distribution of M- and L-cones in the different regions of the retina. Scale bar: 50 microns. (B) Diagram of cone (orange) and rod (gray) photoreceptor densities along the horizontal meridian of a human eye, plotted by the distance in degrees from the foveal center. Data adapted from Osterberg, 1935.

3. Published results: Expression patterns of CYP26A1, FGF8, CDKN1A, and NPVF in the developing rhesus monkey retina

Miranda R. Krueger*¹, Elizabeth Fishman-Williams*¹, Sergi Simó¹, Alice F. Tarantal^{1,2,3}, and Anna La Torre^{1,#}

¹ Department of Cell Biology and Human Anatomy, University of California, Davis, Davis, CA 95616, United States.

² Department of Pediatrics, University of California, Davis, Davis, CA 95616, United States.

³ California National Primate Research Center, University of California, Davis, Davis, CA 95616, United States.

Correspondence: Anna La Torre

Department of Cell Biology and Human Anatomy

School of Medicine

University of California - Davis

One Shields Avenue, 3402 Tupper Hall

Davis, CA, 95616

Phone: 1-530-752-9103

Email: alatorre@ucdavis.edu

* These authors contributed equally to this work.

The following chapter was submitted as a manuscript to *Frontiers in Cell and Developmental Biology* and published on December 14, 2023. The accepted version of this manuscript has been reformatted for this dissertation. The authors of the manuscript were Miranda R. Krueger, Elizabeth Fishman-Williams, Sergi Simó, Alice F. Tarantal, and Anna La Torre, with Miranda and myself contributing equally. I performed sample collection and preparation, hematoxylin and eosin staining, RNAscope *in situ* hybridizations, and immunohistochemistry.

3.1 Keywords

Foveal development, retinal development, CYP26A1, FGF8, NPVF

3.2 Abstract

The *fovea centralis* (fovea) is a specialized region of the primate retina that plays crucial roles in high-resolution visual acuity and color perception. The fovea is characterized by a high density of cone photoreceptors and no rods, and unique anatomical properties that contribute to its remarkable visual capabilities. Early histological analyses identified some of the key events that contribute to foveal development, but the mechanisms that direct the specification of this area are not understood. Recently, the expression of the retinoic acid-metabolizing enzyme *CYP26A1* has become a hallmark of some of the retinal specializations found in vertebrates, including the primate fovea and the high-acuity area in avian species. In chickens, the retinoic acid pathway regulates the expression of *FGF8* to then direct the development of a rod-free area. Similarly, high levels of *CYP26A1*, *CDKN1A*, and *NPVF* expression have been observed in the primate macula using transcriptomic approaches. However, what retinal cells express these genes and their expression dynamics in the developing primate eye remain unknown. Here, we systematically characterize the expression patterns of *CYP26A1*, *FGF8*, *CDKN1A*, and *NPVF* during the development of the rhesus monkey retina, from early stages of development in the first trimester until the third trimester (near term). Our data suggest that some of the markers previously proposed to be fovea-specific are not enriched in the progenitors of the rhesus monkey fovea. In contrast, *CYP26A1* is expressed at high levels in the progenitors of the fovea, while it localizes in

a subpopulation of macular Müller glia cells later in development. Together these data provide invaluable insights into the expression dynamics of several molecules in the nonhuman primate retina and highlight the developmental advancement of the foveal region.

3.3 Introduction

Sight is our most important sense and has provided us with an unparalleled evolutionary advantage for complex tasks, such as decision making, attention, and memory. Vision begins at the retina, an intricate laminar structure that lines the back of the eye³³³. The retina detects light and converts it to neural signals that are then relayed to the visual centers of the brain. To accomplish these functions, the retinal layers contain diverse and specialized sets of cellular populations, including sensory receptors (rod and cone photoreceptors), projection neurons (retinal ganglion cells, RGCs), interneurons (horizontal cells, bipolar cells, and amacrine cells), and a population of glia (Müller glia)³³⁴. It is well established that during development, a single population of multipotent progenitor cells produces these seven main retinal cell types^{80,81}. Moreover, the sequential birth order of these cells is conserved across all vertebrate species, such that RGCs, cones, horizontal cells, and GABAergic amacrine cells are born first, while other amacrine populations, rod photoreceptors, bipolar cells, and Müller glia are generated later during the period of neurogenesis^{20,77,99,101,102,335}.

Despite this conservation, there are species-specific retinal differences due to visual necessities, behaviors, and habitats, namely variations in the ratios of different cell types and populations^{191,336}. Even within a single retina, specialized regions with distinct

cell compositions exist. The primate *fovea centralis* (fovea) is one such example of a specialized retinal region, where cone photoreceptors are the dominant cell population in a sharp contrast to the majority of the retina where rods outnumber cones 20:1^{3,4}. Located at the center of the *macula lutea* (macula), slightly temporal to the optic disk, the fovea contains a particularly high number of densely-packed cone photoreceptors, organized in a bouquet-like spatial arrangement, and no rods^{3,4,337}. Other differences between the macula and the neighboring retina include a different ratio of photoreceptors to RGCs, the output neurons of the retina. The ratio of cones to RGCs in the fovea can be 1:3²⁶⁶, whereas outside the fovea, there is convergence of signals from many photoreceptors onto one RGC. This adaptation results in a higher concentration of RGCs in the macula, such that a region that occupies only 0.002% of the total retinal surface contains 25% of all RGCs²⁶⁷. Additionally, the fovea develops into a pitted invagination by peripherally displacing the inner retinal layers^{204,284,309}. Together with the lack of blood vessels (foveal avascular zone^{296,338}), these specializations minimize light scattering and provide the fovea with the highest visual resolution of the retina.

Even though the development of the retina has been well studied, the mechanisms governing the development of the fovea have remained largely unexplored, mostly due to the lack of a fovea in small animal model organisms. Gaining understanding into the factors governing how the fovea develops is not only critical for unraveling the fundamental principles of retinal development, but also holds tremendous potential for therapeutic strategies aimed at combating retinal diseases and restoring vision.

Besides primates, birds of prey and lizards also have high-acuity vision and foveated retinas^{197,339-341}, and other species, including chickens and zebrafish, have

retinal specializations with the features of a high-acuity area (HAA)^{228,229}. Using some of these models, the retinoic acid (RA) pathway has been proposed as a key regulator of foveal development. RA is an active derivative of vitamin A, and its spatial and temporal distributions result from the regulated expression of RA-synthesizing retinaldehyde dehydrogenases (RALDHs) and RA-metabolizing cytochrome P450s (CYP26) enzymes. Together with FGF8, CYP26A1 expression is an early distinctive feature of the chick HAA, and, in fact, the expression of FGF8 regulated by RA seems to be a requirement for the development of a rod-free region in avian species²²⁸. Notably, transcriptomic approaches using human²³¹ and nonhuman primate (rhesus monkey)²³² samples have also shown high levels of expression of *CYP26A1* in the developing macula, underscoring its potential roles in foveal development. These studies have also identified other genes with higher expression rates in the developing temporal retina, including *NPVF* and *CDKN1A* (P21^{CIP1}). However, their expression patterns in the developing primate retina have yet to be described.

Here, we have investigated the expression dynamics of *CYP26A1*, *FGF8*, *NPVF*, and *CDKN1A* at different developmental stages using the rhesus monkey model (*Macaca mulatta*). The rhesus monkey offers unique advantages, as it shares most of the features of human vision, including our high-resolution central vision³⁴², and it is possible to obtain samples across all stages of gestation. Our data indicate that some of the markers transcriptionally enriched in the fovea at early stages of development are expressed by Müller glia cells, highlighting the developmental advancement of this region, but these markers are not fovea-specific at later stages of development. We also show that *CYP26A1* exhibits high expression levels in the progenitors of the fovea, albeit its

expression is not limited to this region at early stages, while at later, this gene is restricted to the Müller glia cells of the macula. Together, these data underscore the stark advances of the foveal area in comparison to the rest of the retina and suggest that the foveal Müller glia could have unique molecular signatures.

3.4 Materials and methods

3.4.1 Sample collection

All animal procedures conformed to the requirements of the Animal Welfare Act and protocols were approved prior to implementation by the Institutional Animal Care and Use Committee (IACUC) at the University of California at Davis. Healthy adult female rhesus monkeys (*Macaca mulatta*) were time-mated and identified as pregnant using established methods³⁴³. Pregnancy in the rhesus monkey is divided into trimesters by 55-day increments: 0-55 days gestational age represents the first trimester, 56-110 days represents the second trimester, and 111-165 days the third trimester (term 165 ± 10 days). Normal fetal growth and development were confirmed by ultrasound during gestation³⁴⁴. Dams were scheduled for hysterotomy (e.g., approximately 40, 50, 60, 75, 80, 110, 140, and 145 days gestational age; all gestational ages ± 2 days based on timed mating protocol) for fetal tissue collection. Gestational percentages (Table 3.1) are 24% and 30% gestation (1st trimester), 36%, 42%, and 65% gestation (2nd trimester), and 85% and 88% gestation (3rd trimester). For each time point we collected at least two samples with the early stage (40 days gestational age) and later stage (140 days gestational age) represented by three samples. Dams were returned to the breeding colony post-hysterotomy.

The fetal eyes were collected into cold media (DMEM and FBS) then extraneous tissue was removed and the retina was incubated in oxygenated media for 90 min at room temperature. Samples were then fixed in modified Carnoy's fixative (ethanol, formaldehyde, and acetic acid) overnight at 4°C, dehydrated in stepwise ethanol/water solutions, cleared with xylene, and embedded in paraffin blocks. Retinas were sectioned (6 µm) on a horizontal plane and were stored in open slide boxes at room temperature before subsequent staining.

For all comparisons between nasal and foveal regions, the nasal area was selected at the same distance from the ONH as the presumptive fovea (also referred as temporal).

3.4.2 RNAscope *in situ* hybridization and immunohistochemistry

RNAscope detection was performed according to the RNAscope Multiplex Fluorescent Reagent Kit v2 Assay manual. Following sample fixation and preparation described above, sections were treated with heat and three pretreatment steps: After baking for 1 h at 60°C and deparaffinizing with xylene and ethanol, sections were pretreated with hydrogen peroxide for 10 min at room temperature, target retrieval for 15 min at 99°C, and protease plus for 30 min at 40°C. Sections were incubated with the appropriate hybridization probes for 2 h at 40°C, followed by a series of amplification steps and fluorescent labeling with Opal dyes (Opal 520 and 620), as per manufacturer instructions. After the final wash buffer step in the RNAscope protocol, we began an immunohistochemistry protocol to combine the RNA *in situ* with antibody staining. Sections were incubated in PBS for 5 min and blocked in 10% normal donkey serum/PBS-

0.1% Triton X-100 for 1 h at room temperature. Primary antibodies were diluted in blocking solution for an overnight incubation at 4°C. After primary antibody incubation, sections were washed five times (5 min each) in PBS. Species-specific, fluorescently labeled secondary antibodies (Invitrogen, 1:200) were diluted in blocking solution for a 1 h incubation at room temperature. Cell nuclei were counterstained with 4',6-diamidino-2-phenylindole (DAPI, Sigma-Aldrich). The sections were rinsed five times (5 min each) in PBS and mounted for microscopy using a Fluoromount-G (Southern Biotech). See table below for details of antibodies and working dilutions. Images were taken using a Fluoview FV3000 confocal microscope (Olympus) or Axio Imager.M2 with Apotom.2 microscope system (Zeiss). All images were assembled using Photoshop and Illustrator (Adobe).

Antibody	Source	Catalog	Lot	Concentration
Anti-ATOH7 (Rabbit)	Novus Biological	88639	A106752	1:200
Anti-BRN3 (Goat)	Santa Cruz	sc-6026	H2416	1:100
Anti-CRX (Mouse)	Abnova	H00001406-M02	KB191-4G11	1:200
Anti-Glutamine Synthetase (Mouse IgG2a)	Millipore	MAB302	3821584	1:150
Anti-LHX4 (Rabbit)	Proteintech	11183-1AP	00040977	1:200
Anti-NRL (Goat)	R&D Systems	AF2945	VYM032002A	1:400
Anti-OTX2 (Goat)	R&D Systems	AF1979	KRS0320091	1:200
Anti-PAX6 (Rabbit)	Bio Legend	901301	B386304	1:200
Anti-PCNA (Rabbit)	Abcam	AB18197	GR3262110-2	1:100
Anti-PH3 (Rabbit)	Thermo Fisher	PA5-17869		1:100
Anti-TUJ1 (Mouse)	BioLegend	801201	B264428	1:500
Anti-RXRgamma (Mouse)	Santa Cruz	sc-365252	D0623	1:200

3.4.3 Hematoxylin and eosin (H&E) staining

Samples were fixed and prepared as described above. Next, sections were deparaffinized using xylene, rehydrated with stepwise ethanol/water solutions, stained with hematoxylin, rinsed with acid alcohol and ammonia water, counterstained with eosin, and dehydrated in stepwise ethanol/water solutions. Sections were then rinsed with xylene and mounted for microscopy using Permount (Fisher Chemical).

3.4.4 Edu Click-iT

For 5-Ethynyl-2'-deoxyuridine (EdU) labeling experiments, eyes were incubated in oxygenated media for 90 minutes, followed by a 2 h incubation of EdU at 5 mg/ml at 40°C. Eyes were then fixed with modified Carnoy's media (see above), paraffin embedded, and sectioned. Tissue sections were treated with antigen retrieval steps of hot (95°C) 0.01 M sodium citrate pH 8 twice for 5 min each, followed by an acid treatment (2 N HCl and PBS-0.5% Triton X-100/PBS) for 1 h at room temperature in a humidifying chamber. EdU was then detected following the manufacturer instructions (Thermo Fisher Scientific, C10337). RNAscope *in situ* (protocol above) were performed in combination with Edu Click-it kit staining. Here, the EdU protocol was initiated after the final wash buffer steps of the *in situ* protocol. In this case, we did not perform the sodium citrate antigen retrieval.

3.4.5 Statistical methods

Quantifications of retinal length were obtained for each side of the retina (temporal and nasal) from the ONH to the *ora serrata* using three biological replicates. Mean and P-values were obtained using the Student's T-test. Similarly, the GCL thickness was

quantified at the foveal center and at the equivalent distance from the ONH in the nasal side from three biological replicates at 40 days gestational age (first trimester). Student's T-test was used to obtain mean and P-values. All statistical analyses and plot generation was performed using Prism 9 (GraphPad).

3.5 Results

3.5.1 Neurogenesis in the developing rhesus retina follows a fovea-to-periphery gradient

Fetal rhesus monkey samples spanning the three trimesters of gestation were analyzed using H&E staining (Table 3.1). We analyzed samples from the first trimester (~40 days) to the late third trimester (140 days gestational age; term 165 ± 10 days). These experiments revealed the asymmetry of the developing retina from 40 days gestational age (~24% gestation), where the temporal region is larger (1.93-fold larger, p -value: 0.001, Figure 3.1A-B, Table 3.1) and shows a wider ganglion cell layer (GCL) (Figure 3.1C, p -value: 0.011 and Figure 3.1D). We also observed a clear developmental advancement of the foveal region, evidenced by an earlier presence of plexiform layers in the foveal region compared to the equidistant region from the ONH in the nasal region (Figure 3.1E-P). By 50 days gestational age (~30% gestation), the inner plexiform layer (IPL) begins to develop at the center of the foveal anlage, and by 60 days (~36% gestation), the IPL is distinct in the temporal retina but not yet in the nasal retina (Figure 3.1F-G, L-M, arrows). Similarly, by 80 days gestational age (second trimester, ~48% gestation) the IPL is well-defined across the entire retina, with the initial presence of the outer plexiform layer (OPL) only in the foveal region (Figure 3.1H, N). By 110 days

(beginning of the third trimester, ~67% gestation), the foveal pit has started to develop into a shallow depression that already exhibits some lateral RGC displacement (Figure 3.1D, Q, Table1). At 140 days gestational age (~85% gestation), the fovea consists of a deep invagination and part of the GCL has displaced peripherally, as revealed by a thinner GCL at the foveal center (1-2 cells thickness Figure 3.1D,S; Table 3.1). However, the inner nuclear layer (INL) still maintains a uniform thickness between the pit region and the surrounding retina (Figure 3.1S). Similar regions in the nasal side do not present these modifications (Figure 3.1R, T). Immunohistochemistry confirmed that while the majority of CRX+ photoreceptors are NRL+ rods throughout the retina, we did not detect NRL+ cells at the center of the foveal pit, indicating the predominance of cone photoreceptors in this region (Figure 3.1U-V”).

3.5.2 A switch from early to late progenitor competence takes place in the late first trimester at 50 days gestational age in the center of the fovea

We used cell-specific antibodies to evaluate neurogenesis of different retinal populations. Recent analyses have revealed a distinct shift in retinal progenitor cells (RPCs) consistent with their competence to generate early- (*e.g.*, RGCs and cones) versus late-born retinal cell types (*e.g.*, bipolar cells and Müller glia). Early and late RPCs express distinct transcriptional signatures, and single cell “omics” have distinguished broad transitions in RPCs at embryonic day 16 (E16) in mice and between 11 and 15 gestational weeks in humans ^{17,112,231}.

At the earliest stage analyzed (40 days gestational age), we observed BRN3+ TUJ1+ RGCs in the apical side throughout the retina (Figure 3.2A-B', arrows). RPCs divide at the apical side of the retina and as a result, newly born postmitotic neurons need to migrate basally to their appropriate layers. Thus, the presence of BRN3+ TUJ1+ cells in the apical region indicates active RGC neurogenesis. By 50 days, most of the RGCs are localized in the GCL in the temporal side of the retina, suggesting that RGC genesis is completed in the fovea (Figure 3.2C-C'). In contrast, we still detected many BRN3+ RGCs in the most apical part of the retina in the nasal region (Figure 3.2D, arrows).

The basic helix-loop-helix (bHLH) transcription factor ATOH7 plays a critical role in early neurogenesis, and while ATOH7+ progenitors can generate all different cell types, it is necessary for the generation of RGCs^{132,246}. Its expression starts during the final cell division of RPCs and follows a highly-regulated expression pattern that coincides with the first wave of neurogenesis. In mouse retinas, Atoh7 expression initiates at E11, peaks at E14.5, and rapidly decreases after E16.5²⁵². In the rhesus monkey retina, ATOH7 is downregulated first at the center of the fovea at 40 days gestational age, later extending within the temporal side (Figure 3.2E-F'). By 50 days, ATOH7 is not detected in the foveal region by immunohistochemistry, but ATOH7 expression still remains expressed elsewhere within the same retina (Figure 3.2G-H'). Similarly, we observe RXRgamma+ photoreceptors (presumptively cone photoreceptors) first in the temporal retina. By 40 days gestational age, we observe RXRg+ photoreceptors in the foveal region, but only at 50 days, we observe RXRg+ photoreceptors across all regions (Figure 3.2 I-L').

Correspondingly, at this stage, LHX4+ OTX2+ bipolar cells and *RLBP1*+ Müller glia are detected only in the center of the fovea, indicating that by end of the first trimester (50

days gestational age), foveal RPCs are producing late cell types (Figure 3.3). Previous studies have identified LHX4 expression in cone photoreceptors³⁴⁵ and therefore, to further validate that the LHX4+ cells detected at 50 days are indeed bipolar cells, we assessed the expression of LHX4 and OTX2 at different developmental stages (Supplementary Figure 3.1). By 75 days gestational age, we only detected LHX4+ cells in the INL (bipolar cells) and not in OTX2+ cells of the ONL (photoreceptors). By 110 days (beginning of the third trimester), we begin to see LHX4+ cone photoreceptors at the apical side of the ONL in the temporal side, but its expression remains constrained to the INL in the nasal side. These data suggest that LHX4 is expressed in bipolar cells at early stages of development, and only at later stages of maturation is it expressed in cones.

We also analyzed the presence of mitotic cells using phospho-Histone3 (PH3) immunostaining (Supplementary Figure 3.2). At 50 days gestational age, we detected mitotic cells across the retina, but from 60 days onward, we no longer observed PH3+ cells in the center of the foveal region. As development proceeds, the absence of PH3 extended peripherally, but by 80 days gestational age, we still detected PH3+ mitotic RPCs in the nasal side of the retina. By the late third trimester (140 days gestational age), we only detected a few mitotic cells in the ciliary margin, nor did we observe PH3+ RPCs in either side of the retina.

As summarized in Table 3.1, these data indicate that the fovea is developmentally advanced compared to the rest of the retina and that neurogenesis takes place in a wave that begins in the center of the fovea and extends towards the periphery. Our results also indicate that a shift between early and late RPC competence states takes place in the late first trimester (around 50 days gestational age) in the rhesus monkey fovea.

3.5.3 CYP26A1 is highly expressed in the developing rhesus monkey fovea at different stages of development

In order to describe the expression pattern of genes previously proposed to be enriched in foveal RPCs, we used RNAscope *in situ* hybridization (Advanced Cell Diagnostics). In our experiments, the background levels detected with this method are very low (Supplementary Figure 3.3).

At 40 days gestational age, the earliest time-point analyzed, *CYP26A1* is highly enriched in the developing fovea and only expressed at low levels in the nasal region (Figure 3.4A-B'). We also detected *CYP26A1* expression in RPCs surrounding the optic nerve head (ONH, Figure 3.4A-B'), in the ciliary marginal zone, and in the lens epithelium (Figure 3.4A-A', Table 3.2). The cells that expressed the highest levels of *CYP26A1* are PCNA+ (Figure 3.4B-B', Supplementary Figure 3.4A-A'') and some colocalize with EdU (Supplementary Figure 3.4B-C''), indicating that *CYP26A1* is expressed by RPCs. However, even within the foveal anlage, not every EdU+ cell expressed *CYP26A1*. We did not detect colocalization with OTX2+ photoreceptors nor any expression in the GCL, suggesting that *CYP26A1* is not expressed in photoreceptors or RGCs (Supplementary Figure 3.4D-D'', Table 3.2). This expression remains unchanged at 50 days, where the foveal RPCs and a small patch of cells bordering the ONH exhibit the highest levels of *CYP26A1* (Figure 3.4, Table 3.2).

At later stages of development, *CYP26A1* expression is restricted to the Müller glia (Figure 3.5). The Müller glia of the fovea and macula regions (including the foveal center, parafovea and part of the perifovea) express high levels of *CYP26A1*, but this gene is not expressed by the Müller glia of other parts of the retina (Figure 3.5A-D). Thus, *CYP26A1*

colocalizes with *RLBP1* (also known as *CRALBP*), a robust marker of Müller glia cells³⁴⁶, and glutamine synthetase (GS, Figure 3.5E-E' and Supplementary Figure 3.5A-A').

3.5.4 FGF8 is expressed in retinal progenitors in a ONH-to-periphery gradient

In avian species, the RA pathway regulates the expression of *FGF8*, which serves as a molecular marker for the HAA throughout development^{347,348}. We investigated whether this expression is conserved in primates using RNAscope *in situ* hybridization. In contrast with the known expression pattern in chickens, in the early developing rhesus monkey retina, the highest levels of *FGF8* were found localized around the ONH and diffuse in a gradient peripherally (Figure 3.6A, Table 3.2). Co-labeling experiments using *FGF8* and *CYP26A1* showed distinct expression patterns for these two genes (Figure 3.6. A'). This pattern of expression remained unaltered at 50- and 70-days gestational age (Figure 3.6B-G'). At later stages of development, *FGF8* is only detected at low levels of expression in both the ONL and INL, but not in other eye tissues (Figure 3.6. H-J', Table 3.2).

3.5.5 CDKN1A is expressed by the Müller glia and ONH cells

Previous experiments have identified *CDKN1A* (p21^{CIP1}) as a gene enriched in the temporal region of the retina from 50 to 150 day gestational age in rhesus monkeys²³² and in human fetal week 20 samples²³¹. *CDKN1A* was also found in a study aimed at identifying cone-specific transcriptional signatures³⁴⁵. p21^{CIP1} and p27^{XIC1} are G1-

checkpoint CDK inhibitors, and thus, we investigated the intriguing possibility that *CDKN1A* could be enriched in foveal RPCs and/or cone photoreceptors.

RNAscope *in situ* hybridization did not detect expression of *CDKN1A* at 40 days gestational age, but by 50 days, our analyses revealed *CDKN1A* expression in the center of the foveal anlage as well as in the optic nerve head (ONH, Figure 3.7A-A'' arrows, Table 3.2). This expression co-localized with *RLBP1*. The expression of *CDKN1A* extended peripherally as time progressed and by 75 days, it has extended throughout the temporal retina (Figure 3.7E-E'). At this stage of development, we still detected high levels of expression in the ONH (Figure 3.7F-F', arrow). By the late third trimester, we observed *CDKN1A* throughout the whole retina and its expression remained restricted to *RLBP1*+ Müller glia cells in both the temporal and nasal sides of the retina (Figure 3.7H-J'). Together, these data suggest that *CDKN1A* is expressed by Müller glia cells throughout development in the rhesus monkey.

3.5.6 The neuropeptide NPVF is expressed by the Müller glia

Similarly, *NPVF* (Neuropeptide VF precursor) was previously found to be enriched in the temporal primate retina^{231,232}. *NPVF* is expressed by the hypothalamus and regulates sleep in some species³⁴⁹. Expression of *NPVF* was previously correlated with retina aging³⁵⁰, but the pattern of expression during development has not been explored.

Using RNAscope *in situ* hybridization, we observed *NPVF* expression beginning at approximately 50 days gestational age (Figure 3.8). At this stage, *NPVF* is only expressed by a few cells at the center of the macula. The expression of *NPVF* extends laterally as time proceeds and colocalizes with *RLBP1* and GS, indicating that this gene

is expressed by the Müller glia, possibly at somewhat later developmental stages than compared to *CDKN1A* expression (Figure 3.8, Table 3.2).

3.6 Discussion

In the study described herein, we have characterized key morphological characteristics of the developing rhesus monkey fovea, the timing of neurogenesis, and the expression patterns of *CYP26A1*, *FGF8*, *NPVF*, and *CDKN1A* at different ontogenic stages.

We have shown that the embryonic retina undergoes asymmetrical growth, exhibiting a larger temporal region, where the incipient fovea resides (Figure 3.1). This observation mimics published histological images that show that, while the optic cup is symmetrical in its temporal-nasal axis by 30 days gestational age, the temporal side of the optic cup is much larger than the nasal side from 36 days onward ²⁴⁰. We also observed a thicker GCL in the temporal side at 40 days (24% of gestation) and a clear developmental advancement of the foveal region, as the plexiform layers appear first in the center of the fovea before extending towards the periphery. The foveal pit is initially a shallow depression that can be observed by 110 days gestational age (65% of gestation) and then develops into a deeper pit. The development of the pit takes place in conjunction with a lateral displacement of the GCL, similar to prior descriptions in other morphological studies ³¹⁰.

Foundational studies by Hendrickson ^{204,310,351}, Provis ³⁵², and Rakic ^{102,353}, and more recently transcriptomic approaches ^{17,231,232,354,355} have revealed changes in differentiation and maturation rates between the fovea and the rest of the retina. For

instance, late-born cell types, such as bipolar cells and Müller glia, are found in the fovea at much earlier developmental stages compared to the nasal retina ^{102,232,243}. Correspondingly, progenitors exit the cell cycle much sooner in the foveal region ^{232,243,273}. Classic studies from La Vail, Rapaport, and Rakic ¹⁰² used ³H-thymidine labeling at different times during development to define the timing of cell genesis in the rhesus monkey retina. Since these analyses were performed at later stages, several factors could be confounding the data: (1) significant retinal growth takes place after neurogenesis and thus passive cell movements to accompany organ growth could have occurred between cell birth and sample collection, (2) active cell movements towards and away from the fovea have been described during pit formation ^{204,286,308,356}, (3) all the analyses were performed after the period of cell death and RGC culling ³⁵⁷, and (4) all the analyses were based on cell position but no specific markers were used.

In the La Vail dataset, the onset of neurogenesis was defined at ~30 days gestational age, when the first RGCs and horizontal cells are born in the foveal center. The onset of cone genesis was found at ~33 days, and the onset of genesis of late cell types was identified at ~45 days. This study describes a pronounced fovea-to-periphery gradient of cytogenesis. Similarly, *in silico* predictions have been recently used to estimate the onset of neurogenesis for different retinal cell populations ²³². These calculations estimate RGC genesis to begin around 33 days, rod bipolar genesis onset to be ~52 days, and bipolar cell genesis to begin at ~55 days gestational age. To shed light on the timing of cell birth in rhesus monkeys, we have explored neurogenesis during the embryonic period. Our data suggest that RGC genesis begins prior to 40 days and is completed by 50 days in the foveal center (Figure 3.2), while bipolar cells and Müller glia

are found in the center of the foveal anlage by 50 days (late first trimester) (Figure 3.3). *ATOH7*, a transcription factor dynamically expressed in subsets of RPCs and required for RGC formation^{132,246,252}, is downregulated from the fovea by day 50. Together these data validate the dataset published by La Vail and indicate that the shift between early and late competence periods takes place at the end of the first trimester in the primate fovea.

Through the advent of high-throughput sequencing technologies, our understanding of primate retina cell types and their gene expression profiles has broadened^{233,255,350}, spurring the search for reliable foveal markers and the complementing mechanisms driving foveal development. Notably, the RA catabolizing enzyme *CYP26A1* has been previously identified as a foveal marker in several studies^{228,231-233}, and a pathway involving *CYP26A1* and *FGF8* is required for the patterning of the HAA in chickens²²⁸. Our data indicate that *CYP26A1* is highly enriched in primate foveal RPCs, although we also detected some levels of *CYP26A1* expression in other regions of the eye. Contrarily, *FGF8* is not enriched in the developing fovea at any of the gestational ages analyzed. These expression patterns suggest that RA-dependent patterning could be an important aspect regulating the development of the fovea and high acuity areas across species, but the exact molecular mechanism(s) downstream may not be conserved between avian species and primates.

RA is known to participate in dorso-ventral patterning³⁵⁸ and in mice, *Cyp26A1* and *Cyp26C1* cooperate to establish a stripe of lower RA levels within the equatorial rodent retina^{238,239}. Alterations in *Cyp26* expression leads to perturbations of the ratios of cone opsins and RGC projection patterns²³⁸. However, mice do not have foveal

specialization or rod-free regions, and thus, neither *CYP26A1* expression nor lower levels of RA are sufficient to drive foveal development.

At later times in development, *CYP26A1* is expressed by *RLBP1*+ GS+ macular Müller glia, including the Müller glia within the foveola, fovea, parafovea, and part of the perifovea, but *CYP26A1* is not expressed by Müller glia in other parts of the retina. This expression pattern has been observed in the adult rhesus monkey eye²³³. Similarly, novel findings using the zebrafish model also suggest conserved expression patterns of *cyp26a1* in the Müller glia of the HAA²³⁰.

Similar to *CYP26A1*, *CDKN1A* and *NPVF* have been identified in transcriptomic analyses as genes enriched in the developing fovea. In our previous analyses, *NPVF* was shown to have one of the highest enrichments in the temporal retina compared to the nasal retina (420-fold enrichment at 90 days gestational age). *CDKN1A* showed 11.7-fold enrichment in the temporal side, comparable to the 17.9-fold enrichment exhibited by *CYP26A1* at the same developmental time point²³². Here, we observed a clear colocalization between both *CDKN1A* and *NPVF* with *RLBP1*, indicating that these molecules are expressed in Müller glia cells. By 50 days gestational age, we observed substantial levels of *CDKN1A* in the temporal retina, while *NPVF* is only expressed by a few cells in the center of the foveal anlage. As development proceeds, the region that expresses these genes extends peripherally, such that by 140 days gestational age (late third trimester), we observed *CDKN1A* expression in both sides of the retina, while *NPVF* expression had extended in the temporal retina but is only modestly expressed by the Müller glia at the nasal side. Together, these data suggest that these genes are not exclusive of the developing fovea but are instead expressed by Müller glia at different

stages of maturation, and that the enriched expression detected in previous studies is associated with the gradient of Müller glia production and maturation.

The presence of different glial cells in the foveal pit remains poorly understood. Early electron microscopy studies³⁵⁹ observed “cone-shaped Müller glia” in the innermost part of the fovea. Gass³⁶⁰ revisited these preparations and observed that the cytoplasm composing the outer portion of these Müller cells appeared optically empty, indicating that perhaps the Müller glia of the foveola could have unique properties. More recently, one study has identified GFAP+ glial cells in the foveal center but these glia cells do not appear to express *RLBP1* or *GS*³⁶¹. The authors of this study proposed that the glial cells present in the foveal floor are not Müller glia but astrocytes. However, previous primate studies suggest that the avascular zone within the macula remains devoid of astrocytes and vessels at all times²⁹³ and thus, the identity of the glia cells of the foveola remains a contentious topic. In our preparations, we observed a reduction in *RLBP1* in the center of the foveal pit at 140 days gestational age (see Figures 3.7H' and 3.8E'). However, we did not observe a corresponding reduction in *CYP26A1*, *CDKN1A*, or *NPVF*, indicating that Müller glia cells are likely present in this region. Single-cell sequencing studies have reported differences between the glial cells of the fovea and the periphery, but expression of *RLBP1* has been detected in both foveal and peripheral Müller glia³⁶². However, most “omics” studies analyze the tissue obtained within a 2-3 mm punch and thus, these approaches do not distinguish the center of the fovea from the rest of the macula. The possible reduction of *RBLP1* together with the expression of *CYP26A1* only in the macular Müller glia suggests that the Müller glia of the fovea/macula exhibit some unique molecular signatures.

Taken together, our results demonstrate the spatial and temporal expression patterns of several genes, previously hypothesized to be fovea-specific, and reveal that from all the genes analyzed, only *CYP26A1* is enriched in the fovea across different ontogenic stages. However, the dynamic changes of *CYP26A1* expression in different regions of the retina, and in RPCs and Müller glia may pose challenges to be used as a fovea RPC-specific marker for single-cell approaches.

In the future, by integrating the knowledge obtained from diverse species, including primate, chickens, and mice, we can advance our understanding of the intricate roles of RA pathway molecules in retinal patterning and foveal progenitor development. Ultimately, such insights may contribute to unraveling the mechanisms underlying foveal specialization.

3.7 Acknowledgements

We want to thank all members of the La Torre and Simó laboratories for their helpful insights. We also want to thank Drs. Nadean Brown, Tom Glaser, and Nick Marsh-Armstrong for their valuable comments. This study was supported by NIH (R0EY026942; ALT), the California National Primate Research Center base operating grant (P51-OD011107), and a Pilot project grant supported by the Departments of Physiology and Cell Biology and Human Anatomy (to ALT and AFT). We also benefited from the use of the National Eye Institute Core Facilities (supported by P30 EY012576). *In vivo* sonographic imaging was performed by instrumentation obtained through an NIH S10 High-End Instrumentation grant to AFT (S10-OD016261).

3.8 Figures

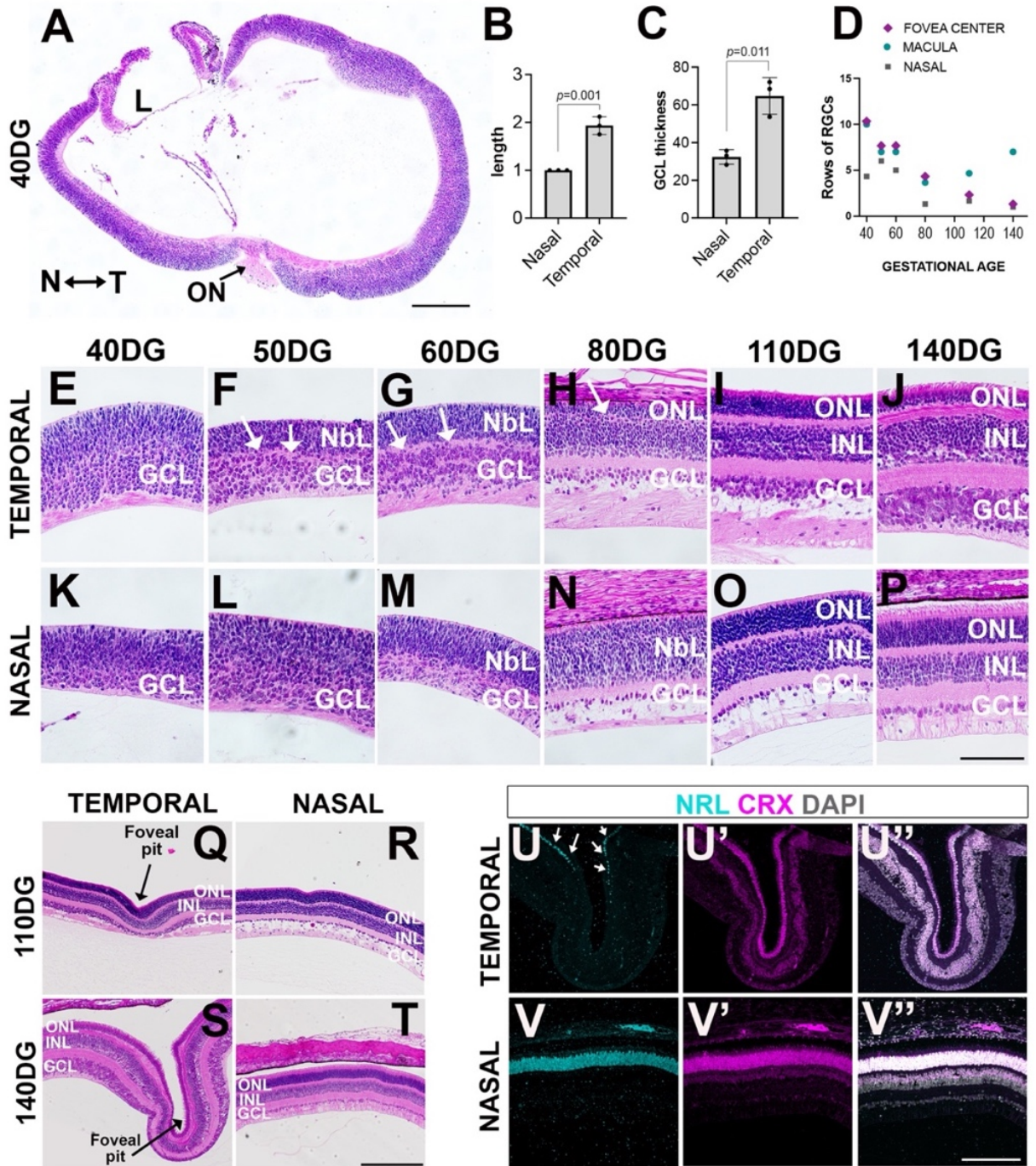


Figure 3.1 The foveal region is developmentally advanced

(A) Hematoxylin and eosin (H&E) staining of a paraffin-embedded section of the eye at 40 days gestational age which shows a larger temporal side. **(B-C)** Quantifications of retinal length (relative to the nasal side) and GCL thickness (microns) at 40 days gestational age. Mean \pm SEM. P-values were obtained using Student's T-test. **(D)** The number of rows of RGCs in the center of the fovea, macula (tissue surrounding the center of the fovea), and nasal regions was quantified at different gestational ages. **(E-P)** H&E staining (40-140 days gestational age). White arrows (F-H) indicate the presence of plexiform layers in the temporal side. **(Q-R)** Development of the foveal pit is observed in the temporal side from ~110 days gestational age. **(S-T)** Mature foveal pit observed near term at 140 days gestational age. **(U-V)** The 140 days gestational age sections were immunostained with NRL (cyan), CRX (magenta), and counterstained with DAPI (gray). Arrows in U indicate NRL+ cells at the edge of the fovea but note that while there are CRX+ photoreceptors, there are no NRL+ rods in the center of the fovea. Scale bars: 250 μ m in A, 100 μ m in O, 200 μ m in S and U. DG: days gestational age, ON: optic nerve, GCL: ganglion cell layer, NBL: neuroblastic layer, ONL: outer nuclear layer, INL: inner nuclear layer.

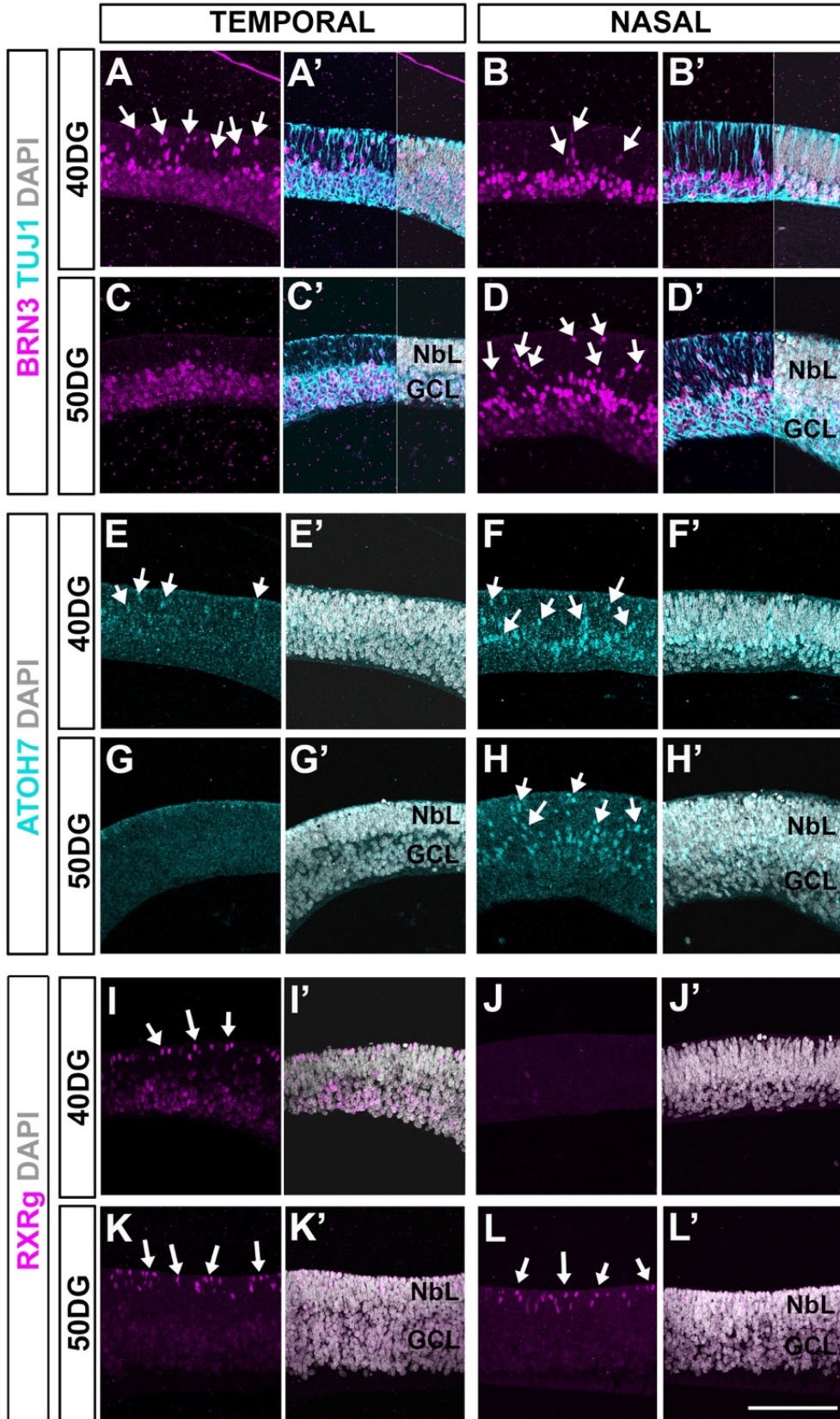


Figure 3.2 Early neurogenesis in the developing rhesus monkey retina

(A-D') RGCs are stained with BRN3 (magenta), TUJ1 (cyan), and counterstained with DAPI (grey) at the gestational ages indicated (40-50 days gestational age). Arrows indicate newly-born RGCs located in the apical side of the retina. **(E-H')** ATOH7 is labeled in cyan (arrows) and the retinas are counterstained with DAPI (grey). Note the absence of ATOH7+ cells in the temporal retina at 50 days gestational age (G-G'). **(I-L')** RXRgamma is labeled in magenta (arrows) and the retinas are counterstained with DAPI (grey). Scale bar: 100 μ m. DG: days gestational age, NbL: neuroblastic layer, GCL: ganglion cell layer.

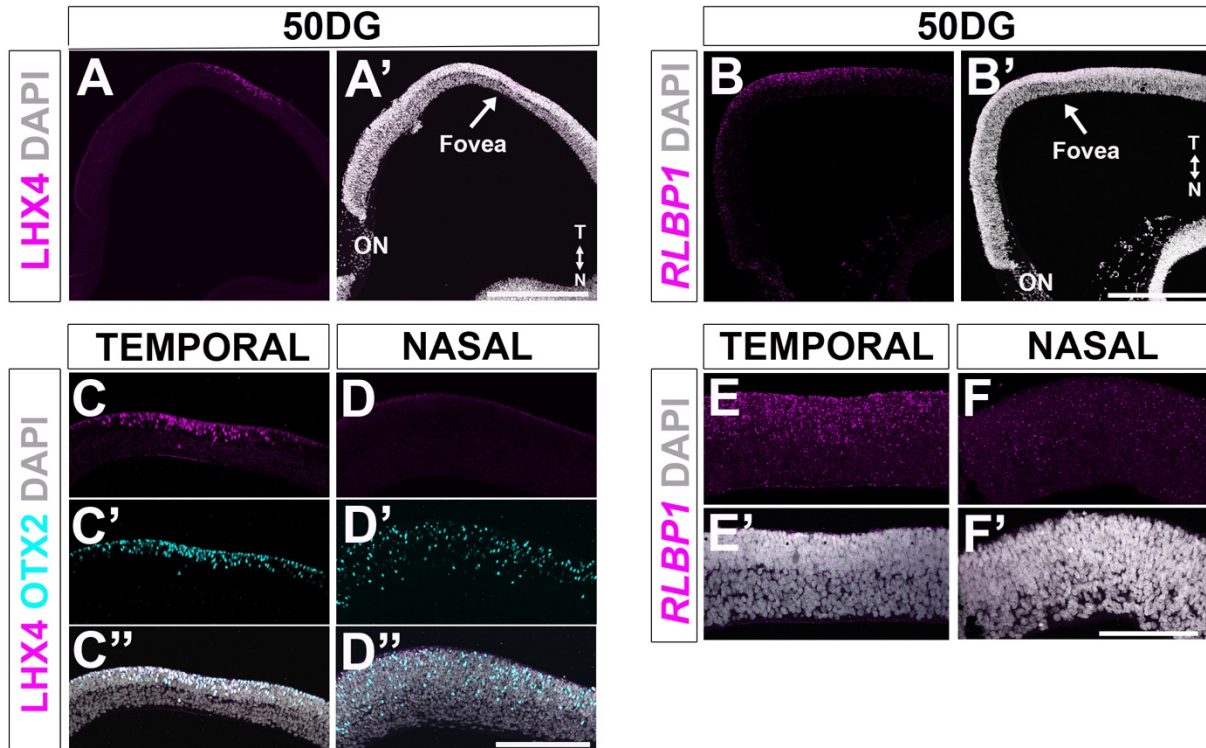


Figure 3.3 Late cell type are detected in the foveal anlage at 50 days gestational age

(A-A') Low magnification image of a 50 days gestational age retina showed the expression of LHX4 protein (magenta). **(B-B')** RNAscope *in situ* hybridization for *RLBP1* (magenta) showed enriched expression in the temporal retina at 50 days gestational age. **(C-D-D'')** LHX4+ cells (magenta) colocalize with OTX2 (cyan). Note the restricted expression of LHX4 in the temporal retina. **(E-F')** *RLBP1* exhibits low levels of expression throughout the retina but it is highly expressed in the foveal region. In all cases, tissues have been counterstained with DAPI (gray). Scale bar: 250 μm in A' and B', 100 μm in D'' and F'. ON: optic nerve, T: temporal, N: nasal.

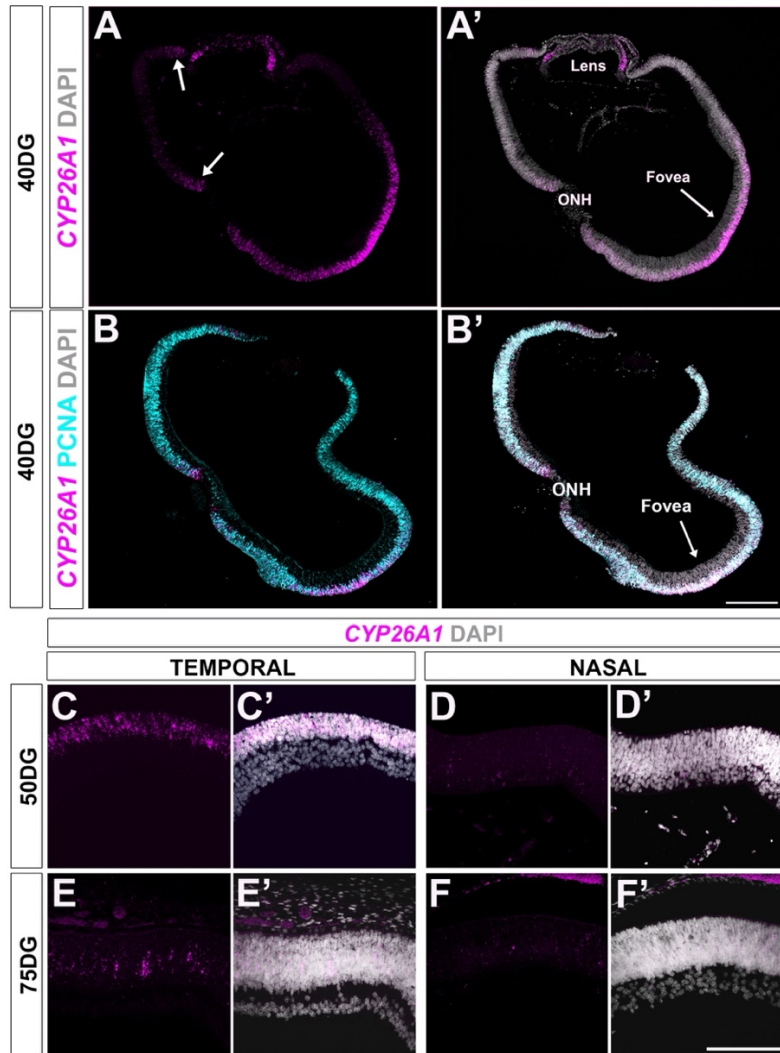


Figure 3.4 CYP26A1 is enriched in the progenitors of the fovea

(A-A') RNAscope *in situ* hybridization for *CYP26A1* (magenta) at 40 days gestational age (DG) revealed enriched expression in the foveal region. Other regions (A, white arrows) such as the lens epithelium, the ciliary margin, and a patch of cells around the optic nerve also expressed *CYP26A1*. (B-B') Colocalization between *CYP26A1* (magenta) and PCNA (cyan) is shown at 40 days gestational age. Retinas were counterstained with DAPI (gray). (C-F') Expression pattern of *CYP26A1* (magenta) in the temporal and nasal retina at indicated ages (50-70 days gestational age). Samples have been counterstained with DAPI (grey). Scale bars: 250 μm in B', 100 μm in F'. ONH: optic nerve head.

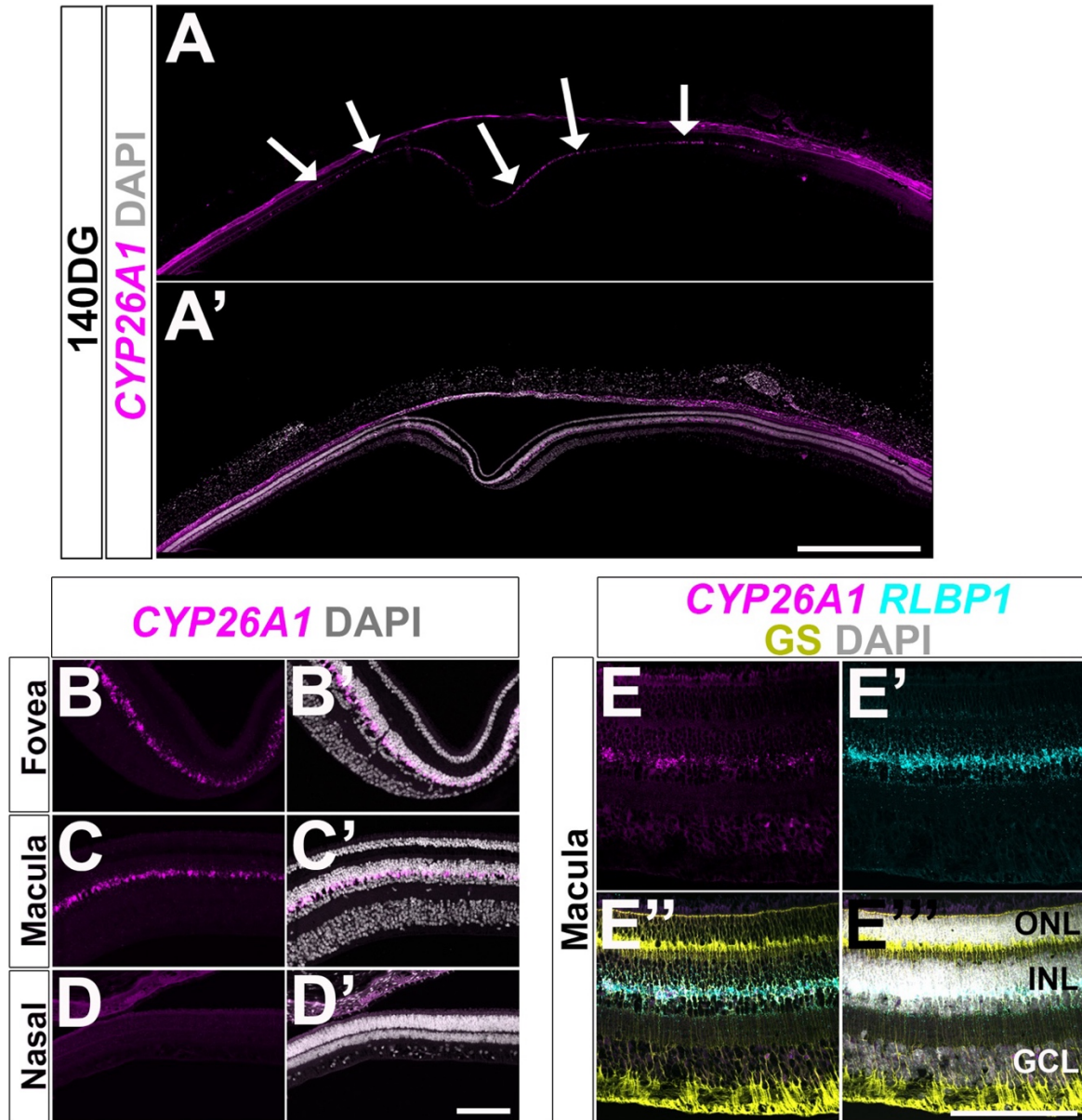


Figure 3.5 At later stages of gestation CYP26A1 colocalized with Müller glia cells

(A-D') *In situ* hybridization for *CYP26A1* (magenta) at ~140 days gestational age (DG) showed expression in the center of the fovea and other macula regions (foveolar, fovea, and perifovea. Arrows in A) but not in the rest of the retina. (E-E''') The expression of *CYP26A1* (magenta) colocalizes with *RLBP1* (cyan) and GS (yellow). All tissues have been counterstained with DAPI (gray). Scale bars: 400 μ m in A', 150 μ m in D', 100 μ m in E'.

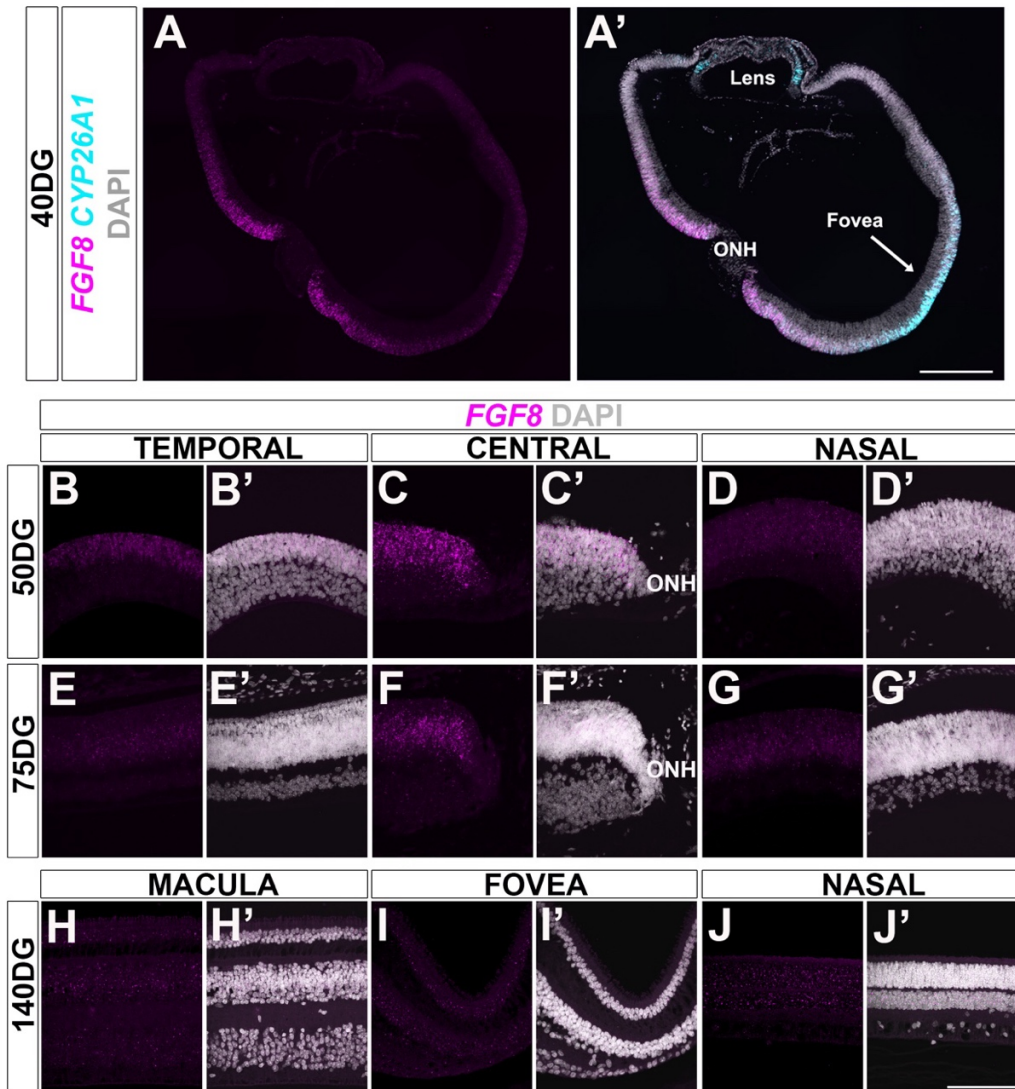


Figure 3.6 *FGF8* is expressed in a central-to-periphery gradient in the developing rhesus monkey retina

(A-A') *FGF8* (magenta) is highly expressed in the cells surrounding the optic nerve and its expression exhibits a gradient that extends peripherally in both temporal and nasal sides of the retina. This expression pattern does not mimic *CYP26A1* expression (cyan, A'). **(B-G')** The expression pattern of *FGF8* (magenta) at 50 and 75 days gestational age show a similar pattern with higher expression in the central part of the retina. Samples were counterstained with DAPI (grey). **(H-J')** At later time points, *FGF8* is only expressed at low levels in both the ONL and INL. Scale bars: 250 μm in A', 100 μm in J'. ONH: optic nerve head.

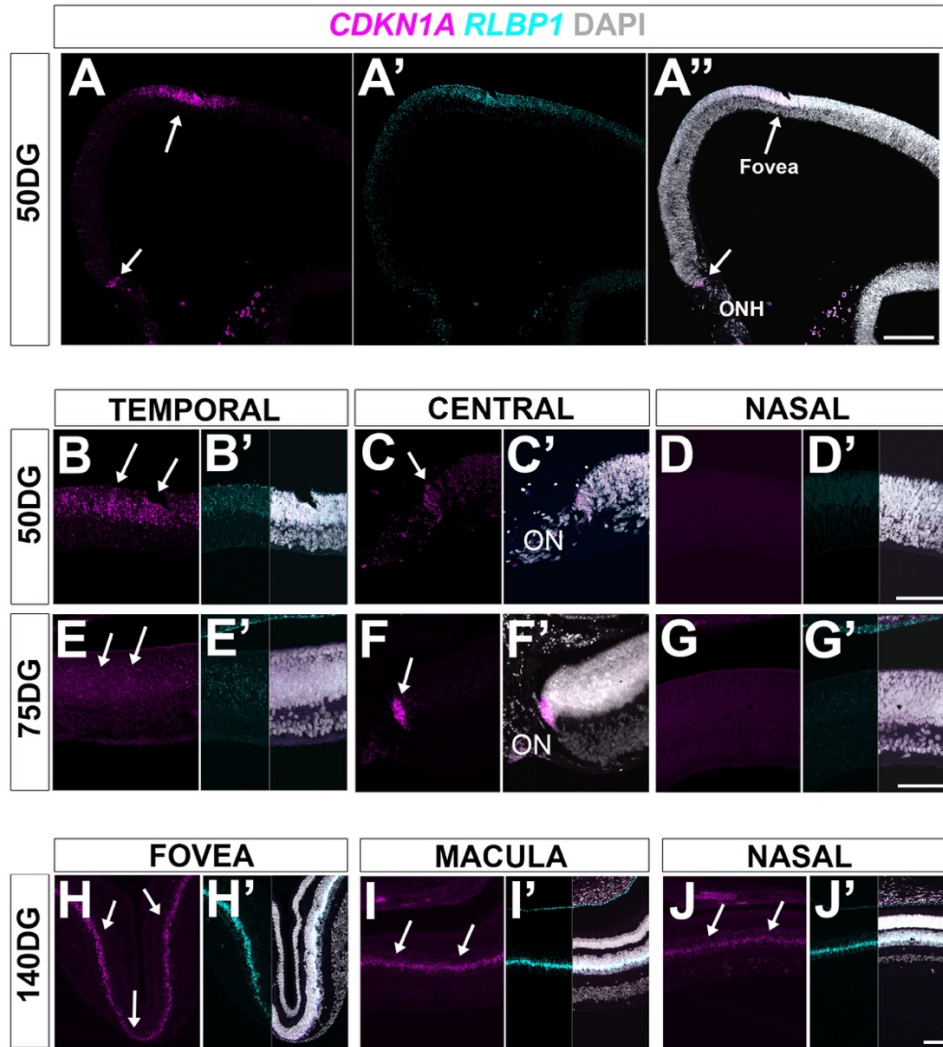


Figure 3.7 CDKN1A is expressed by Müller glia cells

(A-A'') RNAscope *in situ* hybridization for *CDKN1A* (magenta) revealed enriched expression in the foveal region and optic nerve head cells at 50 days gestational age (arrows in A). The enriched expression at the center of the fovea colocalizes with high levels of *RLBP1* (cyan). **(B-G')** Expression of *CDKN1A* (magenta) and *RLBP1* (cyan) in different regions of the retina at 50 and 75 days gestational age. Arrows indicate enriched expression in the temporal retina and optic nerve head. **(H-J')** In the late third trimester (~140 days gestation) *CDKN1A* (magenta) was shown to be expressed by *RLBP1*+ cells (cyan) throughout all regions of the retina. Scale bars: 250 μ m in A', 70 μ m in D', G', and J'. ONH: optic nerve head, ON: optic nerve.

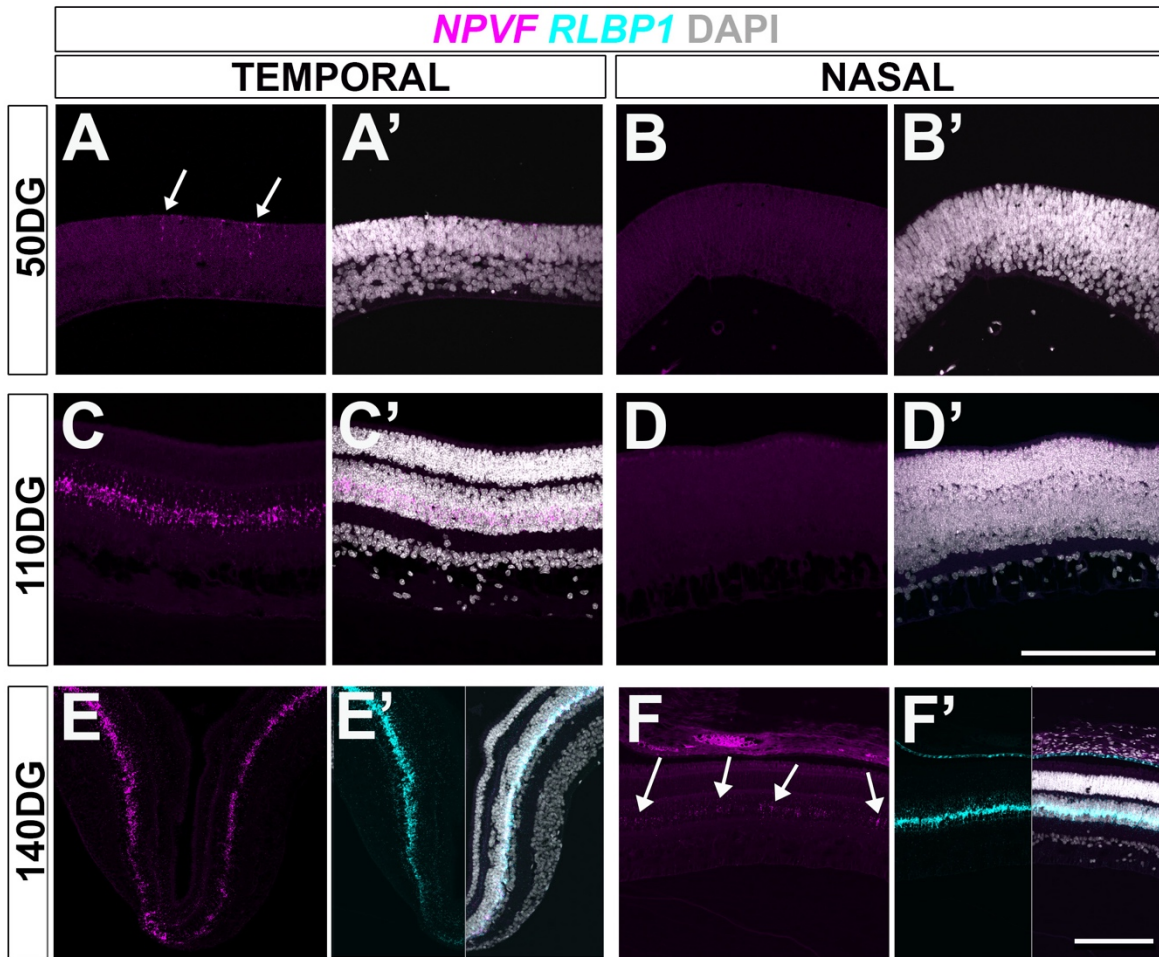


Figure 3.8 NPVF is expressed by Müller glia cells at slightly later times in development

(A-B') *NPVF* (magenta) was only weakly expressed by some cells at the center of the foveal anlage (arrows in A) at 50 days gestational age (late first trimester). (C-D') By 110 days gestational age (early third trimester), the expression of *NPVF* had extended throughout the temporal side of the retina. (E-F') At 140 days gestational age (late third trimester), the expression of *NPVF* can be faintly detected in the nasal retina (arrows in F). The cells that expressed *NPVF* also expressed *RLBP1* (cyan). Scale bar: 100 μ m in D', 150 μ m in F'.

3.9 Tables

Gestation Day	% Gestation	Foveal development and morphology
40	24	Thicker GCL; early cell types are produced
50	30	IPL appears; cones form a continuous row; late-born cells are present in the foveal center
60	26	Clear IPL; neurogenesis is done in the foveal center
70	44	OPL appears
110	65	Shallow foveal pit; OS appear
140	86	GCL is 2 cells thick; 2 layers of elongated cones with IS and OS

Table 3.1 Summary of morphological characteristic and neurogenesis of the fovea at different periods of gestation

GCL: ganglion cell layer; IPL: inner plexiform layer; OPL: outer plexiform layer; OS: outer segments; IS: inner segments.

CYP26A1	DG 40	DG 50	DG 75	DG 110	DG 140-145
<i>RETINA</i>					
RPCs temporal/fovea	++++	++++	n/a	n/a	n/a
RPCs nasal	+	+	-/+	-/+	n/a
RPCs central	++	++	+	-	n/a
RGCs	-	-/+	-/+	-	-
Photoreceptors	-	-	-	-	-
Horizontal cells			-	-	-
Amacrine cells	n/a		-	-	-
Bipolar cells	n/a		-	-	-
Müller glia	n/a	++	+++*	++++*	++++*
<i>ONH</i>					
<i>Optic nerve</i>	-	-	-/+	-/+	-/+
<i>RPE</i>					
<i>Ciliary margin zone</i>	+	+	+	+	+
<i>LENS</i>					
Lens epithelium	++	++	++	++	
Bow region			-	-	
Lens fibers			-	-	
<i>CORNEA</i>					
	-	-	-	-	-
*Exclusively expressed in the macula					

FGF8	DG 40	DG 50	DG 75	DG 110	DG 140-145
<i>RETINA</i>					
RPCs temporal/fovea	++	++	n/a	n/a	n/a
RPCs nasal	+	+	+	+	n/a
RPCs central	++++	++++	++++	++	n/a
RGCs	-	-	-	-/+	-/+
Photoreceptors			+	+	+
Horizontal cells		-/+	-/+	-/+	-/+
Amacrine cells	n/a	-/+	-/+	+	+
Bipolar cells	n/a	-/+	-/+	+	+
Müller glia	n/a		+	+	+
<i>ONH</i>					
	+	+	+	+	+
<i>Optic nerve</i>					
	-	-	-	-	-
<i>RPE</i>					
	-	-	-	-	-
<i>Ciliary margin zone</i>					
	-	-	-	-	-
<i>LENS</i>					

<i>FGF8</i> (continued)	DG 40	DG 50	DG 75	DG 110	DG 140-145
Bow region			-	-	
Lens fibers			-	-	
<i>CORNEA</i>	-	-	-	-	-

<i>NPVF</i>	DG 40	DG 50	DG 75	DG 110	DG 140-145
<i>RETINA</i>					
RPCs temporal/fovea	-	-	n/a	n/a	n/a
RPCs nasal	-	-			n/a
RPCs central	-	-	-	-	n/a
RGCs	-	-	-	-	-
Photoreceptors	-	-	-	-	-
Horizontal cells			-	-	-
Amacrine cells	n/a	-	-	-	-
Bipolar cells	n/a	-	-	-	-
Müller glia	n/a	-	+	++	+++
<i>ONH</i>	-	-	-	-	-
<i>Optic nerve</i>	-	-	-	-	-
<i>RPE</i>	-	-	-/+	-/+	-/+
<i>Ciliary margin zone</i>	-	-	-	-	-
<i>LENS</i>					
Lens epithelium	++	+	-/+	-/+	
Bow region			-	-	
Lens fibers			-	-	
<i>CORNEA</i>					

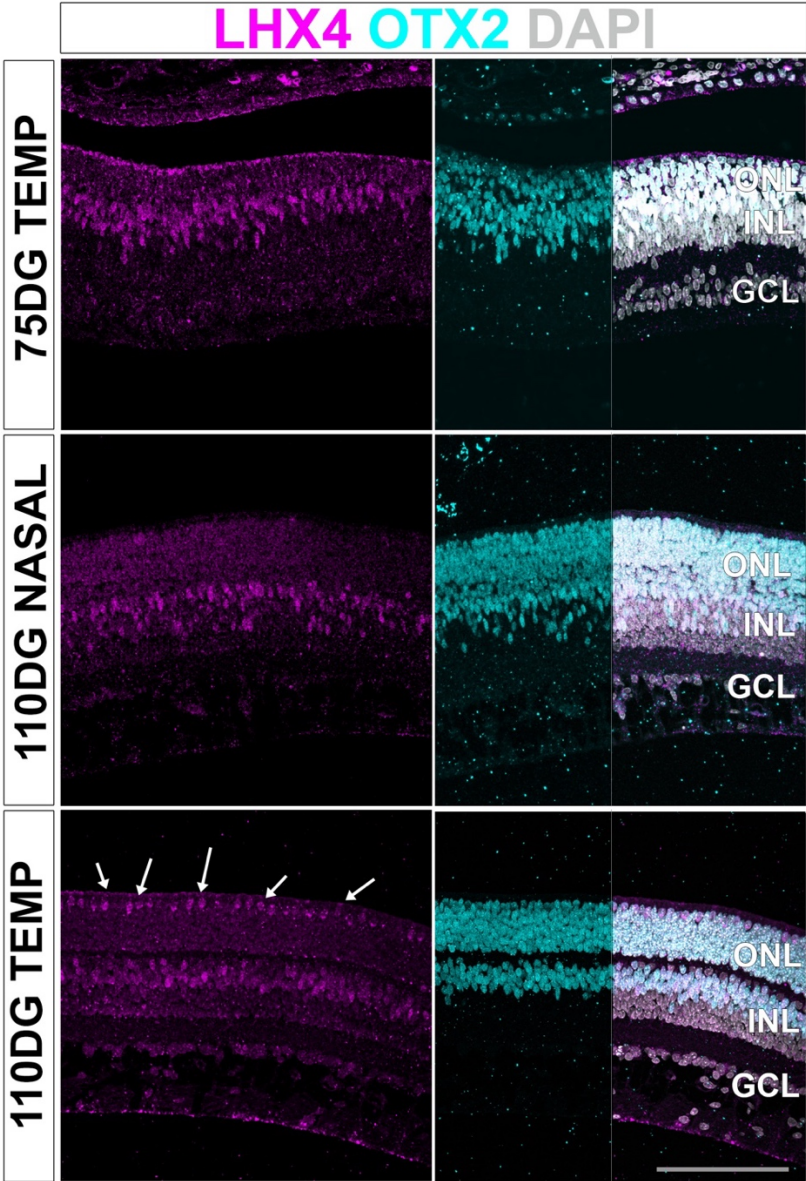
<i>CDKN1A</i>	DG 40	DG 50	DG 75	DG 110	DG 140-145
<i>RETINA</i>					
RPCs temporal/fovea	-	-	n/a	n/a	n/a
RPCs nasal	-	-	-		n/a
RPCs central	-	-	-	-	n/a
RGCs	-	-	-	-	-
Photoreceptors	-	-	-	-	-
Horizontal cells		-	-	-	-
Amacrine cells	n/a	-	-	-	-
Bipolar cells	n/a	-	-	-	-
Müller glia	n/a	++	+++	+++	+++
<i>ONH</i>	++	++	+++	+++	+
<i>Optic nerve</i>	+	+	+	+	-

CDKN1A (continued)	DG 40	DG 50	DG 75	DG 110	DG 140-145
<i>Ciliary margin zone</i>	+/-	+/-	+/-	+/-	+/-
LENS					
Lens epithelium	++	+	-	-	
Bow region			-	-	
Lens fibers			-	-	
CORNEA	++	+	+	+	+

Table 3.2 Expression patterns of *CYP26A1*, *FGF8*, *CDKN1A*, and *NPVF* in the rhesus monkey eye

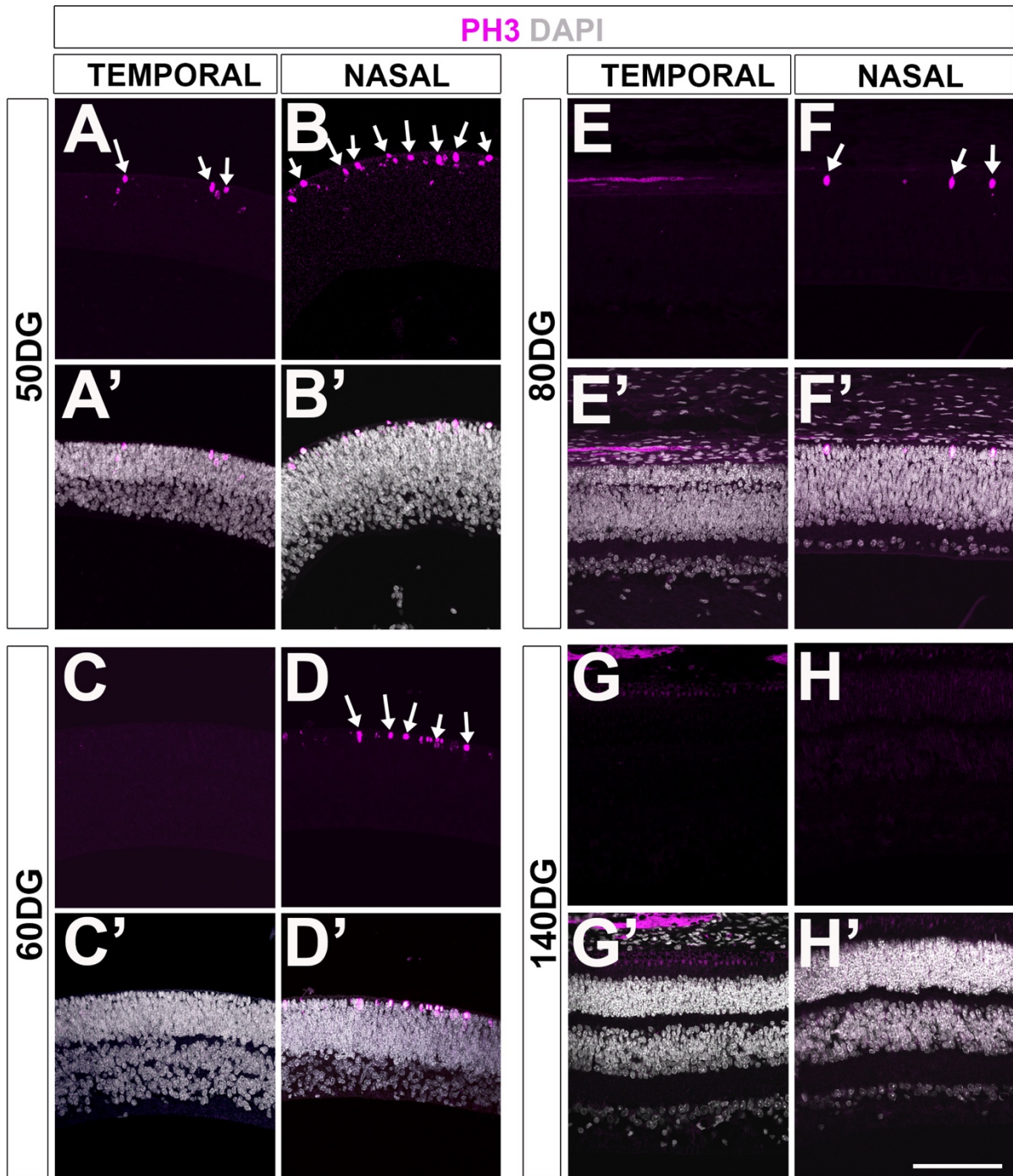
Expression patterns of *CYP26A1*, *FGF8*, *CDKN1A*, and *NPVF* in the rhesus monkey eye. Very low (+/-), low (+), moderate (++) , high (+++), and very high (++++) levels of expression. No detectable expression is indicated (-). N/A (not applicable) indicating that the corresponding areas were not defined at that developmental stage. (*) indicates exclusively expressed in the macula but not in other retinal regions. Empty tables: expression not analyzed. GD: days gestational age; RPC: retinal progenitor cell; ONH: optic nerve head; RPE: retinal pigment epithelium.

3.10 Supplementary figures



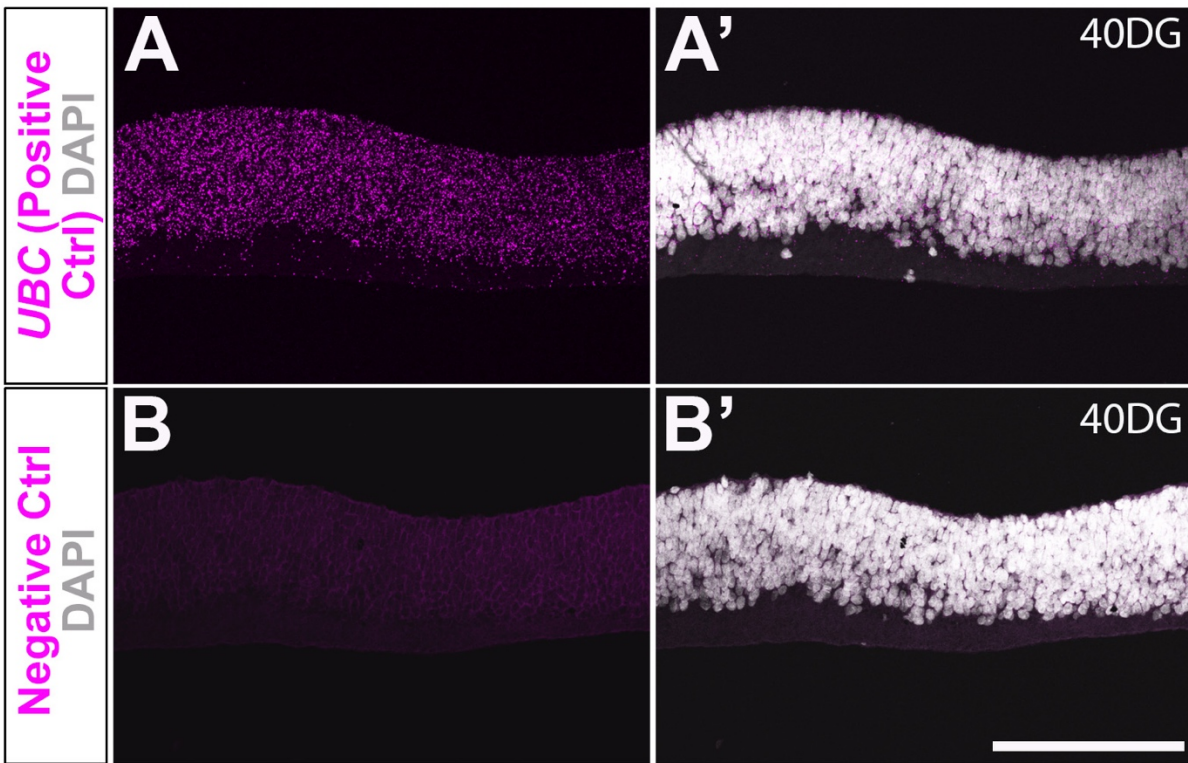
Supplementary Figure 3.1

Expression pattern of LHX4 (magenta) and OTX2 (cyan) at 70 and 110 days gestational age. Retinas have been counterstained with DAPI (gray). Note the expression in the outer part of the ONL only in the temporal region at 110 days (arrows). ONL: outer nuclear layer, INL: inner nuclear layer, GCL: ganglion cell layer. Scale bar: 100 μ m.



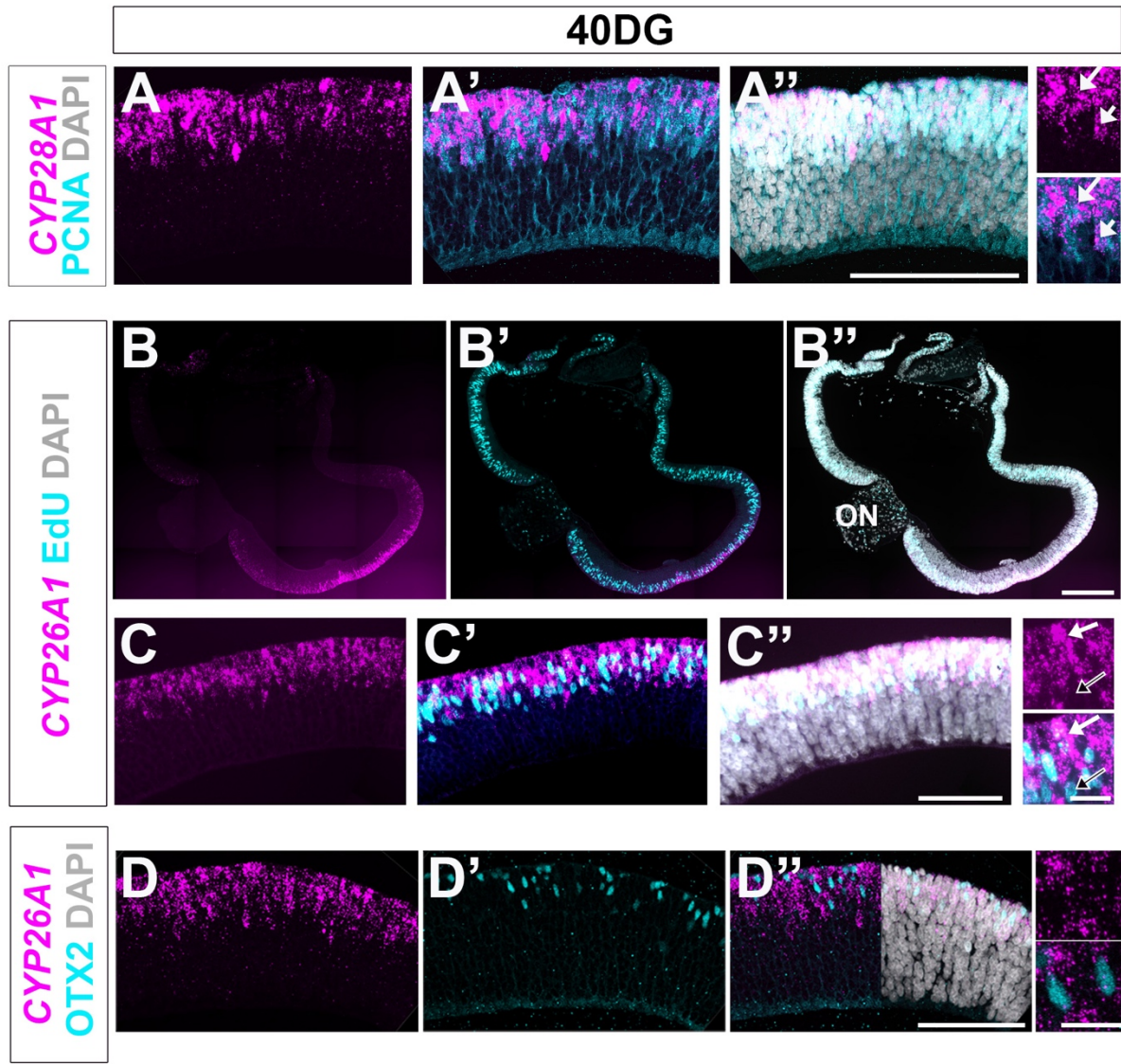
Supplementary Figure 3.2

Mitotic cells are labeled with Phospho-histone3 (PH3, magenta. Arrows in A, B, D, and F). Retinas are counterstained with DAPI (gray). Scale bar: 100 μ m.



Supplementary Figure 3.3

Positive control probe (*UBC*, magenta in A-A') and negative control (RNAscope 3-plex Negative Control Probe, magenta in B-B') are shown at 40 days gestational age. Scale bar: 75 μ m.

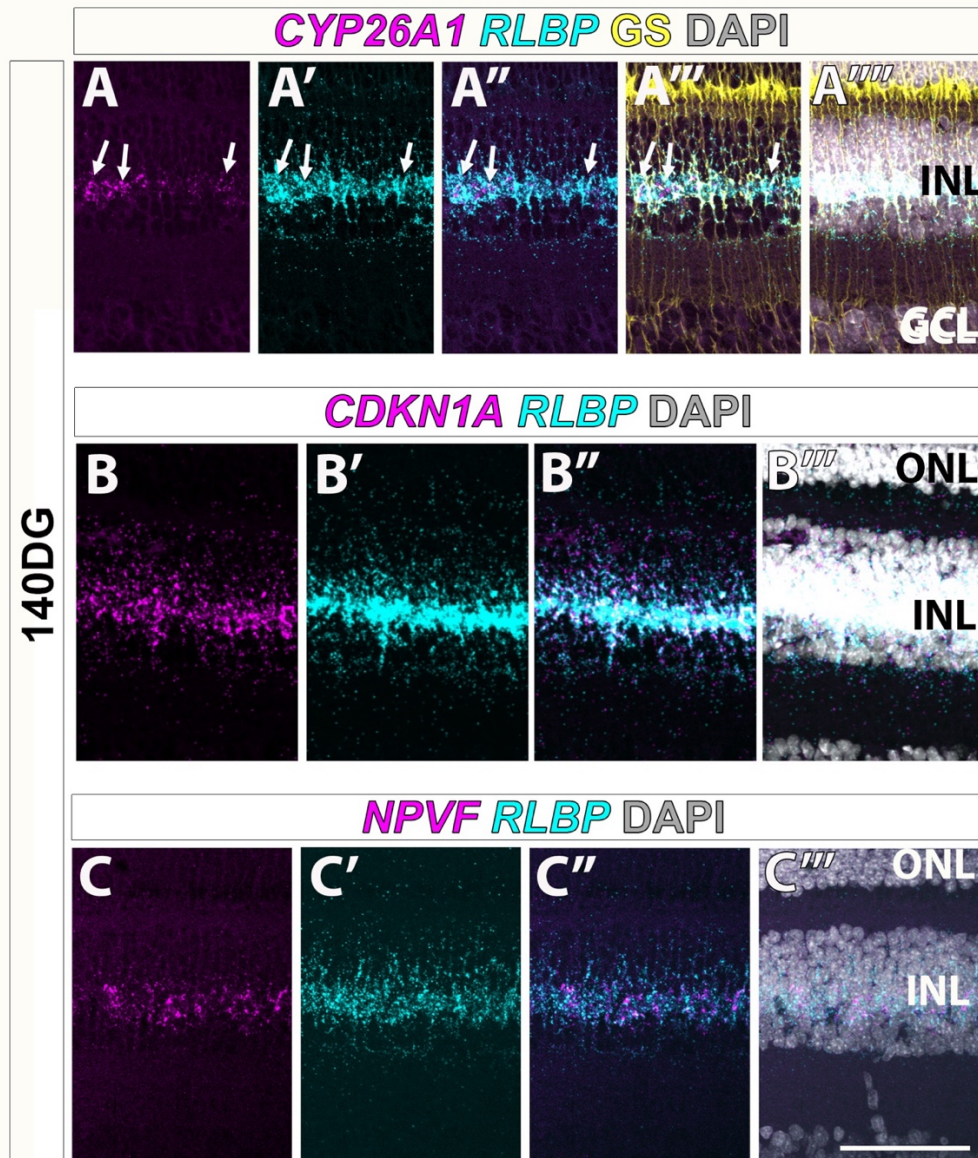


Supplementary Figure 3.4

(A-A'') Expression of *CYP26A1* (magenta) colocalizes with PCNA+ RPCs (cyan, white arrows).

(B-C'') Expression of *CYP26A1* (magenta) was detected in some EdU+ cells (cyan, white arrow) while some EdU+ cells in the center of the fovea do not express *CYP26A1* (black arrow). **(C-C'')**

CYP26A1 (magenta) did not colocalize with OTX2 (cyan). All tissues have been counterstained with DAPI (gray). Scale bars: 75 μ m in A'', B'' and C'', 250 μ m in A'', and 20 μ m in small insets.



Supplementary Figure 3.5

(A-A''') Expression of *CYP26A1* (magenta), *RBLP1* (cyan), *GS* (yellow) is shown at 140 days gestational age (DG). Arrows in A-A''' indicate some of the cells that co-express all the markers.

(B-B''') Expression of *CYP26A1* (magenta) and *RBLP1* (cyan) is shown at 140 days gestational age.

(C-C''') Expression of *CYP26A1* (magenta) and *RBLP1* (cyan) is shown at 140 days gestational age. All samples have been counterstained with DAPI (gray). ONL: outer nuclear layer,

INL: inner nuclear layer, GCL: ganglion cell layer. Scale bar: 75 μ m.

4. Published results: MicroRNA signatures of the developing primate fovea

Elizabeth S. Fishman^{1*}, Mikaela Louie^{1*}, Adam M. Miltner^{1*}, Simranjeet K. Cheema¹, Joanna Wong¹, Nicholas M. Schlaeger¹, Ala Moshiri², Sergi Simó¹, Alice F. Tarantal^{1,3,4}, and Anna La Torre^{1#}

¹ Department of Cell Biology and Human Anatomy, University of California Davis, Davis, 95616

² Department of Ophthalmology, University of California Davis, Davis, 95616

³ Department of Pediatrics, University of California Davis, Davis, 95616

⁴ California National Primate Research Center, University of California Davis, Davis, 95616

* These authors contributed equally to this work

Author for correspondence: alatorre@ucdavis.edu

The following chapter was submitted as a manuscript to *Frontiers in Cell and Developmental Biology* and published on April 8, 2021. The accepted version of this manuscript has been reformatted for this dissertation. The authors of the manuscript were Elizabeth S. Fishman (Elizabeth Fishman-Williams), Mikaela Louie, Adam M. Miltner, Simranjeet K. Chema, Joanna Wong, Nicholas M. Schlaeger, Ala Moshiri, Sergi Simó, Alice F. Tarantula, and Anna La Torre, with myself, Mikaela, and Adam contributing equally. I performed the miRNA *in situ* hybridizations and immunohistochemistry experiments.

4.1 Abstract

Rod and cone photoreceptors differ in their shape, photopigment expression, synaptic connection patterns, light sensitivity, and distribution across the retina. Although rods greatly outnumber cones, human vision is mostly dependent on cone photoreceptors since cones are essential for our sharp visual acuity and color discrimination. In humans and other primates, the *fovea centralis* (fovea), a specialized region of the central retina, contains the highest density of cones. Despite the vast importance of the fovea for human vision, the molecular mechanisms guiding the development of this region are largely unknown. MicroRNAs (miRNAs) are small post-transcriptional regulators known to orchestrate developmental transitions and cell fate specification in the retina. Here, we have characterized the transcriptional landscape of the developing rhesus monkey retina. Our data indicates that nonhuman primate fovea development is significantly accelerated compared to the equivalent retinal region at the other side of the optic nerve head, as described previously. Notably, we also identify several miRNAs differentially expressed in the presumptive fovea, including miR-15b-5p, miR-342-5p, miR-30b-5p, miR-103-3p, miR-93-5p as well as the miRNA cluster miR-183/-96/-182. Interestingly, miR-342-5p is enriched in the nasal primate retina and in the peripheral developing mouse retina, while miR-15b is enriched in the temporal primate retina and increases over time in the mouse retina in a central-to-periphery gradient. Together our data constitutes the first characterization of the developing rhesus monkey retinal miRNome and provides novel datasets to attain a more comprehensive understanding of foveal development.

4.2 Introduction

Sight is often considered our most fundamental sense to perceive and navigate the world and, as a result, vision loss has a devastating impact on everyday life. Visual perception begins when photons of light enter the eye and are absorbed by the photoreceptors, the light-sensitive cells of the retina. There are two classes of photoreceptors named rods and cones because of their distinctive morphologies. While both populations contribute to the information transmitted to the visual centers of the brain by the optic nerve, these two cell types serve different purposes: rods are highly sensitive to light and provide relatively coarse, colorless images, while cones require considerably brighter light and are responsible for our sharp chromatic vision and spatial acuity ³⁵.

All photoreceptors are localized in the outer nuclear layer of the retina and are organized in a mosaic pattern that varies in different organisms to fit their environments and behaviors ^{336,363-366}. In most mammals, rods outnumber cones by orders of magnitude; in the mouse retina, rods constitute 97.2% and cones are 2.8% of all photoreceptors (38:1 rod to cone ratio ^{135,367}), while the human retina contains an average of 92 million rods and 4.6 million cones (20:1 rod to cone ratio ³). In humans and other primates, most of the cones are confined to a small region of the central temporal retina called the *macula lutea* (macula), where the cone concentration is about 200-fold higher than the most eccentric retinal regions ^{3,4,242,309}. At the center of the macula, a small indentation marks the location of the *fovea centralis* (fovea) corresponding with the center of the visual field. At the foveal pit, all photoreceptors are densely packed cones and there are virtually no rods ³⁶⁸⁻³⁷¹. Despite the overall predominance of rod photoreceptors, primates have evolved to primarily utilize cone pathways, and most of our useful photopic

vision depends on the cones in the fovea such that a 2-millimeter lesion in this area will result in legal blindness.

Age-related macular degeneration (AMD), one of the most prevalent types of photoreceptor degeneration, affects millions of people worldwide, and causes irreversible vision loss from the selective degeneration of the photoreceptors of the fovea³⁷². It has been estimated that AMD affects up to 25% of the U.S. population over the age of 80³⁷³, illustrating the urgent need for novel treatments to restore the cones of the fovea. Efforts to develop therapies aimed at cone replacement will inevitably require preclinical studies using nonhuman primates, but our understanding of primate retinogenesis is still incomplete. Similarly, despite the fundamental importance of the fovea for human vision, the molecular mechanisms that guide the development of this region as well as the pathways that regulate the higher ratios of cone production remain largely unresolved.

During retinal development, different classes of retinal populations are consecutively added in a well-known sequence that is conserved in all vertebrates^{1,99,100,374}: Retinal ganglion cells (RGCs), cone photoreceptors, and horizontal cells are the first cell populations to be born, followed by amacrine cells and rod photoreceptors, and finally, bipolar cells and Müller glia are born last. Classic lineage-tracing studies showed that retinal progenitor cells are multipotent such that one single type of progenitor cell has the ability to differentiate into multiple postmitotic cell types. Evidence from heterochronic transplants^{105-107,375}, in which neural progenitors were transplanted into an environment of a different age and, more recently, single-cell transcriptomics^{17,231,376} has revealed that (1) retinal progenitors are intrinsically restricted, and (2) retinal progenitors

pass through waves of competence to acquire and lose the ability to make specific cell types at different developmental stages.

MicroRNAs (miRNAs) are small RNA molecules known to regulate several aspects of development. To date, over 2,000 miRNAs have been recorded in miRbase (miRbase.org) ¹⁷⁷ and both computational and experimental analyses indicate that most protein-coding genes are regulated by one or more miRNAs ^{377,378}. The essential roles of miRNAs in cell fate acquisition and central nervous system (CNS) patterning are well established. miRNAs are known to regulate neural progenitor competence *in vivo* ^{187,188,279,379,380} and *in vitro* ^{381,382}, and some miRNAs have been associated with the production of specific cell types ^{381,383-385}.

Given the vast importance of miRNAs as developmental regulators, we have sought to characterize the miRNome of the early developing nonhuman primate retina, specifically the rhesus monkey (*Macaca mulatta*), an Old World nonhuman primate. We have generated transcriptomic profiles of rhesus retinas at three developmental time points, spanning the major stages of development, and we have used miRNA-sequencing technologies to identify miRNAs differentially expressed in the presumptive fovea (temporal posterior side of the retina) compared to its equivalent region at the other side of the optic nerve head (nasal posterior) at early stages of retinal development. In addition, we have chosen miRNAs with significant differential expression between retinal regions and we have validated their expression using *in situ* hybridization in mouse and human samples. Together, our data provides invaluable resources for studies aimed at understanding the role of miRNAs in retinal development as well as datasets to broaden our knowledge of foveal development.

4.3 Results

4.3.1 Transcriptomic characterization of the developing rhesus monkey retina

Total RNA was obtained from retinal punches (approximately 2.5 mm in diameter) from the prospective fovea (temporal side) and the equivalent region at the other side of the optic nerve head (nasal side), from three different time points spanning the three trimesters (50 days gestational age [late first trimester], 90 days [second trimester], and 150 days [third trimester]; term 165 ± 10 days). Rhesus monkey trimesters are divided by 55-day increments (0-55 days, 56-110, days 111-165 days) ³⁴³. We performed Next Generation Sequencing (NGS) analyses (50 days: 6 samples, 3 temporal and 3 nasal, 90 days and 150 days: 2 samples each, 1 temporal and 1 nasal for each ontogenic stage). After the pre-processing pipeline and quality controls, more than 89% of the reads were aligned with the rhesus monkey genome (reference genome: Mmul_1; annotation reference: Ensembl_75) for each sample. On average, 74.9 million reads were obtained from each sample, and genome mapping was on average 90%.

We used the expression of cell type-enriched genes as a read-out of the timing of retinal histogenesis (Figure 4.1A-E, Supplementary Table 4.1). As expected, by 50 days gestational age, several well-known progenitor genes are highly expressed (*e.g.*, PRTG, FOXP1) but not all progenitor genes reach the highest expression point at these early stages and several progenitor genes such as bHLH transcription factors (*e.g.*, ASCL1, NEUROG2) and genes associated with active proliferation (*e.g.*, CCND1, CDK4, E2F1, E2F2) do not peak until 90 days gestational age (Figure 4.1A and Supplementary Figure 4.1A). Previous reports have identified clear transcriptional differences between early and

late retinal progenitor competence states in mouse and human retinas^{17,231,376}, including a progressive increase in Notch signaling. The activation of the Notch pathway maintains cells in a proliferative state ensuring that a subset of progenitors remains for the consecutive waves of neurogenesis^{386,387}. Notch also regulates fate decisions through the regulation of neurogenic genes^{94,388}. Correspondingly, many genes involved in the Notch signaling pathway show their highest levels of expression at 90 days gestational age in our screening (Supplementary Figure 4.1B), with NOTCH1, NOTCH3, DLL1, DLL3 and HES5 peaking at this time.

Similarly, genes known to be expressed in both mouse and human RGCs exhibit specific expression at different time points (Figure 4.1B). For example, several transcription factors such as ISL1 and SOX11 are highly expressed at early stages of development corresponding with their expression in other species³⁸⁹⁻³⁹¹, while genes associated with RGC synaptic maturation (*e.g.*, NRN1 or SNCG) increase over developmental time and peak in the third trimester. Interestingly, many photoreceptor-specific¹²⁹ and bipolar cell-specific markers²⁵³ are detected first in the temporal samples before the nasal samples starting from 50 days gestational age (Figure 4.1C-D). Accordingly, by this time, the temporal samples exhibit higher levels of cone genes (*e.g.*, PDE6H, 3.5-fold enrichment; Figure 4.1C) and early bipolar genes (*e.g.*, VSX1 shows a 28-fold enrichment, GSG1 shows a 3.1-fold enrichment, and TMEM215 shows an 8.3-fold enrichment; Figure 4.1D). These differences between temporal and nasal regions are more prominent in the second trimester (90 days gestational age), reflecting a vast developmental acceleration in the presumptive fovea. Thus, by this time, the expression of GUCA1B is 14.5-fold higher in the temporal samples, PDE6H shows an enrichment of

5.8-fold (photoreceptor markers), and the bipolar markers VSX1, CABP5, PRDM8, GSG1, TMEM215 are enriched 39.8-, 2.6-, 2.8-, 4.5- and 10.3-fold, respectively. Correspondingly, many Müller glia-specific genes are up-regulated over developmental time, including NFIX, GLUL, CA2 and RLBP1 (Figure 4.1E).

In addition to the cell-specific markers, other genes also exhibit transcriptional differences between the temporal and nasal regions of the developing rhesus eye (Figure 4.1F, Supplementary Tables 4.1 and 4.2). Notably, many of these genes have been previously shown to be differentially expressed in the developing macula or the high-acuity area of other species. For example, FOXP1 is a transcription factor exclusively expressed in the nasal portion of the retina in fish, chicken, mouse, and human^{213,243,392-395}. Hoshino and collaborators demonstrated that CYP11B1 is enriched in the periphery of the human fetal retina²⁴³. Notably, CYP26A1 is higher in the temporal retina at all the ages analyzed and ALDH1A1 is enriched in the nasal retina. CYP26A1 and ALDH1A1 are negative and positive regulators of retinoic acid (RA) levels, respectively and downregulation in RA signaling correlates with the development of a rod-free area in the avian retina³⁹⁶. CYP26A1 and NPVF have also been previously identified as developing macula markers in human samples by different reports^{231,243}. Additionally, our analyses also identify novel genes such as CROC4 (C1orf61), CASQ2, SPARCL1, and WIF1 as genes presenting strong differential expression signatures between the presumptive fovea and the nasal side at different gestational time points (Figure 4.1F). Collectively, these results show that the rhesus monkey presumptive fovea is developmentally advanced relative to the opposite nasal region, confirming the utility of these data as a tool to analyze differences between temporal and nasal expression.

4.3.2 miRNA-sequencing and differential expression profiles between temporal and nasal fetal rhesus monkey retina

miRNA libraries were obtained from retinal punches from the temporal side of the retina (presumptive fovea) and the nasal side of the optic nerve head as described above, at 50 days gestational age (n=3 samples for each anatomical region, 6 samples total). After NGS profiling, an average of 29.9 million reads were obtained per sample, and the data was mapped to miRBase (release 20) and normalized. Principal Component Analysis (PCA) was performed by including the top 50 microRNAs that varied the most across all samples using normalized reads. As shown in Figure 4.2A, the foveal/temporal samples form a relatively robust cluster indicating that the biological differences between these samples are pronounced despite the nasal samples exhibiting larger intra-group variability.

Importantly, our experiments indicate that several miRNAs are differentially expressed in the different regions of the developing primate retina (Figure 4.2B-C). For example, miR-183, miR-96, and miR-182 are significantly enriched in the developing fovea (3.3-fold, 5.21-fold, and 5.11-fold, respectively). miR-183/-96/-182 are co-expressed together as a single primary transcript, are highly expressed in developing photoreceptors in mouse and zebrafish, and play essential roles in photoreceptor development and maintenance^{280,282,397}. Since the temporal region of the developing primate eye exhibits both a developmental acceleration and higher percentage of photoreceptors, it is not surprising that this family is expressed at greater levels in the temporal samples. Additionally, several other miRNAs are significantly enriched in the presumptive fovea compared to the nasal samples, including miR-369-3p (4.86-fold

enrichment with a p -value of $2.45E-7$), miR-15b-5p (3.85-fold enrichment with p -value of $5.6E-7$), miR-30b-5p (3.96-fold enrichment with a p -value of $8.99E-6$), miR-103-3p (2.69-fold enrichment with a p -value of 0.0009), and miR-93-5p (2.57-fold enrichment with a p -value of 0.0019). However, the expression levels of miR-369-3p are fairly low (Figure 4.2B). In contrast, miR-342-5p is significantly enriched in the nasal site (2.71-fold with a p -value of $1.96E-10$).

Interestingly, miRNAs belonging to the same families often show similar expression profiles: all members of the miR-17/-20/-93/-106/-519 family are enriched over two-fold in the temporal samples, miR-15b and miR-16 are enriched 3.85-fold and 2.65-fold respectively, and miR-130a/-130b/-454/-301 are also all expressed at higher levels in the temporal region of the eye (Supplementary Table 4.3). This suggests that these miRNA families are frequently regulated as a whole, perhaps at the primary transcript stage.

Previous studies have indicated that miRNAs coordinately regulate protein levels and thus, miRNAs that target the same complexes are often co-expressed³⁹⁸. We have used MIENTURNET (MicroRNA ENrichment TURned NETwork,³⁹⁹ to gain insight into the possible miRNA networks in the different regions of the primate retina (Supplementary Figure 4.2). The network analyses of some of the highest expressed miRNAs for each region suggest possible differences in cell cycle regulation as several cell cycle genes including CCND1, CDKN1A, TP53, and CCNE1 are potentially regulated by differentially expressed miRNAs (Supplementary Tables 4.4 and 4.5). Similarly, FOXP1 is potentially targeted by miR-30b-5p and miR.103-3p while NFIA and NFIB, two transcription factors involved in fate specification in the retina³⁷⁶, are potentially targeted by miR-30b-5p, miR-

103-3p, and miR-93 (Supplementary Figure 4.2 and Supplementary Table 4.5). Additionally, several genes involved in the NOTCH, WNT, and RA pathways are also targeted by the temporal miRNA network.

Notably, our analyses also reveal several miRNAs that were not previously annotated in the *Macaca mulatta* database but known in other species (Figure 4.3A) as well as putative novel miRNAs (Figure 4.3B), based on counts and putative secondary precursor hairpin structures identified using the miRPara software⁴⁰⁰.

4.3.3 miRNA expression in the developing mouse retina

The miRNAs identified in our screening could be differentially expressed in the developing fovea for various reasons; for example, since the fovea is developmentally accelerated, temporally-regulated miRNAs are expected to increase first in the temporal side of the retina. Similarly, miRNAs enriched in cell populations found in higher percentages in the fovea (*e.g.*, cones) could also exhibit higher expression levels in the temporal samples. Finally, the progenitors of the fovea could possess unique properties and miRNA signatures.

Since miRNA-seq technologies do not offer cellular resolution, and given the costs of primate samples, we first attempted to validate the developmental expression and cellular resolution of the top miRNA candidates using mouse tissue at three different time points: embryonic day 13.5 (E13.5), E16.5, and postnatal day 3 (P3) by *in situ* hybridization (ISH) (Figure 4.4). All the miRNAs tested show some level of expression in the murine samples and, in all cases, the expression detected was above the labeling threshold in negative controls (scrambled probe, Figure 4.4 S-U). miR-15b, miR-30b and

miR-103-3p are up-regulated over the time points analyzed and show the highest levels of expression at P3 (Figure 4.4A-F, J-L). Interestingly, miR-15b exhibits a clear center-to-periphery pattern and it is first detected in the central retina at E13.5 (black arrows, Figure 4.4A and Supplementary Figure 4.3). By E16.5, most of the retina expresses miR-15b, but we found lower levels of expression in the peripheral tips (Figure 4.4B) and the whole retina expresses high levels of miR-15b by P3. miR-30b is expressed throughout the thickness of the retina at P3 but we observed a moderate enrichment in the ganglion cell layer (GCL) and the basal part of the inner nuclear layer, suggesting higher expression in amacrine cells and possibly RGCs (Figure 4.4F and Supplementary Figure 4.3). Interestingly, miR-93 expression is missing from the apical side of the retina at P3, suggesting that this miRNA may be expressed at lower levels in developing murine photoreceptors (Figure 4.4I and Supplementary Figure 4.3). Finally, miR-342-5p shows higher expression levels in the peripheral retina from E16.5 onward (Supplementary Figure 4.3), and this pattern of expression is maintained by P3 (Figure 4.4N-O, black arrows). In contrast, positive control experiments (U6 probe, Figure 4.4P-R) show neither regional differences nor changes in expression coordinated with the stage of development.

4.3.4 Expression in the developing human retina

The experiments using murine samples indicate that several of the miRNAs identified in our miRNA-seq screening are developmentally regulated and that miR-15b and miR-342-5p also show compartmentalized expression with central-to-peripheral differences. To further assess whether these expression patterns are conserved in

primates and relevant to human biology, we used human fetal retina tissue to test miRNA expression of our top candidates (Figure 4.5 and Supplementary Figure 4.3). We collected human fetal samples at gestational ages estimated to be between 77-83 gestational days (28-31% of gestation, Supplementary Figure 4.4). In order to obtain additional data on the developmental stage of the samples assessed, we performed immunohistochemistry using known markers and Hematoxylin and Eosin staining (Supplementary Figure 4.5). At the stage analyzed, there are PCNA+ retinal progenitors in all the quadrants of the retina, but the thickness of the neuroblastic layer where the retinal progenitors reside is thinner on the temporal side (NbL, Supplementary Figure 4.5A-C'). Similarly, we detected fewer PH3+ mitotic cells on the temporal site of the retina compared to the nasal side (arrows, Supplementary Figure 4.5B-C', F), indicating that more progenitors have already exited the cell cycle in this region. Correspondingly, we also detected increased numbers of OTX2+ photoreceptors on the temporal side of the eye (Supplementary Figure 4.5D-G').

Remarkably, miR-15b is expressed at higher levels in the temporal side of the optic nerve head (Figure 4.5A-A'') and miR-342-5p shows higher labeling signals in the nasal side of the eye (Figure 4.5B-B'') as predicted by our miRNA-seq analyses (Figure 4.2B-C). Both miRNAs display stronger signal in the neuroblast layer compared to other regions of the retina, including the GCL and the most apical side of the retina where the developing photoreceptors reside (arrows in Figure 4.5B'', Supplementary Figure 4.7). In contrast, we did not detect significant miR-93 or miR-30b differences between the temporal and nasal retina (Supplementary Figure 4.6). As shown previously, our U6

positive control is ubiquitously expressed (Figure 4.5C) and our negative controls (Figure 4.5D) show very low levels of non-specific labeling.

4.4 Discussion

Our most advanced visual abilities such as reading and recognizing faces are dependent on the highly-specialized structure of the fovea. Unfortunately, the current understanding of retinal development is primarily based on mouse studies. Since the mouse retina does not contain a fovea and the rod-to-cone ratio in rodents resembles the most eccentric regions of the human retina, the molecular events that lead to the formation of the macula and the cone-dominated fovea remain largely unknown.

Previous studies have shown that the primate retina develops over many months and, in fact, the human fovea is not fully developed until four years of age³⁰⁹. Histological data using human and nonhuman primate samples has revealed that retinal development takes place in a dramatically compartmentalized manner such that two regions separated by a few millimeters may be at vastly different ontogenic stages^{242,244,308,401}. Moreover, primate retinal development does not progress in a central-to-peripheral gradient similar to mice but advances in a fovea-to-periphery manner. Consistent with this species-specific difference in patterning, the expression of S-Opsin and L/M-Opsin is first detected in the fovea^{402,403}. Recently, the first transcriptional profiling datasets of the developing human retina have been published using both human fetal tissue and stem cell organoids^{17,231,243}. However, obtaining human tissue at very early or late stages of development is challenging and these resources are subject to ethical and political issues⁴⁰⁴. In contrast, nonhuman primate models offer a unique opportunity to decipher some of the molecular

mechanisms that dictate foveal development. The genus *Macaca*, probably the most extensively used nonhuman primate model ^{405,406}, shares with humans susceptibility genes for AMD ⁴⁰⁷⁻⁴⁰⁹ and for other photoreceptor pathologies such as achromatopsia ⁴¹⁰. Consequently, a comprehensive characterization of the specific mechanisms that regulate rhesus retinal development could facilitate the study of the pathophysiological events that lead to these diseases and enable the development of clinical approaches aimed at vision restoration.

Here, we provide the first spatio-temporal transcriptional datasets of the developing rhesus monkey retina obtained from temporal and nasal regions at three different gestational time points spanning all trimesters. By analyzing the expression of cell-specific markers, our data offers insights into the timing of retinal histogenesis and indicates that by 50 days gestational age, the temporal side of the retina is already more developmentally advanced when compared to the nasal side (Figure 4.1). A model developed by Finlay ⁴¹¹, Clancy ⁴¹², and Workman ⁴¹³ and available at translatingtime.org explores the idea that timing of many neurodevelopmental events - such as the timing of retinal neurogenesis - is highly conserved among species and thus, can be predicted with high accuracy taking into account the growth rates for the different species. According to this model (Supplementary Figure 4.4), by 50 days gestational age (end of the first trimester, 30% gestation), the rhesus monkey retina is at the peak of cone genesis and approximately at the onset of bipolar cell genesis. Assuming that neurogenesis for all the different cell types begins at the foveal region, these predictions appropriately fit our RNA-seq data. Indeed, by 50 days, we detect higher temporal expression of several bipolar genes, including *GSG1* and *TMEM215* (Figure 4.1D), two genes identified by the

Brzezinski group as cone bipolar markers ²⁵³. Our data also indicate that the maturation of photoreceptor cells follows a fovea-to-periphery gradient (Figure 4.1C), in agreement with histological evidence ⁴¹⁴. Importantly, we also distinguish other genes differentially expressed in the presumptive developing fovea (Figure 4.1F), including genes previously identified in the human macula and in the avian high-acuity area as well as novel genes, such as the gene encoding for the calcium-binding protein Calsequestrin-2 and SPARCL1/Hevin. Future studies will shed light on the role of these genes in retinal development.

It has been proposed that the accelerated developmental timing of the fovea may be partially responsible for its unique cellular composition. During the sequence of retinal cell specification, cones are generated earlier than rods and thus, precocious cell cycle exit from the retinal precursor pool would result in increased representation of early cell types (*e.g.*, cones). Comparison between diurnal (foveated) and nocturnal (afoveated) New World primates suggested that alterations in cell cycle kinetics could explain some of the differences between these models, including the higher production of cones in foveated species ²⁷³. However, molecules associated with rod photoreceptor differentiation such as NRL and NR2E3 are never detected in the foveal region while other late cell types (*e.g.*, bipolar cells and Müller glia) are present in the presumptive fovea before the cell movements that lead to pit formation ^{243,303}. Thus, it is feasible that the progenitors of the fovea possess unique characteristics that result in the stark difference in cell composition.

Prior studies have revealed that miRNAs are key regulators of the temporal changes that allow progenitors to produce different cell populations as development

proceeds ^{116,187,380}. Similarly, we have also shown that miRNAs coordinate cell cycle kinetics ²⁷⁶. Given that the fovea exhibits both different cell composition and perhaps different cell cycle dynamics, we have characterized the miRNome of the early developing primate retina with the goal to pinpoint miRNAs differentially expressed in the progenitors of the fovea. We identified several miRNAs with different temporal and nasal expression levels. Among these, miRNA-183/96/182, a miRNA cluster highly expressed in photoreceptors and vital in maintaining cone photoreceptor outer segments ^{415,416} is significantly enriched in the temporal samples. Similarly, other miRNAs including miR-15b and miR-342-5p also showed significant differences in our datasets and we utilized ISH to further validate these differences using mouse and human fetal samples. According to our assessment, the human samples used in this study are in a developmental stage comparable to the rhesus monkey samples we used for the miRNA-seq (Supplementary Figure 4.4). Remarkably, miR-15b showed higher labeling in the temporal retina while miR-342-5p exhibited lower expression in the temporal side of the retina. Past studies in different models and contexts have revealed that miR-15b plays roles in cell cycle regulation and survival ⁴¹⁷ while miR-342-5p acts downstream of Notch to regulate neural stem cell fate choices ⁴¹⁸. This raises the possibility that one or both of these miRNAs may contribute to the molecular events that lead to the development of the central primate retina. Future studies aimed at the identification of the miRNA-mediated networks in conjunction with the existing human and primate expression datasets may shed light on the regulatory events that orchestrate the cytoarchitecture of the primate fovea.

4.5 Materials and methods

4.5.1 Experimental models and subject details

4.5.1.1 *Rhesus monkeys*

All animal procedures conformed to the requirements of the Animal Welfare Act and protocols were approved prior to the implementation by the Institutional Animal Care and Use Committee (IACUC) at the University of California at Davis. Normal, healthy adult female rhesus monkeys (*Macaca mulatta*) were bred and identified as pregnant using established methods³⁴³. Pregnancy in the rhesus monkey is divided into trimesters by 55-day increments, with 0-55 days representing the first trimester, 56-110 days representing the second trimester, and 111-165 days gestational age the third trimester (term 165 ± 10 days). Female rhesus monkeys (n=5) were time-mated and identified as pregnant by ultrasound according to established methods (Tarantal 2005). Normal embryonic/fetal growth and development were confirmed by ultrasound across gestation and until tissue collection (Tarantal 2005). Dams were scheduled for hysterotomy (*e.g.*, approximately 50, 90, or 150 days gestational age) for fetal tissue collection. Dams were returned to the breeding colony post-hysterotomy.

The fetal eyes were collected in cold PBS and the retinas were immediately dissected. With the cornea facing up, we made a small puncture in the center of the cornea with an 18 gauge needle. Using spring scissors (10mm tip), we slowly cut the cornea from the puncture towards the corneo-scleral junction. We successively rotated the eye 90° and made three more cuts and we gently remove the lens. Then, using one of the cuts, we carefully inserted the lower blade of the scissors between the sclera/RPE and the retina and we cut all the way to the optic nerve head being careful not to damage

the retina. We repeated using the other cuts at the corneo-scleral divide. Next, the sclera, RPE, and choroid were carefully removed with fine forceps (World Precision Instruments, Dumont tweezers 0.05 x 0.01mm tips) to dissect the retina away from the rest of the tissues. We performed two cuts in the dorsal and ventral part of the retina to open its cup shape and the temporal and nasal samples were obtained using 2.5mm biopsy punches (World Precision Instruments) at equidistant regions about 0.5mm from the ONH. As the total size of the retina changes during development, the percentage of retina captured at the different stages varied in the different samples. At 50 days gestational age, the biopsy captured more than half of the retina from the ONH to the *ora serrata*, thus extending beyond the foveal anlage.

4.5.1.2 Mice

Pregnant CD-1 IGS females were obtained from Charles River and housed until embryos or neonates were at the proper developmental stage for dissection and fixation. All animals were used with approval from the University of California Davis IACUC. Dams were euthanized and embryos were dissected and fixed for ISH as described below.

4.5.1.3 Human fetal samples

Eyes (n=6) were obtained from discarded de-identified human fetal tissue with permission of the University of California, Davis Institutional Review Board. The age for the human specimens was estimated by clinic intakes.

4.5.2 RNA and miRNA sequencing

4.5.2.1 Library preparation and next generation sequencing

Upon dissection, all the tissues were preserved in RNAlater (Thermo Fisher) at -80°C. Then, total RNA was obtained from all the samples using the Total RNA Purification plus micro kit (Cat #48500, Norgen), and we used an Agilent Bioanalyzer 2100 to evaluate the quality of the RNA obtained.

The sequencing experiments were conducted by Exiqon (Denmark). The library preparation was performed using Illumina TruSeq® Stranded Total RNA (with Ribo-Zero Gold) preparation kit.

The starting material (1000 ng) of total RNA was depleted of rRNAs using ribo-zero gold (to remove both cytoplasmic and mitochondrial rRNA) magnetic bead-based capture-probe system (Illumina Inc.). The remaining RNA (including mRNAs, lincRNAs and other RNA species) was subsequently purified (RNACleanXP) and fragmented using enzymatic fragmentation. Then, first strand synthesis and second strand synthesis were performed, and the double stranded cDNA was purified (AMPure XP). The cDNA was end repaired, 3' adenylated and Illumina sequencing adaptors ligated onto the fragments ends, and the library was purified (AMPure XP). The stranded libraries were amplified with PCR and purified (AMPure XP). The libraries size distribution was validated and quality inspected on a Bioanalyzer (high sensitivity DNA chip). High quality libraries were quantified using qPCR, the concentration normalized, and the samples pooled. The library pool(s) were re-quantified with qPCR and optimal concentration of the library pool used to generate the clusters on the surface of a flowcell before sequencing on a

Nextseq500/ High Output sequencing kit (51 cycles according to the manufacturer instructions (Illumina Inc.) using 50-bp single-end reads and 30 million reads.

4.5.2.2 Sequence analyses

Our data analysis pipeline is based on the Tuxedo software package, including Bowtie2 (v. 2.2.2), Tophat (v2.0.11), and Cufflinks (v2.2.1). CummeRbund was used for post-processing Cufflinks and Cuffdiff results. The heatmap.2 function contained within the ggplot2 R package was used to produce all heat maps. Transcriptomic heat maps were produced by selecting genes that represent specific retinal cell types based on established literature using normalized CPM values.

4.5.2.3 miRNA-sequencing: library preparation and next generation sequencing

For miRNA-sequencing, we used the same samples that we used for RNA-seq. A total of 500 ng of total RNA was converted into microRNA NGS libraries using NEBNext library generation kit (New England Biolabs Inc.) according to the manufacturer's instructions. Each individual RNA sample had adaptors ligated to its 3' and 5' ends and converted into cDNA. Then the cDNA was pre-amplified with specific primers containing sample specific indexes. After 18 PCR cycles the libraries were purified on QiaQuick columns and the insert efficiency evaluated by Bioanalyzer 2100 instrument on high sensitivity DNA chip (Agilent Inc.). The microRNA cDNA libraries were size fractionated on a LabChip XT (Caliper Inc.) and a band representing adaptors and 15-40 bp insert excised using the manufacturer's instructions. Samples were then quantified using qPCR

and concentration standards. Based on quality of the inserts and the concentration measurements the libraries were pooled in equimolar concentrations (libraries to be pooled are of the same concentration). The library pool(s) were finally quantified again with qPCR and optimal concentration of the library pool used to generate the clusters on the surface of a flowcell before sequencing using v2 sequencing methodology according to the manufacturer instructions (Illumina Inc.). Samples were sequenced on the Illumina NextSeq 500 system.

4.5.3 Analyses of RNA-seq and miRNA-seq data

Following sequencing, intensity correction and base calling (into BCL files), FASTQ files were generated using the appropriate bcl2fastq software (Illumina Inc.) which includes quality scoring of each individual base in a read. We found that the vast majority of the data has a Q score greater than 30 (>99.9% correct), indicating that high quality data was obtained for all samples.

PCA was performed on miRNA samples using the base R function. To produce the hierarchically clustered heat map, the miRNA-seq data were initially filtered by removing any miRNAs that had a False Discovery Rate (FDR) of greater than 0.001 to improve readability of the heat map. All miRNAs with an FDR of <0.001 were then hierarchically clustered using the built-in hierarchical clustering algorithm in the heatmap.2 function. The color-key for each heat map was created using predetermined break points to bin the TMM value into colors for each marker. The volcano plot was also obtained using the base R volcano plot function.

4.5.4 *In situ* hybridization (ISH)

All samples were collected and quickly fixed in a modified Carnoy's fixative overnight at 4°C. For the mouse embryonic samples, we fixed whole heads while postnatal day 3 and human fetal samples were fixed as whole eyes. A small hole was made with an 18 gauge needle at the corneal limbus to facilitate the fixation. After fixation, samples were dehydrated and embedded in paraffin as described elsewhere ⁴¹⁹. Horizontal sections of whole embryo heads (mouse E13.5 and E16.5) and sagittal sections of whole eyes (mouse P3 and human 77-83 days) were prepared at 5 µm, collected onto SuperFrost slides, and air dried overnight at room temperature. Paraffin wax-embedded sections were baked for 45 min at 60°C, deparaffinized using xylene, rehydrated with ethanol (stepwise) and PBS, and treated with Proteinase K for 10 min at 37°C. A double digoxigenin (DIG)-labeled locked nucleic acid (LNA) ISH probe (miRCURY LNA Detection probe) was purchased from Exiqon/Qiagen. ISH was performed using the miRCURY LNA microRNA Detection FFPE microRNA ISH Optimization Kit 4 (Exiqon), which includes hybridization buffers and control probes (LNA scramble microRNA and LNA U6 snRNA control probe), according to manufacturer's protocol. The following LNA miRNA probes were used for ISH: miR-15b-5p (Qiagen, Cat# YD00611174-BEG, 1:500), miR-30b-5p (YD00610927-BCG, miR-30b, 1:500), miR-93-5p (Qiagen, Cat# YD00611038, miR-93-5b, 1:300), miR-103-3p (Qiagen Cat# YD00612004, 1:500), miR-342-5p (Qiagen, Cat# YD00611489, 1:625), U6 (Qiagen, Cat#YD00699002-BEG, 1:500), scrambled (Qiagen Cat# YD00699004, 1:300). LNA probes were hybridized for 1 h at 55°C and rinsed with SSC buffer (stepwise from 5x to 0.2x). Sections were blocked in 2% sheep serum/1% bovine serum albumin/PBS-0.01% Tween for 30 min at

room temperature. Detection was performed using an alkaline phosphatase conjugated anti-DIG secondary antibody (Roche) in 1% sheep serum/1% bovine serum albumin/PBS-0.05% Tween for 1 h at room temperature. Following rinsing in PBS-0.1% Tween, sections were incubated in developing solution of sodium chloride 0.1 M/tris pH 9.5 0.1M/magnesium chloride 10 mM/0.1% Tween-20 and NBT (nitroblue tetrazolium)/BCIP (5-bromo-4-chloro-3-indolyl phosphate) stock solution (Roche). After the reactions were deemed complete (1-4 days), sections were fixed with 4% paraformaldehyde and mounted for microscopy using Fluoromount-G (Southern Biotech).

4.5.5 Immunofluorescence

Sections were prepared as described previously ^{420,421}. Sections were then deparaffinized using xylene, rehydrated with ethanol (stepwise), rinsed with PBS-0.3% Triton X-100, and antigen retrieval was performed by treating the slides with 0.1 M sodium citrate. All sections were then blocked in 10% normal donkey serum/PBS-0.1% Triton X-100 in PBS for 1 h at room temperature and incubated in primary antibody in blocking solution overnight at 4°C. The following antibodies were used for immunofluorescence: goat anti-OTX2 (R&D Systems Cat#BAF1979), 1:500; rabbit anti-RBPMS (Phosphosolutions Cat#1832-RBPMS, 1:400, and anti-PCNA (Abcam Cat#ab18197, 1:500), and anti-PH3 (Thermo Fisher Cat#PA5-17869, 1:300). After primary antibody incubation, sections were rinsed in PBS and incubated with appropriate Alexa Fluor-conjugated secondary antibodies (Invitrogen, 1:300) in blocking solution for 1h at 4°C. Cell nuclei were counterstained with DAPI. The sections were rinsed with PBS and mounted for microscopy using a Fluoromount-G (Southern Biotech).

4.5.6 Hematoxylin and eosin staining

Samples were prepared as described previously ⁴²². Next, sections were deparaffinized using xylene, rehydrated with ethanol (stepwise) and water, and stained with hematoxylin and eosin, and dehydrated with ethanol (stepwise). The sections were then rinsed in xylene and mounted for microscopy using a Fluoromount-G (Southern Biotech).

4.5.7 Microscopy

ISH were imaged using an Axio Imager M2 with ApoTome2 microscope system (Zeiss) using tile scan options (ZEN imaging software), and immunolabeling experiments were documented using a Fluoview FV3000 confocal microscope (Olympus). Images were processed using Fiji (ImageJ software), and figures were prepared in Adobe Photoshop 2000.

4.6 Data availability statement

All datasets presented in this study are included in the article/supplementary material. Further inquiries can be directed to the corresponding author.

4.7 Ethics statement

The animal studies were reviewed and approved by the IACUC.

4.8 Author contributions

ESF, ML, AMM, SKC, JW, and NMS conducted experiments and/or analyses. AM conducted sample collection, contributed to the study design, and revised the manuscript. AFT identified, selected, and monitored the pregnancies sonographically, and collected the specimens for analysis, contributed to the study design, and revised the manuscript. SS and ALT supervised and designed the study, conducted experiments, and wrote the manuscript. All authors contributed to the manuscript and approved the submitted version.

4.9 Conflict of interest

The authors declare that the research was conducted in the absence of any commercial or financial relationships that could be construed as a potential conflict of interest.

4.10 Funding

This work was supported by grants from the NIH (R0EY026942; ALT), the California National Primate Research Center base operating grant (P51-OD011107; ALT and AFT), and a Pilot grant from the Departments of Physiology and Cell Biology and Human Anatomy (to ALT and AFT). *In vivo* imaging was performed with instrumentation funded by the NIH (S10 grant #OD016261; AFT) and the National Eye Institute Core Facilities (supported by P30 EY012576).

4.11 Acknowledgements

We thank all the members of the La Torre and Simo laboratories for their support. We thank Dr. Nadean Brown for her insightful advice and generosity with reagents, Keiko Hino and Raenier Reyes for technical support, and Dr. Corinne Fairchild and Brad Shibata for training lab members in *in situ* protocols.

4.12 Figures

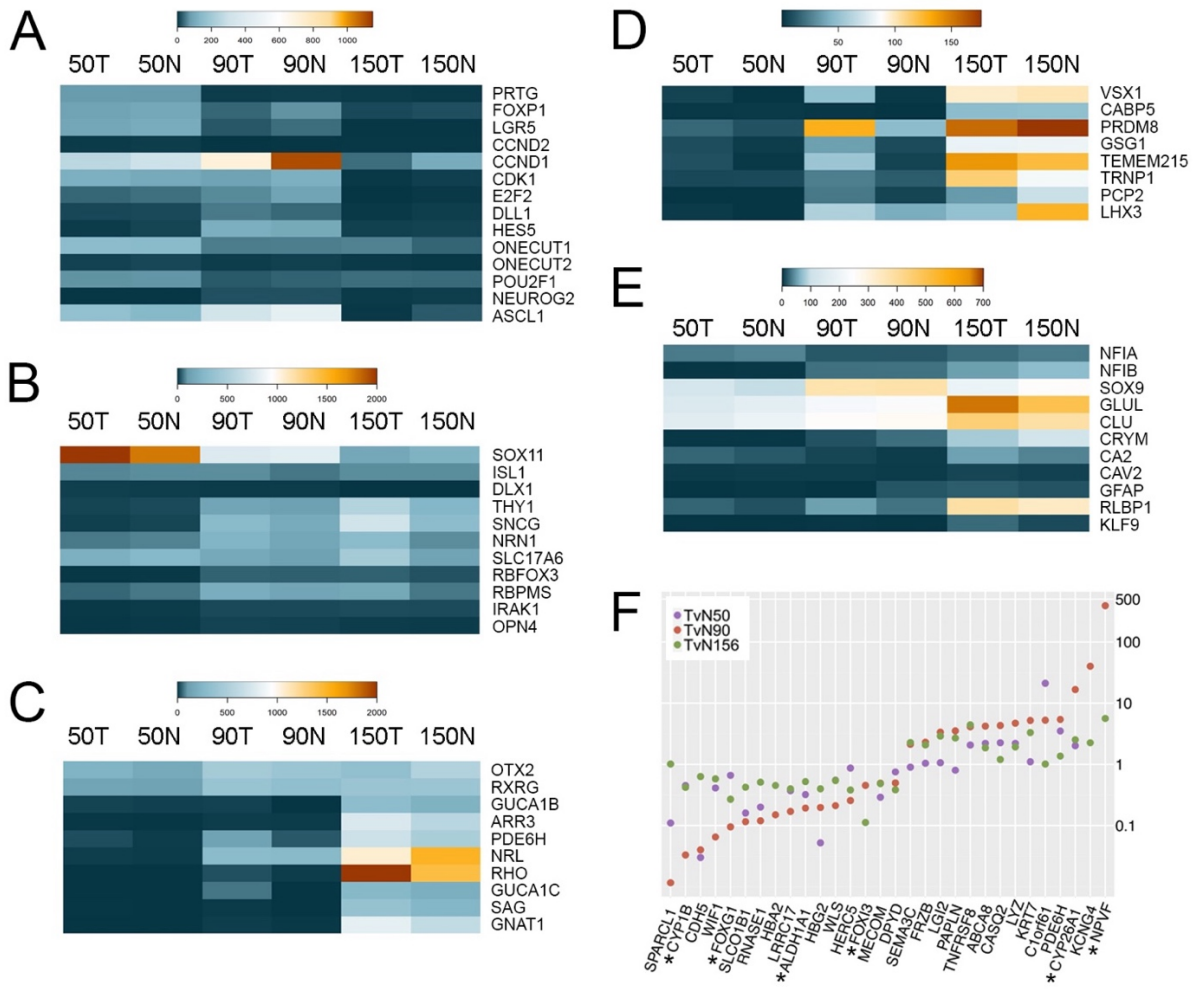
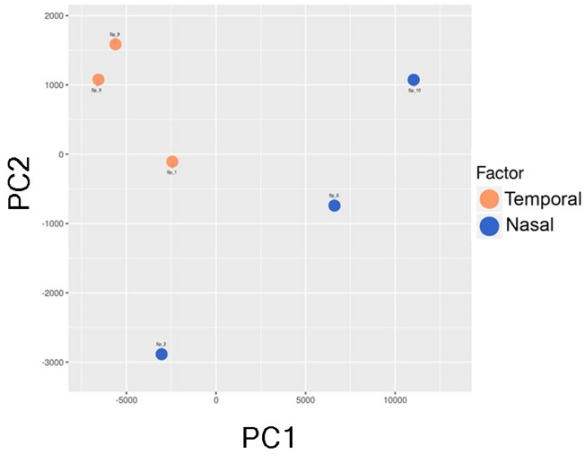


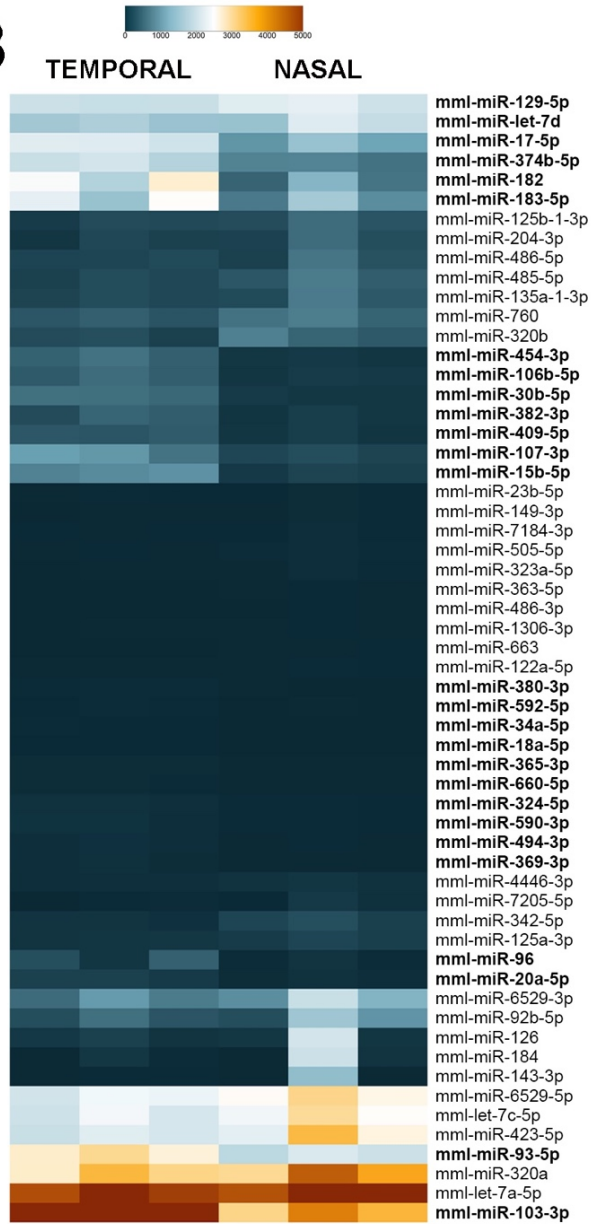
Figure 4.1 RNA-sequencing of *Macaca mulatta* retinas

(A-E) Heatmaps showing expression of cell-specific markers during *Macaca mulatta* retinal development. Comparisons between Temporal (T) and Nasal (N) data is shown at 50, 90, and 150 days gestational age. **(A)** Retinal Progenitor Cell markers. **(B)** Retinal Ganglion Cell markers. **(C)** Photoreceptor cell markers. **(D)** Bipolar cell markers. **(E)** Muller Glia cell markers. All data is shown as CPM (counts per million). **(F)** Scatter plot of genes showing differences between temporal and nasal expression. TvN: Temporal vs Nasal. Stars indicate genes previously identified as macula-enriched.

A



B



C

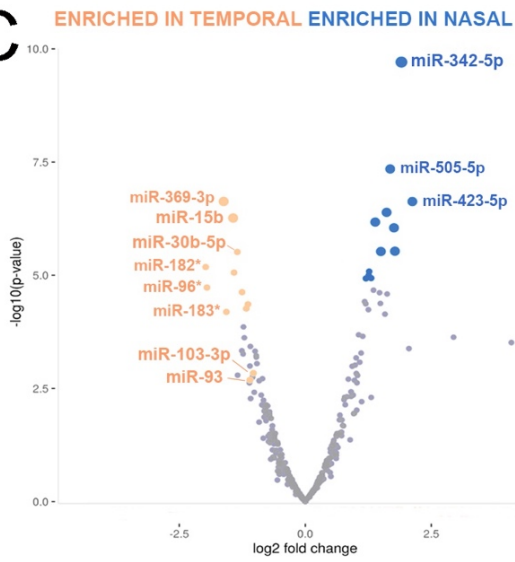


Figure 4.2 MiRNA-sequencing of *Macaca mulatta* retinas

(A) Two-dimensional Principal Component Analysis was used to visualize sample variance between six retinal tissue samples collected at 50 days gestational age. **(B)** Heatmap shows different miRNA expression between temporal and nasal samples. Only miRNAs with a False Discovery Rate (FDR) value of <0.012 between nasal and temporal samples are shown. miRNAs enriched in the temporal samples are shown in bold. **(C)** Volcano plot of miRNA plotted on fold change (\log_2 , x-axis) and P value ($-\log_{10}(\text{p-value})$, y-axis) shows difference in expression between nasal and temporal retina. Stars indicate the photoreceptor enriched miR-183/96/182 cluster.

A

ID	Chr	Strand	Start	Stop	Sequence	Counts
hsa-miR-744-5p	16	+	11829814	11829835	TGCGGGGCTAGGGCTAACAGCA	27596
hsa-miR-4684-5p	1	+	25309179	25309200	CTCTCTACTGACTTGCAACATA	27
bmo-miR-2779	4	+	26617823	26617838	ATCCGGCTCGAAGGAC	14
mmu-miR-7689-3p	5	+	1472793	1472815	TTAGAGCCAGACTGCCTGGGTTT	9
ggo-miR-1291	8	+	56485909	56485923	GTGGCCCTGACTGAA	11
bta-miR-2424	11	+	6658740	6658760	ATCTTTGGTAATCTGATGGCT	140
hsa-miR-1248	2	+	1.79E+08	1.79E+08	ACCTTCTTGTATAAGCACTGTGC	155
hsa-miR-4508	18	+	71266455	71266471	GCGGGGCTGGGCGCGCG	3

B

ID	Chr	Strand	Start	Stop	Sequence	Counts
put-miR-349	2	+	117300472	117300497	TCTGTGGGATTATGACTGAACGCCTC	11196
put-miR-348	2	+	117300369	117300395	GATGTGTTGTTGCCATGGTAATCCTGC	4114
put-miR-92	1	+	95623473	95623499	GTCCGATGGTAGTGGGTTATCAGAACT	3564
put-miR-91	1	+	47709617	47709643	GTAAGTGACGATAAAGTGTGTCTGAGG	3253
put-miR-42	14	+	83661692	83661717	AACGCGCCCGATCTCGTCTGATCTCG	3149
put-miR-66	19	+	34152595	34152621	AGCTACCATCTGTGGGATTATGACTGA	2056
put-miR-300	X	+	39631265	39631288	CGTCTGATCTCGGAAGCTAAGCAG	1819
put-miR-214	6	+	125875024	125875047	CGTCTGATCTCGGAAGCTAAGCAG	1806
put-miR-27	14	+	11231916	11231942	AATGTGACTGAAAGGTATTTCTGAGC	1571
put-miR-65	19	+	22514233	22514256	CCCAGTGCTCTGAATGTCAAAGTG	1443
put-miR-224	7	+	3968825	3968842	TCATCGGAACTGAGGTCC	1301
put-miR-93	1	+	95830029	95830052	AATTGTTTCAAGACGGGACTGATG	1016
put-miR-40	14	+	73584717	73584743	GATTGATTTAGAGGCATTTGTCTGAGA	908
put-miR-15	12	+	63966580	63966606	GATGGTAGTGGGTTATCAGAACTTATT	846
put-miR-4	10	+	51653988	51654013	ATGGTAGTGGGTTATCAGAACTTATT	817

Figure 4.3 Novel *Macaca mulatta* miRNAs at 50 days gestational age

(A) miRNAs previously discovered in other species but unknown to be expressed in *Macaca mulatta* prior to this study. (B) Putative novel miRNAs based on counts and secondary precursor hairpin structure.

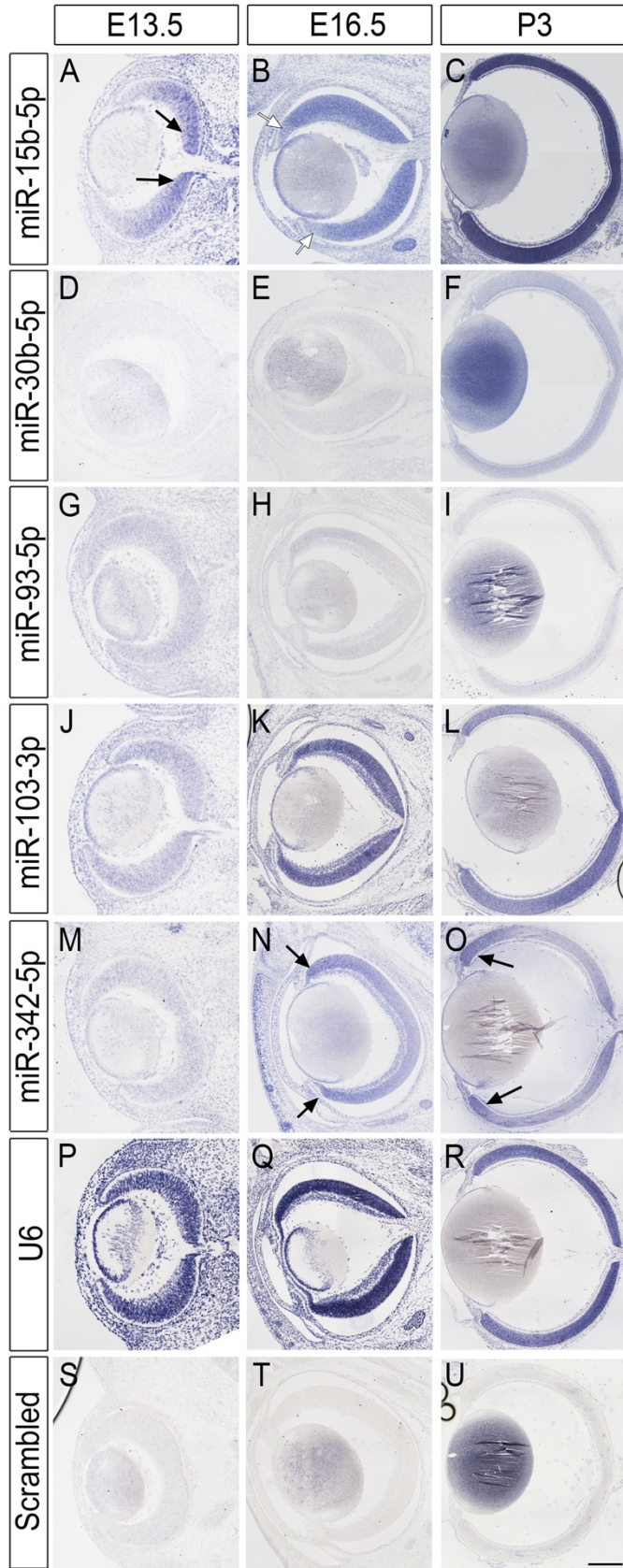


Figure 4.4 miRNA *in situ* hybridization in the mouse retina

(A-U) miRNA expression in the murine retina at E13.5, E16.5, and P3. Rows are labeled with the miRNA probe used, including U6 positive control and scrambled negative control. Each column shows a different developmental time point. Black arrows indicate increased expression in central **(A)** or peripheral **(N, O)** retina regions. White arrows indicate lower expression **(B)**. Scale bars: 40 microns for A, D, G, J, M, P and S (first column), 100 microns for B, E, H, K, N, Q and T (second column), and 500 microns in C, F, I, L, O, R and U (last column).

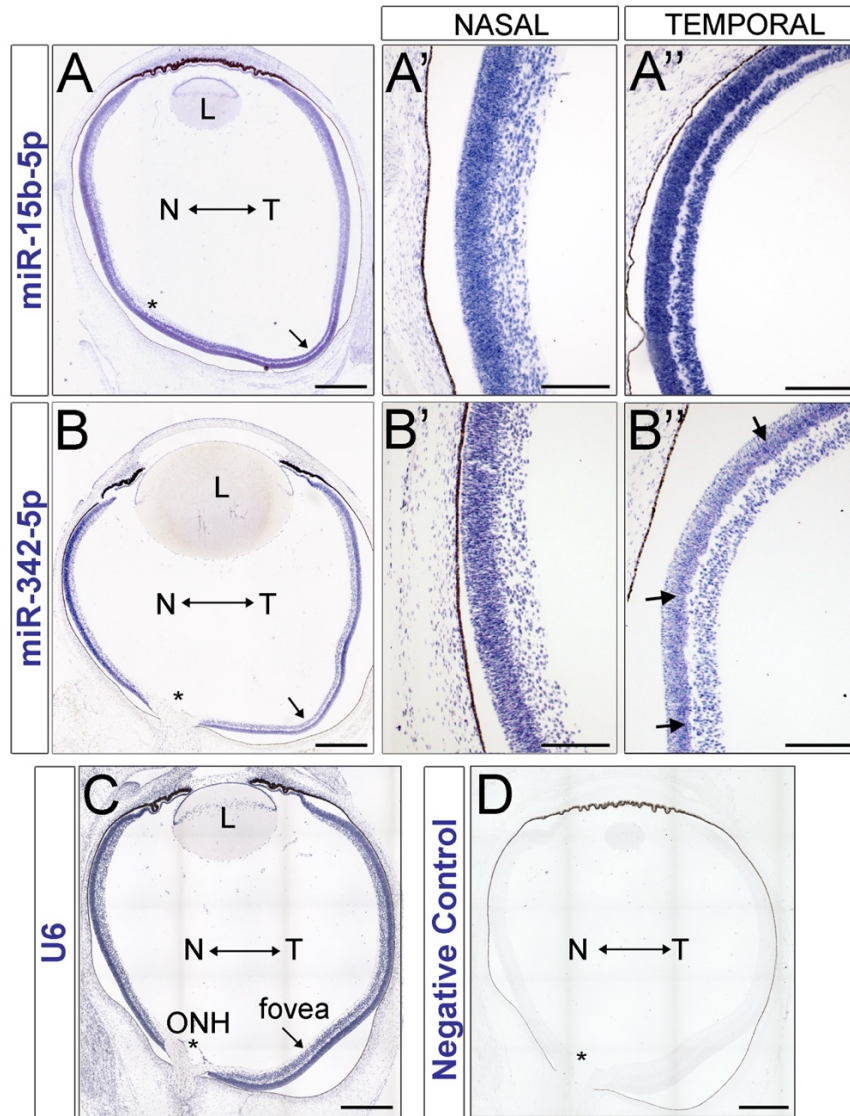
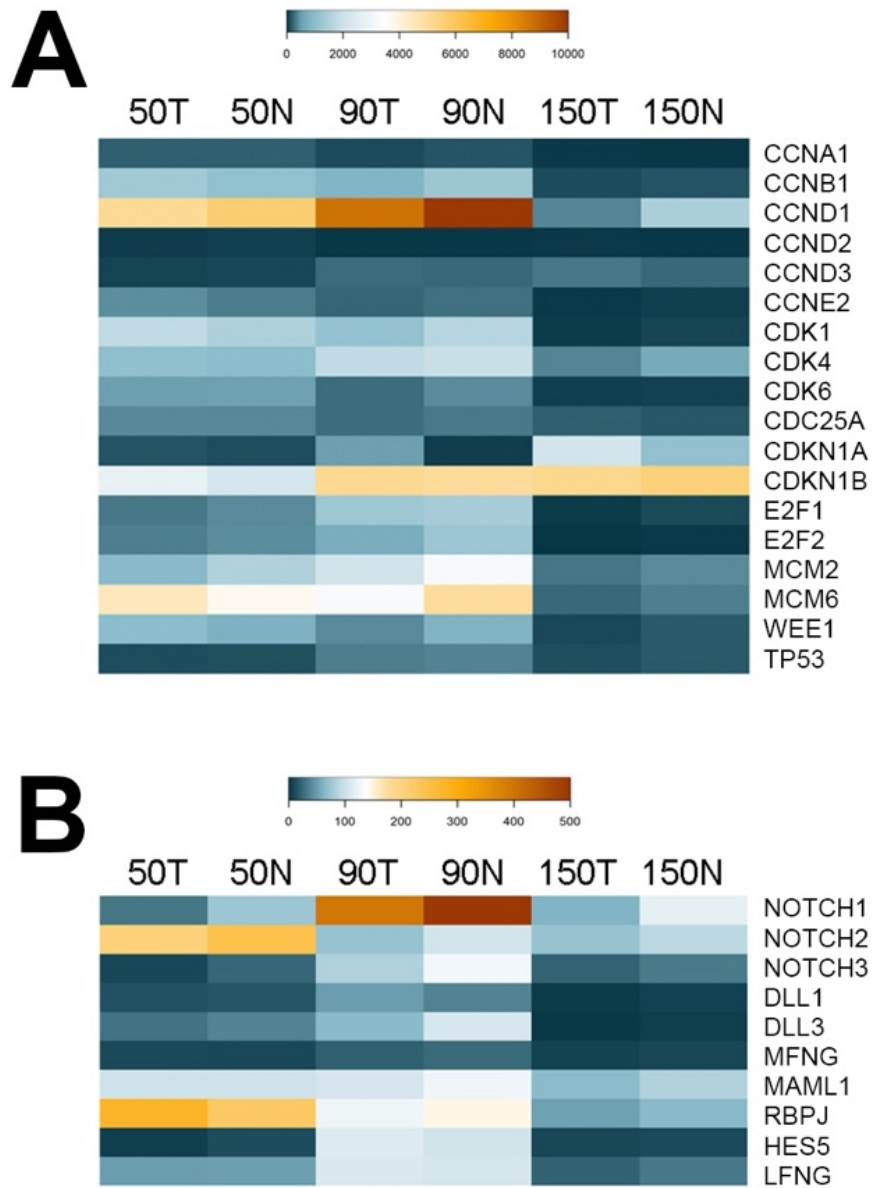


Figure 4.5 miRNA *in situ* hybridization in the human retina

(A-D) miRNA expression in the human fetal retina at 70-82 days gestation. miR-15b (A-A'') and miR-342-5p (B-B'') expression in the developing human retina. (A, B) tiled montage of the whole eye. (A', B') inset of nasal retina. (A'', B'') inset of temporal retina. (C) U6 positive control. (D) ISH negative control. Black arrows indicate the position of the presumptive fovea. L: Lens; N: Nasal; T: Temporal; ONH: Optic Nerve Head. Asterisks indicate the location of the optic nerve head and the arrows indicate the presumptive foveal region. Scale bars: 500 microns in A, B, C and D, 200 microns in A', A'', B' and B''.

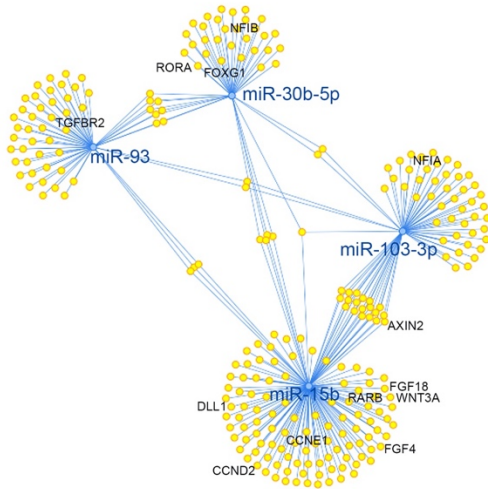
4.13 Supplementary figures



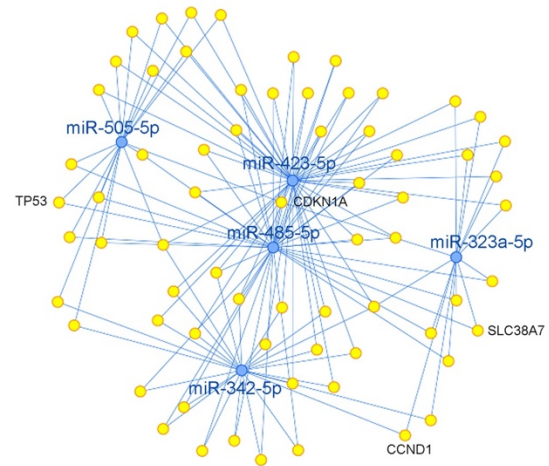
Supplementary Figure 4.1 (related to Figure 4.1)

(A-B) Heatmaps showing expression of cell-specific markers during *Macaca mulatta* retinal development. Comparisons between Temporal (T) and Nasal (N) data is shown at 50, 90 and 150 days gestational age. Expression of genes involved in (A) cell cycle and (B) Notch signaling pathway. All the data is expressed as CPMs.

A miRNA network temporal

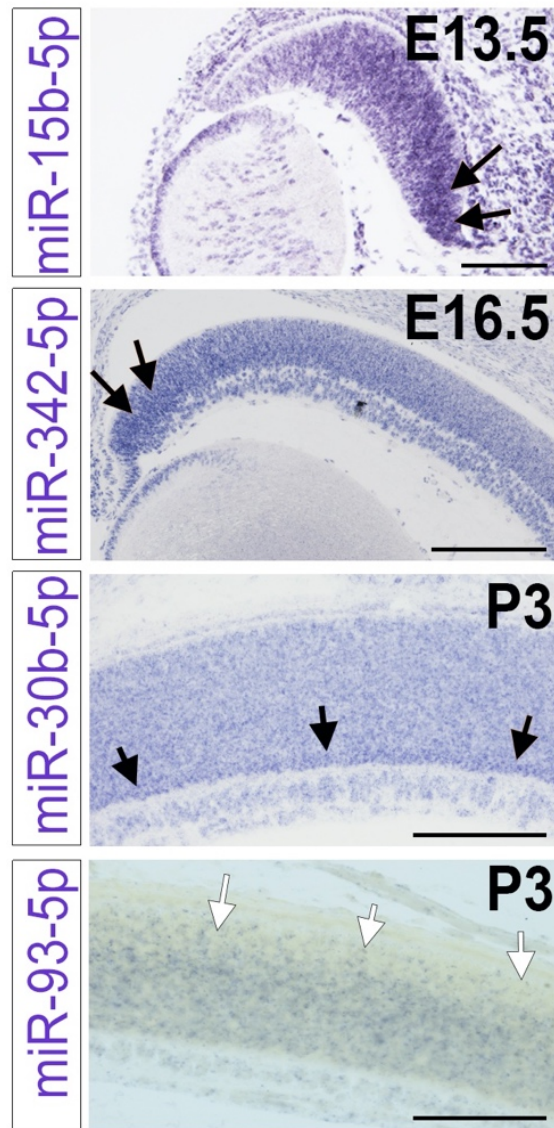


B miRNA network nasal



Supplementary Figure 4.2 (related to figure 4.2) MiENTURNET network analysis of differentially expressed miRNAs

(A) mRNA-miRNAs network of miRNAs enriched in the temporal samples. (B) mRNA-miRNAs network of miRNAs enriched in the nasal samples. miRNAs are indicated as blue dots, while target genes are yellow dots. Relevant targets genes are indicated.



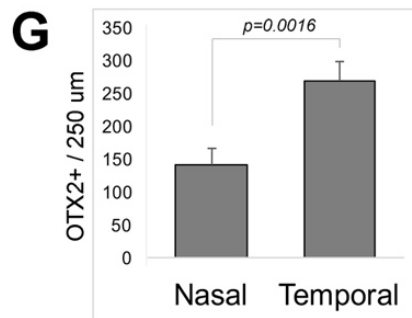
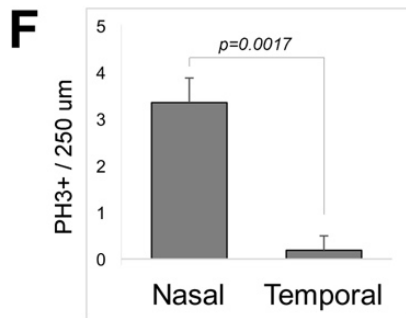
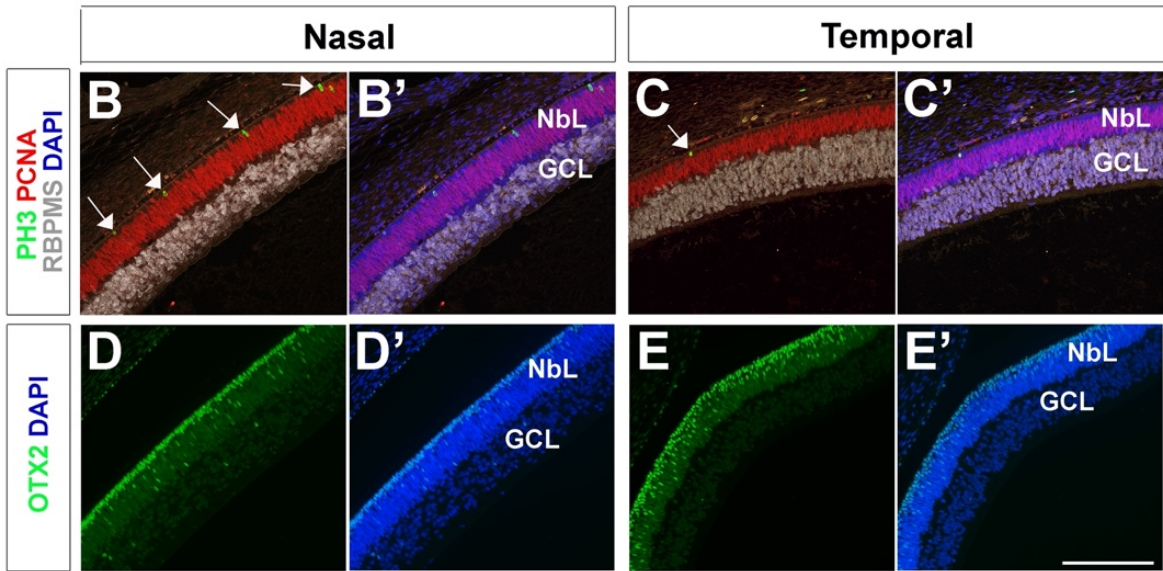
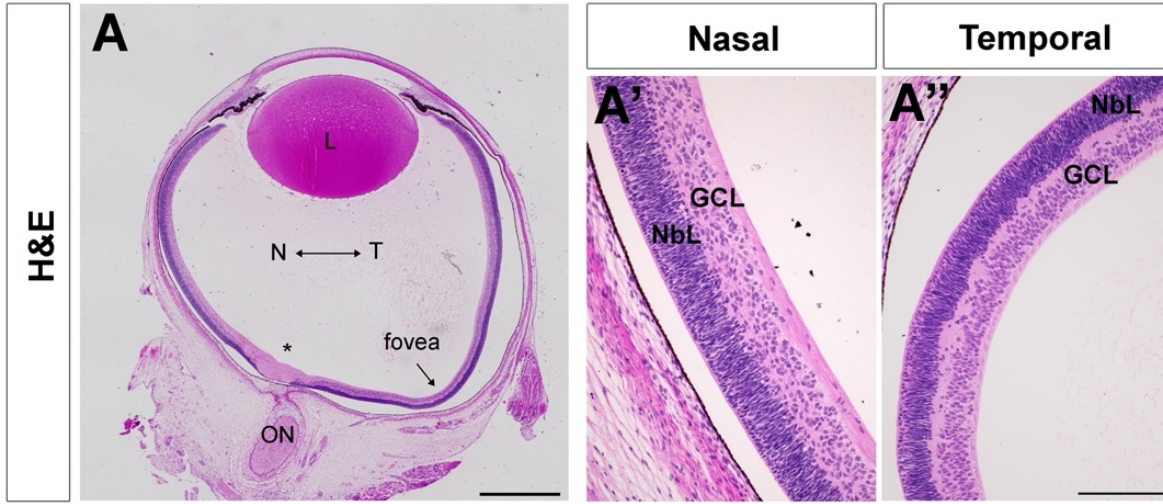
Supplementary Figure 4.3 (related to figure 4.4) Close-ups of miRNA *in situ* hybridization in the mouse retina

Black arrows indicate regions with higher expression level while white arrows indicate areas that display lower levels of expression. Scale bar: 100 microns for the top panel (miR-15b-5p) and 200 microns for the other panels.

	Mouse	Macaque		Human		
	<i>days</i>	<i>days</i>	%	<i>days</i>	<i>week</i>	%
Gestation	18.5	165		270	38	
RGC genesis	11-18	33-59	20-35	33-82	4.7-11.7	12-30
RGC peak	13	42	25	49	7	18
Cone peak	14	50	30	63	9	23
Rod genesis	15-25	52-102	30-61	68-192	10-27	25-71
Rod peak	21	81	62	134	19	50
Bipolar genesis	15-24	54-97	32-59	73-178	10-25	27-65
Bipolar peak	21	83	50	141	20	52
RGC apoptosis	26	108	65	208	30	77

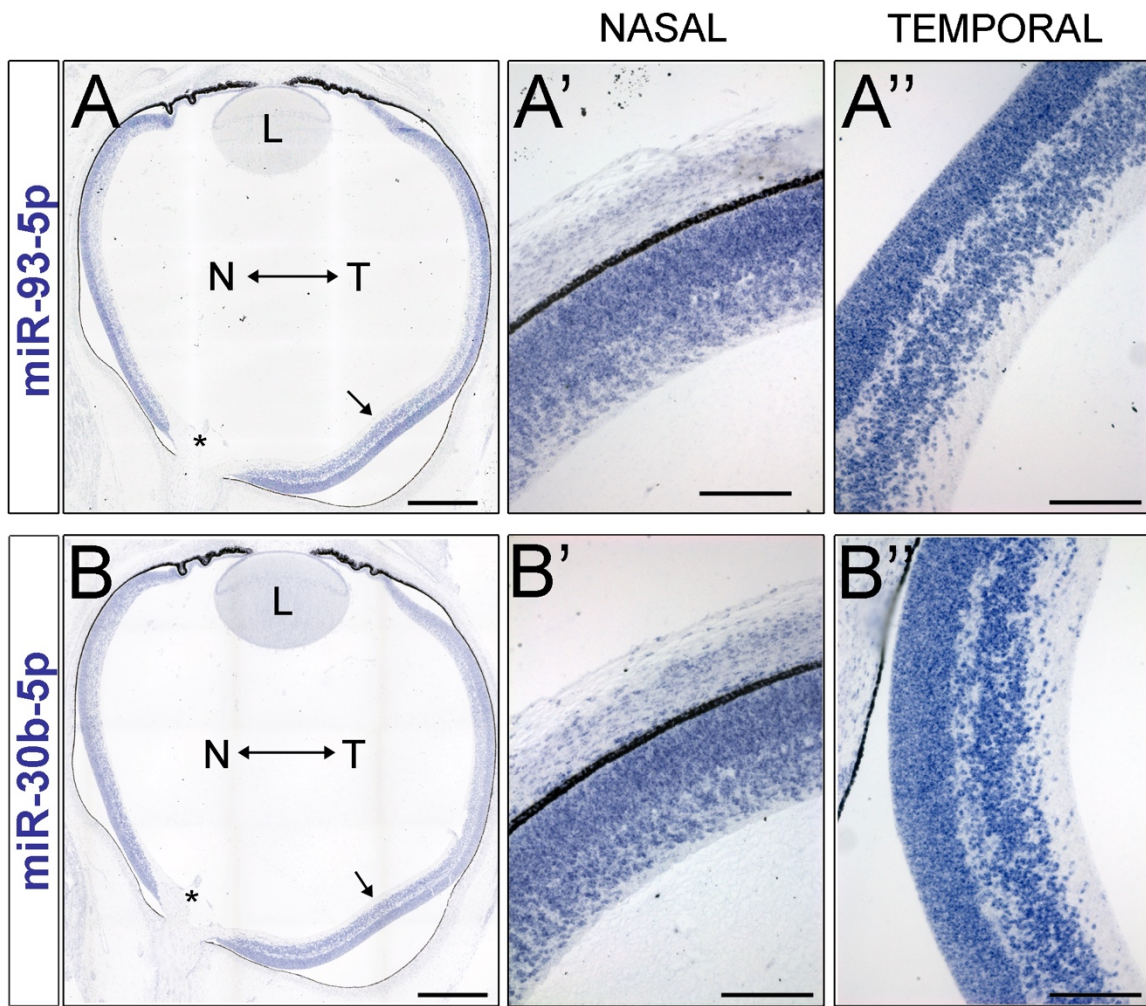
Supplementary Figure 4.4 Comparison between developmental timing in mouse, rhesus monkey, and human

The timing of key events during retinal histogenesis has been calculated using a prediction model previously published (translatingtime.org).



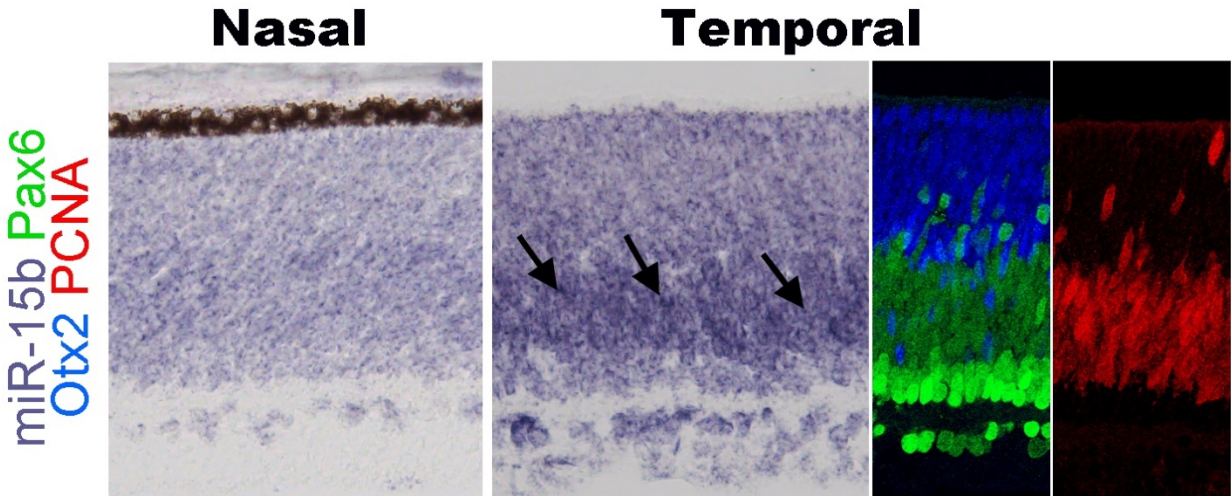
Supplementary Figure 4.5 (related to figure 4.5) Hematoxylin and eosin (H&E) staining and immunohistochemistry of human fetal retinas

(A-A'') H&E staining of human fetal retina at 77 days of gestation (H&E) staining. **(B-C')** Immunohistochemistry using PH3 (green, white arrows in B and C), PCNA (red), RBPMS (gray) antibodies and counterstained with DAPI. **(D-E')** OTX2 staining (green). The samples were also counterstained with DAPI (blue). **(F-G)** Quantification of the number of PH3+ **(F)** and OTX2+ cells **(G)** per 250 μm of retina in the temporal and nasal regions of the retina. L: lens, N: Nasal, T: Temporal, ON: optic nerve, NbL: neuroblastic layer, GCL: Ganglion cell layer, * indicates the localization of the optic nerve head. Scale bars: 500 microns in A, 200 microns in A'-E''. Error bars indicate standard deviation.



Supplementary Figure 4.6 (related to figure 4.5) miRNA *in situ* hybridization in the human retina

(A-D) miRNA expression in the human fetal retina at 70-82 days gestation. miR-93 **(A-A'')** and miR-30b **(B-B'')** expression in the developing human retina. Scale bars: 500 microns in A and B, and 200 microns in A', A'', B' and B''.



Supplementary Figure 4.7 (related to figure 4.5) Close-ups of miRNA *in situ* hybridization in the human fetal retina

miR-15b expression in the human fetal retina at 95 days gestation. miR-15b is enriched in the temporal progenitors (black arrows). Immunolabeling experiments using OTX2 (blue), PAX6 (green) and PCNA (red) using consecutive sections. Scale bar: 50 microns.

4.14 Supplementary Tables

Supplementary Table 4.1 mRNA-sequencing results of *Macaca mulatta* retinas

Supplementary Table 4.2 miRNA-sequencing results of *Macaca mulatta* retinas

Supplementary Table 4.3 MiENTURNET target enrichment for the temporal network

Supplementary Table 4.4 MiENTURNET target enrichment for the nasal network

Supplementary Table 4.5

Supplementary Tables 4.1 through 4.5: These are large tables that are not suitable for print. To view this data, please visit the official publication where all figure and supplemental information may be downloaded.

5. Published literature review: Oscillatory behavior of microRNA networks: emerging roles in retinal development

Elizabeth S. Fishman¹, Jisoo S. Han¹, and Anna La Torre^{1#}

¹ Department of Cell Biology and Human Anatomy, University of California Davis, Davis, 95616

Author for correspondence: alatorre@ucdavis.edu

The following chapter was submitted as a manuscript to *Frontiers in Cell and Developmental Biology* and published on February 2, 2022. The accepted version of this manuscript has been reformatted for this dissertation. The authors of the manuscript were Elizabeth S. Fishman (Elizabeth Fishman-Williams), Jisoo S. Han, and Anna La Torre.

5.1 Abstract

A broad repertoire of transcription factors and other genes display oscillatory patterns of expression, typically ranging from 30 minutes to 24 hours. These oscillations are associated with a variety of biological processes, including the circadian cycle, somite segmentation, cell cycle, and metabolism. These rhythmic behaviors are often prompted by transcriptional feedback loops in which transcriptional activities are inhibited by their corresponding gene target products. Oscillatory transcriptional patterns have been proposed as a mechanism to drive biological clocks, the molecular machinery that transforms temporal information into accurate spatial patterning during development. Notably, several microRNAs (miRNAs)—small non-coding RNA molecules—have been recently shown to both exhibit rhythmic expression patterns and regulate oscillatory activities. Here, we discuss some of these new findings in the context of the developing retina. We propose that miRNA oscillations are a powerful mechanism to coordinate signaling pathways and gene expression, and that addressing the dynamic interplay between miRNA expression and their target genes could be key for a more complete understanding of many developmental processes.

5.2 Key words

miR-183 cluster, let-7, miR-9, circadian rhythm, cell cycle, Notch

5.3 Introduction

The surge of new techniques to survey the transcriptome over the last few decades has led to the identification of numerous types of non-coding RNAs. While protein-coding sequences constitute less than 1.5% of the human genome, large-scale screenings have revealed that virtually the entire genome is transcribed to generate myriads of non-coding RNAs⁴²³⁻⁴²⁶. These RNA molecules are differentially expressed in distinct cell types and dynamically regulated during development^{427,428}.

Among non-protein coding RNAs, microRNAs (miRNAs) have emerged as key post-transcriptional regulators of gene expression⁴²⁹⁻⁴³¹. MiRNAs are small (~22-nucleotide (nt) long), evolutionarily conserved molecules. First described in *Caenorhabditis elegans*⁴³², miRNAs are also present in a wide diversity of organisms in the bacteria, archaea, and eukaryote domains⁴³³.

MiRNAs are transcribed from DNA sequences as long transcripts called primary miRNAs (pri-miRNAs) that contain double-stranded hairpin-like structures in which at least one of the two strands includes a mature miRNA (Figure 5.1). About half of all currently identified miRNAs are intergenic, mostly localized in introns, and controlled by the regulatory elements of the host gene; the other half are intragenic and are regulated independently by their own promoters¹⁷¹. About 25% of all miRNAs are arranged in clusters and transcribed as longer transcripts that contain more than one mature miRNA sequence. Intergenic miRNAs are processed by the splicing machinery while intragenic pri-miRNAs are cleaved by the microprocessor complex that includes Drosha ribonuclease and DiGeorge critical region 8 (DGCR8). In both cases, this first cleavage step produces a precursor miRNA (pre-miRNA) of about 70-nt that is exported out of the

nucleus. Pre-miRNAs are further processed by the enzyme Dicer, which removes the loop of the hairpin, yielding a mature miRNA duplex that can be loaded onto the RNA-Induced Silencing Complex (RISC, Figure 5.1). Mature miRNAs bind to their target mRNAs, usually to the 3' untranslated region (3'UTR), through imperfect base-pairing, hindering the stability and translation of their target mRNAs¹⁷⁶. Hence, miRNAs are part of complex networks where one individual miRNA can regulate a large number of genes, frequently from a similar biochemical pathway, and where a single target mRNA can be regulated concomitantly by multiple miRNAs. Thus far, about 2,500 mature miRNAs have been identified in the human genome (miRBase.org)⁴³⁴, and bioinformatics studies have estimated that over 60% of the human transcriptome is regulated by miRNAs¹⁷⁸.

A large body of research suggests that this previously unknown miRNA-based regulation is crucial for many physiological and pathophysiological events and that the complex interactions between transcription factors and miRNAs could be instrumental in delineating developmental programs.

5.4 miRNAs in the developing retina

To gain further understanding of the roles of miRNAs in ocular tissues, several groups have attempted to characterize the retina miRNome by *in situ* hybridization, computational predictions, and profiling techniques. Hundreds of different miRNAs have been identified in the retina of different species^{232,435-440} and several miRNAs show a significantly enriched expression in the retina compared to other tissues (Table 5.1). Two early reports by Hackler *et al.*⁴³⁸ and Xu *et al.*⁴³⁵ compared miRNA expression patterns at different developmental ages in the mouse retina and brain. Consistent with other

studies ⁴⁴¹, the authors found that miRNAs with identical seed sequences exhibited highly similar expression profiles. Additionally, these studies and others have defined the repertoire of miRNAs expressed at different time points during retinal development (Table 5.1). Two main miRNA categories have been consistently identified: miRNAs expressed primarily at early developmental stages (embryonic day (E)10-E16 in the mouse) and miRNAs present at later stages of retinal development (E16- postnatal day (P)7) and maturation (>P7). Specifically, miR-17, miR-18, miR-19, miR-20, miR-93, miR-106, and miR-130 are down-regulated throughout development while the let-7 family, miR-7, miR-9, miR-9*, miR-96, miR-101, miR-124, miR-181, miR-182, and miR-183 are some of the miRNAs that increase during retinal development from E10 to adulthood in mice. Additional studies have also identified cell-specific expression of subsets of these miRNAs (Table 5.1) ^{116,442,443}.

Dicer and DGCR8 transgenic models ^{116,186,187,279,415,444-448}, miRNA mutants ^{281,282,449}, sponge strategies ²⁸⁰, and miRNA inhibitors ^{187,380,450,451} have been extensively used to shed some light on the specific roles of miRNAs during retinal development. While many miRNA functions have been elucidated using these strategies, far less is known about miRNA target genes and the specific circuits that regulate development and pathophysiological processes in the retina. Furthermore, these global analyses do not capture the dynamic nature of miRNA expression and activity. Importantly, several miRNAs are involved in complex feedback and feed-forward regulations with their target genes, allowing for increased robustness of protein expression towards gene background noise ⁴⁵². MiRNAs also participate in negative feedback loops, where target mRNAs regulate miRNA expression leading to the occurrence of biological rhythms.

Correspondingly, miRNAs have been shown to display rhythmic behaviors in the retina and other organs, and to regulate the circadian clock, the cell cycle, and the Hes1 ultradian oscillator (Figure 5.2). Here, we summarize some of the recent findings on miRNA oscillatory behaviors, their regulatory mechanisms, and some of their possible functions during retinal development.

5.5 miR-183, -96, and -182 and the circadian clock

The textbook view of the circadian clock consists of a light-dark pattern of approximately 24 hours (Figure 5.2A) that governs rhythmicity within the organism and is regulated by two interwoven feedback loops with positive and negative components (Figure 5.3). One of these regulatory mechanisms involves the heterodimeric transcriptional activators CLOCK and BMAL1, which trigger the expression of repressors such as Period (PER1, PER2, and PER3) and Cryptochrome (CRY1 and CRY2) that, in turn, will repress the transcriptional activity of their activators ⁴⁵³⁻⁴⁵⁵. The second loop involves the expression of Rev-Erba and Rora genes also regulated by CLOCK and BMAL1. Subsequently, REV-ERBa and RORa proteins compete for binding to the Bmal1 promoter ⁴⁵⁵. These self-sustaining feedback clocks are reset by fluctuating inputs, including light, temperature, or feeding patterns, to synchronize the molecular clock with the environment and the Earth's rotation. This timing mechanism is controlled by a master pacemaker in the suprachiasmatic nuclei (SCN) of the hypothalamus, but independent circadian oscillators are present throughout the organism. Studies in the early 80s already demonstrated that the circadian clock was present in the *Xenopus* retina ⁴⁵⁶, and further analyses have added that the retinal circadian rhythm controls many aspects of the

vertebrate ocular physiology, including melatonin and dopamine synthesis, photoreceptor disk shedding, visual sensitivity, and intraocular pressure⁴⁵⁷⁻⁴⁶¹. Dysregulation of these retinal circadian clocks can lead to ocular diseases and have impacts on the circadian rhythm of the whole body⁴⁶².

Mathematical modeling predicted decades ago that the regulation of mRNA stability is essential for rhythmic protein output⁴⁶³. More recently, high-throughput analyses have shown that 25-50% of all rhythmically expressed proteins do not exhibit transcriptional rhythmicity⁴⁶⁴. Accordingly, instead of the simplified transcription-translation view, the circadian rhythm undergoes very complex and dynamic regulatory processes that include polyadenylation, RNA splicing, and miRNA regulation.

Numerous miRNAs exhibit circadian rhythmicity, although the mechanisms that regulate these oscillations often remain unclear. In some cases, miRNA coding regions contain E-Box or RORE upstream elements that could be regulated by the core components of the circadian clock⁴⁶⁵. Dicer expression has also been reported to display diurnal rhythmicity⁴⁶⁶, which could lead to a rhythmic pattern of miRNA maturation.

By means of microarray technologies and other tools, early screenings identified the miR-183 cluster (miR-183, miR-96, and miR-182) as miRNAs robustly regulated by the circadian clock^{467,468}. For instance, circadian fluctuations in *dme*-miR-263a and *dme*-miR-263b expression, the *Drosophila* orthologues of the miR-183 cluster, were detected in wild type flies and the levels of these miRNAs were significantly reduced in the arrhythmic clock mutant *cyc*⁰¹⁴⁶⁸. Likewise, in the adult mouse retina, the expression of these miRNAs obeys a circadian rhythm, with the miRNA levels being significantly higher during zeitgeber time (ZT) 17 (midnight) compared to ZT 5 (noon)⁴⁶⁷. The expression of

these miRNAs is also regulated by light in the mammalian retina and the total levels of miR-183, miR-96, and miR-182 shift quickly (within 30 minutes) after light or dark adaptation ⁴⁶⁹.

MiR-183, -96, and -182 are part of a highly-conserved polycistronic miRNA cluster that plays multiple roles in sensory tissues including the retina ^{467,470}, the inner ear ⁴⁷¹, and the olfactory epithelium ⁴⁶⁷. In the vertebrate retina, this cluster has been shown to elicit neuroprotective functions in photoreceptors, modulate outer segment maintenance, and enhance light responses in stem cell-derived retinal organoids ^{281,415,469,472}. Many reports indicate that the miR-183 cluster is a key regulator of apoptosis and programmed cell death and validated target genes include CASP2, FOXO1, SLC1A1, and PDCD4 ⁴¹⁶. Recent studies have indicated that the miR-183 cluster is also an important morphogenetic factor regulating multiple signaling pathways involved in photoreceptor differentiation and maintenance. In this direction, the miR-183 cluster targets PAX6 ⁴⁷³, a highly conserved paired-box transcription factor that is critical for eye morphogenesis in a wide range of species ^{325,326,474,475}.

The exact mechanisms that regulate the oscillatory expression of this miRNA cluster are not well understood. The putative promoter region of the miR-183 cluster contains several binding sites for transcription factors known to regulate the circadian rhythm in the eye, including ROR α ⁴⁶⁷, but there is currently no experimental data to confirm this transcriptional regulation. Genetic variants with abnormal processing of pre-miR-182 have been described ⁴⁷⁶ and neuronal miRNAs have been shown to have very quick turn-over ratios ⁴⁶⁹ compared to nonneuronal cells ^{469,477,478}. Thus, the regulation of

miRNA processing and/or degradation could also play important roles in its oscillatory behavior.

A recent phenotype-driven genome-wide miRNA screen using reporter human cell lines identified several miRNAs with the potential to modulate circadian rhythms ⁴⁷⁹. Among 989 miRNAs tested, this study identified 120 miRNAs that significantly changed the period length in a dose-dependent manner, including let-7, miR-17, and the 183 cluster. Importantly, these changes were tissue-specific and the inactivation of the miR-183 cluster shortened the circadian period in the retina but did not change the period length of the SCN in mice. All three members of the miR-183 cluster can modulate circadian rhythms and luciferase-based assays have shown that miR-182 potentially targets CLOCK ⁴⁷⁶ as well as the circadian rhythm regulators ADCY6 and MITF ⁴⁶⁷, while miR-96 directly targets PER-2 ⁴⁷⁹ (Figure 5.3). Similarly, experimental evidence in zebrafish indicates that miR-183 targets other circadian regulators such as E4BP4-6 and AANAT2 ⁴⁸⁰. However, these results do not exclude possible additional regulation through non-cell autonomous mechanisms.

Finally, while it is not known whether the oscillatory behavior of miR-183 has any effects on retinal development, the removal of circadian clock genes led to defective dorso-ventral patterning of cones, thinner inner retinal nuclear and plexiform layers, and reduced photoreceptor viability ^{481,482}. Future studies might shed light on the role of the miR-183 cluster in these phenotypes and the interplay between the circadian rhythmicity and miRNA roles in photoreceptor differentiation and function.

5.6 Let-7 levels oscillate with the cell cycle in the embryonic retina

The cell cycle is a precisely regulated oscillatory process essential for growth and maintenance of tissues as well as for coordinating the timing of major cellular events during development. The cell cycle is classically divided into four different phases: Gap1 (G1), DNA Synthesis (S), Gap2 (G2), and Mitosis (M)⁸⁸. The ability of the cells to progress through these phases to ultimately produce two daughter cells is generally attributed to two classes of molecules: Cyclin-dependent kinases (CDKs), a large family of serine/threonine kinases, and their binding partners named Cyclins because their concentration varies in a cyclical manner⁸⁹. The abundance of individual Cyclins, and the consequent activation of the appropriate CDKs at specific phases, orchestrates the orderly completion of DNA replication and cell division and constitutes the core cell cycle oscillator (Figure 5.4). Thus, CyclinD/CDK4,6 activity ensures G1 progression, CyclinE/CDK2 promotes the G1/S transition, while CyclinA/CDK2 regulates the transition between S and G2. Finally, CyclinB/CDK1 warrants the G2/M transition and entry of cell into mitosis⁸⁹. However, cell cycle progression is not only regulated by the rise and fall of Cyclin molecules' concentrations, but is tightly regulated at several levels and through many different mechanisms (Figure 5.4).

The first studies on miRNAs published three decades ago already suggested a role for the miRNA let-7 in the cell cycle of *C. elegans*^{483,484}. Let-7 is part of the heterochronic pathway required in the nematode seam cells to determine the timing of stage-specific developmental events^{485,486}. Since then, numerous studies have revealed that let-7 is a master regulator of cell proliferation. Accordingly, let-7 alters cell cycle

progression, controls the timing of cell cycle exit, and inhibits self-renewal, and disruptions in let-7 coding genes can enhance oncogenic transformation ⁴⁸⁷⁻⁴⁸⁹.

Elegant genetic studies from the Ruvkun laboratory ^{490,491} revealed that let-7 is a genetic switch that controls major developmental transitions in bilaterally symmetrical animals, from flies and worms to vertebrates. In the developing mammalian retina, let-7 regulates the developmental transition that allows the retinal progenitors to generate the late cell types (amacrine cells, rod photoreceptors, bipolar cells, and Müller glia) ^{187,492}, and also plays a central role in Müller glia-dependent regeneration ^{380,493}. Similar roles have been described in other parts of the developing CNS, where let-7 is required for the generation of the later cell populations in different species ^{188,381,494}.

In the developing retina, let-7 regulates cell cycle kinetics by both promoting cell cycle exit and lengthening S/G2 phases ²⁷⁶. Notably, no differences were detected in G1 length in time-lapse experiments using the fluorescent reporter FUCCI (Fluorescence Ubiquitination-based Cell Cycle Indicator) in combination with gain-of-function or loss-of-function of let-7 ²⁷⁶. Given that let-7 levels normally increase throughout developmental time in the retina ^{187,492,495} (Table 5.1), these data correlate with classic experiments using ³H-thymidine cumulative labeling that indicated that the cell cycle lengthens during retinal development mainly due to an increase in S-phase length ⁴⁹⁶.

The cell cycle proteins CDC25A, CDC34, CDK4, CDK6, Cyclin A, Cyclin D1, D2, and D3 are known let-7 targets ⁴⁹⁷ (Figure 5.4) as well as TLX ⁴⁸⁸, another cell cycle regulator, and oncogenic chromatin proteins such as HMGA1 and HMGA2 ^{492,498}. However, since the specific effects of let-7 overexpression or inhibition are different in different experimental paradigms (e.g., induction of cell cycle arrest vs cell cycle

lengthening), let-7's ability to target these genes may be concentration and/or context dependent. Similarly, the human genome contains 10 different mature miRNAs in the let-7 family (let-7a, let-7b, let-7c, let-7d, let-7e, let-7f, let-7g, let-7i, mir-98, miR-202), produced from 13 precursor sequences. As each of these miRNAs have identical seed sequences and highly conserved regions for target recognition and thus, the individual roles and targets for each let-7 are not well characterized.

Strikingly, not only does let-7 regulate developmental transitions and cell cycle, but its expression and activities also oscillate concurrently with the cell cycle across the developing CNS, including the retina ²⁷⁶ (Figure 5.2B). Neural progenitors undergo interkinetic nuclear migration between the apical and basal surfaces in concert with the cell cycle ^{86,499,500}. Thus, mitotic cell bodies are only found in the apical surface, and cell somas move basally in G1. Cells in S-phase are found at the most basal positions, which move again apically in G2. Intriguingly, let-7 levels also fluctuate within these regions, suggesting that let-7 oscillates in coordination with cell cycle ²⁷⁶. Mathematical modeling also supports that oscillatory levels of let-7 are required for the complex balance between let-7 and Cyclin/CDK complexes ⁵⁰¹ and more recently, these fluctuations have been validated by flow cytometry analyses and time-lapse imaging ²⁷⁶.

The cell cycle-dependent fluctuation of let-7 suggests that some cell cycle genes may be regulating its expression; however, given that the let-7 family is located in 13 different loci in the genome, the transcriptional regulation of these miRNAs is still poorly understood. E2F transcription factors have been shown to directly regulate let7a-d and let-7i expression and c-MYC represses the expression of several let-7 clusters ⁴⁹⁷. Additionally, CyclinD1 can regulate the expression of Dicer ⁵⁰² and thus, cell-cycle

dependent miRNA processing may have an impact on let-7 fluctuations. Consistent with this idea of negative feedback loops, the miRNA machinery can be directly regulated by miRNAs and for example, a loop involving let-7 and Ago2 is critical to maintain pluripotency⁵⁰³. Importantly, miRNA stability and turn-over rates could also be regulated in a cell cycle-dependent manner.

The specific role(s) of the periodicity of let-7 expression and activity have not been previously explored but it can be speculated that cell cycle-coupled miRNA oscillatory circuits may be an important strategy to coordinate division rates with complex cellular activities as well as the timing of cell cycle exit and fate decisions.

5.7 miR-9 is part of the Notch ultradian oscillator

Proper retina development relies on the tight balance between retinal progenitor cell (RPC) proliferation and differentiation. It is well-documented that Notch activation perpetuates RPC maintenance, whereas Notch pathway disruption leads to neuronal differentiation^{97,504-507}. Notch also regulates neural patterning^{508,509}, cell fate specification^{96,510,511}, is essential for Müller glia development⁵¹²⁻⁵¹⁴, and a key mediator of regeneration^{515,516}. Together, a growing body of literature supports the notion that the Notch pathway is dynamic and remarkably pleiotropic, and that the timing and levels of Notch signaling must be precisely regulated to maintain the temporal control driving normal retinal development.

Since the Notch receptor was first identified in *Drosophila* over 100 years ago⁵¹⁷, genetic and molecular interaction studies have helped map the Notch signaling pathway that is recognized today (Figure 5.5) (reviewed in^{386,518,519}). Briefly, the intracellular

signaling pathway is initiated by cell-cell contacts, where the transmembrane Notch receptor (Notch1-4) on one cell is activated by a ligand (Delta-like (Dll1, Dll3, and Dll4), or Jagged (Jag1 and Jag2)) on a neighboring cell. Ligand binding prompts a series of proteolytic cleavage events that culminates in the release of the Notch receptor's intracellular domain (NICD). NICD translocates into the nucleus, where it forms a transcriptional complex with Rbpj (recombination signal-binding protein for immunoglobulin kappa J region) and Maml1 (Mastermind-like transcriptional co-activator 1) to activate gene expression. The best characterized Notch targets are the Hes (Hes1, Hes3, and Hes5) and related Hey genes⁵²⁰, which encode inhibitory basic helix-loop-helix (bHLH) proteins that suppress pro-neural bHLH genes Ngn1, Ngn2 (Neurogenins 1-2), NeuroD1, NeuroD2, NeuroD4, NeuroD6 (Neuronal Differentiation 1-2,4,6), and Ascl1 (Acheate-Scute)^{521,522}. Importantly, Hes proteins also repress the expression of Notch ligands, affecting the Notch activity of their neighbors⁵²³.

These cross-regulatory activities raise a hypothetical problem: in the absence of Hes1, cells prematurely differentiate into neurons but then, how is the progenitor pool maintained if Hes1 reduces Notch signaling in neighboring cells? Several pioneering studies from the Kageyama laboratory solved the conundrum and showed that the expression of Hes1, Ascl1, and Dll1 display oscillatory behaviors (Figure 5.2C top) using luciferase-based reporters in several contexts⁵²⁴, including neural progenitors^{525,526}. These oscillatory expression patterns are driven by the Hes1 oscillator⁵²⁷. Hes1 protein represses its own expression by binding to N-box regulatory elements in the Hes1 promoter, and both Hes1 protein and mRNA have very short half-lives. Thus, upon repression, the levels of Hes1 decline rapidly leading to the reactivation of Hes1

transcription with a rhythmicity of 2-3 hours⁵²⁷. These oscillations are key in maintaining pools of progenitor cells from precociously differentiating; when Hes1 oscillations are quenched, even if the Notch signaling pathway can still be activated, neural progenitors undergo premature cell cycle exit⁵²⁸. Importantly, these rhythmic patterns can in part explain the heterogeneity of gene expression observed in individual RPCs with “snapshot” techniques such as immunostaining and sequencing^{17,112,529,530}.

Many signaling pathways are common beneficiaries of miRNA-mediated regulation, and the Notch pathway is no exception^{531,532}. In fact, functional relationships between Notch and miRNA pathways have been described in the developing retina as Dicer conditional knockout mice showed downregulation of Notch pathway components and at the same time, overexpression of NICD in Dicer-null retinas did not lead to classic “Notchy” phenotypes such as induction of glial fates²⁷⁹.

MiR-9, a miRNA highly expressed in the developing CNS, interacts with Notch components in several organisms⁵³³. Target prediction analyses have shown that miR-9 may directly target components of the Notch pathway, including Notch ligands, Rbpj, and Maml1⁵³⁴. Additionally, bioinformatics analyses have identified miR-9-binding sites in mouse, rat, and human *Hes1*⁵⁰⁹, zebrafish *her5* and *her9*⁵³⁵, and *Xenopus hairy1*⁵³⁶. Manipulation of miR-9 activity by antisense inhibitors resulted in increased levels of Hes1, and overexpression of miR-9 conversely reduced the half-life of Hes1⁵³⁷.

In humans, miR-9 is transcribed from three independent genomic loci (pri-miR-9-1, pri-miR-9-2, and pri-miR-9-3) that give rise to two functional miRNAs, mir-9-5p and miR-9-3p. Hes1 reduces miR-9 expression, as observed by *in situ* hybridization of pri-miR-9-2 in the mouse cortex and binds to several N-boxes in the putative miR-9

promoters of all three miR-9 genes (Figure 5.6). However, Hes1 only regulates the expression of pri-miR-9-1 and pri-miR-9-2, but not pri-miR-9-3⁵³⁷. These promoters are embedded within CpG islands and thus, they could also be regulated by epigenetic mechanisms or other indirect means.

Importantly, the cross-regulations between miR-9 and Hes1 (Figure 5.6) also contribute to the Hes1 oscillator, and overexpressing or inhibiting miR-9 has been shown to reduce Hes1 oscillations⁵³⁷. The negative feedback loops between miR-9 and Hes1 creates an out-of-phase oscillatory pattern of expression (Figure 5.2C top), which is important for limiting Hes1 oscillations⁵³². As development continues, miR-9 accumulates (due to its longer half-life than the less-stable Hes1 mRNA and protein) until it reaches a threshold for differentiation⁵²⁸. At that point, Hes1 oscillations are dampened, and miR-9 maintains high, steady levels allowing for neural differentiation to proceed (Figure 5.2C bottom)⁵³⁷. Although oscillations of miR-9 have not been observed directly, mathematical modelling analyses incorporating miR-9 into the Hes1 oscillator recapitulate the behaviors observed experimentally⁵³⁸.

During retinal development, miR-9 expression increases in RPCs over developmental time and regulates cell fate acquisition¹⁸⁷, but miR-9 is also important in the mature mouse retina to maintain homeostasis of the Müller glia⁵³⁹ and can potentiate Müller glia conversion into progenitor-like cells in culture in combination with miR-124³⁸⁵. While the molecular mechanisms downstream of these functional roles remain widely unexplored, it can be speculated that the oscillatory interplay between Notch and miR-9 in combination with the increasing levels of mature miR-9 over time may be one of the mechanisms that enables cells with an ability to keep track of time while maintaining the

ability to adapt to external stimuli. This model accommodates the existing evidence indicating that fate decisions during retinal development are both cell autonomous and strongly influenced by external factors.

Recently, a novel CIS-regulatory element of pri-miR-9-2 has been described for its association with retinal diseases such as Macular Telangiectasia Type 2 and Macular degeneration⁵⁴⁰. Interestingly, the deletion of this enhancer leads to reduced miR-9 levels, a decrease in the number of rod photoreceptors, and perturbation of Müller glia homeostasis in human retinal organoids. Transcriptional data indicates that the Notch pathway is affected in these cells but the exact nature of this regulation and whether the oscillatory behaviors and feedback loops between Notch and miR-9 play any roles have not yet been investigated.

5.8 Conclusions and perspectives

During normal development, different cell fates are specified with exquisite spatial and temporal accuracy. Oscillatory feedback circuits that integrate temporal cues are part of the machinery that establishes the robustness of developmental transitions and progenitor outcomes. It is now obvious that miRNAs are functionally integrated in many of these oscillatory pathways. Beyond the examples offered in this review, a reciprocal relationship between miRNAs and transcription factors that in turn regulate miRNA expression may be a common theme in a variety of developmental contexts.

Despite all the evidence accumulated in the last few years, we are only starting to understand the relevance of these rhythmic behaviors, largely because most of the miRNA expression data to date comes from studies that used sequencing technologies

that do not capture dynamic changes of expression within a cell. Thus, efforts to develop tools to show miRNA levels longitudinally with cellular resolution need to be advanced.

In addition, our understanding of miRNA transcriptional regulation is still quite limited. The complex regulation of miRNA processing and turn-over may similarly open new avenues to further understand the regulatory networks that govern neural development.

5.9 Author contributions

ESF and ALT wrote the manuscript. JSH and ALT created the figures, and ESF, JSH and ALT reviewed the manuscript.

5.10 Conflict of interest

The authors declare that the research was conducted in the absence of any commercial or financial relationships that could be construed as a potential conflict of interest.

5.11 Funding

This work was supported by a grant from NIH (R0EY026942; ALT) and support from a training grant (T32 to ESF).

5.12 Acknowledgements

We thank all the members of the La Torre and Simó laboratories for their support.

5.13 Figures

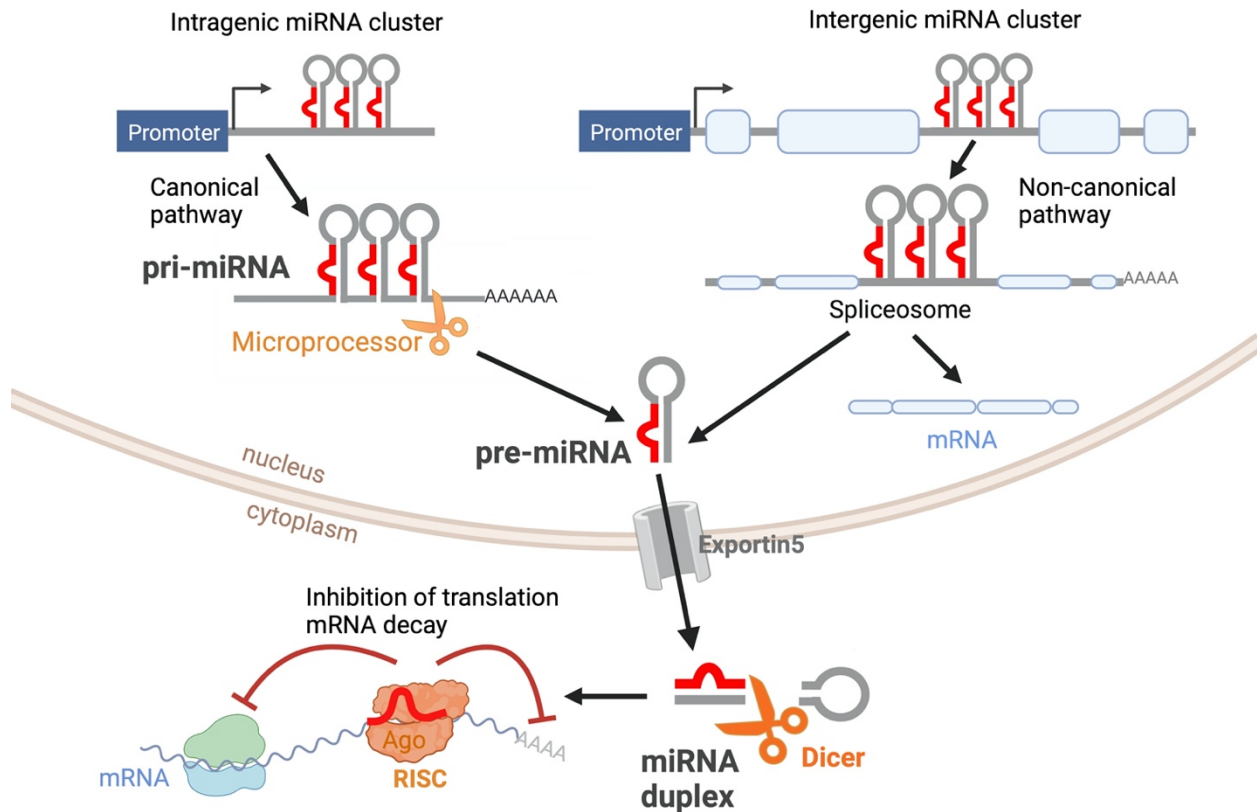


Figure 5.1 miRNA biogenesis

Primary miRNAs (pri-miRNAs) are transcribed as double-stranded hairpin-like structures. Intragenic pri-miRNAs are processed via the canonical pathway, where the clusters of hairpin-like structures are cleaved into individual precursor miRNAs (pre-miRNAs) by the microprocessor complex. Intergenic pri-miRNAs are processed by the splicing machinery. The resultant pre-miRNA from both pathways is an individual hairpin-like structure of 70-nt. After being exported from the nucleus via Exportin5, pre-miRNAs are further processed by Dicer into mature miRNA duplexes. One miRNA strand is loaded into the RNA-Induced Silencing Complex (RISC). Mature miRNA binds to its target mRNA, inhibiting mRNA translation and inducing mRNA decay. This figure was created with BioRender.com.

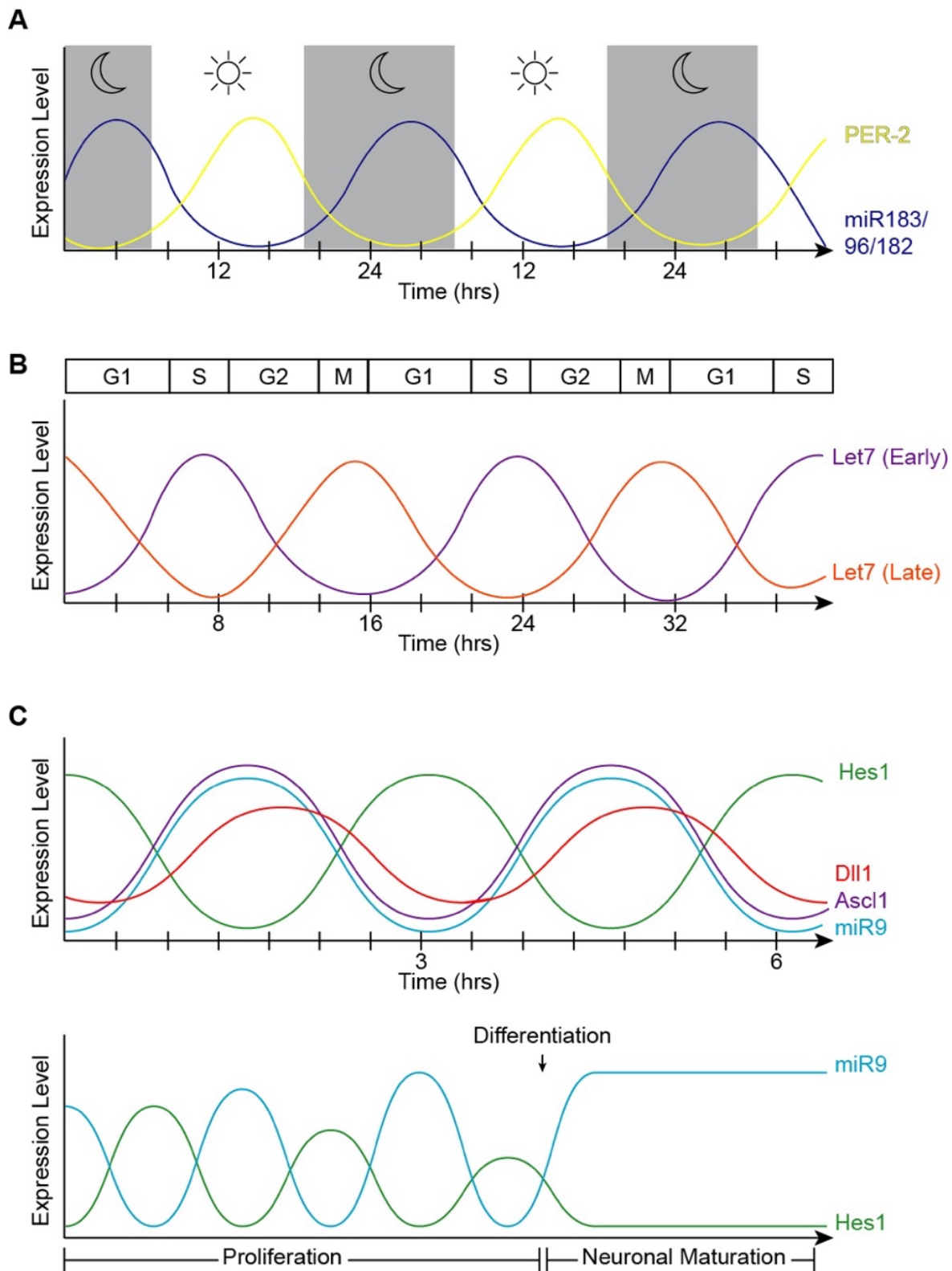


Figure 5.2 Oscillatory patterns of miRNAs in biological processes

(A) Oscillatory behavior of the miR-183 complex. miR-96 directly targets PER2, causing an out-of-phase oscillation pattern with PER-2 peaking during light and miR-183/96/182 peaking in dark hours. **(B)** Let-7 oscillatory behavior. The fluctuation of let-7 expression in accordance with the cell cycle changes at different stages of development. Early in development (let-7 early), let-7 expression is at its lowest at the start of the cell cycle in G1, and peaks in S-phase. The phase of oscillation shifts later in development (let-7 late), when let-7 expression is at its highest in mitosis and lowest in S-phase. **(C)** Hes1/miR-9 ultradian oscillator. **(Top)** Hes1 oscillation is self-driven with a rhythmicity of 2-3 hours. The Hes1 oscillator represses Ascl1 and Notch ligands, consequently driving their oscillation patterns. MiR-9 and Hes1 participate in a negative feedback loop, creating an out-of-phase expression pattern. **(Bottom)** Hes1 and miR-9 have out-of-phase expression patterns and are dependent on one another. As miR-9 continues to accumulate during proliferation, Hes1 is consequently dampened. RPC differentiation is induced when miR-9 levels reach a threshold to maintain high, steady levels while dulling Hes1 oscillations, resulting in neuronal maturation.

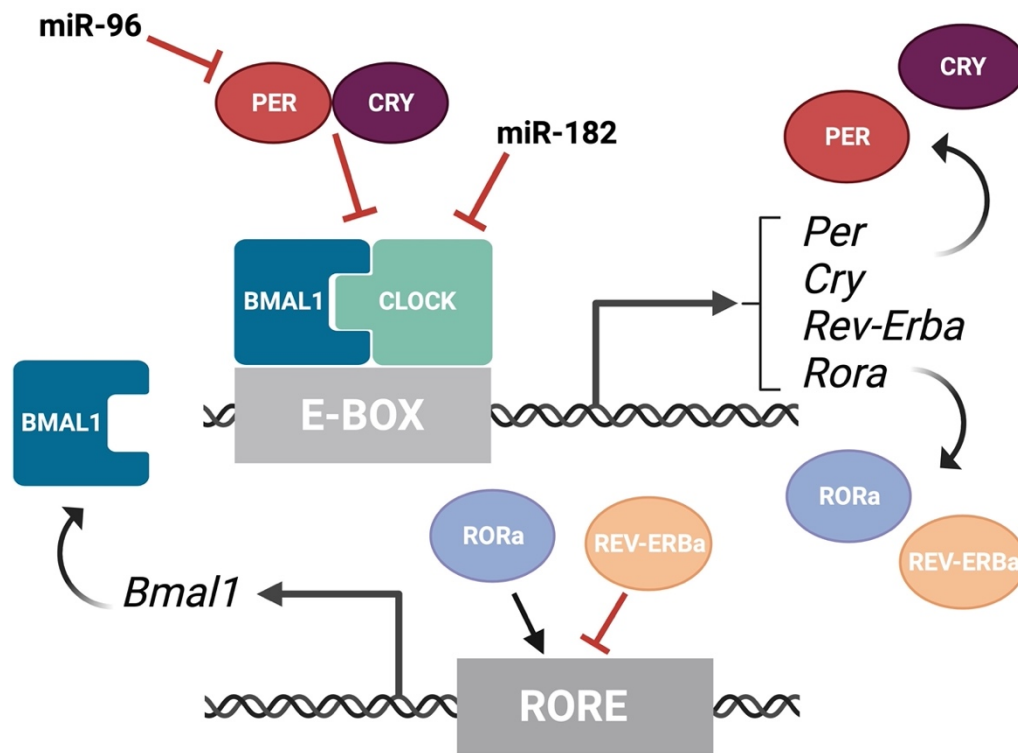


Figure 5.3 Overview of the molecular components of the circadian rhythm

Circadian rhythm is regulated by two interwoven feedback loops. The first loop involves CLOCK and BMAL1 activating regulatory elements containing E-boxes to induce expression of repressors. PER and CRY proteins bind to CLOCK/BMAL1 to repress the transcriptional activity of their activators. PER and CRY proteins bind to CLOCK/BMAL1 to repress the transcriptional activity of their activators. MiR-182 targets CLOCK, among other circadian rhythm regulators, and miR-9 targets PER-2. The second loop involves REV-ERBa and RORa competing for binding on RORE binding elements, which promotes Bmal1 transcription. This figure was created with BioRender.com.

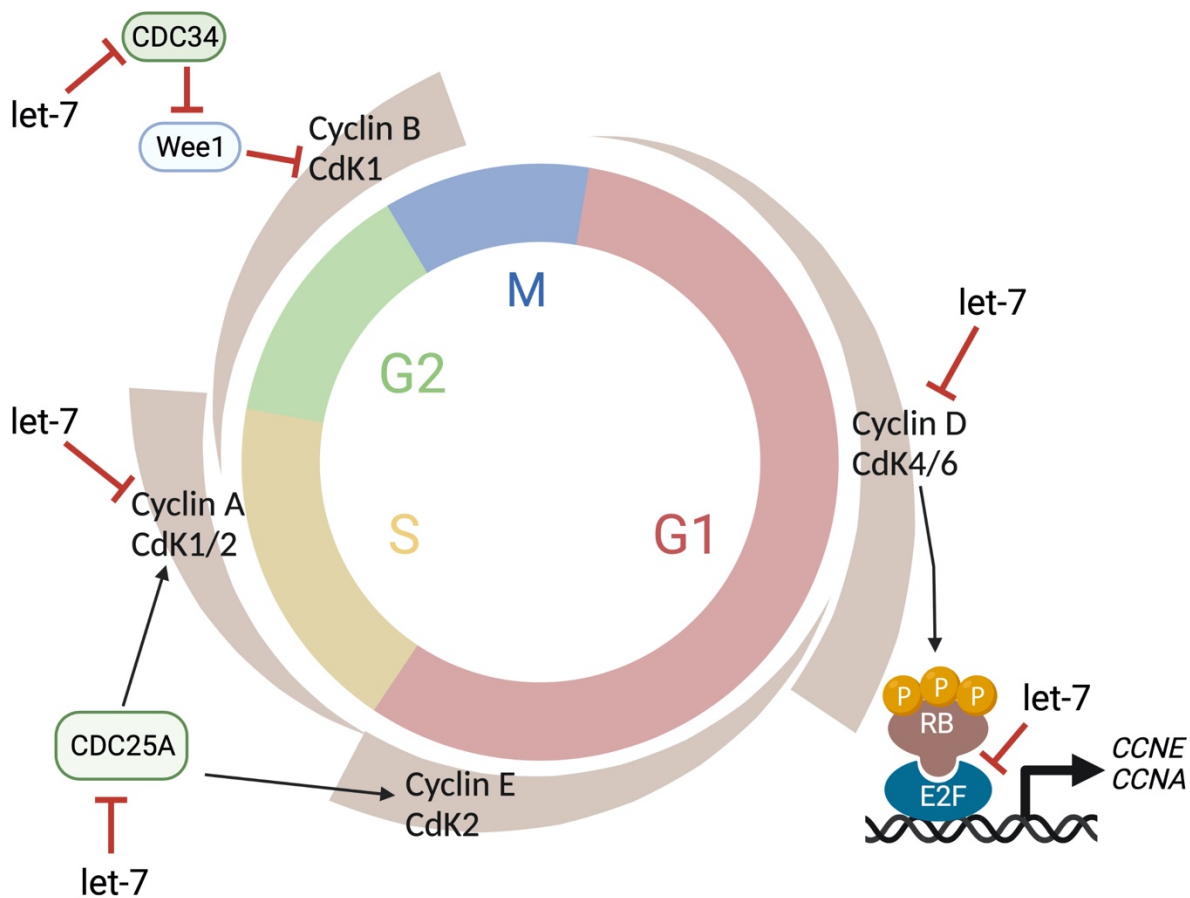


Figure 5.4 Let-7 regulation of the cell cycle

Let-7 regulates the cell cycle kinetics by both promoting cell cycle exit and lengthening distinct phases. Let-7 targets Cyclin D, CDK4, and CDK6, CDC25A, Cyclin A, and CDC34, affecting the G1/S, S/G2, and G2/M transitions, respectively. This figure was created with BioRender.com.

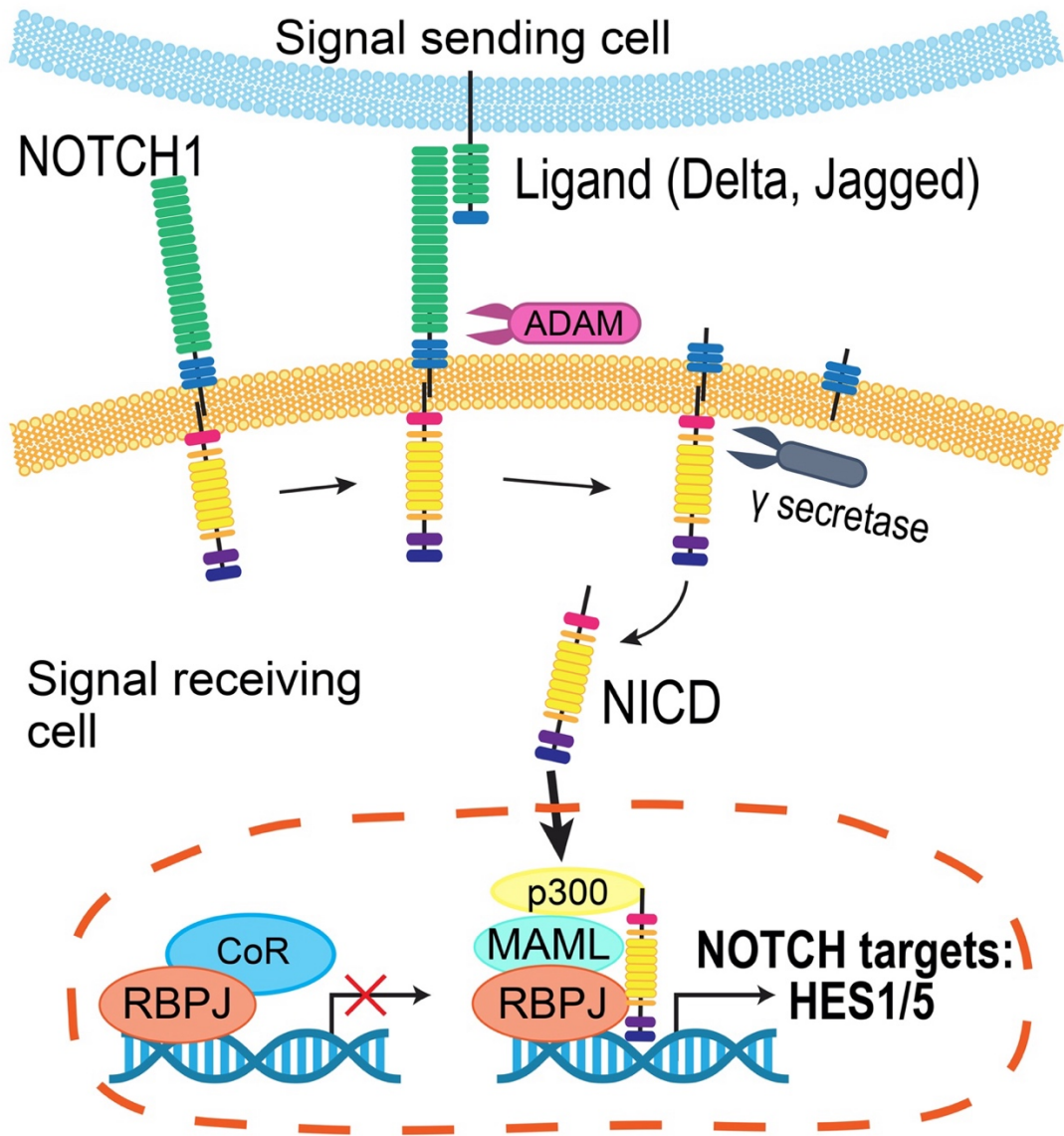


Figure 5.5 Summary of the Notch pathway

Notch signaling is initiated when a transmembrane Notch receptor (Notch1-4) on one cell is activated by a neighboring cell's ligand (Delta, Jagged/Serrate), prompting proteolytic cleavage events by ADAM and γ -secretase to release the Notch receptor's intracellular domain (NICD). Inside the cell, NICD translocates into the nucleus to form a transcriptional complex with a number of co-activators to in turn, activate the expression of genes, including the Hes and Hey families. The miRNA miR-9 regulates several members of this pathway.

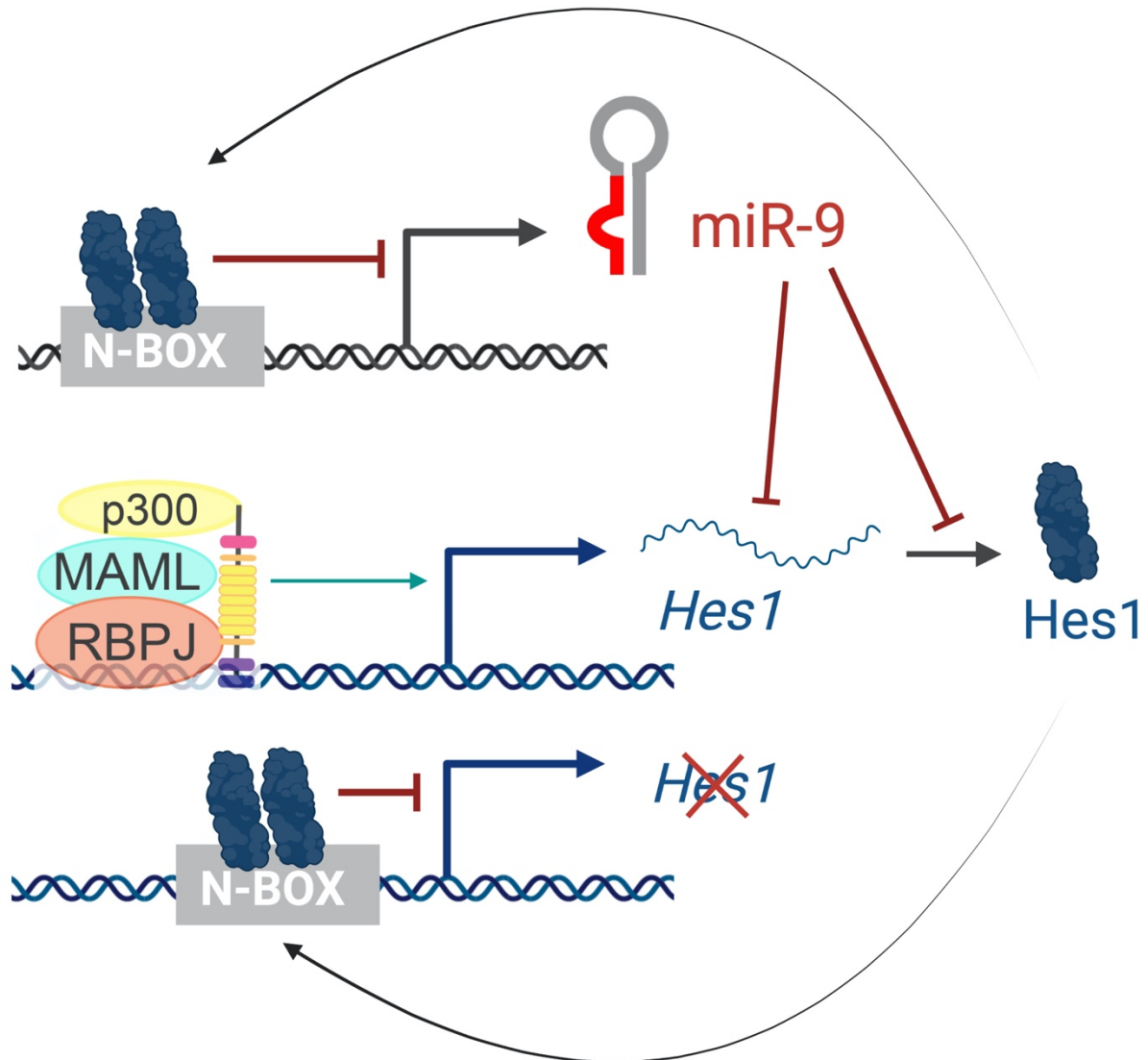


Figure 5.6 The Hes1/miR-9 oscillator

Activation of the Notch pathway leads to the activation of Hes1 transcription. Hes1 protein then dimerizes and binds to N-box domains to repress its own expression as well as miR-9 transcription. In turn, miR-9 reduces Hes1 levels by controlling the stability of *Hes1* mRNA and inhibiting its translation, resulting in oscillatory behaviors.

5.14 Tables

miRNA	Enriched in retina	Development expression	Known function	Proposed roles in retinal diseases	References
Let-7a	no	late development	neural differentiation; competence progression, repression of regeneration	Retinoblastoma	116,187,276,437, 492,495,541-543
Let-7b	no	late development	neural differentiation; competence progression, repression of regeneration	Retinoblastoma, diabetic retinopathy	276,279,437,492, 541,543-545
Let-7c	no	late development	neural differentiation; competence progression, repression of regeneration	AMD, Retinoblastoma,	276,279,437,492, 541,543,546
Let-7d	no	late development	neural differentiation; competence progression, repression of regeneration	Retinoblastoma	187,276,279,437, 541,543
Let-7e	no	late development	neural differentiation; competence progression, repression of regeneration	Retinoblastoma	279,437,541,543
Let-7f	no	late development	neural differentiation; competence progression, repression of regeneration	Retinoblastoma	187,279,437,541, 542,547
miR-101a		late development			279,495
miR-103		late development			232,467
miR-106	yes	early development		AMD	187,467,541,546
miR-107		early development			467,495,541
miR-124	no	late development	neuronal fate determination	AMD and other neuro-degenerations	380,437,467,472, 495,544,547-551
miR-125b	no	late development/ no change	Competence progression neuronal differentiation	AMD, Retinoblastoma	116,437,472,541, 544,547,552,553
miR-127	no	late development			467,541
miR-128a	no				437,467
miR-129		early development	photoreceptor/bipolar fate		450
miR-139					467,495
miR-140	yes				467,495
miR-15a		downregulated postnatally			443

miR-15b		enriched in fovea, downregulated postnatally		Diabetic retinopathy	232,443,554
miR-151	yes				467
miR-155		early development	photoreceptor/bipolar fate	AMD	450
miR-16	no	early development			116,495,541
miR-17	no	early development	Retinal progenitor proliferation, circadian oscillator regulator	AMD, Retinoblastoma	279,443,495,541, 552,555,556
miR-18	no	early development		Retinoblastoma	279,541,553
miR-181a		late development		Glaucoma, LHON	440,472,495,541, 557
miR-181b		late development		Glaucoma, LHON	467,495,544,547, 557-559
miR-181c	yes	late development			467,495,541
miR-182	yes	enriched in photoreceptors	photoreceptor physiology, circadian oscillator regulator		232,279,281,282, 415,437,440,467, 472,495,541,547, 558-560
miR-183	yes	enriched in photoreceptors	photoreceptor physiology, circadian oscillator regulator	RP	232,279,281,282, 415,437,440,467, 472,495,541,547, 558-560
miR-184	yes			AMD	437,440,467,472, 559,561
miR-185	yes				467,559
miR-191					279
miR-194	yes				467
miR-200b*				AMD, Diabetic retinopathy, Glaucoma	279,562,563
miR-204			retina and lens development	AMD, Coloboma, Glaucoma	440,467,547,548, 558,561,564,565
miR-21	no	late development		AMD	541,544
miR-210	yes				437,467,541
miR-211	yes				437,467,495
miR-214		early development	photoreceptor/bipolar fate		450
miR-219	yes				467,495
miR-222		early development	photoreceptor/bipolar fate		450

miR-24a		late development	inhibition of apoptosis	AMD, Glaucoma	561,566
miR-25	yes	downregulated postnatally	circadian oscillator regulator	Retinoblastoma	443,467,495,553
miR-26a	yes		circadian oscillator regulator	AMD	279,472,546,547
miR-29b		late development		AMD, Diabetic retinopathy, Glaucoma	467,495,541,561, 563,565
miR-29c		late development		Glaucoma	439,495,541,565
miR-30	no	late development			232,279,437,495, 541,547,558
miR-31	yes				437,467,472,547
miR-320	yes			Diabetic retinopathy	467,545
miR-342-5p		late development, enriched in peripheral/nasal retina	neural stem cell proliferation	AMD	232,418,546
miR-361	yes				467
miR-550		late development			279
miR-690		late development			279
miR-7	no	early development			279,437,467,495
mir-709		late development			279
miR-720					187,279
miR-9/9*	yes	late development	neuronal fate determination	AMD, Macular Telangiectasia Type 2	187,279,467,472, 495,540,541,548, 558
miR-92	yes	progenitors		Retinoblastoma	467,548,556,567
miR-93		early development			232,279,495,541
miR-96	yes	late development	photoreceptor physiology, circadian oscillator regulator	RP	232,279,281,282, 415,437,440,467, 472,495,541,547, 558,559

Table 5.1 Summary of miRNAs highly expressed in the developing retina

Retina enrichment is defined as increased expression compared to brain samples; early development refers to E10-E16 and late development refers to E16-P7, as defined by the progenitor states in Clark et al. ¹¹². Acronyms: AMD: age-related macular degeneration, LHON: Leber's hereditary optic neuropathy, RP: retinitis pigmentosa.

6. Published results: Notch directs telencephalic development and controls neocortical neuron fate determination by regulating microRNA levels

Jisoo S. Han^{1§}, Elizabeth Fishman-Williams^{1§}, Steven C. Decker^{1§}, Keiko Hino¹, Raenier V. Reyes¹, Nadean L. Brown¹, Sergi Simó^{1#*} and Anna La Torre^{1#*}

¹ Department of Cell Biology and Human Anatomy, University of California Davis, Davis, 95616

§ These authors contributed equally to this work

Co-senior authors

* Author for correspondence: alatorre@ucdavis.edu and ssimo@ucdavis.edu

The following chapter was submitted as a manuscript to *Development* and published on June 1, 2023. The accepted version of this manuscript has been reformatted for this dissertation. The authors of the manuscript were Jisoo S. Han, Elizabeth Fishman-Williams, Steven C. Decker, Keiko Hino, Raenier V. Reyes, Nadean L. Brown, Sergi Simó, and Anna La Torre, with Jisoo, myself, and Steven contributing equally. I performed hematoxylin and eosin staining, EdU/BrdU staining and quantifications, and immunohistochemistry experiments.

6.1 Introduction to cortical development (unpublished)

There are many structures in the CNS, beyond the retina, that require the coordinated effort of cell fate specification and cell migration for proper development. The cortex is one such highly-organized, laminated structure. Derived from the telencephalon, the cerebral cortex gives rise to both the hippocampus and the neocortex⁵⁶⁸. The hippocampus will become responsible for memory, learning, and emotion, and the neocortex will be important for cognition and sensation perception.

All the projection neurons and most of the glia of the cortex are born from a single population of multipotent progenitor cells, called radial glia cells (RGs, not to be confused with retinal ganglion cells)⁵⁶⁹⁻⁵⁷³. RGs are found in the ventricular zone (VZ), and their processes extend the entire width. This allows for the RGs to participate in interkinetic nuclear migration (INM)⁵⁷⁴⁻⁵⁷⁶. With that, the nucleus is most basal, near the pial surface, during S-phase and most apical, near the ventricular surface, during M-phase. These RGs can either symmetrically divide into the same cell type or asymmetrically divide into two different cell types. A cycling RG may divide into a combination of three different cell types: more RGs, intermediate progenitors (IPs), and post-mitotic neurons. IPs are similar to RGs in their ability to proliferate and produce more progenitors or post-mitotic neurons, but they are limited in their number of cell divisions before terminally differentiating⁵⁷⁷⁻⁵⁷⁹. IPs are found in the basal VZ, or even more basal in their own layer, the subventricular zone (SVZ).

Similar to the development of the retina, the cortex is built by the consecutive addition of different classes of cells in a stereotypic sequence that is well-conserved⁵⁶⁹⁻⁵⁷³. There are distinct early-born cell populations, and others generated as late-born cells.

When the first cell population (fated for layer VI) is born, it uses the RGs processes as a scaffold to migrate radially across. Future cell populations will continue to differentiate and migrate across the RG atop the previous layer. Such a migration pattern forms an “inside out” lamination, where the deeper layers in the apical cortex (e.g. layer VI) contain early-born neurons, and the higher layers in the more basal region (e.g. layers II-III) contain late-born neurons ⁵⁷⁹.

MiRNAs have been implicated in regulating cortical fate determination. Experiments manipulating Dicer showed that miRNAs are required to have both early-born and late-born neurons in the fully developed cortex ^{379,382}. Both miR-17 and miR-92 are involved in the production of IPs ^{383,580}. Similar to the LP-miRNAs of the retina, let-7 and miR-125b are part of the molecular mechanisms that enable RGs and IPs to differentiate into late fates ^{187,188}. One study showed that miR-9, miR-128, and let-7 are expressed in temporally opposite gradients to specify the production of each cortical layer ¹⁸⁸.

6.2 Abstract

The central nervous system (CNS) contains myriads of different cell types produced from multipotent neural progenitors. Neural progenitors acquire distinct cell identities depending on their spatial position, but they are also influenced by temporal cues to give rise to different cell populations over time. For instance, the progenitors of the cerebral neocortex generate different populations of excitatory projection neurons following a well-known sequence. The Notch signaling pathway plays crucial roles during this process but the molecular mechanisms by which Notch impacts progenitor fate

decisions have not been fully resolved. Here, we show that Notch signaling is essential for neocortical and hippocampal morphogenesis, and for the development of the corpus callosum and choroid plexus. Our data also indicate that in the neocortex, Notch controls projection neuron fate determination through the regulation of two microRNA (miRNA) clusters that include let-7, miR-99a/100, and miR-125b. Our findings collectively suggest that balanced Notch signaling is crucial for telencephalic development and that the interplay between Notch and miRNAs is critical to control neocortical progenitor behaviors and neuron cell fate decisions.

6.3 Key words

Cortical development, neurogenesis, cell fate, Notch, miRNA

6.4 Introduction

The mammalian telencephalon contains an unparalleled diversity of neural populations generated during development in a tightly regulated series of events. Despite the astounding intricacies of the mature cerebrum, the telencephalon arises from a relatively simple neuroepithelial sheet composed solely of neural progenitors^{581,582}. An exquisitely orchestrated interplay of intrinsic and extrinsic factors choreographs the emergence of distinct territories along the different axes. The posterior medio-dorsal region will develop into the hippocampus, cortical hem, and choroid plexus, while the embryonic dorsal telencephalon will develop into the neocortex in the anterior and lateral aspects⁵⁸³⁻⁵⁸⁵.

At early stages of development, neural progenitors called radial glial cells (RGs) expand the whole thickness of the neocortex from the ventricular (apical) surface to the pial (basal) surface. As development proceeds and the cortex grows, the somas of the RGs remain close to lateral ventricles, forming the ventricular zone where RGs can divide symmetrically to self-renew or asymmetrically to yield intermediate progenitors and post-mitotic neurons ^{586,587}. Importantly, these progenitors produce excitatory projection neurons in a conserved sequential manner ⁵⁸⁸⁻⁵⁹¹. Throughout neurogenesis, newly-born excitatory projection neurons use the RGs as a scaffold to migrate radially across the existing cortex and position themselves atop, forming an 'inside-out' lamination pattern ⁵⁷⁹. Accordingly, the deeper neocortical layers (e.g., layer VI) are formed by early-born neurons, while the more superficial layers (e.g., layer II-III) contain late-born cells.

The Notch signaling pathway is a pivotal regulator of numerous developmental processes in the telencephalon, including regulating the balance between proliferation and differentiation of progenitor populations, cell fate acquisition, and glial cell specification, among other roles ^{504,505,592-594}. Ligands such as Delta-like or Jagged/Serrate bind to the transmembrane Notch receptors (Notch 1-4), causing the proteolytic release of the Notch intracellular domain (NICD). NICD then translocates to the nucleus ⁵⁹⁵ and binds to a complex that includes RBPJ (recombination signal-binding protein for immunoglobulin κ J region, also known as CSL and CBF1), MAML1 (mastermind-like transcriptional co-activator1), p300, and other proteins, to transcriptionally activate downstream genes ^{596,597}. Well-known effector targets of the Notch pathway include the HES (Hairy and Enhancer of Split) and HEY (Hairy Ears, Y-linked) families. Previous studies have reported that HES1-deficient mice exhibited

accelerated neuronal differentiation in the neocortex while either HES1⁵⁹⁸ or HES5⁵⁹⁹ overexpression led to an expansion of the neural progenitor pool and prolonged production of superficial layer neurons and astrocytes. Such findings suggest that the timing and levels of Notch signaling must be properly regulated to maintain the temporal control of neurogenesis.

Importantly, the Notch signaling pathway also engages in complex feedback loops with several microRNA (miRNAs)²⁷⁸. MiRNAs regulate the expression of Notch pathway components, including HES1 and HES5^{279,381}. At the same time, Notch activity regulates the transcription of several miRNAs in different paradigms^{532,533,600}. MiRNAs have recently emerged as key regulators of cortical fate acquisition and developmental timing. In particular, let-7 and miR-125b are part of the heterochronic pathway that regulates many developmental transitions in bilaterally-symmetrical animals and are key components of the molecular machinery that allows neural progenitors to generate late cell populations in the cortex and retina^{187,188}.

Here, we show that balanced Notch signaling is necessary for proper development of the neocortex, corpus callosum, hippocampus, and choroid plexus. Additionally, we show that Notch signaling regulates neurogenesis and cortical laminar organization. At a molecular level, Notch coordinates the expression of several transcription factors, including bHLH neurogenic transcription factors as well as two miRNA clusters, *miR99ahg* and *miR100hg*, the host genes for the miRNAs miR-99a, let-7c, and miR-125b-2; and miR-100, let-7a, and miR-125b-1, respectively. Strikingly, we demonstrate that inhibition of these miRNAs partially rescues Notch gain-of-function phenotypes *in vivo*. Together

our data indicate that complex interactions between the Notch pathway and miRNAs are essential for proper cell fate specification and overall telencephalic development.

6.5 Results

6.5.1 Notch signaling regulates corpus callosum and hippocampal development

To investigate the roles of the Notch pathway during early telencephalic development, we generated Notch gain-of-function (GOF) and dominant negative (DN) mouse transgenic lines. A GOF strain was generated by crossing $ROSA26^{loxP-stop-loxP-Notch1-ICD}$ ⁶⁰¹ with the *Emx1-Cre* driver ⁶⁰². The resulting mouse line, hereafter referred to as *Emx1-NICD*, overexpresses Notch1-ICD in the dorsal telencephalon from embryonic day 10.5 (E10.5). Similarly, we generated a DN line by overexpressing a truncated MAML1 protein that acts as a dominant negative ($ROSA26^{loxP-stop-loxP-dnMAML1}$ ⁶⁰³) using the same *Emx1-Cre* driver (hereafter *Emx1-dnMAML*). In both lines, CRE recombinase mediates excision of the loxP-flanked STOP cassette, allowing for the expression of either NICD or dnMAML. Littermates containing no CRE were used as controls for all experiments. In both cases, the constructs are inserted at the *ROSA26* locus and thus, they are equivalent, avoiding expression differences due to the surrounding genomic DNA.

Emx1-NICD mice fail to thrive (Supplemental Figure 6.1A) and die around two weeks of age, whereas *Emx1-dnMAML* mice show no differences in animal size or survival rates compared to their control littermates. At a global level, neither of these strains show significant brain size differences at birth (Postnatal day 0, P0), but by P10,

Emx1-dnMAML animals exhibit smaller telencephalons compared to controls (Supplemental Figure 6.1B-D).

Analyses of these mice at P0 revealed several telencephalic gross morphological defects. Emx1-NICD brains exhibit enlarged lateral ventricles, aberrant hippocampi, thinner cortices, and agenesis of corpus callosum (Figure 6.1A-B, D-E, G-H, J-L). In contrast, Emx1-dnMAML show smaller lateral ventricle volumes, smaller hippocampi, and dysgenesis of corpus callosum (Figure 6.1C, F, I-L), with stronger deficiencies in the posterior corpus callosum, including misrouted axons (Figure 6.1F).

The corpus callosum is a large commissure that connects the right and left hemispheres and is formed by the axons of SATB2⁺ neurons that are found in all cortex layers, but particularly abundant in upper layers^{604,605}. Since Notch signaling regulates neuronal differentiation, one possibility is that the SATB2⁺ neurons are not correctly produced in Emx1-NICD brains, thus resulting in a lack of callosal cells^{606,607}. To test this hypothesis, we quantified the number of SATB2⁺ neurons in the neocortex of Emx1-NICD mice at P0. Strikingly, Emx1-NICD exhibits increased numbers of SATB2⁺ neurons compared to their littermate controls (2.49-fold increase, p-value: 0.004, Supplemental Figure 6.2A-B), indicating that the observed phenotype is not caused by a deficiency in the production of callosal neurons, but possibly due to deficiencies in axon pathfinding or midline defects. In this direction, we observed Probst bundles by H&E staining and L1 axon immunolabeling, suggesting that aberrant axon bundles fail to extend across the midline (arrows in Figure 6.1B and E). We labeled neurons with mCherry fluorescent protein in E13.5 control and Emx1-NICD embryos by *in utero* electroporation (IUE), when the first SATB2⁺ neurons are born⁶⁰⁸, then collected P0 mice for analysis. In control mice,

we detected mCherry-labeled axons through the midline. In Emx1-NICD mice, some mCherry+ axons extended towards the midline but failed to cross to the other hemisphere, resulting in an aberrant accumulation of axon fascicles (Supplemental Figure 6.2C).

The hippocampus is also affected in both Emx1-NICD and Emx1-dnMAML mice (Figure 6.1G-I). The hippocampus is comprised of the dentate gyrus (DG), which includes the granule cells (Calbindin+), and the hippocampus proper, which contains pyramidal neurons (DKK3+) ^{609,610}. Emx1-NICD hippocampi are smaller than the controls and show a severe disorganization of both cell types at P10, without increased apoptosis at P0 (Figure 6.1H-L, Supplemental Figure 6.3). Conversely, upon dnMAML expression, the hippocampus is organized correctly, but all regions are drastically reduced in size (Figure 6.1I, L). We also noticed instances of mispositioned DKK3+ neurons in the Emx1-dnMAML hippocampi, namely DKK3+ cells cross the upper DG blade and/or ectopically clustering in the hippocampal fissure (Supplemental Figure 6.3D, arrows).

6.5.2 Notch signaling is not a main mediator of dorsal telencephalic patterning but regulates Cajal-Retzius cell production

During the course of CNS patterning, the dorsal telencephalic midline gets organized into three distinct regions: the choroid plexus (ChP), the cortical hem (CH), and the hippocampal primordium, which is contiguous with the neocortex ⁶¹¹ (Figure 6.2A-A').

Since both Emx1-NICD and Emx1-dnMAML mice exhibit abnormal hippocampi and enlarged or smaller lateral ventricles respectively, we hypothesized that the dorsal telencephalic midline patterning could be affected in our models. Consistent with this idea, a triple knockout of the Notch signaling effectors *Hes1*, *Hes3*, and *Hes5* exhibited defects

in ChP development⁶¹². To identify possible patterning alterations, we labeled E13.5 coronal sections with FOXG1 and MSX1 to distinguish the hippocampal primordium, CH, and ChP regions (Figure 6.2A-C'). Emx1-NICD mice exhibit elongated hippocampi and CH, while these structures are significantly shorter in Emx1-dnMAML, compared to their littermate controls (Figure 6.2A-C', G-J). These changes could be reflecting alterations in cell cycle dynamics, but the general patterning and localization of these territories is maintained.

An important function of the CH is the production of Cajal-Retzius cells that secrete the extracellular glycoprotein Reelin⁶¹³, which is essential for cortical and hippocampal neuron migration and lamination⁶¹⁴⁻⁶¹⁹. Since the size of the CH is altered in both Emx1-NICD and Emx1-dnMAML mice, we labeled and quantified the number of Cajal-Retzius cells, using Reelin as a marker. Although the CH is larger in Emx1-NICD brains, we found a reduction in Reelin+ cells in both the cortical marginal zone (Figure 6.2D, E, K, Supplemental Figure 6.4A, C) and in the hippocampus at P0 (Supplemental Figure 6.4B). Interestingly, despite fewer Reelin+ cells present in the cortex and hippocampus, we identified ectopic patches of Reelin+ cells within the ChP of Emx1-NICD mice (Figure 6.2 M-N). In order to further confirm whether these cells are indeed Cajal-Retzius cells or cells that have aberrantly upregulated the expression of Reelin, we tested two other Cajal-Retzius markers: Calretinin and TBR1⁶²⁰. Notably, the ectopic Reelin+ cells express Calretinin but not TBR1 (Supplemental Figure 6.4F-H"). Emx1-dnMAML mice showed a significant increase in Reelin+ cells at E13.5 in the cortical marginal zone (Figure 6.2C, L), although no changes were observed in the hippocampus (Supplemental Figure 6.4D).

6.5.3 Early-born projection neuron production is limited by Notch signaling during neocortical development

Since our Emx1-NICD animals showed increased numbers of SATB2⁺ cells, we assessed if other cortical cell types were also affected by NICD overexpression. To avoid staining or counting biases, we used a semi-automatic cell counter platform (RapID⁶²¹) and we normalized each quantification to their corresponding littermate controls. In Emx1-NICD cortices, we observed a dramatic reduction of CTIP2⁺ and TBR1⁺ neurons and an increase in CUX1⁺ cells in comparison to controls (Figure 6.3A-D). Despite the significant changes in the ratio of cell populations in these cortices and the reduction in Reelin⁺ cells, lamination was largely normal, with CUX1⁺ projection neurons located at the top of the cortex and TBR1⁺ neurons located in the most apical layer of the cortical plate (Figure 6.3A).

To further investigate the changes in cell populations, we performed birth-dating experiments using EdU (5-ethynyl-2'-deoxyuridine) to label dividing progenitors. We injected EdU at E13.5 and then we analyzed the cortices at P0 to assess the fate outcomes of the EdU-labeled progenitors. The number of neurons that were both EdU⁺ and CUX1⁺, CTIP2⁺, or TBR1⁺ were quantified and normalized by the total number of EdU⁺ neurons (Figure 6.3E-H). Whereas in control brains EdU-labeled E13.5 neural progenitor cells mostly gave rise to CTIP2⁺ layer V neurons (Figure 6.3E, G), we observed a strong decrease of EdU⁺ CTIP2⁺ cells in Emx1-NICD brains. Concomitantly, the presence of EdU⁺ CUX1⁺ cells increased almost two-fold in Emx1-NICD brain in comparison to their control littermates (Figure 6.3E, F). At this stage of development, RGs

have already passed beyond the period of production of layer VI neurons, and we did not observe a significant change in EdU+ TBR1+ cell production (Figure 6.3H).

Next, we evaluated the consequences of blocking Notch signaling in the developing cortex using the Emx1-dnMAML model. Unfortunately, the anti-CUX1 antibody that we were using (Santa Cruz Biotechnology) was discontinued and we had to switch to a new vendor (Proteintech). The new antibody only labels CUX1+ neurons efficiently after P10 and thus, we switched the age of all subsequent CUX1 analyses from P0 to P10. In this case, we found a significant decrease in CUX1+ projection neurons, whereas CTIP2+ and TBR1+ neurons were overrepresented (Figure 6.4A-G). We also performed birth-dating experiments to measure whether the changes in cortical neuron composition are linked to changes in the timing of neurogenesis, similar to the experiments described before. We found a significant decrease in EdU+ CUX1+ neurons and corresponding increases in EdU+ CTIP2+ and EdU+ TBR1+ neurons, suggesting that the neural progenitors in the Emx1-dnMAML mice continue to produce TBR1+ neurons beyond the normal time window of layer VI neurogenesis (Figure 6.4J-O).

In contrast with the normal lamination observed in Notch GOF, Emx1-dnMAML mice neocortices also show severe disruption of the cortical layers in the dorsomedial region with milder lamination defects in the lateral aspects of the neocortex (Supplemental Figure 6.5). To quantify this phenotype, we divided the cortical plate into eight bins and counted the number of CTIP2+ and TBR1+ neurons in each bin. In control animals, TBR1+ neurons are mainly positioned at the bottom of the cortical plate as expected (bins 6-8 contain 63.5% of all TBR1+ neurons) and CTIP2+ cells are enriched in more basal locations (bins 3-4 contain 49.2% of all CTIP2+ cells). Conversely, both CTIP2+ and

TBR1+ neurons are dispersed across the whole thickness of the cortical plate in Emx1-dnMAML samples (bins 6-8 contain only 27.8% of all TBR1+ cells while bins 3-4 include 29.9% of CTIP2+ neurons) (Figure 6.4H-I).

Despite MAML having clear roles in the Notch signaling pathway, several studies suggest broader functions for MAML1 as a cofactor for multiple signaling pathways, including Wnt, Hippo, and Sonic Hedgehog⁶²²⁻⁶²⁵. To determine whether the defects observed in Emx1-dnMAML mice are caused by MAML's role in the MAML-RBPJ-NICD trimeric protein complex, we generated a Notch1 conditional knockout line by crossing Notch1^{ff} mice⁶²⁶ with the Emx1-CRE driver (hereafter Notch1cKO). Similar to Emx1-dnMAML1 mice, Notch1cKO exhibited dysgenesis of the corpus callosum and smaller lateral ventricles and hippocampi (Supplemental Figure 6.6A-D). We also observed thinner cortices that had considerably reduced upper layers (II-III) and dispersed cortical neurons, but this phenotype was not as severe as in the Emx1-dnMAML model (Supplemental Figure 6.6E, F). We performed birth-dating experiments as described above. Experiments showed a 2.4-fold increase in TBR1+ population production (*i.e.*, TBR1+ EdU+) compared to littermate controls, whereas no differences were observed for CTIP2+ population (Supplemental Figure 6.6G-J). These data indicate that Notch1cKO closely mimic Emx1-dnMAML phenotypes, suggesting that the overall defects we observe in Emx1-dnMAML mice are mainly due to the imbalance downstream of Notch.

Given the migration defects observed in both LOF models, we hypothesized that defects in the RGs could be contributing to these phenotypes, as described before in Emx1-RBPJ^{ff} mice⁶²⁷. We labeled RGs using Nestin at E13 and P0 (Supplemental Figure 6.7). Surprisingly, we did not observe changes in the organization or distribution of the

RGs. At P0, we observed a depletion of Nestin signal in the most medial region of the cortex but not in the lateral aspects in the Emx1-dnMAML model, suggesting a possible depletion of ventricular progenitors at this age.

6.5.4 Notch signaling regulates radial glia cell cycle dynamics

Notch signaling is required for maintaining the progenitor pool, and *Hes* genes downstream of Notch repress bHLH transcription factors, especially those with proneural functions^{388,505,521,628-631}. Overexpression of Delta1, HES1, or activated Notch1 prolongs mitotic activity in different types of progenitor cells^{504,628,632,633}. For these reasons, we characterized the cortical neural progenitors in our transgenic models at E13.5. We observed decreased numbers of TUJ1+ post-mitotic neurons at E13.5 in Emx1-NICD mice as expected (Figure 6.5A, left panels), but we also found that all Emx1-NICD embryos exhibit a complete depletion of TBR2+ intermediate progenitors (Figure 6.5A, right panels). To further validate that the intermediate progenitors were absent, as opposed to a downregulation of TBR2 protein, we labeled all mitotic cells with Phosphohistone H3 (PH3). While we did not observe any changes in the number of mitotic cells adjacent to the ventricle (RGs), the basally located PH3+ cells (intermediate progenitors) were absent in Emx1-NICD mice (Figure 6.5B-D). In order to discriminate whether the lack of TBR2+ progenitors observed is a developmental delay or a permanent loss of intermediate progenitors, we extended these analyses to E15.5. Interestingly, at E15.5, we observed TBR2+ cells at ratios similar to the controls (Supplemental Figure 6.8), suggesting that the lack of intermediate progenitors at E13.5 reveals a developmental delay.

To further characterize the cell cycle dynamics in our different genetic models, we measured the length of the cell cycle using dual-window labeling with the thymidine analogs EdU and BrdU (5-bromo-2'-deoxy-uridine) as described before⁶³⁴. Pregnant mice at E13.5 were injected with a pulse of EdU followed by a pulse of BrdU two hours later. All animals were euthanized 30 minutes after the second pulse (150 minutes total) and the tissues were processed and stained for EdU, BrdU, and PAX6. Since NICD mice were missing the TBR2⁺ intermediate progenitors, we limited the quantification to PAX6⁺ apical RGs. RGs labeled by EdU but not BrdU (PAX6⁺ EdU⁺ BrdU⁻) left S-phase during the 2-hour period between pulses. The ratio of PAX6⁺ EdU⁺ BrdU⁻ cells over the total number of cells in S-phase (PAX6⁺ EdU⁺) equals 2h/Time of S-phase (2h/T_s). The ratio between the number of cells in S-phase at one given timepoint (PAX6⁺ BrdU⁺) and the total PAX6⁺ proliferating population is proportional to the ratio T_s/total cell cycle time (T_s/T_c). Using these parameters, we estimated the percentage of cells in S-phase for each sample and then calculated the average T_s and T_c, normalizing each value to their littermate controls to avoid staining or imaging biases.

While the length of S-phase was not significantly altered in any of the models (9.02h in control, 9.12h in Emx1-NICD and 9.20h in Emx1-dnMAML, Figure 6.5E-G), the total length of cell cycle was significantly longer in Emx1-NICD progenitors (7.9 hours longer or 1.42-fold increase ± 0.19 , p-value: 0.040) and shorter in Emx1-dnMAML RGs (6.7 hours shorter or 1.38-fold reduction ± 0.59 , p-value: 0.003).

These data together show that activation of Notch signaling results in depletion of intermediate progenitors at early time-points but not at E15.5 and lengthening of the cell cycle without affecting the total length of S-phase.

6.5.5 Overactivation of Notch signaling results in transcriptomic changes of Notch effectors, bHLH transcription factors, and miRNAs *let-7*, *miR-99a/100*, and *miR-125b*

To identify the downstream targets of Notch activation that may play a role in neurogenesis and/or cell cycle regulation within the progenitor population, we profiled E13.5 RG transcriptomes using RNA sequencing (RNAseq), facilitated by specific labeling of RGs using FlashTag⁶³⁵. As described previously, FlashTag utilizes carboxyfluorescein esters (CFSEs) that, when injected into the ventricles, label cells in contact with the cerebrospinal fluid. Since the apical RGs are transiently in contact with the ventricle walls during mitosis, this technique allows for a specific labeling of the RG population. We confirmed that 1 hour after injection, all FlashTag-labeled cells were PAX6+ RGs (Figure 6.6A). Next, we used FlashTag to label RGs in control (n=3) and *Emx1-NICD* (n=5) littermate embryos at E13.5. We dissected the neocortices 1 hour post-injection, isolated the labeled RGs using FACS, and performed RNAseq. Multidimensional scaling analysis showed a clear clustering of all the *Emx1-NICD* samples (Supplemental Figure 6.9A). Gene ontology (GO) enrichment analyses using PANTHER revealed that processes overrepresented in *Emx1-NICD* cortices include the terms: “regulation of Notch signaling pathway” (GO:0008593, p-value: 0.00135), “negative regulation of cell differentiation” (GO:0045596, p-value 2.22×10^{-9}), “cell fate commitment” (GO:0045165, p-value: 1.73×10^{-8}), and “regulation of cell cycle” (GO:0051762, p-value: 0.00026); processes downregulated include the terms: “neuron differentiation” (GO:0030182, p-value: 4.36×10^{-17}), “forebrain development”

(GO:0030900, p-value: 1.65×10^{-10}), and “axon guidance” (GO:0007411, p-value: 0.00148) (Supplemental Figure 6.9B).

As expected, known Notch effectors such as *Hes1*, *Hes5*, *Hey1*, and *Hey2* were upregulated by NICD, while the Notch receptors, *Dll1* and *Dll3*, were downregulated along with *Mfng* (Manic Fringe Homolog), a glycosyltransferase that modulates Notch activity (Figure 6.6B-C). *Hes* and *Hey* genes negatively regulate the expression of proneural basic helix-loop-helix (bHLH) transcription factors in several contexts and accordingly, we observed a reduction in *Neurog1*, *Neurog2*, *Neurod1*, *Neurod2*, *Neurod6*, and *Ascl1* (Figure 6B-C). Even though we only analyzed the RG transcriptome, we observed a significant downregulation of some deep-layer markers (e.g., *Tbr1*, *Myt1* and *Rprm*), layer V genes (*Bcl11b/Ctip2*), and intermediate progenitor markers (e.g., *Eomes/Tbr2*), but we did not observe differences in upper-layer markers (e.g., *Cux1* and *Satb2*).

Strikingly, we also observed upregulation of *miR100hg* and *miR99ahg*, which are the host genes for two miRNA clusters (Figure 6.6C, purple data points). *MiR100hg* (miR-100 host gene) includes miR-100, let-7a-2, and miR-125b-1, while *miR99ahg* (mir-99a host gene) encodes for miR-99a, miR-125b-2, and let-7c. Upregulation of these miRNAs in Emx1-NICD samples was further confirmed by miRNA sequencing of FlashTag-labeled purified RGs (Figure 6.6D and Supplemental Table 6.2), as described before. To further confirm the sequencing results, we performed single molecule *in situ* hybridization (RNAscope) of *miR99ahg*; as expected, *miR99ahg* expression is increased in Emx1-NICD samples compared to controls (Supplemental Figure 6.10).

6.5.6 Let-7, miR-125b, and miR-99/100 are required downstream of Notch to restrict early-born projection neuron fates

To test whether the upregulation of let-7, miR-125b and/or miR-99a/100 play any roles in the cortical phenotypes observed, we performed IUE using microRNA sponges^{187,636} to inhibit miRNA activity in Emx1-NICD mice, and we analyzed the consequent effects on cell fate. Plasmids expressing specific miRNA sponges together with an mScarlet plasmid were IUEd into Emx1-NICD E13.5 embryos, and the electroporated brains were collected at P0 (Figure 6.7A-F). These samples were processed, labeled with CTIP2 antibodies, and the numbers of CTIP2⁺ mScarlet⁺ cells were determined. Whereas in control animals we observed 19.4% \pm 8.4 of CTIP2⁺ mScarlet⁺ /mScarlet⁺ cells, we did not observe any CTIP2⁺ mScarlet⁺ cells in Emx1-NICD brains (Figure 6.7A-B), in agreement with our data showing that upon NICD overexpression, E13.5 RGs generate upper-layer cells instead of layer V neurons. We did not observe any significant changes when either let-7, miR-125b or miR-100 were inhibited (5.56% \pm 2.9, 0% and 2.83% \pm 2.6, respectively, Figure 6.7D,E,G). Notably, when we electroporated the three sponges together (let-7, miR-125b and miR-100) in Emx1-NICD mice, significantly more electroporated cells were now CTIP2⁺ (11.15% \pm 7.4, Figure 6.7F,G). Similarly, we quantified the distribution of the electroporated cells throughout the cortical plate (Figure 6.7H). In control samples, most of the electroporated cells locate in bins 4-5 whereas NICD overexpression shifts the cells to bins 2-3. Inhibition with the three sponges reduces the number of cells in the upper bins (p-value: 0.041). Together these data suggest that these miRNAs are downstream effectors of Notch signaling and necessary to produce upper-layer neurons, possibly through epistatic mechanisms.

6.6 Discussion

6.6.1 Multifaceted functions of Notch during telencephalic morphogenesis

The Notch pathway has long been recognized for its roles in cell specification, patterning, differentiation, and regeneration ^{97,388,505,508,510,515,592,630,637}. However, its contributions to telencephalic development remain unresolved. Utilizing GOF and DN transgenic mouse lines, we demonstrate that balanced Notch signaling is required for hippocampal and corpus callosum development, and we also show that Notch is a key regulator of neurogenesis in the neocortex.

Given the vast array of gross morphological defects observed in both GOF and DN models, we examined whether Notch regulates the patterning of the dorsal telencephalic midline, perhaps affecting the development of the hippocampus and ChP, changing brain fluid homeostasis and the volume of the ventricles. Although there are obvious differences in the size of the hippocampal, CH, and ChP areas in the transgenic mice, the establishment of the different territories is not affected by Notch changes.

While the ChP is properly patterned and establishes a sharp boundary with the CH, we identified ectopic Reelin⁺ cells in the ChP region at E13.5 in Emx1-NICD brains. Notably, these ectopic cells express Reelin and Calretinin (both markers of Cajal-Retzius) but not TBR1, a marker normally detected in Cajal-Retzius cells at E13.5, but not expressed in these cells at later stages ⁶²⁰. A previous study using lineage-tracing analysis of the prospective ChP region indicated that these progenitors sequentially give rise to Reelin⁺ Cajal-Retzius cells first and later to nonneural ChP epithelial fates ⁶¹². Inactivation of *Hes1*, *Hes3* and *Hes5* genes led to an enhanced development of Cajal-

Retzius cells at the expense of ChP cell fates, suggesting that Notch signaling regulates the progenitor transition from cells that produce Cajal-Retzius cells to progenitors that will generate nonneural ChP epithelial cell identities. However, around E12.5, the levels of HES1 and HES5 are downregulated after ChP cell fate specification⁶¹². The presence of ectopic Reelin⁺ cells suggests that this later downregulation of Notch signaling may be required to maintain the ChP fate and that ChP progenitors can transdifferentiate to neural fates, or at least express some neural markers, upon sustained HES1/5 activity. The ectopic Reelin⁺ cells observed could alternatively be the consequence of aberrant migratory patterns from the CH. In fact, Notch has been shown to regulate migration patterns in the cortex through interactions with the Reelin-Dab1 signaling pathway⁶³⁸.

Alternatively, Notch could also be affecting the tangential expansion of the progenitor pool, indirectly affecting the volume of the ventricles. In some large mammals, including humans, the cerebral cortex undergoes a massive expansion that takes place by a growth in surface area rather than in thickness and is the basis for gyrencephaly⁶³⁹. In this direction, recent work has shown that local disruption of Notch signaling can trigger cortical folding⁶⁴⁰.

6.6.2 Balanced Notch signaling is essential for the development of the corpus callosum

Transgenic models overexpressing *Hes5* in the neocortex⁵⁹⁹ and *Hes1/Hes3/Hes5* and *RBPJ* knockouts has been described before^{612,627,630}, but to our knowledge, our study is the first to report corpus callosum defects upon alterations of Notch signaling in mice.

In Emx1-NICD mice, we observed an increase of SATB2+ cells together with the presence of Probst bundles, indicating that callosal axons are present but unable to cross the midline. One possibility is that the defects in the corpus callosum may be directly caused by the changes in the cortical cell ratios observed in our different models. The pioneering axons, the first axons to cross the midline during development, are known to guide later axons and experimental approaches indicate that later axons are unable to find the correct path in the absence of pioneering axons⁶⁴¹. SATB2+ neurons are normally detected from E13.5 as CUX1+ upper layer neurons, but a small percentage colocalize with CTIP2 or TBR1⁶⁰⁶. Thus, it is possible that the lack of CTIP2+ SATB2+ or TBR1+ SATB2+ pioneering axons is causing this phenotype. Alternatively, deficiencies in the midline glia (glial wedge and indusium griseum), which secrete guidance cues, or changes in the expression of the appropriate receptors in the SATB2+ neurons could also result in the failure to cross the midline. In this direction, our RNAseq results indicate that several guidance receptors are altered upon NICD overexpression, including *Slit1*, *DCC1*, *UNC5a*, *Plxna4*, and *Nrp1* (Supplemental Table 6.1), even though our analyses were restricted to RGs and not postmitotic neurons.

6.6.3 Notch regulates radial glia cell cycle length and cortical neurogenesis

In the present study, we show that the switch between generating deep to upper-layer projection neurons is regulated by Notch, as RGs labeled with EdU generated upper-layer fates sooner in Emx1-NICD mice and they generated deep-layer cells for longer periods upon the expression of dnMAML compared to their respective littermate

controls. These results parallel phenotypes observed in Hes5 KO and Hes5-overexpression models where the timing of neurogenesis was also affected ⁵⁹⁹.

Since the length of the cell cycle is longer in Emx1-NICD RGs, the fate acquisition changes do not seem to correlate with the number of cell divisions. However, the length of the cell cycle and the timing of cell cycle exit could be influencing these neurogenic fate decisions. For example, during bristle patterning in *Drosophila*, Notch signaling controls cell cycle progression, such that cells with elevated Notch signaling divide first while those with lower signaling extend their G2 phase, making them more sensitive to lateral inhibition and consequently change their cell fate ⁶⁴². Our data could fit a similar model in which NICD extends RG cell cycle time, making these cells more susceptible to fate determinant factor(s).

Even though effects driven by the ectopic expression of NICD or dnMAML in post-mitotic neurons cannot be completely ruled out, our data support the idea that fate decisions are decided at the progenitor stage. In this direction, pro-neural bHLH transcription factors, a family of transcriptional regulators known to play key roles in fate determination, are expressed in the terminal cell cycle of neural progenitors from S-phase or G2 ⁶⁴³, and are known to regulate both cell cycle exit and fate choices ⁶⁴⁴⁻⁶⁴⁶. Surprisingly, we also detected the presence of transcripts normally associated with specific subpopulations of postmitotic neurons in our sequencing experiments using purified RGs. As suggested before, low levels of these mRNAs in RGs may not lead to detectable protein expression but might prime the cells for differentiation upon cell cycle exit. While we distinguished significant differences in the expression of IP markers (*EOMES/Tbr2*) and deep-layer genes (*Tbr1*, *Myt1*, *Ctip2*), we did not observe any

differences in upper-layer markers (*Cux1*, *Satb2*). Published reports have shown that TBR1/CTIP2 and TBR1/FEZF2 initially overlap in their expression before genetic repression and depression networks establish the distinct layer subtype identities⁶⁴⁷. For instance, FEZF2 is a transcriptional repressor that acts by repressing genes that would be inappropriate for layer V, including *Tbr1*⁶⁴⁸ and layer II-IV genes⁶⁴⁹. Our data may suggest that the reduction in deep-layer genes in RGs may be affecting the expression of upper-layer genes later (*i.e.*, upon cell cycle exit).

6.6.4 miRNAs downstream of Notch are required for upper-layer neuron fate acquisition

We identified two miRNA clusters—*miR100hg* and *miR99ahg*—with increased expression in Emx1-NICD cortices. Both clusters encode for let-7, miR-125b, and miR-99a/100. Let-7 and miR-125b are essential regulators of developmental timing in various organisms^{485,490,494}. In the mammalian retina, let-7 and miR-125b regulate the switch from progenitors that produce early cell fates to retinal progenitors that yield late-born cell fates^{187,492}. In the cortex, let-7 has been recognized as an important factor to maintain homeostasis⁶⁵⁰ and vital in the generation of late cell types^{188,381}. Moreover, we have recently shown that let-7 also regulates progenitor cell cycle dynamics in the cortex²⁷⁶. While there is limited literature on the roles of miR-99a/100 in the CNS, the miR-99a/100, let-7, miR-125b tricistrons have been shown to regulate hematopoietic progenitor homeostasis⁶⁵¹.

Strikingly, the inhibition of these miRNAs' activity using specific miRNA sponges is sufficient to partially rescue the Emx1-NICD phenotype. We have previously shown that

let-7 inhibition leads to a shortening of the S/G2 phase of cell cycle²⁷⁶, but further inquiry is needed to discern if the effects of these sponges are mediated by the regulation of cell cycle or through other downstream targets. A widely-recognized target of let-7 is the chromatin remodeler HMGA2⁴⁹⁸, an important regulator of neocortical neurogenesis¹⁸⁸. Let-7 also regulates the levels of the nuclear receptor TLX⁴⁸⁸ and the cell cycle genes Cyclin D1, Cyclin D2, CDK4, CDK6 and CDC25A⁴⁹⁷. Further experiments aimed at understanding the molecular mechanisms downstream of let-7 and the possible cooperative activities between the different miRNAs will shed light on the machinery that instructs cortical fate acquisition.

Importantly, *miR100hg* is located in a human chromosome region (11q24.1) whose deletion is associated with Jacobsen syndrome (JBS, OMIM #147791). This syndrome involves intellectual disability, abnormal head shape, microphthalmia, and increased likelihood of autism spectrum disorders⁶⁵²⁻⁶⁵⁴. The JBS patient deletions range from 7 to 20 Mb. The heterogeneity of phenotypes supports the hypothesis that JBS is a contiguous gene deletion syndrome where the loss of different combinations of genes causes particular phenotypes. Owing to the rarity of reported cases, it has not yet been possible to tease out the requirements of individual genes, including *miR100hg*. Notably, a rare microtriplication of 1.8 Mb in the 11q24.1 region (partial trisomy), which includes *miR100hg* and only a handful of other genes (11 in total), also results in intellectual disability with severe verbal impairment⁶⁵⁵. Thus, a further understanding of the roles that *miR99ahg* and *miR100hg* play in telencephalic development will also allow us to gain further insights into the molecular underpinnings of developmental brain disorders.

6.7 Acknowledgments

We want to thank all members of the Brown, Simó, and La Torre laboratories for their helpful insights. We also want to thank Drs. Tom Glaser and Nick Marsh-Armstrong for their valuable comments and generosity with reagents. This study was supported by the National Institute of Neurological Disorders and Stroke (National Institutes of Health) [R21 NS101450 to SS and ALT, R01 NS109176 to SS] and National Eye Institute [R01 EY013612 and R01 EY031724 to NLB]. We also benefited from the use of the National Eye Institute Core Facilities [supported by P30 EY012576] and the Flow Cytometry Laboratory with funding from the NCI [P30 CA0933730] and NCRR [C06-RR12088, S10 RR12964] with technical assistance from Ms. Bridget McLaughlin and Mr. Jonathan Van Dyke. The sequencing library preparations and the sequencing were carried out at the UC Davis Genome Center DNA Technologies and Expression Analysis Core, supported by NIH Shared Instrumentation Grant 1S10OD010786-01 and analyzed by the UC Davis Bioinformatics Core. Non-commercial reagents used in this paper are available upon request.

6.8 Experimental models and subject details

6.8.1 Animals

All animals were used with approval from the University of California Davis Institutional Animal Care and Use Committees and housed and cared for in accordance with the guidelines provided by the National Institutes of Health. B6N.129-*Gt(ROSA)26Sor^{tm1(MAML1)Wsp}/J* (*ROSA26^{loxP-stop-loxP-dnMAML1}*) and *Notch1^{tm2Rko}/GridJ* (*Notch1^{ff}*) were generous gifts from Dr. Ivan Maillard and Dr. Raphael Kopan,

respectively. *Gt(ROSA)26Sor^{tm1(Notch1)Dam}/J* (ROSA26^{loxP-stop-loxP-Notch1-ICD}) and B6.129S2-*Emx1^{tm1(cre)Krl}/J* (Emx1-Cre) mice were obtained from The Jackson Laboratory. All animals are currently available at The Jackson Laboratory (Cat. #008159⁶⁰¹, #032613⁶⁰³, #006951⁶²⁶ and #005628⁶⁰², respectively). To drive NICD and dnMAML expression in the developing mouse telencephalon, ROSA26^{loxP-stop-loxP-Notch1-ICD} or ROSA26^{loxP-stop-loxP-dnMAML1} were crossed with Emx1-Cre/+ mice. To generate Emx1-Cre/+; Notch1^{ff} (Notch1cKO) mice, Notch1^{ff} were crossed with Emx1-Cre/+ mice to generate an intermediate stock and then Emx1-Cre/+; Notch1^{f/+} were bred with Notch1^{ff}.

6.8.2 Constructs

The MSCV puro let-7 sponge was a gift from Dr. Phil Sharp (Addgene plasmid #29766)⁶⁵⁶, the pRNA-U6-let-7 sponge was a gift from Dr. Phillip Zamore (Addgene plasmid #35664), and the MG-miR-125b-sponge-bulge was a gift from Dr. David Baltimore (Addgene plasmid #45790)⁶⁵⁷. The miR-100 sponge was designed using the miRNAsong algorithm⁶³⁶ (5'- CACAAGTTCGGATCTACGGGTTAATTCACAAGTTCGGATCTACGGGTT-3'). MiR-100 sponge sequences were cloned in tandem into a pCAG backbone⁶¹⁷ to obtain a 12mer miR-100 sponge sequences. miR-100 sponge is expected to also target miR-99a based on sequence homology.

6.8.3 Histology and immunohistochemistry

Brains were collected at indicated ages and prepared for cryoembedding or paraffin embedding. Samples to be cryoembedded were fixed in 3.7% formalin/PBS by

submersion overnight at 4°C, cryoprotected with 30% sucrose/PBS solution, embedded in Optimum Cutting Temperature (OCT) compound (Tissue-Tek, Torrance, CA), and quickly frozen using dry-ice. Samples for paraffin embedding were fixed in modified Carnoy's fixative (ethanol, formaldehyde, and acetic acid) overnight at 4°C, dehydrated, cleared with xylene, and embedded in paraffin blocks. OCT embedded brain blocks were cryo-sectioned (15 µm) and paraffin embedded blocks were sectioned (5 µm), both on a coronal plane. Immunostainings were performed in free-floating cryoprotected sections and mounted paraffin sections with agitation. Paraffin sections were deparaffinized using xylene, rehydrated with ethanol, and rinsed with PBS/0.3% Triton X-100. Antigen retrieval was performed on all samples with hot 0.01 M sodium citrate pH 8 for 20 min. Some samples required further antigen retrieval, which included an additional acid wash (2N HCl and PBS/0.5% Triton X-100) for 1h at room temperature. All sections were then blocked with PBS/0.1% Triton X-100 and either 5% milk or 10% normal donkey serum for 1h at room temperature. Blocking solution was used for primary antibody incubation (overnight, 4°C). After primary antibody incubation, free-floating sections were washed three times (10 min each) in PBS/0.1% Triton X-100 and mounted sections were washed five time (5 min each) in PBS. Species-specific, fluorescently-labelled secondary antibodies were used in blocking solution (60-90 minutes, room temperature). 4',6-diamidino-2- phenylindole (DAPI) (Sigma-Aldrich) was used for nuclear staining. The list and concentrations of antibodies used in this work are described in the table below. Images were taken in a Fluoview FV3000 confocal microscope (Olympus, Center Valley, PA) or Axio Imager.M2 with Apotome.2 microscope system (Zeiss, Dublin, CA). All images were assembled using Photoshop and Illustrator (Adobe, San, Jose, CA).

Antibody	Source	Catalog	Lot	Concentration
Anti-BrdU (Mouse)	ThermoFisher	B35128	2125239	1:100
Anti-Calbindin (Mouse)	Millipore Sigma	C9848-100UL	079M4794V	1:200
Anti-Calretinin (Goat)	Swant	CG1	N/A	1:50
Anti-Cleaved Caspase-3 (Rabbit)	Cell Signaling Technologies	9664S	22	1:200
Anti-CTIP2 (Rat)	Abcam	ab18465	GR3462350-1	1:500
Anti-CUX1 (Rabbit)	Proteintech	11733-1-AP	00098340	1:1000
Anti-CUX1 (Rabbit)	Santa Cruz Biotechnologies	sc-13024, discontinued	CDP M-222X	1:50
Anti-DKK3 (Rabbit)	Sino Biological	50247-RP02	HB04MA1301-B	1:200
Anti-EOMES (TBR2) (Rat)	ThermoFisher	14-4875-82	2504948	1:200
Anti-FOXP1 (Rabbit)	Abcam	ab196868	GR3242662-8	1:100
Anti-GFAP (Mouse)	Antibodies Incorporated	73-240	455-8JD-45C	1:100
Anti-L1 (Rat)	Millipore Sigma	MAB5272	3663105	1:500
Anti-MSX1 (Goat)	R&D Systems	AF5045	CALG0119111	1:100
Anti-Nestin (Mouse)	BD Biosciences	556309	6084618	1:100
Anti-PAX6 (Rabbit)	BioLegend	901301	B386304	1:200
Anti-PH3 (Rabbit)	Millipore Sigma	06-570	3795233	1:100
Anti-Reelin (Mouse)	Millipore Sigma	MAB5364	3439219	1:100
Anti-RFP (Rabbit)	Novus Biologicals	NBP2-25157	71615	1:1000
Anti-RFP (Goat)	Origene	AB0040-200	N/A	1:1000
Anti-SATB2 (Mouse)	Abcam	51502	N/A	1:200
Anti-TBR1 (Rabbit)	Invitrogen	PA5-34582	WG3332981A	1:1000
Anti-TBR2 (Rabbit)	Abcam	ab23345	GR3230866-2	1:200
Anti- β -III-Tubulin (TUJ1) (Mouse)	BioLegend	801201	B264428	1:500

6.8.4 In utero electroporation

In utero microinjection and electroporation was performed at embryonic day (E)13.5 as described previously⁶¹⁷, using timed pregnant Emx1-NICD mice. For control electroporations, DNA solutions containing 0.5 mg/ml pCAG-ChFP plasmids were mixed in 10 mM Tris, pH 8.0, with 0.01% Fast Green and 1 μ l of the solution was injected per embryo. Tweezertrodes electrodes (BTX) with 5-mm pads were used for electroporation

(five 50ms pulses of 30V). To express the miRNA sponges, a solution containing 1 mg/ml of each sponge individually, or combined, and 0.5 mg/ml pCAG-ChFP was used. All experimental manipulations were performed in accordance with protocols approved by the University of California, Davis Institutional Animal Care and Use Committee (IACUC). At P0, electroporated brains were collected and processed as described.

6.8.5 FlashTag NSC labelling and FACS

Labelling of cortical neuronal progenitors with carboxyfluorescein esters (CFSEs) was achieved as described elsewhere⁶³⁵. Briefly, 1µl of a 5mM solution of CellTrace CFSE (from the CellTrace CFSE Cell Proliferation Kit, Invitrogen #C34554) and 0.01% FastGreen in DMSO was injected into the 3rd ventricle of E13.5 control and Emx1-NICD embryos. Dams were allowed to recover and injected embryos were collected 1 hour post-injection. Embryonic cortices were dissected individually and dissociated into single cells using Papain Dissociation System (Worthington, # LK003150) manufacturer's protocol. Cells were resuspended in FACS media (DMEM/F12 without phenol red supplemented with 10% FBS and B-27) and sorted using a Beckman Coulter Astrios EQ Cell Sorter.

6.8.6 RNA and miRNA sequencing

Total RNA from control (n=3) and Emx1-NICD (n=5) sorted cells was extracted using the Total RNA Purification Plus Kit (NORGEN Biotek Corp., #48300). Gene expression profiling was carried out using a 3'-Tag-RNA-Seq protocol. Barcoded sequencing libraries were prepared using the QuantSeq FWD kit (Lexogen, Vienna,

Austria) for multiplexed sequencing according to the recommendations of the manufacturer using both the UDI-adaptor and UMI Second-Strand Synthesis modules (Lexogen). The fragment size distribution of the libraries was verified via micro-capillary gel electrophoresis on a LabChip GX system (PerkinElmer). Barcoded miRNA-Seq libraries were prepared using the NEXTflex Small RNA Sequencing kit V3 (PerkinElmer) with sequence randomized adapters according to the recommendations of the manufacturer. The fragment size distribution of the libraries was verified via micro-capillary gel electrophoresis on a Bioanalyzer 2100 (Agilent). Both sets of libraries were quantified by fluorometry on a Qubit instrument (Life Technologies, Carlsbad, CA), and then pooled in equimolar ratios. The library pools were quantified by qPCR with a Kapa Library Quant kit (Kapa Biosystems/Roche). Finally, both library sets were sequenced on a HiSeq 4000 sequencer (Illumina) with single-end 100 bp reads.

6.8.7 Data availability

All relevant data can be found within the article and its supplementary information. Moreover, information about next generation sequencing including raw data, quality controls, and experimental pipeline are available at: [doi:10.25338/B8RM0H](https://doi.org/10.25338/B8RM0H). Custom scripts used to process sequencing data are available upon request.

6.8.8 Edu and BrdU labeling

For Edu birth-dating experiments, pregnant dams were injected intraperitoneally with 25mg Edu/kg body weight at E13.5 and pups were sacrificed at birth. For the Edu/BrdU dual window labeling experiments, pregnant dams were injected

intraperitoneally with 12.5mg/kg body weight of EdU at E13.5 and injected again with 12.5mg/kg body weight of BrdU after 2 hours. Brains were collected 30 minutes post BrdU injection. EdU was detected following manufacturer instructions (ThermoFisher Scientific, #C10337). Prior to detection of BrdU by immunofluorescence as previously described, tissue was treated with hot 0.01 M sodium citrate pH 8 for 20 min followed by an acid wash (2N HCl and PBS/0.5% Triton X-100) for 1h at room temperature.

6.8.9 Statistical methods

Specific number of biological replicates (Ns) and statistical methods used are specified in each figure or figure legend. For cortical thickness, the thickness of the somatosensory cortex in three consecutive brain slices was measured and averaged per brain. The same strategy was used to measure the corpus callosum thickness. The hippocampal area was measured from both hippocampal hemispheres of three sections containing the dorsal hippocampus in which the habenula was visible. These measures were averaged and represented the results for a single brain. For histological and IUE quantifications, single or double fluorescently labelled cells were quantified for at least three consecutive sections in each brain and their results averaged.

To measure cell distribution in the cortex we used RapID ⁶²¹. Briefly, a grid containing eight equally-sized bins was manually placed in the cortex with bin 1 mainly covering the marginal zone and bin 8 covering the intermediate zone. The quantification of fluorescently labelled cells was automatically determined by the software.

All statistical analyses and plot generation were performed using Prism 9 (GraphPad, San Diego, CA).

6.9 Figures

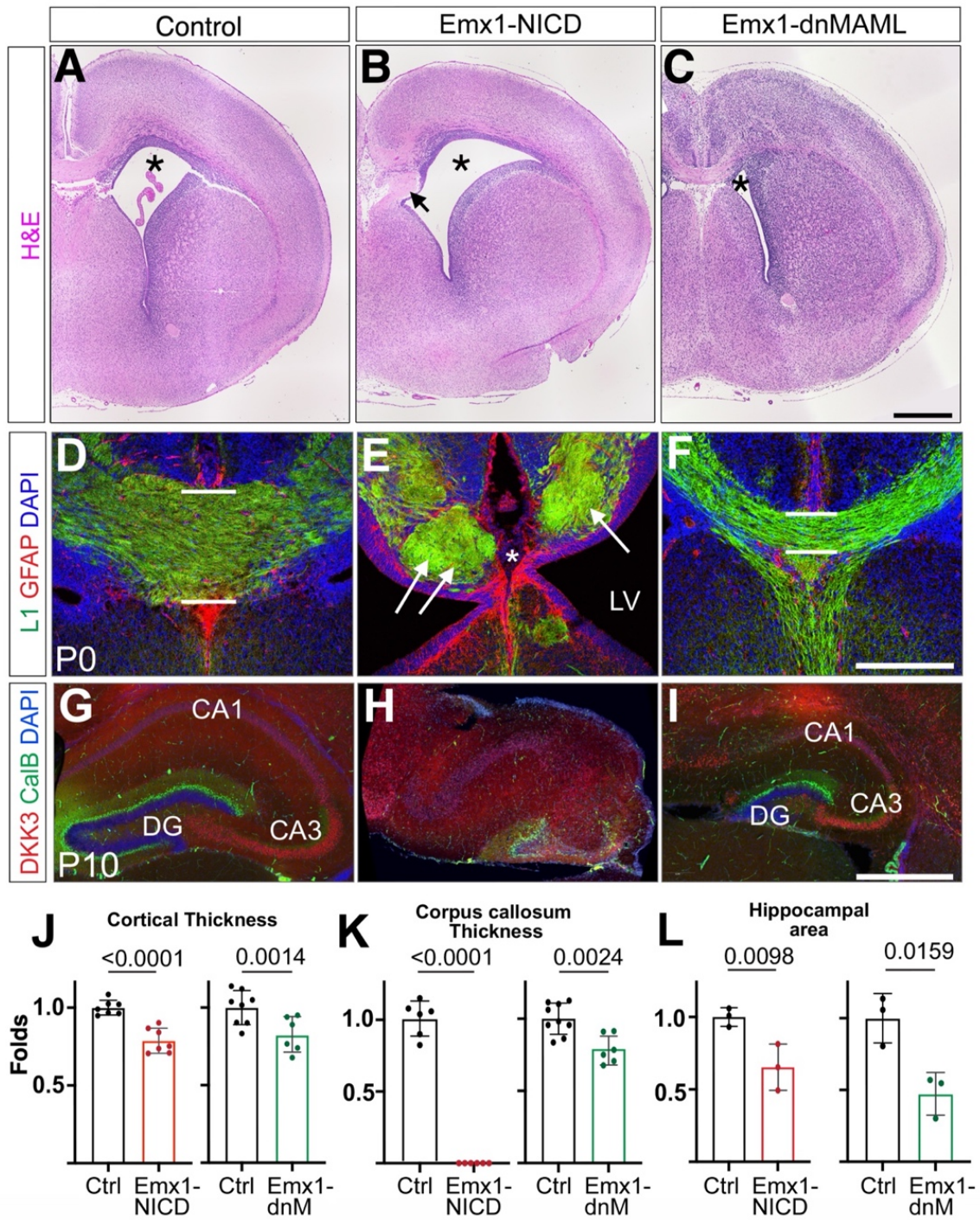


Figure 6.1 Morphological defects in Emx1-NICD and Emx1-dnMAML models

(A-C) Hematoxylin and eosin staining (H&E) of Control **(A)**, Emx1-NICD **(B)** and Emx1-dnMAML **(C)** P0 brains. Lateral ventricles are indicated with an asterisk. Arrow in B indicates axon Probst bundles. **(D-F)** P0 cortical slices were immunolabeled against GFAP (red) and L1 (green) and counterstained with DAPI (blue). The thickness of the corpus callosum is indicated in D and F with white bars. White arrows in E point at Probst bundles and asterisk indicates lack of corpus callosum. **(G-I)** P10 slices were immunolabeled against DKK3 (red) and Calbindin (green) and counterstained with DAPI (blue). Note the disorganization of the hippocampus in Emx1-NICD **(H)**. **(J-L)** Quantifications of cortical thickness **(J)**, corpus callosum thickness **(K)**, and hippocampal area **(L)**. Mean \pm SEM. P-values were obtained using Student's T-test. LV: lateral ventricle, DG: dentate gyrus, CA1-CA3: cornu ammonis hippocampal regions. Scale bars: 500 μ m A-C and G-I, 250 μ m D-F.

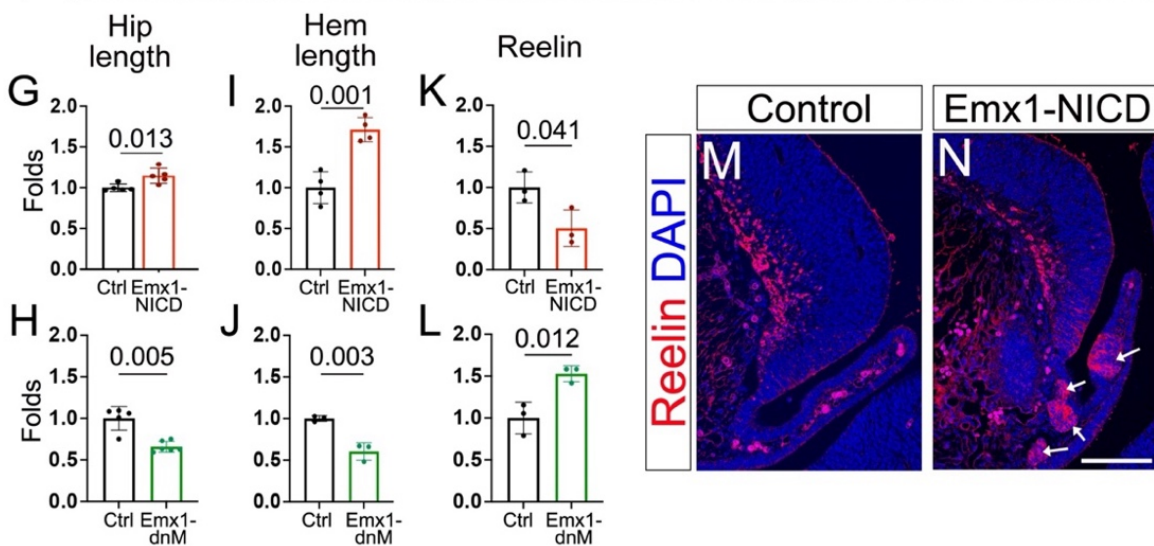
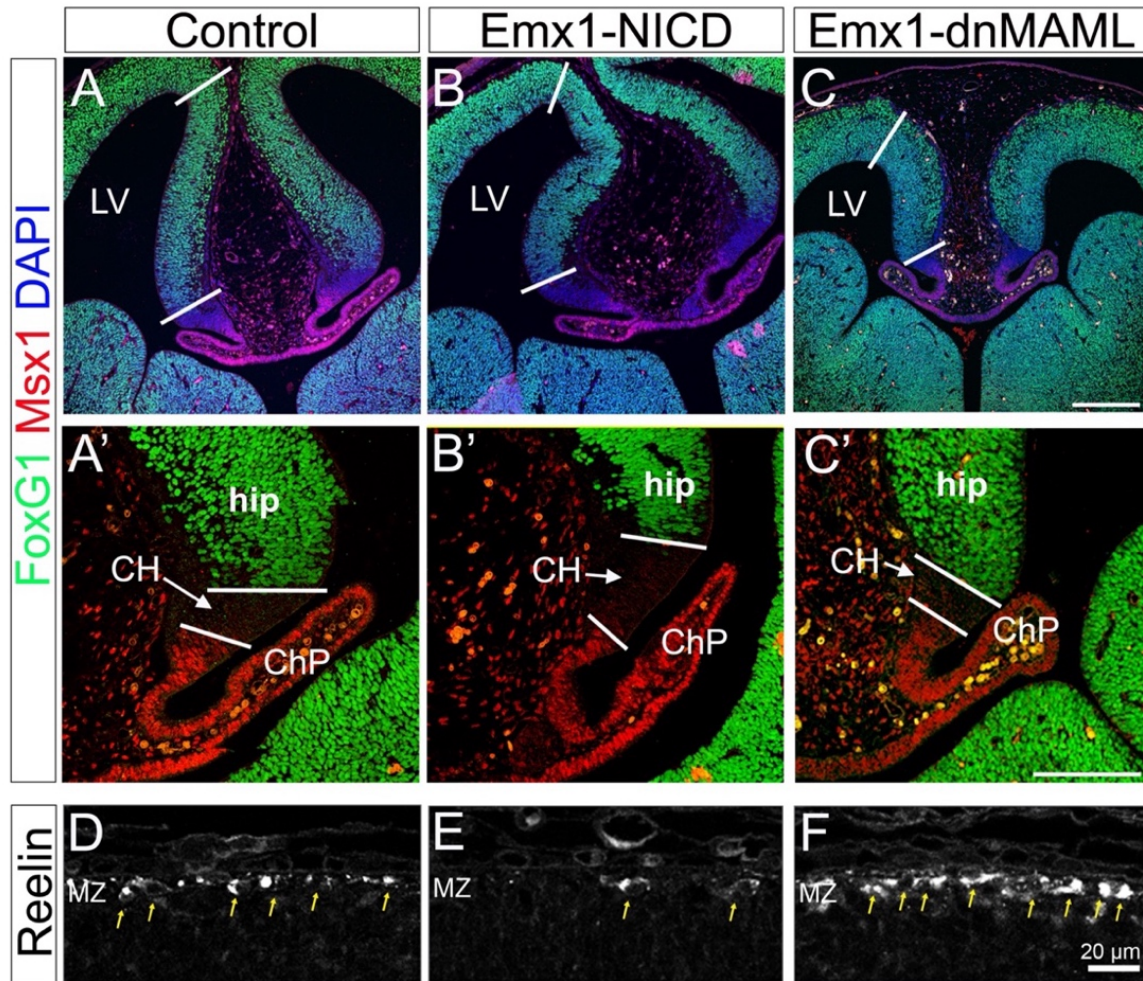


Figure 6.2 Midline patterning and production of Cajal-Retzius cells in Emx1-NICD and Emx1-dnMAML telencephalons

(A-C') Embryonic day 13.5 sections were immunolabeled against MSX1 (red), FoxG1 (green), and counterstained with DAPI (blue). White bars indicate hippocampal primordia **(A-C)** and cortical hem **(A'-C')** regions. **(D-F)** Reelin (white) labeling in the marginal zone of the neocortex identifies Cajal-Retzius cells (yellow arrows). **(G-L)** Quantifications of hippocampal length **(G-H)**, cortical hem length **(I-J)**, and number of Reelin+ cells/area **(K-L)** are shown as fold change compared to each control littermate. Mean \pm SEM. P-values were obtained using Student's T-test. **(M-N)** Emx1-NICD mice show patches of ectopic Reelin+ cells at E13.5 (white arrows). LV: lateral ventricle; hip: hippocampal primordia; CH: cortical hem; ChP: choroid plexus; MZ: marginal zone. Scale bars: 250 μ m A-C, 100 μ m A'-C' and M-N, 20 μ m D-F.

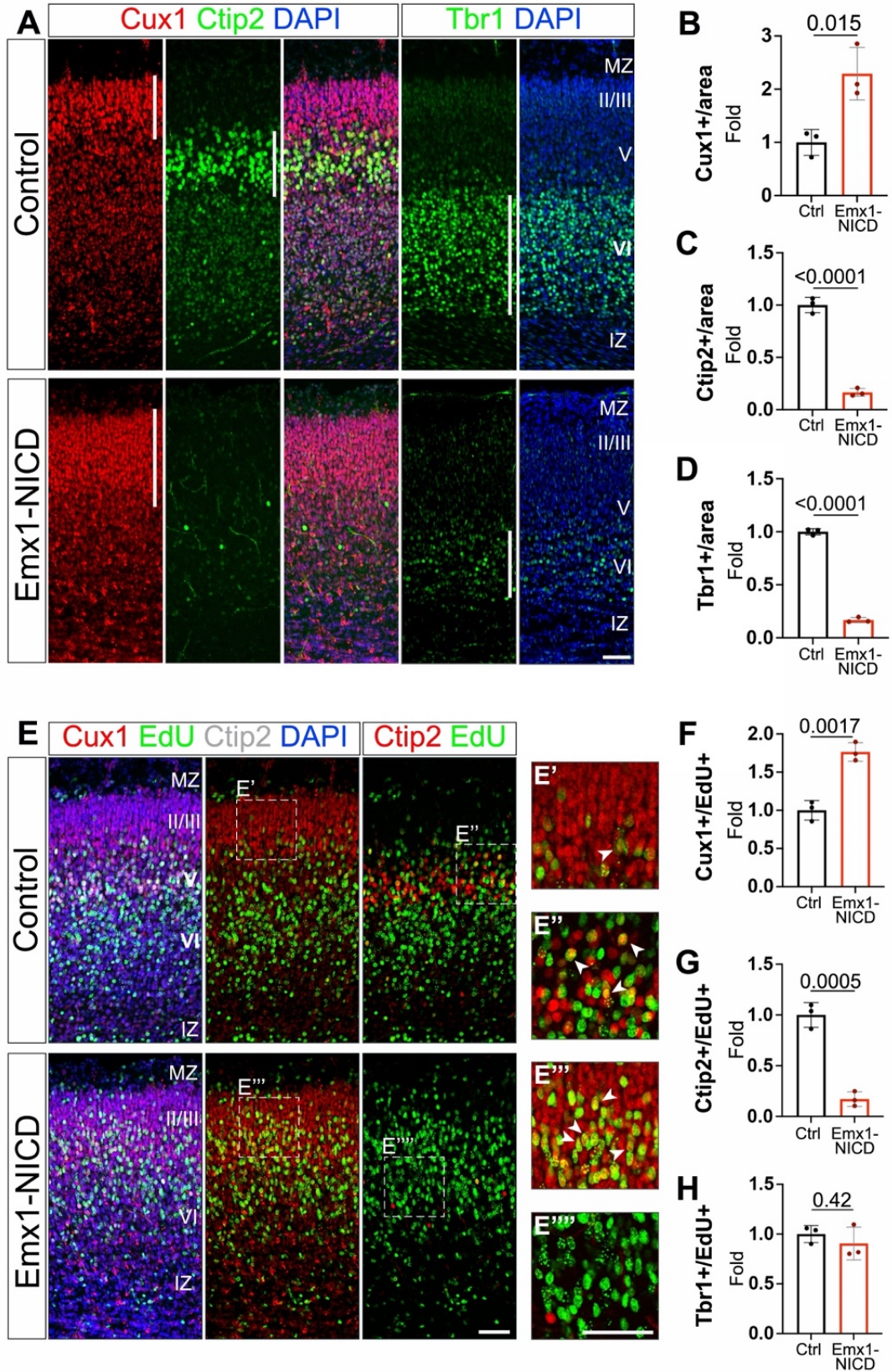


Figure 6.3 Emx1-NICD neocortices exhibit increased ratios of upper-layer neurons

(A) P0 cortical brain section immunolabeled with CUX1 (red), CTIP2 (green), and TBR1 (green) antibodies, and counterstained with DAPI (blue). **(B-D)** Quantifications of the number of cells per area are shown as fold change compared to their control littermates. **(E)** Cortical section labelings of EdU (green), CUX1 (red), CTIP2 (white left, red right) are counterstained with DAPI (blue). **(F-H)** Quantifications of the number of cells per area are shown normalized to their corresponding control littermates. Mean \pm SEM (B-D and F-H). P-values were obtained using Student's T-test. Scale bars: 50 μ m.

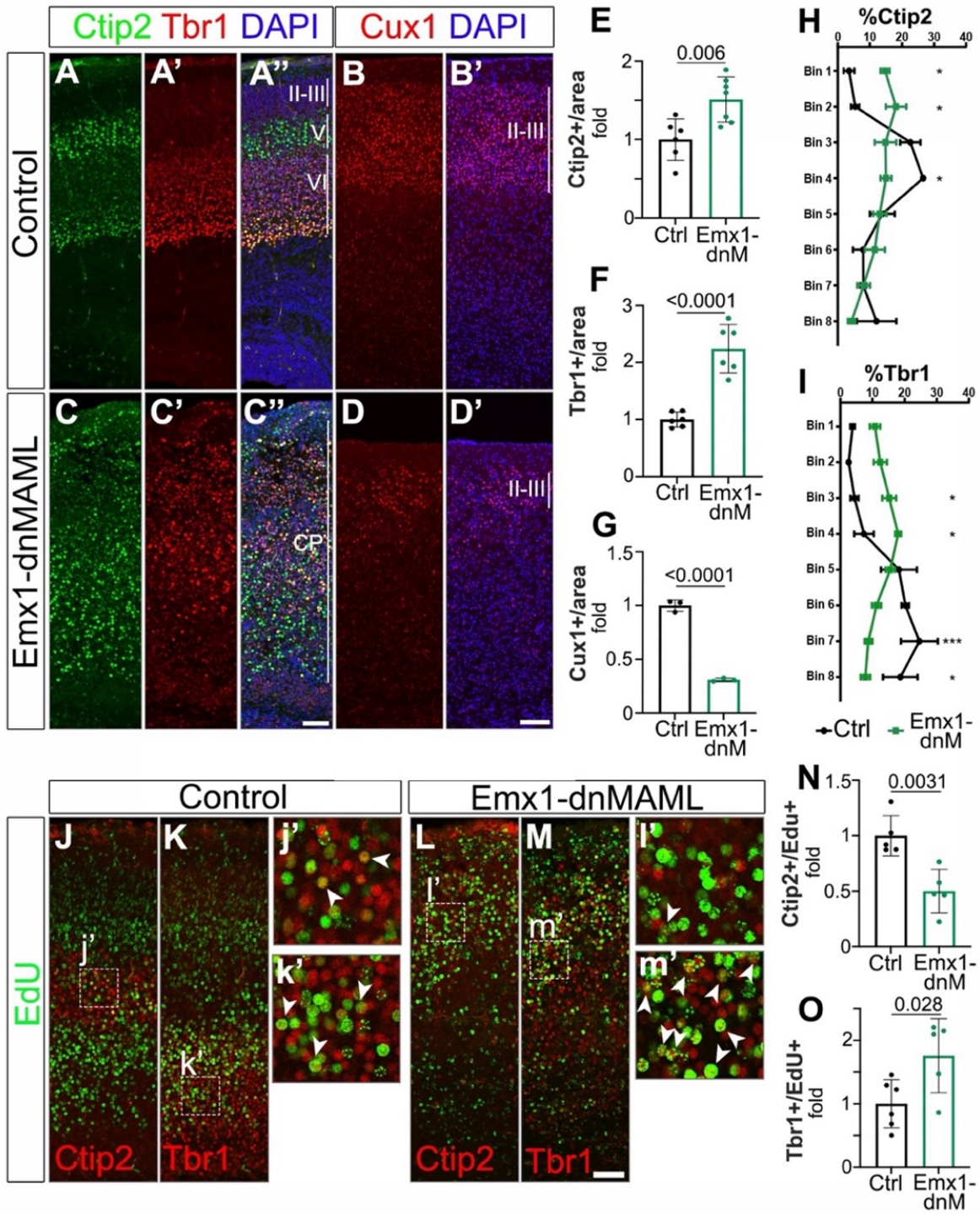


Figure 6.4 Emx1-dnMAML neocortices exhibit increased numbers of deep-layer neurons and lamination defects

(A-D') P0 cortical coronal section immunolabeled with CTIP2 (green) and TBR1 (red) **(A-A'' and C-C'')** and P10 coronal section immunolabeled with CUX1 (red) antibodies. Tissues were counterstained with DAPI (blue). **(E-G)** Quantifications of the number of cells per area are shown as fold change compared to their control littermates. **(H-I)** Distribution of CTIP2+ **(H)** and TBR1+ **(I)** cells in control (Ctrl) and Emx1-dnMAML (dnM) in P0 cortical brain slices. **(J-M')** Cortical section labelings of EdU (green), CTIP2 (red), and TBR1 (red) are counterstained with DAPI (blue). **(N-O)** Quantifications of the number of cells per area are normalized to their corresponding control littermates. Mean \pm SEM. P-values in (E-G) and (N-O) were obtained using Student's T-test. For cell distribution in (H-I), multiple unpaired T tests (one per bin) with Welch correction were performed (*, Adjusted P value <0.05; ***, Adjusted p-value <0.001). Scale bar: 50 μ m.

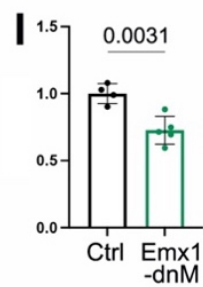
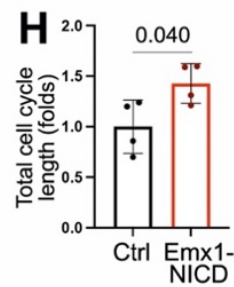
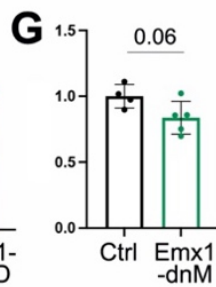
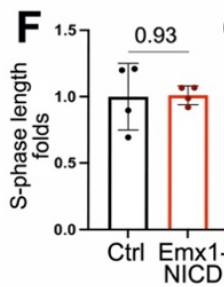
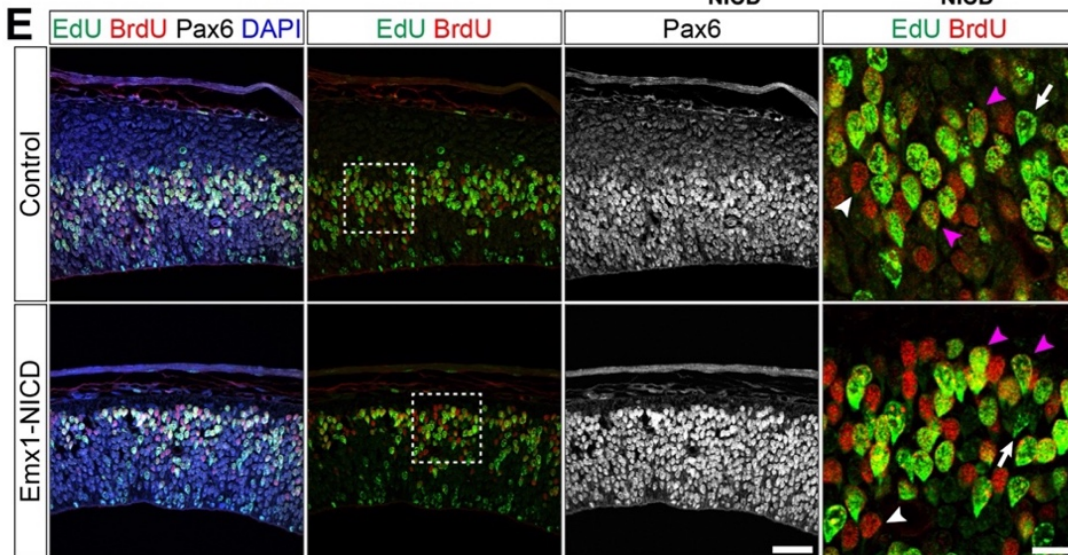
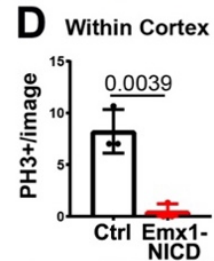
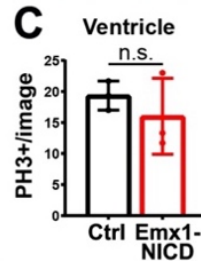
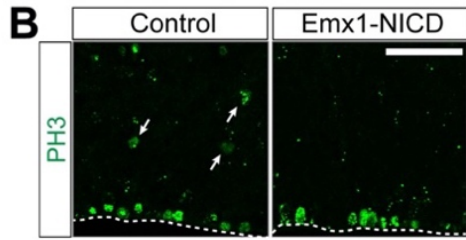
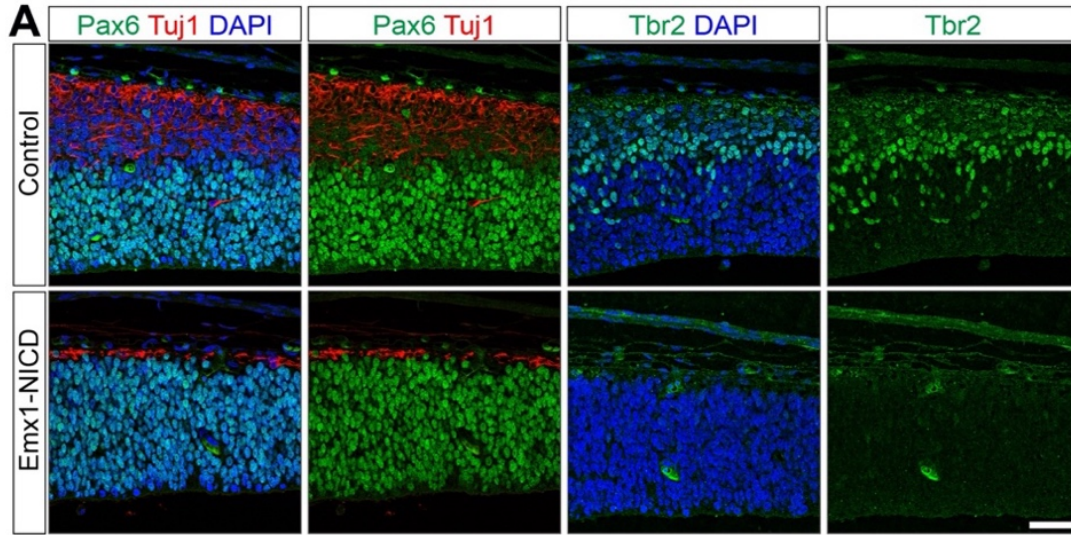


Figure 6.5 Notch regulates Radial Glia cell cycle dynamics

(A) Cortical slices from E13.5 control and Emx1-NICD embryos immunostained against PAX6 (green), β -III-Tubulin (Tuj1, red), TBR2 (green) and DAPI (blue). **(B)** Cortical slices from E13.5 control and Emx1-NICD embryos immunostained against phospho-Histone3 (PH3, green). **(C-D)** Quantification of PH3⁺ cells in the ventricular surface (C) and anywhere else in the cortex area above the ventricular surface (D). **(E)** E13.5 cortical section labelings of EdU (green), BrdU (red), and PAX6 (white), and DAPI (blue). **(F-G)** Quantification of S-phase length in Emx1-NICD (**F**) and Emx1-dnMAML (dnM) (**G**) mice in comparison to their control littermates. **(H-I)** Quantification of total cell cycle length in Emx1-NICD (**H**) and Emx1-dnMAML (dnM) (**I**) mice in comparison to their control littermates. Mean \pm SEM (F-I). P-values were obtained using Student's T-test. Scale bars: 50 μ m A, B and E (except for the right panels in E, 20 μ m).

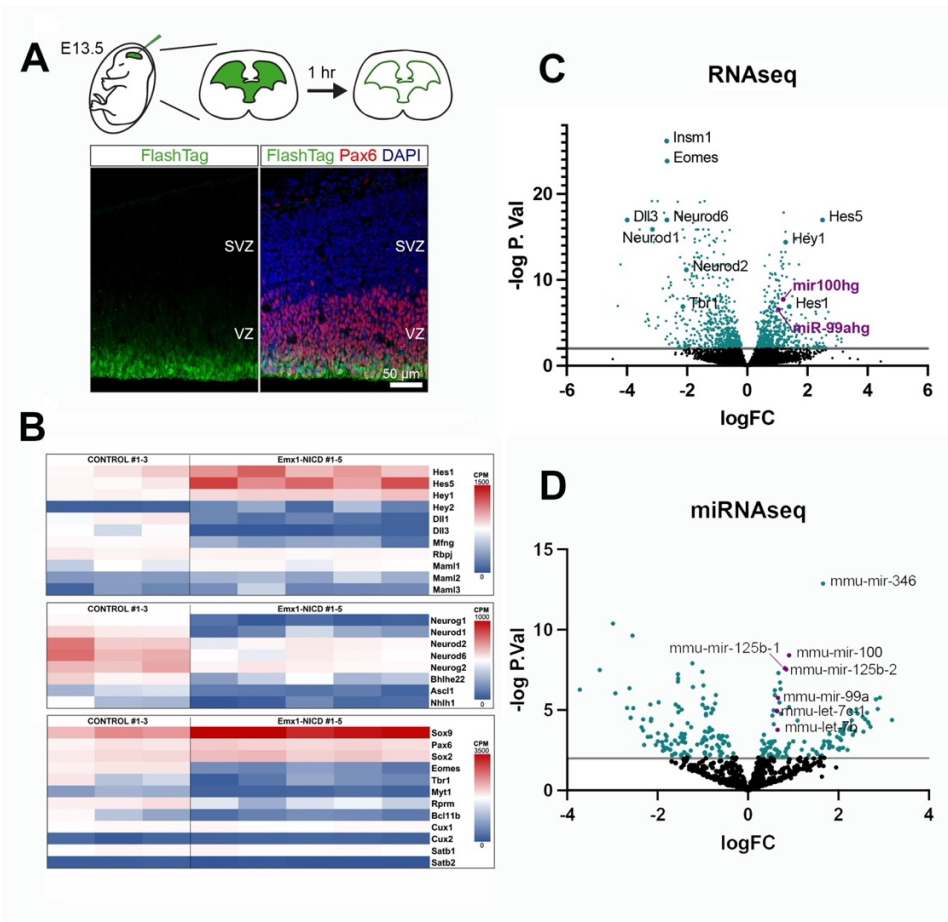


Figure 6.6 Transcriptional changes in Emx1-NICD Radial Glia

(A) Experimental design (top). Only the PAX6+ RGs (red) closest to the ventricular surface were labeled with FlashTag (green) 1h post-injection (bottom). **(B)** Heatmaps showing RNA-seq analysis of selected Notch signaling-related genes (top), bHLH genes (middle), and cortical markers (bottom). **(C-D)** Volcano plots representing differential gene **(C)** and miRNA **(D)** expression between Emx1-NICD (n=5) and control (n=3) RGs samples. Ratio of counts per million between Emx1-NICD and control per gene or miRNA is plotted. The x-axis represents the logarithmic fold ratio of Emx1-NICD/control per gene and miRNA identified. The y-axis represents the logarithmic adjusted p-value (false discovery rate) calculated by the Benjamini-Hochberg Procedure. Genes with fewer than 5 counts per million reads in all samples were filtered prior to analysis, leaving 12,556 genes. MiRNAs present in fewer than 3 samples were filtered prior to analysis, leaving 779 miRNAs.

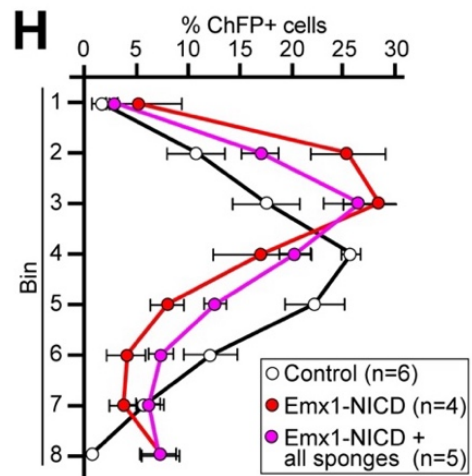
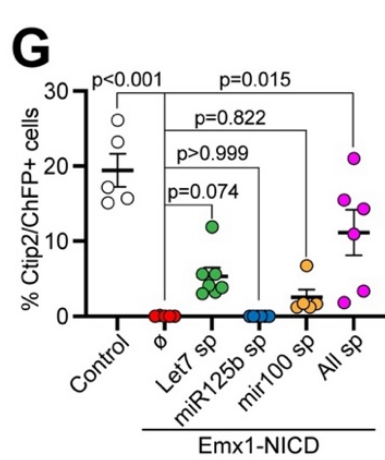
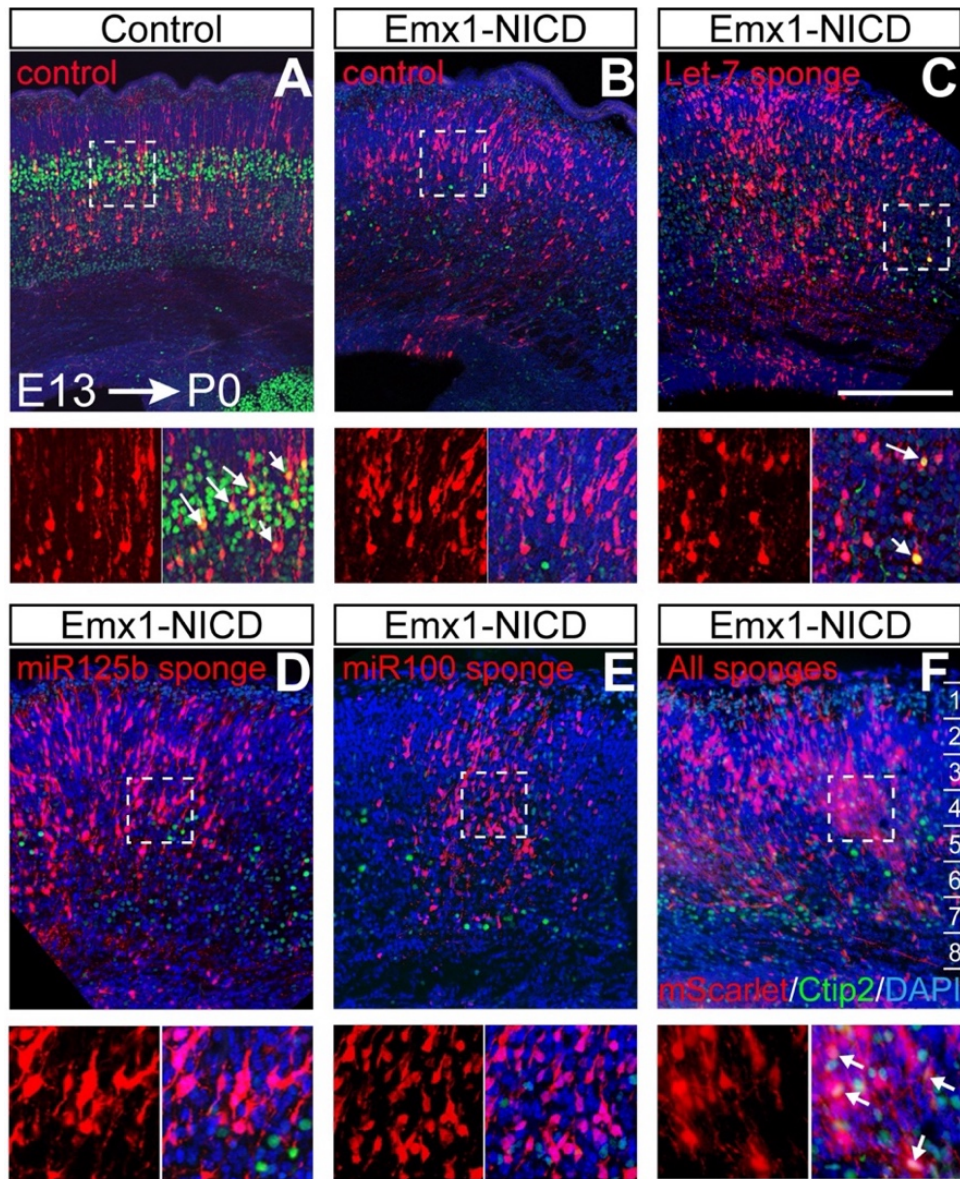
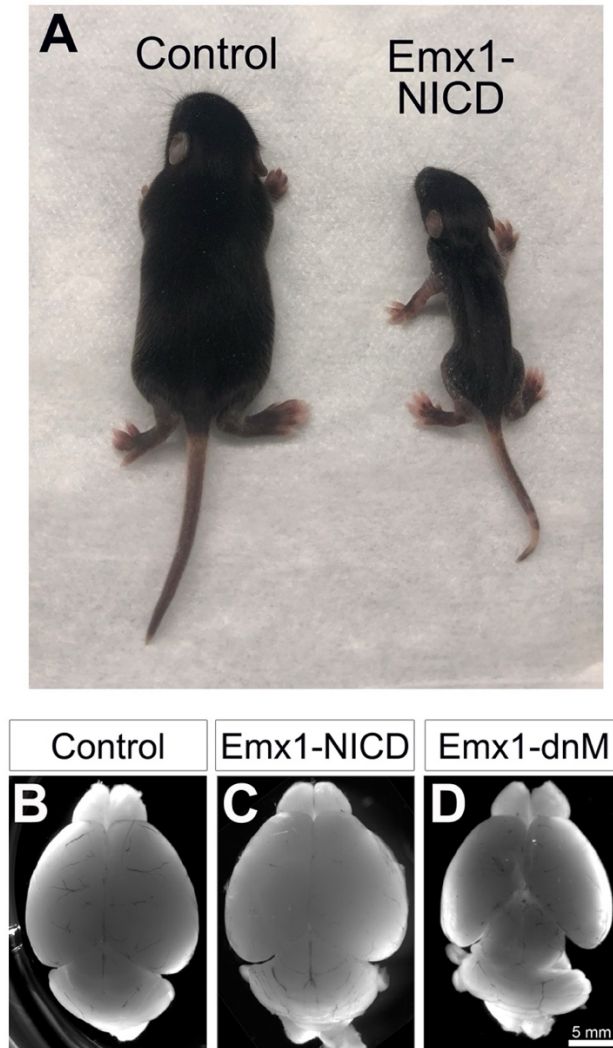


Figure 6.7 Inhibition of let-7, miR-125b, and miR-100 expression rescues cortical cell fate defects in Emx1-NICD mice

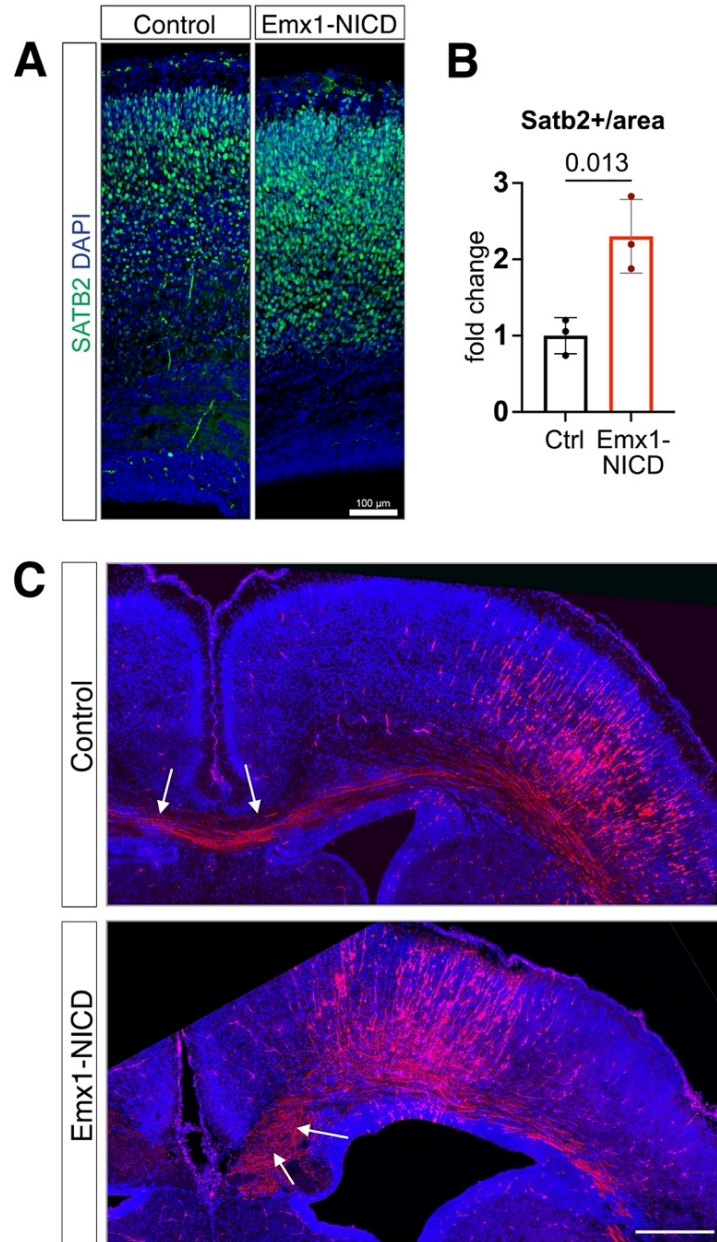
(A-B) Representative images of control **(A)** and Emx1-NICD **(B)** mice electroporated with control plasmid (mScarlet, red) and Emx1-NICD mice co-electroporated with mScarlet and miRNA sponges against let-7 **(C)** miR-125b **(D)**, miR-100 **(E)**, or all three sponges **(F)**. Quantification of the percentage of CTIP2+/mScarlet+ cells in each condition **(G)**. Mean \pm SEM. Adjusted p-values were obtained with Kruskal-Wallis test and Dunn's post-hoc test. **(H)** Distribution of mScarlet+ cells from (A), (B), and (F) electroporations. Mean \pm SEM. Adjusted p-values were obtained with Kruskal-Wallis test and Dunn's post-hoc test. Scale bar: 250 μ m.

6.10 Supplementary figures



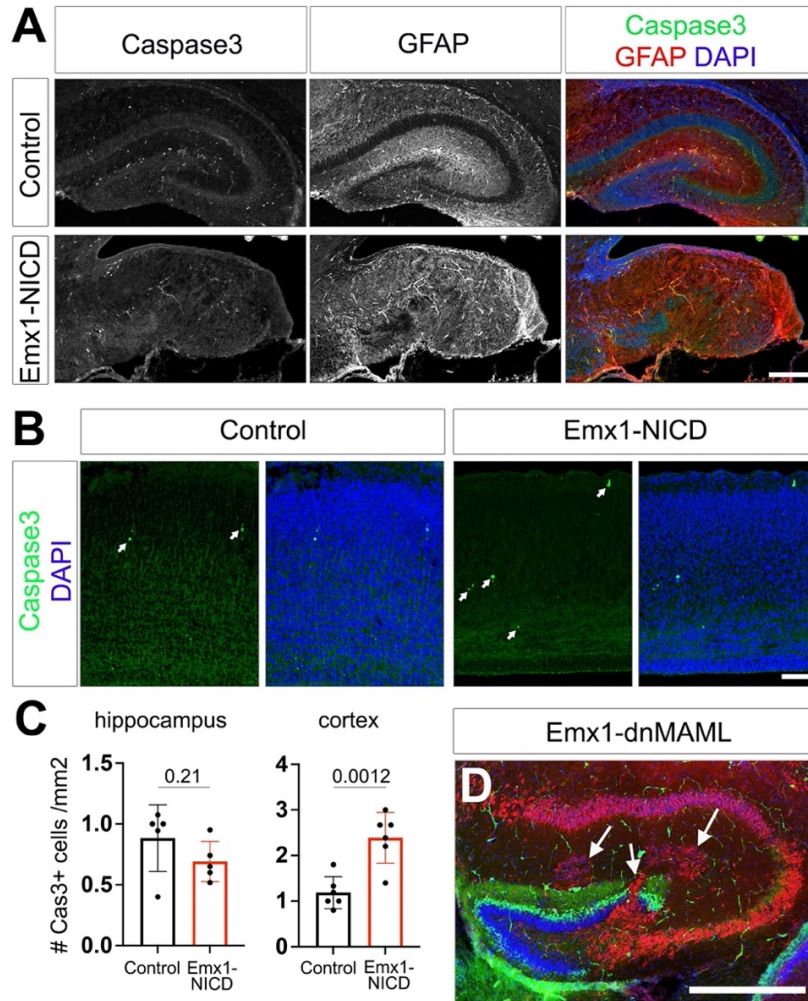
Supplementary Figure 6.1 Emx1-NICD and Emx1-dnMAML mice

(A) At P14, Emx1-NICD mice are smaller in size compared to their control littermates. **(B)** At P0, the size of the brain is significantly smaller in Emx1-dnMAML mice compared to their littermate controls but no significant differences were observed in Emx1-NICD. Scale bar B-D: 5mm.



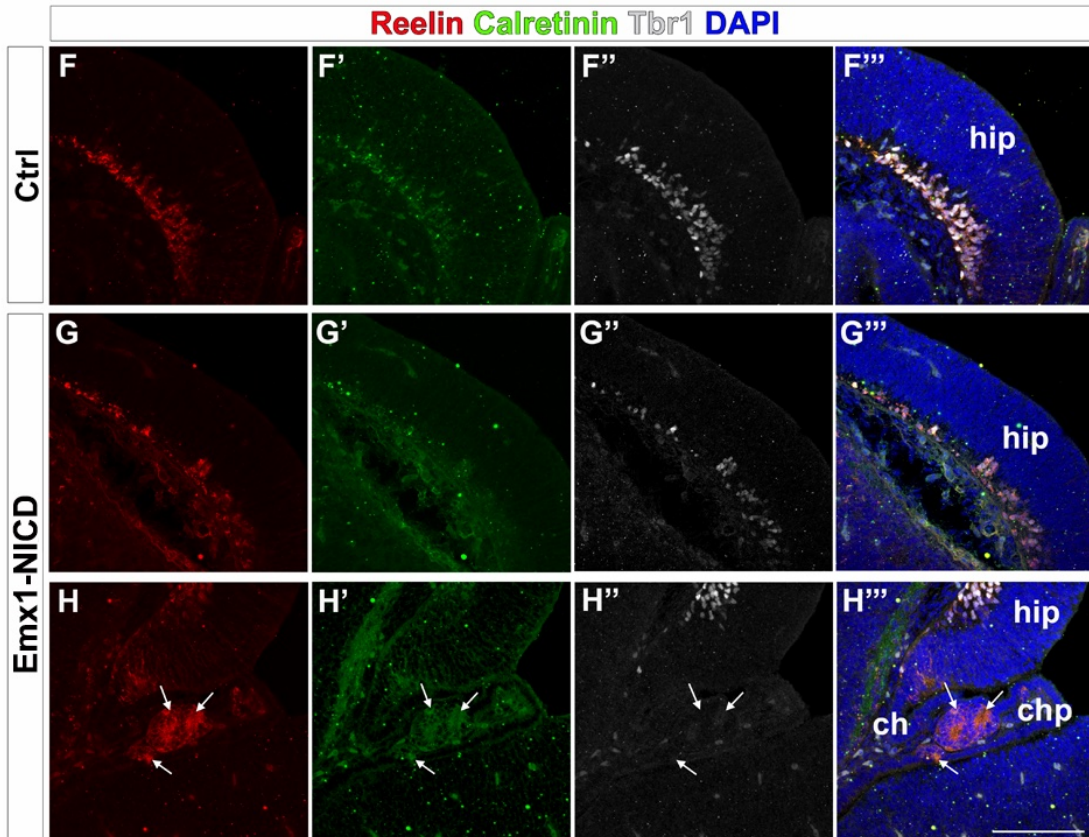
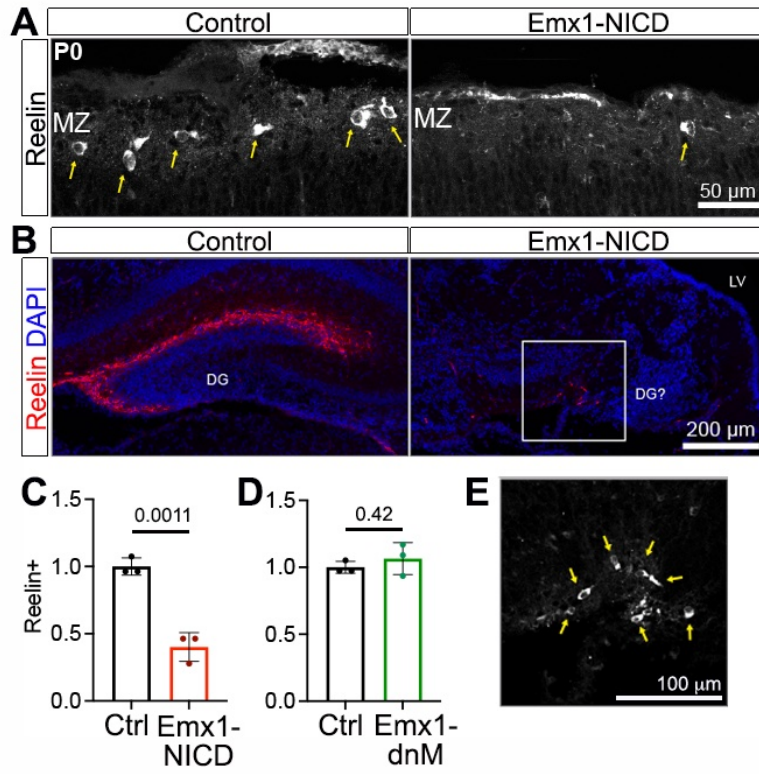
Supplementary Figure 6.2 Agenesis of the corpus callosum in EMX1-NICD mice

(A-B) At P0, Emx1-NICD cortices exhibit increased ratios of SATB2⁺ callosal neurons (green) compared to their littermates, DAPI (blue) was used for counterstaining. P-value was obtained using Student's T-test. Scale bar: 100 microns. **(C)** Upon *in utero* electroporation of mCherry (red), labeled axons (while arrows) cross the midline in control animals but result in aberrant bundles in Emx1-NICD mice. Scale bars: 100mm A-B; 250mm C.



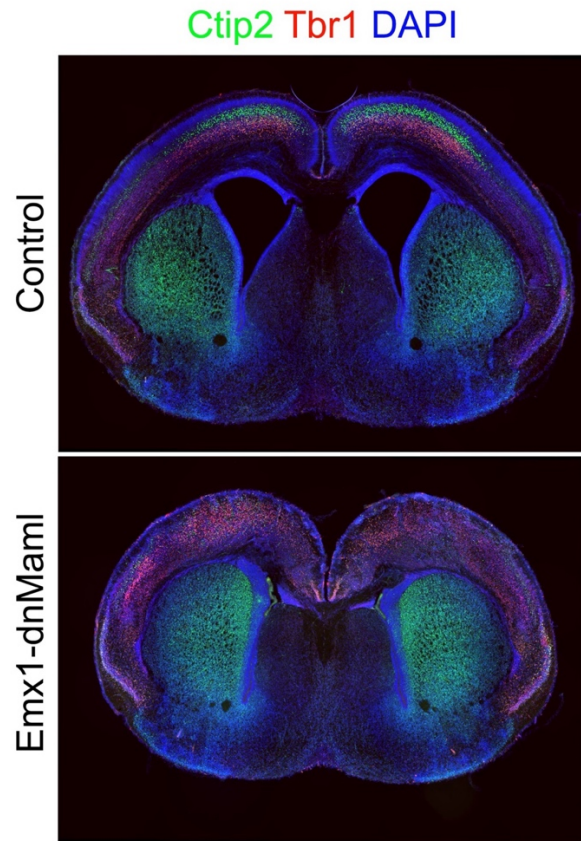
Supplementary Figure 6.3 Hippocampal defects in Emx1-NICD and Emx1-dnMAML mice

(A) Caspase3 (green) and GFAP (red) immunolabeling of control and Emx1-NICD hippocampi at P0, counterstained with DAPI (blue). Scale bar: 100 microns. **(B)** Caspase3 (green) immunolabeling of control and Emx1-NICD neocortices at P0. White arrows point at Caspase3+ cells. Scale bar: 70 microns. **(C)** Quantification of Caspase3+ cells in hippocampus and cortex, p-values were obtained using Student's T-test. **(D)** Immunolabeling using DKK3 (red) and Calbindin (green) antibodies, counter-stained with DAPI (blue) of Emx1-dnMAML hippocampal section. Note the ectopic location of some DKK3+ cells (white arrows). Scale bars: 100mm A, 70mm B, 200mm D.



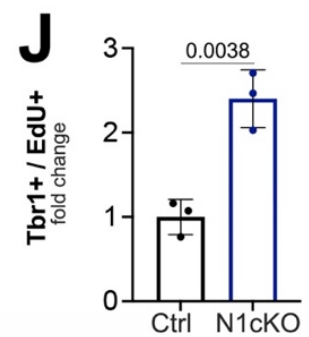
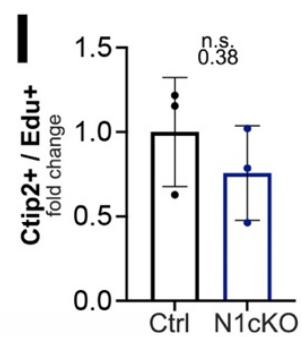
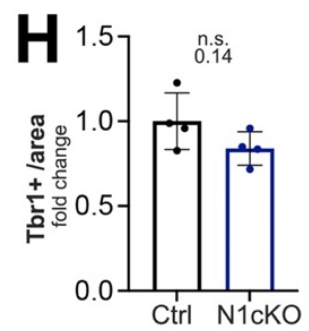
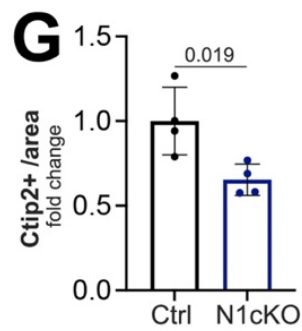
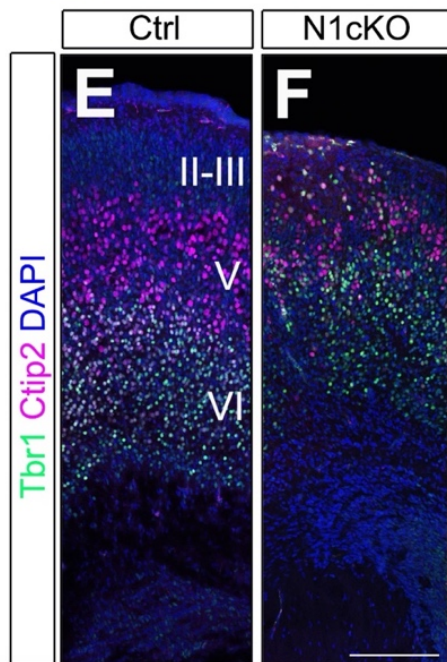
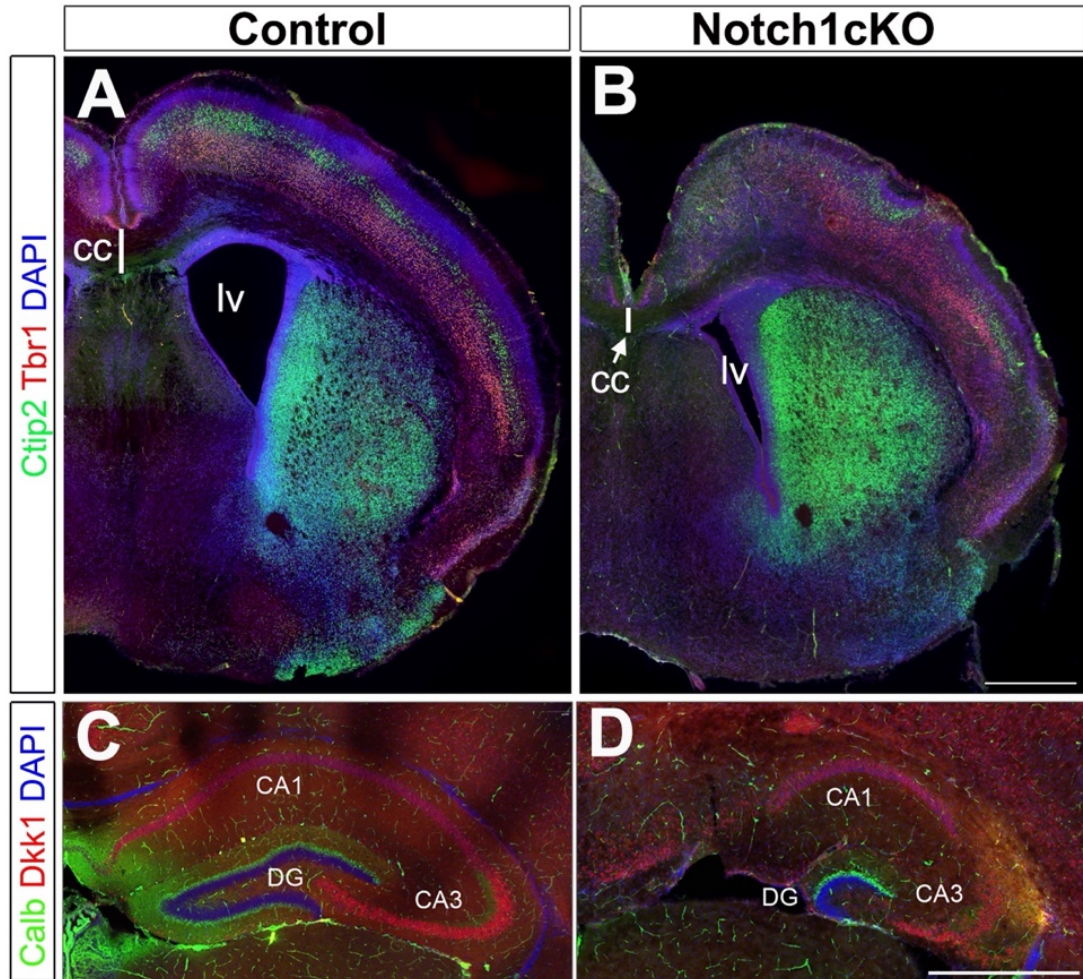
Supplementary Figure 6.4 Aberrant production of Cajal-Retzius cells in Emx1-NICD and Emx1-dnMAML mice

(A) Emx1-NICD cortices exhibit less Reelin⁺ (white label, yellow arrows) than their littermate controls at P0. Scale bar: 50 microns. MZ: marginal zone. **(B)** Immunolabeling with Reelin (red) in control and Emx1-NICD hippocampal sections. The white inset box is shown in E. LV: lateral ventricle, DG: dentate gyrus. Scale bar: 200 microns. **(C-D)** Quantification of number of Reelin⁺ cells/area in Emx1-NICD and Emx1-dnMAML hippocampi at P0. P-Values were obtained using Student's T-tests. **(E)** Only a handful of Reelin⁺ cells (white, noted with yellow arrows) are detected in Emx1-NICD hippocampi. F-H". Emx1-NICD hippocampi have fewer Cajal-Retzius cells compared to controls at E13.5. Cajal-Retzius cells are detected using a combination of Reelin, Calretinin, and Tbr1 markers. Ectopic patches are detected in the choroid plexus regions of Emx1-NICD mice, which co-express Calretinin but not TBR1. Hip: hippocampal primordia; CH: cortical hem; ChP: choroid plexus. Scale bars: 50mm A, 200mm B, 100mm E and F-H".



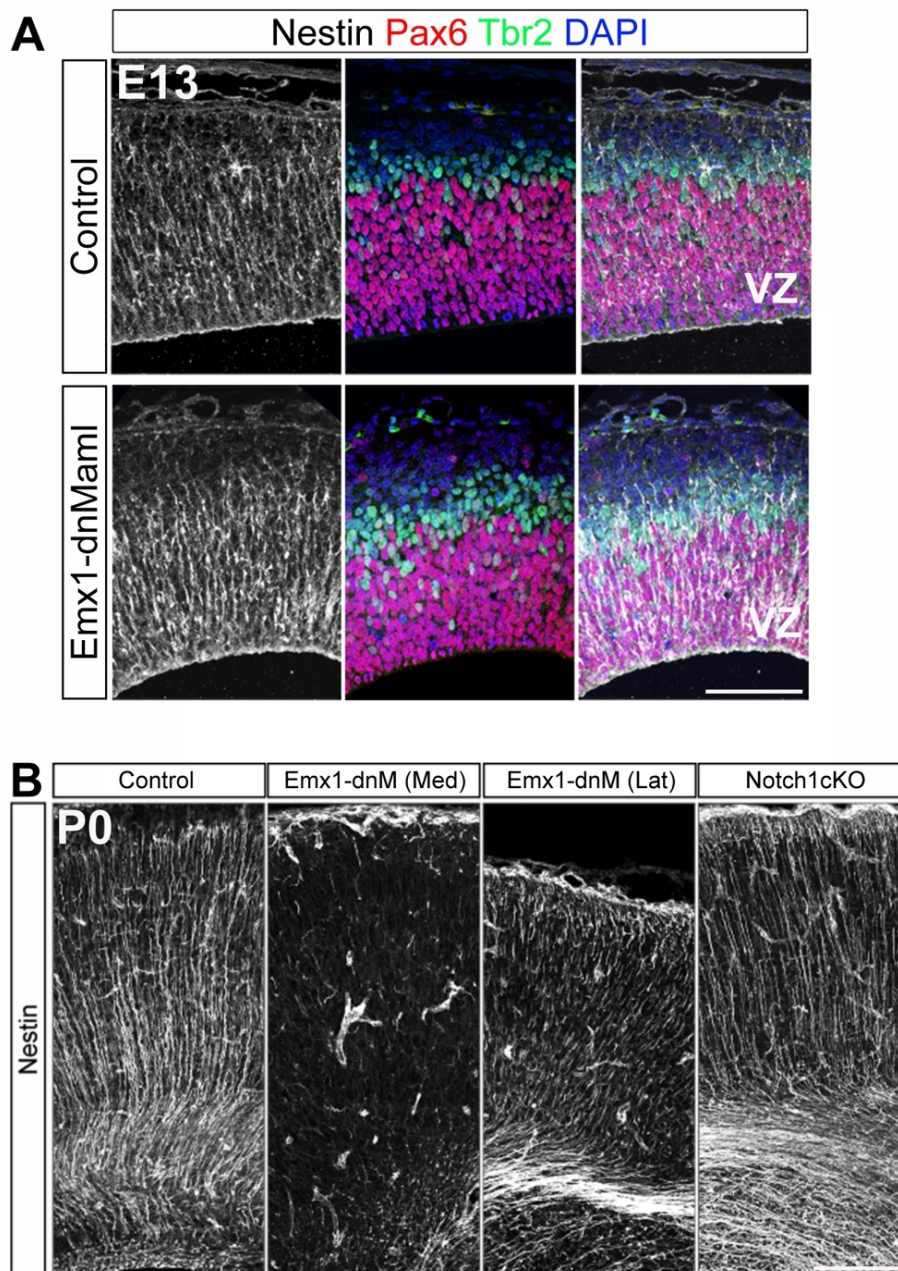
Supplementary Figure 6.5 Lamination defects in Emx1-dnMAML neocortices

Brain coronal sections immunolabeled against CTIP2 (green), TBR1 (red), and counterstained with DAPI (blue). Scale bar: 500mm.



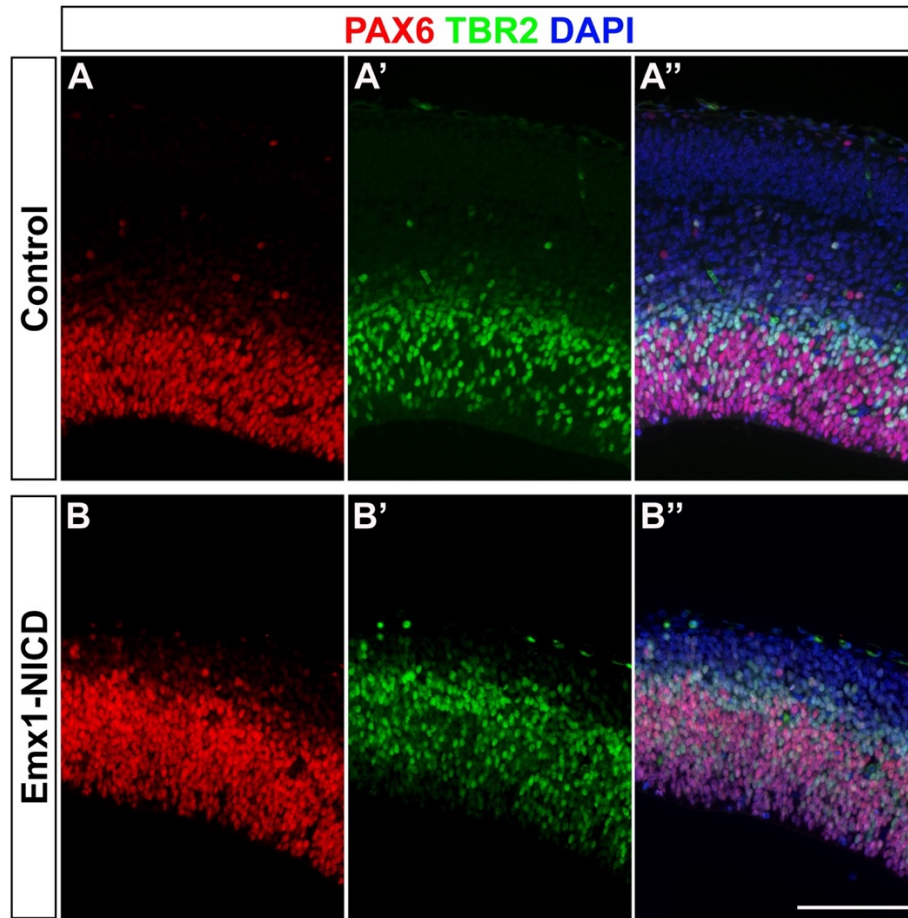
Supplementary Figure 6.6 Notch1cKO phenotypes

(A-B) Brain coronal sections immunolabeled against CTIP2 (green), TBR1 (red), and counterstained with DAPI (blue). The thickness of the corpus callosum is indicated with a white bar. Scale bar: 500 microns. CC: corpus callosum; LV: lateral ventricle. **(C-D)** Hippocampal sections stained against Calbindin (green) and DKK3 (red) and counterstained with DAPI (blue). Scale bar: 250 microns. CA1-CA3: hippocampal regions, DG: dentate gyrus. **(E-F)** Cortical sections stained with TBR1 (green) and CTIP2 (magenta), and counterstained with DAPI (blue). Scale bar: 100 microns. **(G-H)** Quantifications of CTIP2⁺ and TBR1⁺ cells/area, respectively in control and Notch1cKO samples. **(I-J)** Quantification of ratio of EdU⁺ cells colabeled with either CTIP2 or TBR1. For all quantifications (G-J), p-values were obtained using Student's T-tests. Scale bars: 500mm A-B, 250mm C-D, 100mm E-F.



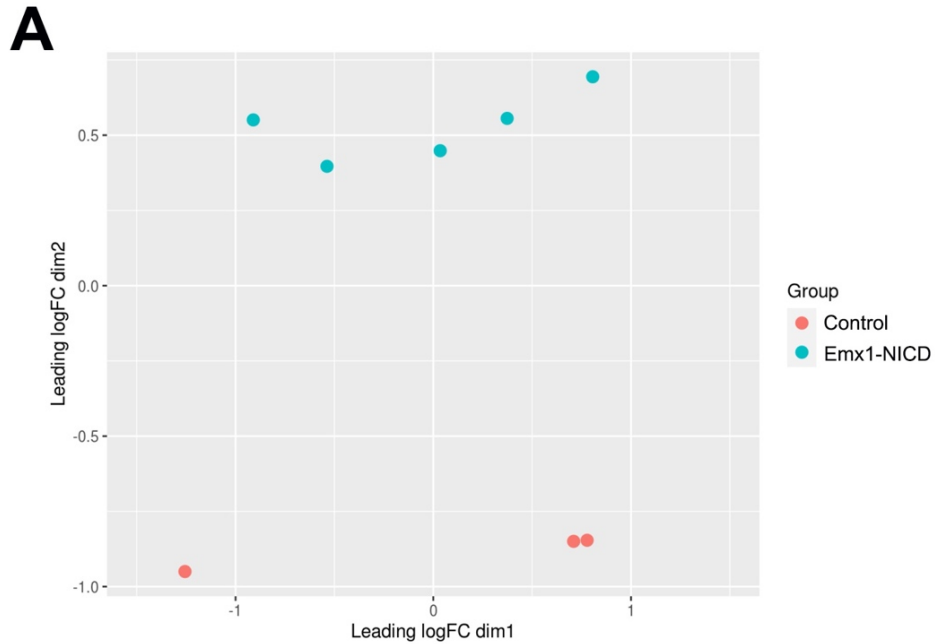
Supplementary Figure 6.7 Radial glia in Emx1-dnMAML and Emx1-Notch1cKO

(A) Nestin (white), PAX6 (red) and TBR2 (green) antibody labeling of control and Emx1-dnMAML cortices were counterstained with DAPI (blue). **(B)** Nestin (white) immunolabeling of cortices from control samples, Emx1-dnMAML, and Emx1-Notch1cKO. Note the difference between the medial (dnMAML-med) and lateral aspects (dnMAML-lat) of the cortices upon dnMAML upregulation. VZ: ventricular zone. Scale bar: 100mm.



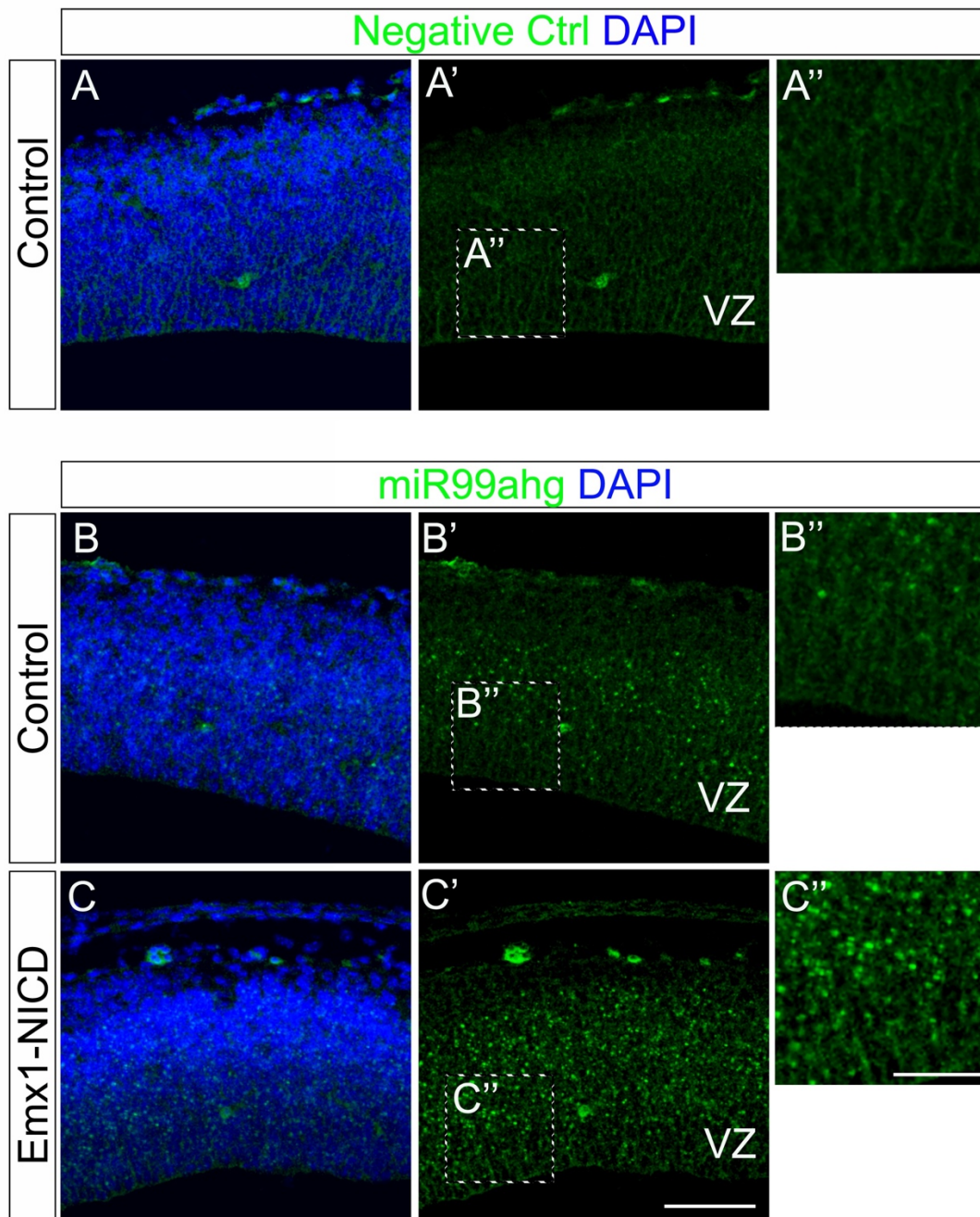
Supplementary Figure 6.8 TBR2+ intermediate progenitors at E15.5

PAX6 (red), TBR2 (green) and DAPI (blue) in Control (A-A'') and Emx1-NICD (B-B'') cortices at E15.5. Scale bar: 100µm.



Supplementary Figure 6.9 RNA sequencing

(A) Multidimensional scaling analysis (MDS) showing control samples (orange) and Emx1-NICD samples (teal). (B) Gene Ontology (GO) analyses using PANTHER Classification System.



Supplementary Figure 6.10 Validation of RNA sequencing using RNAscope

(A-A'') Negative control probe (green) counterstained with DAPI (blue). (B-C'') miR99ahg probe signal is shown in green in control (B-B'') and Emx1-NICD mice (C-C''). These samples have also been counterstained with DAPI (blue). Scale bar: 100mm in C' and 50mm in C''.

6.11 Supplementary tables

Supplementary Table 6.1 RNA-seq differential expression

Normalized counts of Emx1-NICD vs Control samples.

Supplementary Table 6.2 microRNA-seq differential expression

Normalized counts of Emx1-NICD vs Control samples.

Supplementary Tables 6.1 and 6.2: These are large tables that are not suitable for print.

To view this data, please visit the official publication where all figure and supplemental information may be downloaded.

7. Concluding remarks

7.1 Summary

In this dissertation, I explore the mechanisms that drive cell fate specification in the central nervous system. My studies on retina development extend across models with variable visual acuity, from non-human primate and humans to mice models, and the cortical development experiments were conducted in the mouse model.

Chapter 3 characterizes normal retinal development in the non-human primate. Modern labeling techniques were used to define key stages of neurogenesis that lay critical groundwork for future comparative studies with other organisms. We investigated how molecules of the retinoic acid pathway, which have previously been implicated in the development of the specialized region of the chicken retina, are expressed in a foveated retina. Interestingly, we found CYP26A1 to be expressed in progenitors not limited to the fovea in early retinal development and later in Müller glia. My findings contrast those from other studies that stated this molecule is exclusively expressed in foveal progenitors in the human retina. While FGF8 is required for the development of the HAA in chickens, it is not fovea-specific in the developing non-human primate retina. Such findings further emphasize that the avian HAA and primate fovea are not analogous. This examination of gene expression patterns reveals that the specialized retinal regions are not defined by the same mechanisms. However, the distinct mechanisms to make the HAA and fovea may be leveraged to further discern the roles of molecules involved in foveal development (See “Interpreting results with additional models” section, page 246).

Chapter 4 analyzed what distinguishes genes with distinct temporal and nasal expression patterns in the developing non-human primate retina. We identified genes and

miRNAs highly differentially expressed across the non-human primate retina. We further validated those miRNAs unique to either the temporal or the nasal retina in the sequencing experiments through *in situ* hybridizations in the human and mouse retinas. The miRNAs enriched in the temporal non-human primate and human retinas were enriched in the central mouse retina, and those enriched in the nasal foveated retinas were enriched in the peripheral afoveated retina. These results suggest that the miRNAs found to be highly differentially expressed across the primate retina are indicating older and newer regions of the retina.

Chapter 6 explored how the Notch pathway and miRNAs influence cell fate specification in the mouse cortex. Using a gain-of-function mutant to increase Notch expression, we showed that Notch signal limits early-born neuron production. A dominant negative model revealed that inhibiting Notch extends the production of early-born neurons. Over activating Notch caused general transcriptome changes of miRNAs, namely of the miR-100 and miR-99 host genes. Overexpressing Let-7, miR-125b, and miR-100 showed that miRNAs are required to restrict early-born neurons. Both the retina and cortex are derived from a single population of multipotent progenitors that are temporally regulated to differentiate into early- and late-born cell populations. The ability to perform manipulations of miRNAs *in vivo* via IUEs makes the cortex a valuable system to study how miRNAs influence cell cycle dynamics and cell fate specification.

Together, these studies identify a subset of the molecular mechanisms that drive cell fate specification in the central nervous system. They show that miRNAs do not act alone in this process, but are instead part of a concerted effort of various molecules and pathways.

7.2 Utilizing microRNAs to advance stem cell protocols

The ultimate future goal of this research is to develop and optimize stem cell protocols to increase cone yield. Successful protocols exist to culture and differentiate human embryonic stem cells into retinal organoids. While these organoids appropriately resemble the retina, none have existed that possess a fovea. With the findings from this research, we hypothesize that miRNAs could be targeted during retinal organoid development to increase cone production.

7.2.1 Organoid protocols

Organoid production is an involved process that requires months of attention, and then maintaining the retinal organoids is an act of patience. There are a seemingly infinite number of opportunities to manipulate development, as the cells are accessible at every stage of proliferation, differentiation, and organogenesis. Current organoid protocols include the timely introduction of various medias, including neural induction media, retinal differentiation media, retinal maintenance media, and photoreceptor induction media. The sequential modification of nutrients and factors mimics the environment of *in vivo* eye development to encourage the transitions of embryoid body to optic vesicle and then retinal differentiation to photoreceptor maturation. There is a wide variability among protocols. One study suggests a combination of B27, fetal bovine serum (FBS), and taurine to create a cone-rich retinal organoid⁶⁵⁸. Some groups are looking more specifically at manipulating retinoic acid and thyroid hormone levels to influence cone subtypes^{16,659}. There are conflicting findings about the usefulness of retinoic acid in differentiation protocols, with some studies claiming it is wholly unnecessary and other

claiming that it increases rod photoreceptor yield⁶⁶⁰⁻⁶⁶². Additionally, studies are looking at the usefulness of all-trans retinoic acid (ATRA) or 9-cis-retinoic acid⁶⁶⁰. While it is valuable to be able to make retinal organoids enhanced for various cell types, the field is not yet there for the cone-rich retinal organoids needed for transplantations.

I hypothesize that manipulating miRNAs in various steps of retinal organoid differentiation will be necessary for increasing cone yield. First, extend the window of cone production. This could be accomplished by limiting RPCs from undergoing the competence switch, and consequently losing the ability to make early-born cell types. The LP-miRNAs—Let-7, miR-9, and miR-125b—have been shown to promote RPCs to switch their competence from making early-born to making late-born cells. Perhaps these miRNAs may be targeted to prevent the RPCs in the organoids from transitioning to the late competence state, increasing early-born cell production at the expense of late-born cell types. Second, target miRNAs that directly contribute to cone fate specification. The list of miRNAs differentially expressed across the developing non-human primate retina (Chapter 4) may contain prime candidates for cone production regulators. Further validation of expression, mRNA regulation, and the upstream factors that regulate expression of the candidates will reveal if these miRNAs (individually or grouped together) influence cone production. After identifying miRNAs that increase cone production, it will be imperative to identify the appropriate windows to do so during organoid differentiation. The LP-miRNAs would be targeted after optic vesicle formation, and the miRNAs more specific to cone fate targeted after.

There are a number of modalities to manipulate the miRNAs in stem cells. It is worth considering that the resultant neurons are intended for human transplantation, so

minimizing unnecessary genetic modification is important. Some options include nanoparticle and lipid molecules to deliver specific miRNAs or antagomiRs⁶⁶³. Such methods are currently being investigated to deliver RNA interference (RNAi) in cancer models and show promise⁶⁶⁴.

7.2.2 microRNAs and the cell cycle

The timing at which cells exit the cell cycle affects their final cell fate. One hypothesis for the unique cell composition of the fovea is that the foveal progenitors are the first in the retina to differentiate, so their precocious exit from the cell cycle primes them for early cell fates. Supporting this, one study experimentally lengthened the cell cycle in neural progenitors and caused premature cell fate switches⁶⁶⁵. Another study comparing nocturnal (avoveated) and diurnal (foveated) New World primates reported differences in cell cycle length²⁷³. This close relationship between cell cycle dynamics and cell fate specification has been well documented in many developmental systems and contexts⁶⁶⁶⁻⁶⁷⁵. Thus, the molecular mechanisms that regulate cell cycle could be playing a fundamental role in regulating the higher production of early cell types (e.g. cones) in the fovea. To complement this, miRNAs have been implicated in controlling cell cycle dynamics. Our lab has shown that Let-7d, miR-9, and miR-125b coordinately guide cell cycle length in neural progenitors by specifically regulating the length of S/G2²⁷⁶. Perhaps miRNAs could be used to manipulate cell cycle dynamics in the RPCs of organoids to increase cone yield.

In Chapter 4, we identified miRNAs highly differentially expressed across the developing retina. We defined a list of top candidate miRNAs that were upregulated in the

non-human primate temporal (miR-15, miR-30, miR-93, and miR-103) or nasal (miR-342) retina. These candidates are a great starting place for investigating the role of specific miRNAs in cell fate specification. Some of these miRNAs have already been shown to contribute to cell fate determination; miR-15b regulates cell proliferation in many cell types and promote neurogenesis in neocortical development⁶⁷⁶, miR-30 has been shown to regulate neurogenesis and proliferation⁶⁷⁷⁻⁶⁷⁹, and miR-342 regulates fate decisions downstream of Notch⁴¹⁸.

One interesting avenue to follow with these miRNAs is their influence on the cell cycle. Perhaps these miRNAs, either individually or synergistically, are the link between the unique cell cycle dynamics (the initially symmetrical retina forming a bulge at the incipient fovea during early embryonic development) and cell composition (peak cone photoreceptor density) of the fovea. During my preliminary experiments into this question, I performed cumulative EdU labeling on human embryonic retina (HER10) cells, a stable line of undifferentiated retinal progenitors that already express these candidate miRNAs. This is a standard method to calculate cell cycle parameters, including cell cycle length, S-phase duration, and growth fraction. I transfected HER10 cells with either mimic (miRNA overexpression) or antagomiR (miRNA inhibitor) oligonucleotides for miRNA-342, together with mCherry RNA as a transfection control. After a 24-hour (h) incubation, I continuously pulsed the cells with EdU for incremental periods of time (30 minutes, 4h, 8h, 12h, 24h, and 48h) before collection. EdU irreversibly labels replicating DNA during S-phase of the cell cycle. This time course allowed me to label the full length of S-phase in various fractions of the asynchronous cell population. The percentage of EdU+ cells was quantified for each time point, and the cell cycle parameters were calculated using a

regression calculation. Notably, overexpression of miR-342 resulted in a significant increase in the duration of HER10 cells cycle (control: 36.5h; miR-342 mimic: 42.75h, 17% increase; miR-342 antagomiR: 33.29h, 8.8% reduction) without significant changes in cell cycle exit. Given that miR-342 is enriched in the nasal retina and lengthens the cell cycle, these findings could suggest that differentially expressed miRNAs are responsible for the bulge that forms in the incipient fovea in early retinal development. According to this hypothesis, miRNAs in the temporal retina would shorten the cell cycle in foveal progenitors and allow for faster cell cycling and relatively increased tissue growth. If these miRNAs indeed influence cell cycle length, the findings would be the first to directly link miRNAs in the fovea with the unique cell cycle dynamics observed during early development. Additionally, these miRNAs may be regulating cell cycle length to facilitate precocious cell cycle exit and consequent early-born fate specification. With a better understanding of the role of these miRNAs on cell cycle regulation and cell fate specification, these miRNAs could be overexpressed or inhibited in organoid protocols to shorten cell cycle length and increase cone yield.

However, this link between miRNAs and cell cycle length does not necessarily link miRNAs with cell fate specification. There are other avenues through which miRNAs control cell fate. MiRNA target prediction algorithms based on sequence comparison (TargetScan and TarBase) and experimental data (miRDB and miRWalk) are useful to identify genes potentially targeted by the top miRNA candidates. These computational prediction platforms show that these miRNAs are potentially targeting genes controlling early retinal patterning (*e.g.* CYP26A1, PALDH1, DIO2, FOXG1, RBPJ) ^{215,228,680}, transcriptional factors known to be involved in progenitor competence regulation (*e.g.*

IKZF1 and CASZ1)^{681,682}, and transcriptional factors crucial for the determination and differentiation of specific cell types (e.g. ONECUT1, POU4F1, NRL, NR2E3)⁶⁸³. For example, Nrl acts as a photoreceptor-specific fate switch to promote rod fates; Nrl-null mice exhibit an increase of cones at the expense of rods^{147,684}. It is controversial if rods are trans-fating into cone-like cells in the Nrl-null models, or if these new PRs are dysfunctional cone-rod hybrids. While regulating Nrl through our target miRNAs could bias the ratios of photoreceptor types towards cones, more experiments are needed to confirm the appropriate developmental time to do so and the functionality of these new cones. Similarly, experimental manipulations of Onecut1 (OC1) have suggested that this transcription factor plays a role in promoting cone and HC fates¹⁶⁵. The 3'UTR of OC1 is highly regulated by miRNAs¹⁸⁷. Further validation is needed to establish pathways through which the candidate miRNAs may regulate the differences of fate determination assays. Novel technologies, such as miRNA enhanced cross linking and immunoprecipitation (miR-eCLIP), allow for experimental confirmation of miRNA-mRNA interactions. Given that we intend to manipulate miRNA levels to induce cone production, it is important to fully understand which mRNAs our target miRNAs regulate, beyond the theoretical interactions obtained in bulk sequencing experiments.

7.3 Alternative models

Of course, choosing the appropriate model to study the development of cones in is paramount. The human retina is presumably the best model, as the findings of this research are intended to inform treatment of human eye diseases. However, healthy human retinal tissue is sparse and the age range available for collection is limiting and

unlikely to include early developmental ages. To truly study the mechanisms that drive foveal progenitors to preferentially differentiate into cone photoreceptors, we must study the fovea prior to the onset of retinal neurogenesis. The foveal progenitors are first to undergo neurogenesis, so the optimal developmental age to investigate is almost unobtainably early. Therefore, we turn to alternative models to study early retinal development.

7.2.1 Primate model

The non-human primate is an important research model, as its development closely resembles that of humans. This model provides access to a much wider age range of embryonic samples than are possible in research on humans. Retinal tissue is accessible across the entire length of gestation in non-human primates, and because matings are scheduled, the developmental age of retinal samples is accurate. There are caveats to working with non-human primate tissue, namely the timeline and the cost. Rhesus macaques breed seasonally and have lengthy gestation, so collecting tissue at a desired development stage is not readily available at any given time. What is most limiting are the costs associated with studying non-human primates, as they are expensive. Obtaining the retinas from one non-human primate involves impregnating an adult female via medical assistance, monitoring the pregnancy, housing and feeding her through the desired length of gestation, and employing a trained surgical team, including a veterinarian and ophthalmologist, to retrieve the tissue. Such expenses would force even the most well-funded lab to reconsider studying the non-human primate. Additionally, there is a widespread movement to stop non-human primate research. Whereas the

National Institutes of Health (NIH) has been funding National Primate Research Centers for over 50 years, there are currently only seven facilities across the country. These hurdles make studying non-human primates challenging but should not overshadow the usefulness of this model and how informative findings are for better understanding human development. So how do we study the fovea, or cone specification more broadly, if not in a human or non-human primate?

7.2.2 Avian model

Avian species hold great potential for studying cone development. Many avian species, namely birds of prey, notably have foveas—some even have two. However, these species are usually protected and not accessible for this scientific research. Many birds have a specialized retinal region that is responsible for high acuity vision, called the high acuity area (HAA). While the HAA does not have a thinning of the retina to form a pit, and thus cannot be called a true fovea, this specialized region contains a rod-free zone (RFZ).

The goal of studying avian retinal development is to better understand the molecular mechanisms regulating cone development for optimizing organoid protocols and increasing cone yield. With that, it is preferential to study species whose visual system most closely resembles that of humans. How do we know how well different species can see? We turn to RGC density maps to better understand the visual acuity of an animal. These retinal maps represent regions responsible for higher or lower visual acuity by the RGC outputs. In the majority of the retina that employs parasol circuitry, where the photoreceptors' signals are considerably simplified by convergence onto

interneurons and RGCs, RGCs will appear at low density. In regions of high acuity vision, where the photoreceptors participate in more directed connections via midget circuitry, RGCs appear at a higher density. We can see in a mouse retina that there are no regions of increased RGC density, but a human retina has a sharp increase of RGC density right outside of the fovea. So how does the avian HAA survey on a RGC density map? The chicken retina shows two peaks of RGC density, one that coincides with the HAA. While the highest peak of RGC density is four times less than that at the human fovea, it is still notable. The quail retina is even more remarkable. Similar to the chicken retina, there are two peaks of RGC density. However, the quail retina's highest peak of RGC density is over double that of the chicken retina, and less than half that of the human retina. This suggests that quails have higher acuity vision than chicken do. This is not wildly unexpected, as vision is directly correlated to lifestyle. Most chicken are bred for food, not flight. They can only fly for short distances and are known to struggle to find food, even when it is right in the front of their visual field. On the other hand, quails were domesticated much later, so their vision would more closely reflect that of wild quails. Both wild and domesticated quails require keen vision for their flying activities. It is an exciting prospect to introduce quails as a new model for studying cone photoreceptor development.

This is not to say that chickens and quails have not been studied as models in other contexts. Utilizing the remarkably similar embryonic development of these two avian species, Dr. Nicole Le Douarin led a hallmark study to create chimeric chicken and quail embryos ^{685,686}. This experiment of substituting quail cells for chicken cells can be performed *in ovo*, and the hatched chicken will have quail cells at the graft sites. Importantly, a large nucleolus with concentrated heterochromatin makes the quail cells

easily distinguishable from the diffuse nuclei of the chicken cells ⁶⁸⁷. Additionally, quail-specific antigens will discern the quail cells from the chicken cells. The opportunity to create such a chimera, with the different cell origins distinguishable, could open exciting avenues for retinal research. The ease of manipulation of these species *in ovo*, simply by creating a window in the shell, introducing desired molecules, and closing the window with parafilm for development to continue, would make it one of the easiest models to manipulate.

7.2.3 Interpreting results with additional models

The findings from my research are ready to move into the quail model. In my published works, I identified molecules differentially expressed across the primate retina. Such enrichment in the temporal retina could suggest a number of roles: (1) the molecules are expressed in the temporal retina for patterning, (2) the molecules are expressed in cells enriched in the temporal retina, or (3) the molecules are first expressed in the fovea, and the central and peripheral retinas will express the molecules when they reach that same stage of development.

My preliminary, unpublished findings in the chicken and quail retinas suggest that further investigation into these models will provide clarity for discerning the roles of the previously identified molecules differentially expressed across the primate retina. In the primate eye, the fovea resides in the temporal retina. While the eye cup and retina initially develop symmetrically on the nasal-temporal axis, an abrupt shift occurs when growth on the temporal side accelerates, leaving the retina asymmetrical. It is in this incipient fovea, where relatively faster growth occurs, that neurogenesis begins. On this basis, I expected

to observe a similar developmental pattern of the nasally-residing HAA in the chicken and quail retinas. Instead, and very interestingly, I observed a different pattern. These avian retinas are always asymmetrical; the temporal retina is longer at first, and then growth in the nasal retina accelerates. Although the relatively faster growth occurs in the region that will become the HAA, this is not where neurogenesis begins; the first cells differentiate in the temporal retina of chicken and quails.

Incorporating multiple models, each with species-specific development and ratios of retinal cells, will provide clarity on those molecules found to be highly differentially expressed across the primate retina. This distinction between the development of the primate fovea and quail HAA is valuable, and future experiments will be very telling. If molecules are enriched in the temporal primate retina and nasal quail retina, then they are expressed in cells enriched in the HAA. If molecules are enriched in the temporal retina of both primates and quails, then they are expressed where neurogenesis begins. Supplementing these experiments with the mouse model could be even more informative. While mice do not have a fovea or HAA, it is well-known that neurogenesis begins in the central retina and proceeds in a wave towards the periphery. Molecules that are enriched in the temporal retina of primates and quails and the nasal mouse retina would be further validated as connected to the origin of neurogenesis. Those molecules that are present in the primate and quail retinas but not in the mouse retina may contribute to the development of the specialized retinal regions.

The results of this dissertation help elucidate some of the miRNAs and molecules that regulate cell fate specification in the CNS. Future studies continuing the work of this dissertation include characterizing development of the quail retina and assessing the expression patterns of both the candidate miRNAs identified in these studies and the molecules associated with the retinoic acid pathway that have been implicated in the development of the chicken retina. Manipulating these miRNAs and molecules *in ovo* will reveal pathways that regulate cone development. Such findings will further inform protocols to increase cone yields in retinal organoids.

These efforts address the first steps in the pipeline to curing blindness in patients affected by cone degeneration. There are many components to this task, including sourcing, isolating, and transplanting cones, as well as achieving integration of the transplanted neurons into the existing circuitry. We are one of many research groups addressing different steps of this pipeline, making the prospect of using organoid-derived cones for curing blindness promising.

8. References

- 1 Livesey, F. J. & Cepko, C. L. Vertebrate neural cell-fate determination: lessons from the retina. *Nat Rev Neurosci* **2**, 109-118 (2001). <https://doi.org/10.1038/35053522>
- 2 Bassett, E. A. & Wallace, V. A. Cell fate determination in the vertebrate retina. *Trends Neurosci* **35**, 565-573 (2012). <https://doi.org/10.1016/j.tins.2012.05.004>
- 3 Curcio, C. A., Sloan, K. R., Jr., Packer, O., Hendrickson, A. E. & Kalina, R. E. Distribution of cones in human and monkey retina: individual variability and radial asymmetry. *Science* **236**, 579-582 (1987). <https://doi.org/10.1126/science.3576186>
- 4 Curcio, C. A., Sloan, K. R., Kalina, R. E. & Hendrickson, A. E. Human photoreceptor topography. *J Comp Neurol* **292**, 497-523 (1990). <https://doi.org/10.1002/cne.902920402>
- 5 Klein, R. *et al.* Prevalence of age-related macular degeneration in the US population. *Arch Ophthalmol* **129**, 75-80 (2011). <https://doi.org/10.1001/archophthalmol.2010.318>
- 6 Lamba, D. A., Karl, M. O., Ware, C. B. & Reh, T. A. Efficient generation of retinal progenitor cells from human embryonic stem cells. *Proc Natl Acad Sci U S A* **103**, 12769-12774 (2006). <https://doi.org/10.1073/pnas.0601990103>
- 7 Osakada, F. *et al.* Toward the generation of rod and cone photoreceptors from mouse, monkey and human embryonic stem cells. *Nat Biotechnol* **26**, 215-224 (2008). <https://doi.org/10.1038/nbt1384>
- 8 Meyer, J. S. *et al.* Optic vesicle-like structures derived from human pluripotent stem cells facilitate a customized approach to retinal disease treatment. *Stem Cells* **29**, 1206-1218 (2011). <https://doi.org/10.1002/stem.674>
- 9 Eiraku, M. *et al.* Self-organizing optic-cup morphogenesis in three-dimensional culture. *Nature* **472**, 51-56 (2011). <https://doi.org/10.1038/nature09941>
- 10 La Torre, A., Lamba, D. A., Jayabalu, A. & Reh, T. A. Production and transplantation of retinal cells from human and mouse embryonic stem cells. *Methods Mol Biol* **884**, 229-246 (2012). https://doi.org/10.1007/978-1-61779-848-1_16
- 11 Nakano, T. *et al.* Self-formation of optic cups and storable stratified neural retina from human ESCs. *Cell Stem Cell* **10**, 771-785 (2012). <https://doi.org/10.1016/j.stem.2012.05.009>
- 12 Carr, A. J. *et al.* Development of human embryonic stem cell therapies for age-related macular degeneration. *Trends Neurosci* **36**, 385-395 (2013). <https://doi.org/10.1016/j.tins.2013.03.006>
- 13 Al-Shamekh, S. & Goldberg, J. L. Retinal repair with induced pluripotent stem cells. *Transl Res* **163**, 377-386 (2014). <https://doi.org/10.1016/j.trsl.2013.11.002>
- 14 Phillips, M. J. *et al.* Modeling human retinal development with patient-specific induced pluripotent stem cells reveals multiple roles for visual system homeobox 2. *Stem Cells* **32**, 1480-1492 (2014). <https://doi.org/10.1002/stem.1667>

- 15 Zhong, X. *et al.* Generation of three-dimensional retinal tissue with functional photoreceptors from human iPSCs. *Nat Commun* **5**, 4047 (2014). <https://doi.org/10.1038/ncomms5047>
- 16 Eldred, K. C. *et al.* Thyroid hormone signaling specifies cone subtypes in human retinal organoids. *Science* **362** (2018). <https://doi.org/10.1126/science.aau6348>
- 17 Sridhar, A. *et al.* Single-Cell Transcriptomic Comparison of Human Fetal Retina, hPSC-Derived Retinal Organoids, and Long-Term Retinal Cultures. *Cell Rep* **30**, 1644-1659 e1644 (2020). <https://doi.org/10.1016/j.celrep.2020.01.007>
- 18 Cowan, C. S. *et al.* Cell Types of the Human Retina and Its Organoids at Single-Cell Resolution. *Cell* **182**, 1623-1640 e1634 (2020). <https://doi.org/10.1016/j.cell.2020.08.013>
- 19 Demb, J. B. & Singer, J. H. Functional Circuitry of the Retina. *Annu Rev Vis Sci* **1**, 263-289 (2015). <https://doi.org/10.1146/annurev-vision-082114-035334>
- 20 Wallace, V. A. Concise review: making a retina--from the building blocks to clinical applications. *Stem Cells* **29**, 412-417 (2011). <https://doi.org/10.1002/stem.602>
- 21 Gollisch, T. & Meister, M. Eye smarter than scientists believed: neural computations in circuits of the retina. *Neuron* **65**, 150-164 (2010). <https://doi.org/10.1016/j.neuron.2009.12.009>
- 22 Fuhrmann, S. Eye morphogenesis and patterning of the optic vesicle. *Curr Top Dev Biol* **93**, 61-84 (2010). <https://doi.org/10.1016/B978-0-12-385044-7.00003-5>
- 23 Tanna, A. P. & Veto, K. Myelinated Retinal Nerve Fiber Layer. *Mayo Clin Proc* **97**, 819 (2022). <https://doi.org/10.1016/j.mayocp.2022.02.006>
- 24 Alonso, J. M., Yeh, C. I., Weng, C. & Stoelzel, C. Retinogeniculate connections: A balancing act between connection specificity and receptive field diversity. *Prog Brain Res* **154**, 3-13 (2006). [https://doi.org/10.1016/S0079-6123\(06\)54001-4](https://doi.org/10.1016/S0079-6123(06)54001-4)
- 25 Perry, V. H., Oehler, R. & Cowey, A. Retinal ganglion cells that project to the dorsal lateral geniculate nucleus in the macaque monkey. *Neuroscience* **12**, 1101-1123 (1984). [https://doi.org/10.1016/0306-4522\(84\)90006-x](https://doi.org/10.1016/0306-4522(84)90006-x)
- 26 Masland, R. H. The fundamental plan of the retina. *Nat Neurosci* **4**, 877-886 (2001). <https://doi.org/10.1038/nn0901-877>
- 27 Hecht, S., Schlaer, S. & Pirenne, M. H. Energy, Quanta, and Vision. *J Gen Physiol* **25**, 819-840 (1942). <https://doi.org/10.1085/jgp.25.6.819>
- 28 Baylor, D. A., Lamb, T. D. & Yau, K. W. Responses of retinal rods to single photons. *J Physiol* **288**, 613-634 (1979).
- 29 Perkins, B. D. & Fadool, J. M. Photoreceptor structure and development analyses using GFP transgenes. *Methods Cell Biol* **100**, 205-218 (2010). <https://doi.org/10.1016/B978-0-12-384892-5.00007-4>
- 30 Lamb, T. D. & Pugh, E. N., Jr. Phototransduction, dark adaptation, and rhodopsin regeneration the proctor lecture. *Invest Ophthalmol Vis Sci* **47**, 5137-5152 (2006). <https://doi.org/10.1167/iovs.06-0849>
- 31 Lamb, T. D. & Pugh, E. N., Jr. Dark adaptation and the retinoid cycle of vision. *Prog Retin Eye Res* **23**, 307-380 (2004). <https://doi.org/10.1016/j.preteyeres.2004.03.001>

- 32 Burns, M. E. & Pugh, E. N., Jr. Lessons from photoreceptors: turning off g-protein signaling in living cells. *Physiology (Bethesda)* **25**, 72-84 (2010). <https://doi.org/10.1152/physiol.00001.2010>
- 33 Heidelberger, R., Thoreson, W. B. & Witkovsky, P. Synaptic transmission at retinal ribbon synapses. *Prog Retin Eye Res* **24**, 682-720 (2005). <https://doi.org/10.1016/j.preteyeres.2005.04.002>
- 34 Sterling, P. & Matthews, G. Structure and function of ribbon synapses. *Trends Neurosci* **28**, 20-29 (2005). <https://doi.org/10.1016/j.tins.2004.11.009>
- 35 Arshavsky, V. Y. & Burns, M. E. Photoreceptor signaling: supporting vision across a wide range of light intensities. *J Biol Chem* **287**, 1620-1626 (2012). <https://doi.org/10.1074/jbc.R111.305243>
- 36 Gurevich, V. V., Hanson, S. M., Song, X., Vishnivetskiy, S. A. & Gurevich, E. V. The functional cycle of visual arrestins in photoreceptor cells. *Prog Retin Eye Res* **30**, 405-430 (2011). <https://doi.org/10.1016/j.preteyeres.2011.07.002>
- 37 Terakita, A. The opsins. *Genome Biol* **6**, 213 (2005). <https://doi.org/10.1186/gb-2005-6-3-213>
- 38 Schnapf, J. L., Kraft, T. W., Nunn, B. J. & Baylor, D. A. Spectral sensitivity of primate photoreceptors. *Vis Neurosci* **1**, 255-261 (1988). <https://doi.org/10.1017/s0952523800001917>
- 39 Molday, R. S. & Moritz, O. L. Photoreceptors at a glance. *J Cell Sci* **128**, 4039-4045 (2015). <https://doi.org/10.1242/jcs.175687>
- 40 Applebury, M. L. *et al.* The murine cone photoreceptor: a single cone type expresses both S and M opsins with retinal spatial patterning. *Neuron* **27**, 513-523 (2000). [https://doi.org/10.1016/s0896-6273\(00\)00062-3](https://doi.org/10.1016/s0896-6273(00)00062-3)
- 41 Jacobs, G. H. Evolution of colour vision in mammals. *Philos Trans R Soc Lond B Biol Sci* **364**, 2957-2967 (2009). <https://doi.org/10.1098/rstb.2009.0039>
- 42 Strettoi, E. A Survey of Retinal Remodeling. *Front Cell Neurosci* **9**, 494 (2015). <https://doi.org/10.3389/fncel.2015.00494>
- 43 Kamermans, M. *et al.* Hemichannel-mediated inhibition in the outer retina. *Science* **292**, 1178-1180 (2001). <https://doi.org/10.1126/science.1060101>
- 44 Kramer, R. H. & Davenport, C. M. Lateral Inhibition in the Vertebrate Retina: The Case of the Missing Neurotransmitter. *PLoS Biol* **13**, e1002322 (2015). <https://doi.org/10.1371/journal.pbio.1002322>
- 45 Barnes, S., Grove, J. C. R., McHugh, C. F., Hirano, A. A. & Brecha, N. C. Horizontal Cell Feedback to Cone Photoreceptors in Mammalian Retina: Novel Insights From the GABA-pH Hybrid Model. *Front Cell Neurosci* **14**, 595064 (2020). <https://doi.org/10.3389/fncel.2020.595064>
- 46 Twig, G., Levy, H. & Perlman, I. Color opponency in horizontal cells of the vertebrate retina. *Prog Retin Eye Res* **22**, 31-68 (2003). [https://doi.org/10.1016/s1350-9462\(02\)00045-9](https://doi.org/10.1016/s1350-9462(02)00045-9)
- 47 Ahnelt, P. & Kolb, H. Horizontal cells and cone photoreceptors in primate retina: a Golgi-light microscopic study of spectral connectivity. *J Comp Neurol* **343**, 387-405 (1994). <https://doi.org/10.1002/cne.903430305>

- 48 Kolb, H. *et al.* Are there three types of horizontal cell in the human retina? *J Comp Neurol* **343**, 370-386 (1994). <https://doi.org/10.1002/cne.903430304>
- 49 Yan, W. *et al.* Mouse Retinal Cell Atlas: Molecular Identification of over Sixty Amacrine Cell Types. *J Neurosci* **40**, 5177-5195 (2020).
<https://doi.org/10.1523/JNEUROSCI.0471-20.2020>
- 50 Masland, R. H. The tasks of amacrine cells. *Vis Neurosci* **29**, 3-9 (2012).
<https://doi.org/10.1017/s0952523811000344>
- 51 Perez De Sevilla Muller, L., Shelley, J. & Weiler, R. Displaced amacrine cells of the mouse retina. *J Comp Neurol* **505**, 177-189 (2007).
<https://doi.org/10.1002/cne.21487>
- 52 Diamond, J. S. Inhibitory Interneurons in the Retina: Types, Circuitry, and Function. *Annu Rev Vis Sci* **3**, 1-24 (2017). <https://doi.org/10.1146/annurev-vision-102016-061345>
- 53 Grunert, U. & Martin, P. R. Cell types and cell circuits in human and non-human primate retina. *Prog Retin Eye Res*, 100844 (2020).
<https://doi.org/10.1016/j.preteyeres.2020.100844>
- 54 Walia, S., Fishman, G. A., Edward, D. P. & Lindeman, M. Retinal nerve fiber layer defects in RP patients. *Invest Ophthalmol Vis Sci* **48**, 4748-4752 (2007).
<https://doi.org/10.1167/iovs.07-0404>
- 55 Kim, U. S., Mahroo, O. A., Mollon, J. D. & Yu-Wai-Man, P. Retinal Ganglion Cells-Diversity of Cell Types and Clinical Relevance. *Front Neurol* **12**, 661938 (2021). <https://doi.org/10.3389/fneur.2021.661938>
- 56 Weinreb, R. N., Aung, T. & Medeiros, F. A. The pathophysiology and treatment of glaucoma: a review. *JAMA* **311**, 1901-1911 (2014).
<https://doi.org/10.1001/jama.2014.3192>
- 57 Zhang, C. *et al.* Circuit Reorganization Shapes the Developing Human Foveal Midget Connectome toward Single-Cone Resolution. *Neuron* **108**, 905-918 e903 (2020). <https://doi.org/10.1016/j.neuron.2020.09.014>
- 58 Calkins, D. J., Schein, S. J., Tsukamoto, Y. & Sterling, P. M and L cones in macaque fovea connect to midget ganglion cells by different numbers of excitatory synapses. *Nature* **371**, 70-72 (1994). <https://doi.org/10.1038/371070a0>
- 59 MacDonald, R. B. *et al.* Muller glia provide essential tensile strength to the developing retina. *J Cell Biol* **210**, 1075-1083 (2015).
<https://doi.org/10.1083/jcb.201503115>
- 60 Reichenbach, A. & Bringmann, A. New functions of Muller cells. *Glia* **61**, 651-678 (2013). <https://doi.org/10.1002/glia.22477>
- 61 Bejarano-Escobar, R., Sanchez-Calderon, H., Otero-Arenas, J., Martin-Partido, G. & Francisco-Morcillo, J. Muller glia and phagocytosis of cell debris in retinal tissue. *J Anat* **231**, 471-483 (2017). <https://doi.org/10.1111/joa.12653>
- 62 Vecino, E., Rodriguez, F. D., Ruzafa, N., Pereiro, X. & Sharma, S. C. Glia-neuron interactions in the mammalian retina. *Prog Retin Eye Res* **51**, 1-40 (2016).
<https://doi.org/10.1016/j.preteyeres.2015.06.003>
- 63 Blackshaw, S. *et al.* Genomic analysis of mouse retinal development. *PLoS Biol* **2**, E247 (2004). <https://doi.org/10.1371/journal.pbio.0020247>

- 64 Bringmann, A. & Wiedemann, P. Muller glial cells in retinal disease. *Ophthalmologica* **227**, 1-19 (2012). <https://doi.org/10.1159/000328979>
- 65 Heavner, W. & Pevny, L. Eye development and retinogenesis. *Cold Spring Harb Perspect Biol* **4** (2012). <https://doi.org/10.1101/cshperspect.a008391>
- 66 Sparrow, J. R. *et al.* Fundus autofluorescence and the bisretinoids of retina. *Photochem Photobiol Sci* **9**, 1480-1489 (2010). <https://doi.org/10.1039/c0pp00207k>
- 67 Kevany, B. M. & Palczewski, K. Phagocytosis of retinal rod and cone photoreceptors. *Physiology (Bethesda)* **25**, 8-15 (2010). <https://doi.org/10.1152/physiol.00038.2009>
- 68 Crouch, R. K. *et al.* Interphotoreceptor retinoid-binding protein and alpha-tocopherol preserve the isomeric and oxidation state of retinol. *Photochem Photobiol* **56**, 251-255 (1992). <https://doi.org/10.1111/j.1751-1097.1992.tb02154.x>
- 69 McBee, J. K., Van Hooser, J. P., Jang, G. F. & Palczewski, K. Isomerization of 11-cis-retinoids to all-trans-retinoids in vitro and in vivo. *J Biol Chem* **276**, 48483-48493 (2001). <https://doi.org/10.1074/jbc.M105840200>
- 70 Strauss, O. The retinal pigment epithelium in visual function. *Physiol Rev* **85**, 845-881 (2005). <https://doi.org/10.1152/physrev.00021.2004>
- 71 Ambati, J. & Fowler, B. J. Mechanisms of age-related macular degeneration. *Neuron* **75**, 26-39 (2012). <https://doi.org/10.1016/j.neuron.2012.06.018>
- 72 Martinez-Morales, J. R., Cavodeassi, F. & Bovolenta, P. Coordinated Morphogenetic Mechanisms Shape the Vertebrate Eye. *Front Neurosci* **11**, 721 (2017). <https://doi.org/10.3389/fnins.2017.00721>
- 73 Casey, M. A., Lusk, S. & Kwan, K. M. Eye Morphogenesis in Vertebrates. *Annu Rev Vis Sci* **9**, 221-243 (2023). <https://doi.org/10.1146/annurev-vision-100720-111125>
- 74 Tam, P. P. & Behringer, R. R. Mouse gastrulation: the formation of a mammalian body plan. *Mech Dev* **68**, 3-25 (1997). [https://doi.org/10.1016/s0925-4773\(97\)00123-8](https://doi.org/10.1016/s0925-4773(97)00123-8)
- 75 Diacou, R. *et al.* Cell fate decisions, transcription factors and signaling during early retinal development. *Prog Retin Eye Res* **91**, 101093 (2022). <https://doi.org/10.1016/j.preteyeres.2022.101093>
- 76 Bosze, B. *et al.* Multiple roles for Pax2 in the embryonic mouse eye. *Dev Biol* **472**, 18-29 (2021). <https://doi.org/10.1016/j.ydbio.2020.12.020>
- 77 Zhang, X., Leavey, P., Appel, H., Makrides, N. & Blackshaw, S. Molecular mechanisms controlling vertebrate retinal patterning, neurogenesis, and cell fate specification. *Trends Genet* **39**, 736-757 (2023). <https://doi.org/10.1016/j.tig.2023.06.002>
- 78 Hemesath, T. J. *et al.* microphthalmia, a critical factor in melanocyte development, defines a discrete transcription factor family. *Genes Dev* **8**, 2770-2780 (1994). <https://doi.org/10.1101/gad.8.22.2770>

- 79 Hodgkinson, C. A. *et al.* Mutations at the mouse microphthalmia locus are associated with defects in a gene encoding a novel basic-helix-loop-helix-zipper protein. *Cell* **74**, 395-404 (1993). [https://doi.org/10.1016/0092-8674\(93\)90429-t](https://doi.org/10.1016/0092-8674(93)90429-t)
- 80 Holt, C. E., Bertsch, T. W., Ellis, H. M. & Harris, W. A. Cellular determination in the *Xenopus* retina is independent of lineage and birth date. *Neuron* **1**, 15-26 (1988). [https://doi.org/10.1016/0896-6273\(88\)90205-x](https://doi.org/10.1016/0896-6273(88)90205-x)
- 81 Turner, D. L. & Cepko, C. L. A common progenitor for neurons and glia persists in rat retina late in development. *Nature* **328**, 131-136 (1987). <https://doi.org/10.1038/328131a0>
- 82 Turner, D. L., Snyder, E. Y. & Cepko, C. L. Lineage-independent determination of cell type in the embryonic mouse retina. *Neuron* **4**, 833-845 (1990). [https://doi.org/10.1016/0896-6273\(90\)90136-4](https://doi.org/10.1016/0896-6273(90)90136-4)
- 83 Wetts, R. & Fraser, S. E. Multipotent precursors can give rise to all major cell types of the frog retina. *Science* **239**, 1142-1145 (1988). <https://doi.org/10.1126/science.2449732>
- 84 Baye, L. M. & Link, B. A. Nuclear migration during retinal development. *Brain Res* **1192**, 29-36 (2008). <https://doi.org/10.1016/j.brainres.2007.05.021>
- 85 Azizi, A. *et al.* Nuclear crowding and nonlinear diffusion during interkinetic nuclear migration in the zebrafish retina. *Elife* **9** (2020). <https://doi.org/10.7554/eLife.58635>
- 86 Norden, C., Young, S., Link, B. A. & Harris, W. A. Actomyosin is the main driver of interkinetic nuclear migration in the retina. *Cell* **138**, 1195-1208 (2009). <https://doi.org/10.1016/j.cell.2009.06.032>
- 87 Agathocleous, M. & Harris, W. A. From progenitors to differentiated cells in the vertebrate retina. *Annu Rev Cell Dev Biol* **25**, 45-69 (2009). <https://doi.org/10.1146/annurev.cellbio.042308.113259>
- 88 Norbury, C. & Nurse, P. Animal cell cycles and their control. *Annu Rev Biochem* **61**, 441-470 (1992). <https://doi.org/10.1146/annurev.bi.61.070192.002301>
- 89 Malumbres, M. & Barbacid, M. To cycle or not to cycle: a critical decision in cancer. *Nat Rev Cancer* **1**, 222-231 (2001). <https://doi.org/10.1038/35106065>
- 90 Dyer, M. A. & Cepko, C. L. Regulating proliferation during retinal development. *Nat Rev Neurosci* **2**, 333-342 (2001). <https://doi.org/10.1038/35072555>
- 91 Geng, Y. *et al.* Deletion of the p27Kip1 gene restores normal development in cyclin D1-deficient mice. *Proc Natl Acad Sci U S A* **98**, 194-199 (2001). <https://doi.org/10.1073/pnas.98.1.194>
- 92 Lu, Z. & Hunter, T. Ubiquitylation and proteasomal degradation of the p21(Cip1), p27(Kip1) and p57(Kip2) CDK inhibitors. *Cell Cycle* **9**, 2342-2352 (2010). <https://doi.org/10.4161/cc.9.12.11988>
- 93 Besson, A., Dowdy, S. F. & Roberts, J. M. CDK inhibitors: cell cycle regulators and beyond. *Dev Cell* **14**, 159-169 (2008). <https://doi.org/10.1016/j.devcel.2008.01.013>
- 94 Kageyama, R., Ohtsuka, T. & Kobayashi, T. Roles of Hes genes in neural development. *Dev Growth Differ* **50 Suppl 1**, S97-103 (2008). <https://doi.org/10.1111/j.1440-169X.2008.00993.x>

- 95 Bao, Z. Z. & Cepko, C. L. The expression and function of Notch pathway genes in the developing rat eye. *J Neurosci* **17**, 1425-1434 (1997). <https://doi.org/10.1523/JNEUROSCI.17-04-01425.1997>
- 96 Yaron, O., Farhy, C., Marquardt, T., Applebury, M. & Ashery-Padan, R. Notch1 functions to suppress cone-photoreceptor fate specification in the developing mouse retina. *Development* **133**, 1367-1378 (2006). <https://doi.org/10.1242/dev.02311>
- 97 Nelson, B. R., Hartman, B. H., Georgi, S. A., Lan, M. S. & Reh, T. A. Transient inactivation of Notch signaling synchronizes differentiation of neural progenitor cells. *Dev Biol* **304**, 479-498 (2007). <https://doi.org/10.1016/j.ydbio.2007.01.001>
- 98 Wall, D. S. *et al.* Progenitor cell proliferation in the retina is dependent on Notch-independent Sonic hedgehog/Hes1 activity. *J Cell Biol* **184**, 101-112 (2009). <https://doi.org/10.1083/jcb.200805155>
- 99 Young, R. W. Cell differentiation in the retina of the mouse. *Anat Rec* **212**, 199-205 (1985). <https://doi.org/10.1002/ar.1092120215>
- 100 Cepko, C. L., Austin, C. P., Yang, X., Alexiades, M. & Ezzeddine, D. Cell fate determination in the vertebrate retina. *Proc Natl Acad Sci U S A* **93**, 589-595 (1996). <https://doi.org/10.1073/pnas.93.2.589>
- 101 Sidman, R. Histogenesis of the mouse retina studied with thymidine-H3. (1961).
- 102 La Vail, M. M., Rapaport, D. H. & Rakic, P. Cytogenesis in the monkey retina. *J Comp Neurol* **309**, 86-114 (1991). <https://doi.org/10.1002/cne.903090107>
- 103 Stiemke, M. M. & Hollyfield, J. G. Cell birthdays in *Xenopus laevis* retina. *Differentiation* **58**, 189-193 (1995). <https://doi.org/10.1046/j.1432-0436.1995.5830189.x>
- 104 Ohsawa, R. & Kageyama, R. Regulation of retinal cell fate specification by multiple transcription factors. *Brain Res* **1192**, 90-98 (2008). <https://doi.org/10.1016/j.brainres.2007.04.014>
- 105 Rapaport, D. H., Patheal, S. L. & Harris, W. A. Cellular competence plays a role in photoreceptor differentiation in the developing *Xenopus* retina. *J Neurobiol* **49**, 129-141 (2001). <https://doi.org/10.1002/neu.1070>
- 106 Belliveau, M. J., Young, T. L. & Cepko, C. L. Late retinal progenitor cells show intrinsic limitations in the production of cell types and the kinetics of opsin synthesis. *J Neurosci* **20**, 2247-2254 (2000). <https://doi.org/10.1523/JNEUROSCI.20-06-02247.2000>
- 107 McConnell, S. K. Migration and differentiation of cerebral cortical neurons after transplantation into the brains of ferrets. *Science* **229**, 1268-1271 (1985). <https://doi.org/10.1126/science.4035355>
- 108 Cayouette, M., Barres, B. A. & Raff, M. Importance of intrinsic mechanisms in cell fate decisions in the developing rat retina. *Neuron* **40**, 897-904 (2003). [https://doi.org/10.1016/s0896-6273\(03\)00756-6](https://doi.org/10.1016/s0896-6273(03)00756-6)
- 109 Gomes, F. L. *et al.* Reconstruction of rat retinal progenitor cell lineages in vitro reveals a surprising degree of stochasticity in cell fate decisions. *Development* **138**, 227-235 (2011). <https://doi.org/10.1242/dev.059683>

- 110 Belliveau, M. J. & Cepko, C. L. Extrinsic and intrinsic factors control the genesis of amacrine and cone cells in the rat retina. *Development* **126**, 555-566 (1999). <https://doi.org/10.1242/dev.126.3.555>
- 111 Shiau, F., Ruzycski, P. A. & Clark, B. S. A single-cell guide to retinal development: Cell fate decisions of multipotent retinal progenitors in scRNA-seq. *Dev Biol* **478**, 41-58 (2021). <https://doi.org/10.1016/j.ydbio.2021.06.005>
- 112 Clark, B. S. *et al.* Single-Cell RNA-Seq Analysis of Retinal Development Identifies NFI Factors as Regulating Mitotic Exit and Late-Born Cell Specification. *Neuron* **102**, 1111-1126 e1115 (2019). <https://doi.org/10.1016/j.neuron.2019.04.010>
- 113 Lillien, L. Changes in retinal cell fate induced by overexpression of EGF receptor. *Nature* **377**, 158-162 (1995). <https://doi.org/10.1038/377158a0>
- 114 Anchan, R. M., Reh, T. A., Angello, J., Balliet, A. & Walker, M. EGF and TGF- α stimulate retinal neuroepithelial cell proliferation in vitro. *Neuron* **6**, 923-936 (1991). [https://doi.org/10.1016/0896-6273\(91\)90233-p](https://doi.org/10.1016/0896-6273(91)90233-p)
- 115 Brzezinski, J. A. t., Kim, E. J., Johnson, J. E. & Reh, T. A. Ascl1 expression defines a subpopulation of lineage-restricted progenitors in the mammalian retina. *Development* **138**, 3519-3531 (2011). <https://doi.org/10.1242/dev.064006>
- 116 Georgi, S. A. & Reh, T. A. Dicer is required for the transition from early to late progenitor state in the developing mouse retina. *J Neurosci* **30**, 4048-4061 (2010). <https://doi.org/10.1523/JNEUROSCI.4982-09.2010>
- 117 Jasoni, C. L. & Reh, T. A. Temporal and spatial pattern of MASH-1 expression in the developing rat retina demonstrates progenitor cell heterogeneity. *J Comp Neurol* **369**, 319-327 (1996). [https://doi.org/10.1002/\(SICI\)1096-9861\(19960527\)369:2<319::AID-CNE11>3.0.CO;2-C](https://doi.org/10.1002/(SICI)1096-9861(19960527)369:2<319::AID-CNE11>3.0.CO;2-C)
- 118 He, J. *et al.* How variable clones build an invariant retina. *Neuron* **75**, 786-798 (2012). <https://doi.org/10.1016/j.neuron.2012.06.033>
- 119 Waid, D. K. & McLoon, S. C. Ganglion cells influence the fate of dividing retinal cells in culture. *Development* **125**, 1059-1066 (1998). <https://doi.org/10.1242/dev.125.6.1059>
- 120 Reh, T. A. Cell-specific regulation of neuronal production in the larval frog retina. *J Neurosci* **7**, 3317-3324 (1987). <https://doi.org/10.1523/JNEUROSCI.07-10-03317.1987>
- 121 Muranishi, Y. *et al.* An essential role for RAX homeoprotein and NOTCH-HES signaling in Otx2 expression in embryonic retinal photoreceptor cell fate determination. *J Neurosci* **31**, 16792-16807 (2011). <https://doi.org/10.1523/JNEUROSCI.3109-11.2011>
- 122 Nishida, A. *et al.* Otx2 homeobox gene controls retinal photoreceptor cell fate and pineal gland development. *Nat Neurosci* **6**, 1255-1263 (2003). <https://doi.org/10.1038/nn1155>
- 123 Koike, C. *et al.* Functional roles of Otx2 transcription factor in postnatal mouse retinal development. *Mol Cell Biol* **27**, 8318-8329 (2007). <https://doi.org/10.1128/MCB.01209-07>

- 124 Wang, S., Sengel, C., Emerson, M. M. & Cepko, C. L. A gene regulatory network controls the binary fate decision of rod and bipolar cells in the vertebrate retina. *Dev Cell* **30**, 513-527 (2014). <https://doi.org/10.1016/j.devcel.2014.07.018>
- 125 Kim, D. S., Matsuda, T. & Cepko, C. L. A core paired-type and POU homeodomain-containing transcription factor program drives retinal bipolar cell gene expression. *J Neurosci* **28**, 7748-7764 (2008). <https://doi.org/10.1523/JNEUROSCI.0397-08.2008>
- 126 Brzezinski, J. A. t., Lamba, D. A. & Reh, T. A. Blimp1 controls photoreceptor versus bipolar cell fate choice during retinal development. *Development* **137**, 619-629 (2010). <https://doi.org/10.1242/dev.043968>
- 127 Katoh, K. *et al.* Blimp1 suppresses Chx10 expression in differentiating retinal photoreceptor precursors to ensure proper photoreceptor development. *J Neurosci* **30**, 6515-6526 (2010). <https://doi.org/10.1523/JNEUROSCI.0771-10.2010>
- 128 Brzezinski, J. A. t., Uoon Park, K. & Reh, T. A. Blimp1 (Prdm1) prevents re-specification of photoreceptors into retinal bipolar cells by restricting competence. *Dev Biol* **384**, 194-204 (2013). <https://doi.org/10.1016/j.ydbio.2013.10.006>
- 129 Brzezinski, J. A. & Reh, T. A. Photoreceptor cell fate specification in vertebrates. *Development* **142**, 3263-3273 (2015). <https://doi.org/10.1242/dev.127043>
- 130 Adler, R. & Hatlee, M. Plasticity and differentiation of embryonic retinal cells after terminal mitosis. *Science* **243**, 391-393 (1989). <https://doi.org/10.1126/science.2911751>
- 131 Brown, N. L., Patel, S., Brzezinski, J. & Glaser, T. Math5 is required for retinal ganglion cell and optic nerve formation. *Development* **128**, 2497-2508 (2001). <https://doi.org/10.1242/dev.128.13.2497>
- 132 Brzezinski, J. A. t., Prasov, L. & Glaser, T. Math5 defines the ganglion cell competence state in a subpopulation of retinal progenitor cells exiting the cell cycle. *Dev Biol* **365**, 395-413 (2012). <https://doi.org/10.1016/j.ydbio.2012.03.006>
- 133 Wang, S. W. *et al.* Requirement for math5 in the development of retinal ganglion cells. *Genes Dev* **15**, 24-29 (2001). <https://doi.org/10.1101/gad.855301>
- 134 Yang, Z., Ding, K., Pan, L., Deng, M. & Gan, L. Math5 determines the competence state of retinal ganglion cell progenitors. *Dev Biol* **264**, 240-254 (2003). <https://doi.org/10.1016/j.ydbio.2003.08.005>
- 135 Jeon, C. J., Strettoi, E. & Masland, R. H. The major cell populations of the mouse retina. *J Neurosci* **18**, 8936-8946 (1998). <https://doi.org/10.1523/JNEUROSCI.18-21-08936.1998>
- 136 Hafler, B. P. *et al.* Transcription factor Olig2 defines subpopulations of retinal progenitor cells biased toward specific cell fates. *Proc Natl Acad Sci U S A* **109**, 7882-7887 (2012). <https://doi.org/10.1073/pnas.1203138109>
- 137 Tomita, K., Nakanishi, S., Guillemot, F. & Kageyama, R. Mash1 promotes neuronal differentiation in the retina. *Genes Cells* **1**, 765-774 (1996). <https://doi.org/10.1111/j.1365-2443.1996.tb00016.x>

- 138 Chen, S. *et al.* Crx, a novel Otx-like paired-homeodomain protein, binds to and transactivates photoreceptor cell-specific genes. *Neuron* **19**, 1017-1030 (1997). [https://doi.org/10.1016/s0896-6273\(00\)80394-3](https://doi.org/10.1016/s0896-6273(00)80394-3)
- 139 Freund, C. L. *et al.* Cone-rod dystrophy due to mutations in a novel photoreceptor-specific homeobox gene (CRX) essential for maintenance of the photoreceptor. *Cell* **91**, 543-553 (1997). [https://doi.org/10.1016/s0092-8674\(00\)80440-7](https://doi.org/10.1016/s0092-8674(00)80440-7)
- 140 Furukawa, T., Morrow, E. M. & Cepko, C. L. Crx, a novel otx-like homeobox gene, shows photoreceptor-specific expression and regulates photoreceptor differentiation. *Cell* **91**, 531-541 (1997). [https://doi.org/10.1016/s0092-8674\(00\)80439-0](https://doi.org/10.1016/s0092-8674(00)80439-0)
- 141 Li, S. *et al.* Foxn4 controls the genesis of amacrine and horizontal cells by retinal progenitors. *Neuron* **43**, 795-807 (2004). <https://doi.org/10.1016/j.neuron.2004.08.041>
- 142 Morrow, E. M., Furukawa, T., Lee, J. E. & Cepko, C. L. NeuroD regulates multiple functions in the developing neural retina in rodent. *Development* **126**, 23-36 (1999). <https://doi.org/10.1242/dev.126.1.23>
- 143 Liu, H. *et al.* NeuroD1 regulates expression of thyroid hormone receptor 2 and cone opsins in the developing mouse retina. *J Neurosci* **28**, 749-756 (2008). <https://doi.org/10.1523/JNEUROSCI.4832-07.2008>
- 144 Jadhav, A. P., Mason, H. A. & Cepko, C. L. Notch 1 inhibits photoreceptor production in the developing mammalian retina. *Development* **133**, 913-923 (2006). <https://doi.org/10.1242/dev.02245>
- 145 Akhmedov, N. B. *et al.* A deletion in a photoreceptor-specific nuclear receptor mRNA causes retinal degeneration in the rd7 mouse. *Proc Natl Acad Sci U S A* **97**, 5551-5556 (2000). <https://doi.org/10.1073/pnas.97.10.5551>
- 146 Corbo, J. C. & Cepko, C. L. A hybrid photoreceptor expressing both rod and cone genes in a mouse model of enhanced S-cone syndrome. *PLoS Genet* **1**, e11 (2005). <https://doi.org/10.1371/journal.pgen.0010011>
- 147 Mears, A. J. *et al.* Nrl is required for rod photoreceptor development. *Nat Genet* **29**, 447-452 (2001). <https://doi.org/10.1038/ng774>
- 148 Sapkota, D. *et al.* Onecut1 and Onecut2 redundantly regulate early retinal cell fates during development. *Proc Natl Acad Sci U S A* **111**, E4086-4095 (2014). <https://doi.org/10.1073/pnas.1405354111>
- 149 Sato, S. *et al.* Dkk3-Cre BAC transgenic mouse line: a tool for highly efficient gene deletion in retinal progenitor cells. *Genesis* **45**, 502-507 (2007). <https://doi.org/10.1002/dvg.20318>
- 150 Marquardt, T. *et al.* Pax6 is required for the multipotent state of retinal progenitor cells. *Cell* **105**, 43-55 (2001). [https://doi.org/10.1016/s0092-8674\(01\)00295-1](https://doi.org/10.1016/s0092-8674(01)00295-1)
- 151 Fu, Y. *et al.* Feedback induction of a photoreceptor-specific isoform of retinoid-related orphan nuclear receptor beta by the rod transcription factor NRL. *J Biol Chem* **289**, 32469-32480 (2014). <https://doi.org/10.1074/jbc.M114.605774>
- 152 Roberts, M. R., Hendrickson, A., McGuire, C. R. & Reh, T. A. Retinoid X receptor (gamma) is necessary to establish the S-opsin gradient in cone photoreceptors of

- the developing mouse retina. *Invest Ophthalmol Vis Sci* **46**, 2897-2904 (2005).
<https://doi.org/10.1167/iovs.05-0093>
- 153 Ng, L. *et al.* Two transcription factors can direct three photoreceptor outcomes from rod precursor cells in mouse retinal development. *J Neurosci* **31**, 11118-11125 (2011). <https://doi.org/10.1523/JNEUROSCI.1709-11.2011>
- 154 Roberts, M. R., Srinivas, M., Forrest, D., Morreale de Escobar, G. & Reh, T. A. Making the gradient: thyroid hormone regulates cone opsin expression in the developing mouse retina. *Proc Natl Acad Sci U S A* **103**, 6218-6223 (2006).
<https://doi.org/10.1073/pnas.0509981103>
- 155 Livne-Bar, I. *et al.* Chx10 is required to block photoreceptor differentiation but is dispensable for progenitor proliferation in the postnatal retina. *Proc Natl Acad Sci U S A* **103**, 4988-4993 (2006). <https://doi.org/10.1073/pnas.0600083103>
- 156 Swaroop, A., Kim, D. & Forrest, D. Transcriptional regulation of photoreceptor development and homeostasis in the mammalian retina. *Nat Rev Neurosci* **11**, 563-576 (2010). <https://doi.org/10.1038/nrn2880>
- 157 Peng, G. H., Ahmad, O., Ahmad, F., Liu, J. & Chen, S. The photoreceptor-specific nuclear receptor Nr2e3 interacts with Crx and exerts opposing effects on the transcription of rod versus cone genes. *Hum Mol Genet* **14**, 747-764 (2005).
<https://doi.org/10.1093/hmg/ddi070>
- 158 Chen, J., Rattner, A. & Nathans, J. The rod photoreceptor-specific nuclear receptor Nr2e3 represses transcription of multiple cone-specific genes. *J Neurosci* **25**, 118-129 (2005). <https://doi.org/10.1523/JNEUROSCI.3571-04.2005>
- 159 Cheng, H., Khan, N. W., Roger, J. E. & Swaroop, A. Excess cones in the retinal degeneration rd7 mouse, caused by the loss of function of orphan nuclear receptor Nr2e3, originate from early-born photoreceptor precursors. *Hum Mol Genet* **20**, 4102-4115 (2011). <https://doi.org/10.1093/hmg/ddr334>
- 160 Cheng, H. *et al.* In vivo function of the orphan nuclear receptor NR2E3 in establishing photoreceptor identity during mammalian retinal development. *Hum Mol Genet* **15**, 2588-2602 (2006). <https://doi.org/10.1093/hmg/ddl185>
- 161 Cheng, H. *et al.* Photoreceptor-specific nuclear receptor NR2E3 functions as a transcriptional activator in rod photoreceptors. *Hum Mol Genet* **13**, 1563-1575 (2004). <https://doi.org/10.1093/hmg/ddh173>
- 162 Oh, E. C. *et al.* Transformation of cone precursors to functional rod photoreceptors by bZIP transcription factor NRL. *Proc Natl Acad Sci U S A* **104**, 1679-1684 (2007). <https://doi.org/10.1073/pnas.0605934104>
- 163 Glaschke, A., Glosmann, M. & Peichl, L. Developmental changes of cone opsin expression but not retinal morphology in the hypothyroid Pax8 knockout mouse. *Invest Ophthalmol Vis Sci* **51**, 1719-1727 (2010). <https://doi.org/10.1167/iovs.09-3592>
- 164 Glaschke, A. *et al.* Thyroid hormone controls cone opsin expression in the retina of adult rodents. *J Neurosci* **31**, 4844-4851 (2011).
<https://doi.org/10.1523/JNEUROSCI.6181-10.2011>
- 165 Emerson, M. M., Surzenko, N., Goetz, J. J., Trimarchi, J. & Cepko, C. L. Otx2 and Onecut1 promote the fates of cone photoreceptors and horizontal cells and

- repress rod photoreceptors. *Dev Cell* **26**, 59-72 (2013).
<https://doi.org/10.1016/j.devcel.2013.06.005>
- 166 Stevens, C. B., Cameron, D. A. & Stenkamp, D. L. Plasticity of photoreceptor-
generating retinal progenitors revealed by prolonged retinoic acid exposure. *BMC*
Dev Biol **11**, 51 (2011). <https://doi.org/10.1186/1471-213X-11-51>
- 167 Hyatt, G. A., Schmitt, E. A., Fadool, J. M. & Dowling, J. E. Retinoic acid alters
photoreceptor development in vivo. *Proc Natl Acad Sci U S A* **93**, 13298-13303
(1996). <https://doi.org/10.1073/pnas.93.23.13298>
- 168 Kelley, M. W., Turner, J. K. & Reh, T. A. Ligands of steroid/thyroid receptors
induce cone photoreceptors in vertebrate retina. *Development* **121**, 3777-3785
(1995). <https://doi.org/10.1242/dev.121.11.3777>
- 169 Hoover, F., Seleiro, E. A., Kielland, A., Brickell, P. M. & Glover, J. C. Retinoid X
receptor gamma gene transcripts are expressed by a subset of early generated
retinal cells and eventually restricted to photoreceptors. *J Comp Neurol* **391**, 204-
213 (1998).
- 170 Mori, M., Ghyselinck, N. B., Chambon, P. & Mark, M. Systematic
immunolocalization of retinoid receptors in developing and adult mouse eyes.
Invest Ophthalmol Vis Sci **42**, 1312-1318 (2001).
- 171 Ha, M. & Kim, V. N. Regulation of microRNA biogenesis. *Nat Rev Mol Cell Biol*
15, 509-524 (2014). <https://doi.org/10.1038/nrm3838>
- 172 Han, J. *et al.* The Drosha-DGCR8 complex in primary microRNA processing.
Genes Dev **18**, 3016-3027 (2004). <https://doi.org/10.1101/gad.1262504>
- 173 Kim, V. N., Han, J. & Siomi, M. C. Biogenesis of small RNAs in animals. *Nat Rev*
Mol Cell Biol **10**, 126-139 (2009). <https://doi.org/10.1038/nrm2632>
- 174 Borchert, G. M., Lanier, W. & Davidson, B. L. RNA polymerase III transcribes
human microRNAs. *Nat Struct Mol Biol* **13**, 1097-1101 (2006).
<https://doi.org/10.1038/nsmb1167>
- 175 Lee, Y. *et al.* MicroRNA genes are transcribed by RNA polymerase II. *EMBO J*
23, 4051-4060 (2004). <https://doi.org/10.1038/sj.emboj.7600385>
- 176 Eulalio, A., Huntzinger, E. & Izaurralde, E. Getting to the root of miRNA-mediated
gene silencing. *Cell* **132**, 9-14 (2008). <https://doi.org/10.1016/j.cell.2007.12.024>
- 177 Kozomara, A. & Griffiths-Jones, S. miRBase: annotating high confidence
microRNAs using deep sequencing data. *Nucleic Acids Res* **42**, D68-73 (2014).
<https://doi.org/10.1093/nar/gkt1181>
- 178 Friedman, R. C., Farh, K. K., Burge, C. B. & Bartel, D. P. Most mammalian
mRNAs are conserved targets of microRNAs. *Genome Res* **19**, 92-105 (2009).
<https://doi.org/10.1101/gr.082701.108>
- 179 Naeli, P., Winter, T., Hackett, A. P., Alboushi, L. & Jafarnejad, S. M. The intricate
balance between microRNA-induced mRNA decay and translational repression.
FEBS J **290**, 2508-2524 (2023). <https://doi.org/10.1111/febs.16422>
- 180 Sako, H. *et al.* microRNAs slow translating ribosomes to prevent protein
misfolding in eukaryotes. *EMBO J* **42**, e112469 (2023).
<https://doi.org/10.15252/emj.2022112469>

- 181 Reh, T. A. & Hindges, R. MicroRNAs in Retinal Development. *Annu Rev Vis Sci*
4, 25-44 (2018). <https://doi.org/10.1146/annurev-vision-091517-034357>
- 182 Cheloufi, S., Dos Santos, C. O., Chong, M. M. & Hannon, G. J. A dicer-
independent miRNA biogenesis pathway that requires Ago catalysis. *Nature* **465**,
584-589 (2010). <https://doi.org/10.1038/nature09092>
- 183 Cifuentes, D. *et al.* A novel miRNA processing pathway independent of Dicer
requires Argonaute2 catalytic activity. *Science* **328**, 1694-1698 (2010).
<https://doi.org/10.1126/science.1190809>
- 184 Stavast, C. J. & Erkeland, S. J. The Non-Canonical Aspects of MicroRNAs: Many
Roads to Gene Regulation. *Cells* **8** (2019). <https://doi.org/10.3390/cells8111465>
- 185 Bernstein, E. *et al.* Dicer is essential for mouse development. *Nat Genet* **35**, 215-
217 (2003). <https://doi.org/10.1038/ng1253>
- 186 Damiani, D. *et al.* Dicer inactivation leads to progressive functional and structural
degeneration of the mouse retina. *J Neurosci* **28**, 4878-4887 (2008).
<https://doi.org/10.1523/JNEUROSCI.0828-08.2008>
- 187 La Torre, A., Georgi, S. & Reh, T. A. Conserved microRNA pathway regulates
developmental timing of retinal neurogenesis. *Proc Natl Acad Sci U S A* **110**,
E2362-2370 (2013). <https://doi.org/10.1073/pnas.1301837110>
- 188 Shu, P. *et al.* Opposing Gradients of MicroRNA Expression Temporally Pattern
Layer Formation in the Developing Neocortex. *Dev Cell* **49**, 764-785 e764
(2019). <https://doi.org/10.1016/j.devcel.2019.04.017>
- 189 Klapper, S. D., Swiersy, A., Bamberg, E. & Busskamp, V. Biophysical Properties
of Optogenetic Tools and Their Application for Vision Restoration Approaches.
Front Syst Neurosci **10**, 74 (2016). <https://doi.org/10.3389/fnsys.2016.00074>
- 190 Hughes, A. in *The Visual System in Vertebrates* (ed F. Crescitelli) (Springer-
Verlag Berlin Heidelberg, 1977).
- 191 Baden, T. Vertebrate vision: Lessons from non-model species. *Semin Cell Dev*
Biol **106**, 1-4 (2020). <https://doi.org/10.1016/j.semcd.2020.05.028>
- 192 Carroll, J. & Conway, B. R. Color vision. *Handb Clin Neurol* **178**, 131-153 (2021).
<https://doi.org/10.1016/B978-0-12-821377-3.00005-2>
- 193 Drasdo, N., Millican, C. L., Katholi, C. R. & Curcio, C. A. The length of Henle
fibers in the human retina and a model of ganglion receptive field density in the
visual field. *Vision Res* **47**, 2901-2911 (2007).
<https://doi.org/10.1016/j.visres.2007.01.007>
- 194 Lujan, B. J., Roorda, A., Knighton, R. W. & Carroll, J. Revealing Henle's fiber
layer using spectral domain optical coherence tomography. *Invest Ophthalmol*
Vis Sci **52**, 1486-1492 (2011). <https://doi.org/10.1167/iovs.10-5946>
- 195 Collin, S. P. in *Encyclopedia of Neuroscience* 1459-1466 (Springer, Berlin,
Heidelberg, 2009).
- 196 Shimizu, T., Patton, T.B., Szafranski G., Butler, A.B. in *Encyclopedia of*
Neuroscience 1466-1472 (Springer, Berlin, Heidelberg, 2009).
- 197 Mitkus, M., Olsson, P., Toomey, M. B., Corbo, J. C. & Kelber, A. Specialized
photoreceptor composition in the raptor fovea. *J Comp Neurol* **525**, 2152-2163
(2017). <https://doi.org/10.1002/cne.24190>

- 198 Buzzi, F. *Opuscoli Scelti Sulle Scienze e Sulle Arti Tomo V.* (Presso Giuseppe Marelli, 1782).
- 199 Soemmerring, S. T. in *Commentationes Societatis Regiae Scientiarum Gottingensis* Vol. 13 3-13 (Joann Christian Dieterich, 1799).
- 200 Chievitz, J. H. *Entwicklund der fovea centralis retinae.*, (Anat. Anzeig., 1888).
- 201 Magitot, M. A. Etude sur le développement de la rétine humaine. *Annales d'Occulistique* **143**, 241-282 (1910).
- 202 Back, L., Seefelder, R. *Entwicklungsgeschichte des menschlichen auges.*, (W. Engelmann, 1914).
- 203 Mann, I. *The development of the human eye.* (Cambridge University Press. The British Journal of Ophthalmology, 1928).
- 204 Hendrickson, A. & Kupfer, C. The histogenesis of the fovea in the macaque monkey. *Invest Ophthalmol Vis Sci* **15**, 746-756 (1976).
- 205 Packer, O., Hendrickson, A. E. & Curcio, C. A. Photoreceptor topography of the retina in the adult pigtail macaque (*Macaca nemestrina*). *J Comp Neurol* **288**, 165-183 (1989). <https://doi.org/10.1002/cne.902880113>
- 206 Curcio, C. A. H., A. E. in *Prog Retin Res* Vol. 10 Ch. 5, 89-120 (1991).
- 207 Martin, P. R. & Grunert, U. Analysis of the short wavelength-sensitive ("blue") cone mosaic in the primate retina: comparison of New World and Old World monkeys. *J Comp Neurol* **406**, 1-14 (1999). [https://doi.org/10.1002/\(sici\)1096-9861\(19990329\)406:1<1::aid-cne1>3.0.co;2-1](https://doi.org/10.1002/(sici)1096-9861(19990329)406:1<1::aid-cne1>3.0.co;2-1)
- 208 Franco, E. C., Finlay, B. L., Silveira, L. C., Yamada, E. S. & Crowley, J. C. Conservation of absolute foveal area in New World monkeys. A constraint on eye size and conformation. *Brain Behav Evol* **56**, 276-286 (2000). <https://doi.org/10.1159/000047211>
- 209 Casey, M. A., Lusk, S. & Kwan, K. M. Build me up optic cup: Intrinsic and extrinsic mechanisms of vertebrate eye morphogenesis. *Dev Biol* **476**, 128-136 (2021). <https://doi.org/10.1016/j.ydbio.2021.03.023>
- 210 Yuasa, J., Hirano, S., Yamagata, M. & Noda, M. Visual projection map specified by topographic expression of transcription factors in the retina. *Nature* **382**, 632-635 (1996). <https://doi.org/10.1038/382632a0>
- 211 Hatini, V., Tao, W. & Lai, E. Expression of winged helix genes, BF-1 and BF-2, define adjacent domains within the developing forebrain and retina. *J Neurobiol* **25**, 1293-1309 (1994). <https://doi.org/10.1002/neu.480251010>
- 212 Hernandez-Bejarano, M. *et al.* Foxd1-dependent induction of a temporal retinal character is required for visual function. *Development* **149** (2022). <https://doi.org/10.1242/dev.200938>
- 213 Hernandez-Bejarano, M. *et al.* Opposing Shh and Fgf signals initiate nasotemporal patterning of the zebrafish retina. *Development* **142**, 3933-3942 (2015). <https://doi.org/10.1242/dev.125120>
- 214 Takahashi, H., Sakuta, H., Shintani, T. & Noda, M. Functional mode of FoxD1/CBF2 for the establishment of temporal retinal specificity in the developing chick retina. *Dev Biol* **331**, 300-310 (2009). <https://doi.org/10.1016/j.ydbio.2009.05.549>

- 215 Picker, A. *et al.* Dynamic coupling of pattern formation and morphogenesis in the developing vertebrate retina. *PLoS Biol* **7**, e1000214 (2009). <https://doi.org/10.1371/journal.pbio.1000214>
- 216 Yamagata, M., Mai, A., Pollerberg, G. E. & Noda, M. Regulatory interrelations among topographic molecules CBF1, CBF2 and EphA3 in the developing chick retina. *Dev Growth Differ* **41**, 575-587 (1999). <https://doi.org/10.1046/j.1440-169x.1999.00462.x>
- 217 Takahashi, H., Shintani, T., Sakuta, H. & Noda, M. CBF1 controls the retinotectal topographical map along the anteroposterior axis through multiple mechanisms. *Development* **130**, 5203-5215 (2003). <https://doi.org/10.1242/dev.00724>
- 218 Herrera, E. *et al.* Foxd1 is required for proper formation of the optic chiasm. *Development* **131**, 5727-5739 (2004). <https://doi.org/10.1242/dev.01431>
- 219 Sakuta, H. *et al.* Ventroptin: a BMP-4 antagonist expressed in a double-gradient pattern in the retina. *Science* **293**, 111-115 (2001). <https://doi.org/10.1126/science.1058379>
- 220 Behesti, H., Holt, J. K. & Sowden, J. C. The level of BMP4 signaling is critical for the regulation of distinct T-box gene expression domains and growth along the dorso-ventral axis of the optic cup. *BMC Dev Biol* **6**, 62 (2006). <https://doi.org/10.1186/1471-213X-6-62>
- 221 Marcus, R. C., Gale, N. W., Morrison, M. E., Mason, C. A. & Yancopoulos, G. D. Eph family receptors and their ligands distribute in opposing gradients in the developing mouse retina. *Dev Biol* **180**, 786-789 (1996). <https://doi.org/10.1006/dbio.1996.0347>
- 222 Connor, R. J., Menzel, P. & Pasquale, E. B. Expression and tyrosine phosphorylation of Eph receptors suggest multiple mechanisms in patterning of the visual system. *Dev Biol* **193**, 21-35 (1998). <https://doi.org/10.1006/dbio.1997.8786>
- 223 Hornberger, M. R. *et al.* Modulation of EphA receptor function by coexpressed ephrinA ligands on retinal ganglion cell axons. *Neuron* **22**, 731-742 (1999). [https://doi.org/10.1016/s0896-6273\(00\)80732-1](https://doi.org/10.1016/s0896-6273(00)80732-1)
- 224 Marin, O., Blanco, M. J. & Nieto, M. A. Differential expression of Eph receptors and ephrins correlates with the formation of topographic projections in primary and secondary visual circuits of the embryonic chick forebrain. *Dev Biol* **234**, 289-303 (2001). <https://doi.org/10.1006/dbio.2001.0268>
- 225 Schulte, D. & Cepko, C. L. Two homeobox genes define the domain of EphA3 expression in the developing chick retina. *Development* **127**, 5033-5045 (2000). <https://doi.org/10.1242/dev.127.23.5033>
- 226 Petros, T. J., Shrestha, B. R. & Mason, C. Specificity and sufficiency of EphB1 in driving the ipsilateral retinal projection. *J Neurosci* **29**, 3463-3474 (2009). <https://doi.org/10.1523/JNEUROSCI.5655-08.2009>
- 227 Lambot, M. A., Depasse, F., Noel, J. C. & Vanderhaeghen, P. Mapping labels in the human developing visual system and the evolution of binocular vision. *J Neurosci* **25**, 7232-7237 (2005). <https://doi.org/10.1523/JNEUROSCI.0802-05.2005>

- 228 da Silva, S. & Cepko, C. L. Fgf8 Expression and Degradation of Retinoic Acid Are Required for Patterning a High-Acuity Area in the Retina. *Dev Cell* **42**, 68-81 e66 (2017). <https://doi.org/10.1016/j.devcel.2017.05.024>
- 229 Yoshimatsu, T., Schroder, C., Nevala, N. E., Berens, P. & Baden, T. Fovea-like Photoreceptor Specializations Underlie Single UV Cone Driven Prey-Capture Behavior in Zebrafish. *Neuron* **107**, 320-337 e326 (2020). <https://doi.org/10.1016/j.neuron.2020.04.021>
- 230 Lahne, M. Y., T.; MacDonald, R.B. Retinoic acid signaling in the developing zebrafish high acuity zone. *Invest Ophthalmol Vis Sci* **64** (2023).
- 231 Lu, Y. *et al.* Single-Cell Analysis of Human Retina Identifies Evolutionarily Conserved and Species-Specific Mechanisms Controlling Development. *Dev Cell* **53**, 473-491 e479 (2020). <https://doi.org/10.1016/j.devcel.2020.04.009>
- 232 Fishman, E. S. *et al.* MicroRNA Signatures of the Developing Primate Fovea. *Front Cell Dev Biol* **9**, 654385 (2021). <https://doi.org/10.3389/fcell.2021.654385>
- 233 Peng, Y. R. *et al.* Molecular Classification and Comparative Taxonomics of Foveal and Peripheral Cells in Primate Retina. *Cell* **176**, 1222-1237 e1222 (2019). <https://doi.org/10.1016/j.cell.2019.01.004>
- 234 Molotkov, A., Molotkova, N. & Duester, G. Retinoic acid guides eye morphogenetic movements via paracrine signaling but is unnecessary for retinal dorsoventral patterning. *Development* **133**, 1901-1910 (2006). <https://doi.org/10.1242/dev.02328>
- 235 Kelley, M. W., Turner, J. K. & Reh, T. A. Retinoic acid promotes differentiation of photoreceptors in vitro. *Development* **120**, 2091-2102 (1994). <https://doi.org/10.1242/dev.120.8.2091>
- 236 Amamoto, R., Wallick, G. K. & Cepko, C. L. Retinoic acid signaling mediates peripheral cone photoreceptor survival in a mouse model of retina degeneration. *Elife* **11** (2022). <https://doi.org/10.7554/eLife.76389>
- 237 Meire, F. *et al.* Nonsyndromic bilateral and unilateral optic nerve aplasia: first familial occurrence and potential implication of CYP26A1 and CYP26C1 genes. *Mol Vis* **17**, 2072-2079 (2011).
- 238 Sakai, Y., Luo, T., McCaffery, P., Hamada, H. & Drager, U. C. CYP26A1 and CYP26C1 cooperate in degrading retinoic acid within the equatorial retina during later eye development. *Dev Biol* **276**, 143-157 (2004). <https://doi.org/10.1016/j.ydbio.2004.08.032>
- 239 Wagner, E., McCaffery, P. & Drager, U. C. Retinoic acid in the formation of the dorsoventral retina and its central projections. *Dev Biol* **222**, 460-470 (2000). <https://doi.org/10.1006/dbio.2000.9719>
- 240 Townes-Anderson, E. & Raviola, G. The formation and distribution of intercellular junctions in the rhesus monkey optic cup: the early development of the cilio-iridic and sensory retinas. *Dev Biol* **85**, 209-232 (1981). [https://doi.org/10.1016/0012-1606\(81\)90252-9](https://doi.org/10.1016/0012-1606(81)90252-9)
- 241 Krueger, M. R., Fishman-Williams, E., Simo, S., Tarantal, A. F. & La Torre, A. Expression patterns of CYP26A1, FGF8, CDKN1A, and NPVF in the developing

- rhesus monkey retina. *Differentiation* **135**, 100743 (2023).
<https://doi.org/10.1016/j.diff.2023.100743>
- 242 Hendrickson, A. Development of Retinal Layers in Prenatal Human Retina. *Am J Ophthalmol* **161**, 29-35 e21 (2016). <https://doi.org/10.1016/j.ajo.2015.09.023>
- 243 Hoshino, A. *et al.* Molecular Anatomy of the Developing Human Retina. *Dev Cell* **43**, 763-779 e764 (2017). <https://doi.org/10.1016/j.devcel.2017.10.029>
- 244 Xiao, M. & Hendrickson, A. Spatial and temporal expression of short, long/medium, or both opsins in human fetal cones. *J Comp Neurol* **425**, 545-559 (2000).
- 245 Fei, Y. Development of the cone photoreceptor mosaic in the mouse retina revealed by fluorescent cones in transgenic mice. *Mol Vis* **9**, 31-42 (2003).
- 246 Brown, N. L. *et al.* Math5 encodes a murine basic helix-loop-helix transcription factor expressed during early stages of retinal neurogenesis. *Development* **125**, 4821-4833 (1998). <https://doi.org/10.1242/dev.125.23.4821>
- 247 Kay, J. N., Finger-Baier, K. C., Roeser, T., Staub, W. & Baier, H. Retinal ganglion cell genesis requires lakritz, a Zebrafish atonal Homolog. *Neuron* **30**, 725-736 (2001). [https://doi.org/10.1016/s0896-6273\(01\)00312-9](https://doi.org/10.1016/s0896-6273(01)00312-9)
- 248 Kanekar, S. *et al.* Xath5 participates in a network of bHLH genes in the developing *Xenopus* retina. *Neuron* **19**, 981-994 (1997).
[https://doi.org/10.1016/s0896-6273\(00\)80391-8](https://doi.org/10.1016/s0896-6273(00)80391-8)
- 249 Khan, K. *et al.* Next generation sequencing identifies mutations in Atonal homolog 7 (ATOH7) in families with global eye developmental defects. *Hum Mol Genet* **21**, 776-783 (2012). <https://doi.org/10.1093/hmg/ddr509>
- 250 Ghasvand, N. M. *et al.* Deletion of a remote enhancer near ATOH7 disrupts retinal neurogenesis, causing NCRNA disease. *Nat Neurosci* **14**, 578-586 (2011).
<https://doi.org/10.1038/nn.2798>
- 251 Miesfeld, J. B. *et al.* The Atoh7 remote enhancer provides transcriptional robustness during retinal ganglion cell development. *Proc Natl Acad Sci U S A* **117**, 21690-21700 (2020). <https://doi.org/10.1073/pnas.2006888117>
- 252 Miesfeld, J. B., Glaser, T. & Brown, N. L. The dynamics of native Atoh7 protein expression during mouse retinal histogenesis, revealed with a new antibody. *Gene Expr Patterns* **27**, 114-121 (2018).
<https://doi.org/10.1016/j.gexp.2017.11.006>
- 253 Park, K. U., Randazzo, G., Jones, K. L. & Brzezinski, J. A. t. Gsg1, Trnp1, and Tmem215 Mark Subpopulations of Bipolar Interneurons in the Mouse Retina. *Invest Ophthalmol Vis Sci* **58**, 1137-1150 (2017). <https://doi.org/10.1167/iovs.16-19767>
- 254 Wohlschlegel, J. *et al.* ASCL1 induces neurogenesis in human Muller glia. *Stem Cell Reports* (2023). <https://doi.org/10.1016/j.stemcr.2023.10.021>
- 255 Yan, W. *et al.* Cell Atlas of The Human Fovea and Peripheral Retina. *Sci Rep* **10**, 9802 (2020). <https://doi.org/10.1038/s41598-020-66092-9>
- 256 Osterberg, G. Topography of the layer of rods and cones in the human retina. *Acta Ophthalmologica* **13**, 6-97 (1935).

- 257 Ahnelt, P., Keri, C. & Kolb, H. Identification of pedicles of putative blue-sensitive cones in the human retina. *J Comp Neurol* **293**, 39-53 (1990). <https://doi.org/10.1002/cne.902930104>
- 258 Williams, D. R., MacLeod, D. I. & Hayhoe, M. M. Punctate sensitivity of the blue-sensitive mechanism. *Vision Res* **21**, 1357-1375 (1981). [https://doi.org/10.1016/0042-6989\(81\)90242-x](https://doi.org/10.1016/0042-6989(81)90242-x)
- 259 Ahnelt, P. K., Kolb, H. & Pflug, R. Identification of a subtype of cone photoreceptor, likely to be blue sensitive, in the human retina. *J Comp Neurol* **255**, 18-34 (1987). <https://doi.org/10.1002/cne.902550103>
- 260 Curcio, C. A. *et al.* Distribution and morphology of human cone photoreceptors stained with anti-blue opsin. *J Comp Neurol* **312**, 610-624 (1991). <https://doi.org/10.1002/cne.903120411>
- 261 Onishi, A. *et al.* Variations in long- and middle-wavelength-sensitive opsin gene loci in crab-eating monkeys. *Vision Res* **42**, 281-292 (2002). [https://doi.org/10.1016/s0042-6989\(01\)00293-0](https://doi.org/10.1016/s0042-6989(01)00293-0)
- 262 Roorda, A. & Williams, D. R. The arrangement of the three cone classes in the living human eye. *Nature* **397**, 520-522 (1999). <https://doi.org/10.1038/17383>
- 263 Hofer, H., Singer, B. & Williams, D. R. Different sensations from cones with the same photopigment. *J Vis* **5**, 444-454 (2005). <https://doi.org/10.1167/5.5.5>
- 264 Simic, N., Westall, C., Astzalos, E. V. & Rovet, J. Visual abilities at 6 months in preterm infants: impact of thyroid hormone deficiency and neonatal medical morbidity. *Thyroid* **20**, 309-315 (2010). <https://doi.org/10.1089/thy.2009.0128>
- 265 Schein, S. J. Anatomy of macaque fovea and spatial densities of neurons in foveal representation. *J Comp Neurol* **269**, 479-505 (1988). <https://doi.org/10.1002/cne.902690403>
- 266 Sjostrand, J., Olsson, V., Popovic, Z. & Conradi, N. Quantitative estimations of foveal and extra-foveal retinal circuitry in humans. *Vision Res* **39**, 2987-2998 (1999). [https://doi.org/10.1016/s0042-6989\(99\)00030-9](https://doi.org/10.1016/s0042-6989(99)00030-9)
- 267 Curcio, C. A. & Allen, K. A. Topography of ganglion cells in human retina. *J Comp Neurol* **300**, 5-25 (1990). <https://doi.org/10.1002/cne.903000103>
- 268 Dacey, D. in *The Cognitive Neurosciences* (ed M.S. Gazzaniga) (MIT Press, 2004).
- 269 Masri, R. A., Percival, K. A., Koizumi, A., Martin, P. R. & Grunert, U. Survey of retinal ganglion cell morphology in marmoset. *J Comp Neurol* **527**, 236-258 (2019). <https://doi.org/10.1002/cne.24157>
- 270 Masri, R. A. *et al.* Composition of the Inner Nuclear Layer in Human Retina. *Invest Ophthalmol Vis Sci* **62**, 22 (2021). <https://doi.org/10.1167/iovs.62.9.22>
- 271 Finlay, B. L. The developing and evolving retina: using time to organize form. *Brain Res* **1192**, 5-16 (2008). <https://doi.org/10.1016/j.brainres.2007.07.005>
- 272 Finlay, B. L., Hersman, M. N. & Darlington, R. B. Patterns of vertebrate neurogenesis and the paths of vertebrate evolution. *Brain Behav Evol* **52**, 232-242 (1998). <https://doi.org/10.1159/000006566>

- 273 Dyer, M. A. *et al.* Developmental sources of conservation and variation in the evolution of the primate eye. *Proc Natl Acad Sci U S A* **106**, 8963-8968 (2009). <https://doi.org/10.1073/pnas.0901484106>
- 274 Wikler, K. C. & Rakic, P. Distribution of photoreceptor subtypes in the retina of diurnal and nocturnal primates. *J Neurosci* **10**, 3390-3401 (1990). <https://doi.org/10.1523/JNEUROSCI.10-10-03390.1990>
- 275 De Pietri Tonelli, D. *et al.* miRNAs are essential for survival and differentiation of newborn neurons but not for expansion of neural progenitors during early neurogenesis in the mouse embryonic neocortex. *Development* **135**, 3911-3921 (2008). <https://doi.org/10.1242/dev.025080>
- 276 Fairchild, C. L. A. *et al.* Let-7 regulates cell cycle dynamics in the developing cerebral cortex and retina. *Sci Rep* **9**, 15336 (2019). <https://doi.org/10.1038/s41598-019-51703-x>
- 277 Han, J. S. *et al.* Notch directs telencephalic development and controls neocortical neuron fate determination by regulating microRNA levels. *Development* **150** (2023). <https://doi.org/10.1242/dev.201408>
- 278 Fishman, E. S., Han, J. S. & La Torre, A. Oscillatory Behaviors of microRNA Networks: Emerging Roles in Retinal Development. *Front Cell Dev Biol* **10**, 831750 (2022). <https://doi.org/10.3389/fcell.2022.831750>
- 279 Georgi, S. A. & Reh, T. A. Dicer is required for the maintenance of notch signaling and gliogenic competence during mouse retinal development. *Dev Neurobiol* **71**, 1153-1169 (2011). <https://doi.org/10.1002/dneu.20899>
- 280 Zhu, Q. *et al.* Sponge transgenic mouse model reveals important roles for the microRNA-183 (miR-183)/96/182 cluster in postmitotic photoreceptors of the retina. *J Biol Chem* **286**, 31749-31760 (2011). <https://doi.org/10.1074/jbc.M111.259028>
- 281 Lumayag, S. *et al.* Inactivation of the microRNA-183/96/182 cluster results in syndromic retinal degeneration. *Proc Natl Acad Sci U S A* **110**, E507-516 (2013). <https://doi.org/10.1073/pnas.1212655110>
- 282 Fogerty, J., Stepanyan, R., Cianciolo, L. T., Tooke, B. P. & Perkins, B. D. Genomic non-redundancy of the mir-183/96/182 cluster and its requirement for hair cell maintenance. *Sci Rep* **9**, 10302 (2019). <https://doi.org/10.1038/s41598-019-46593-y>
- 283 Gariano, R. F., Iruela-Arispe, M. L. & Hendrickson, A. E. Vascular development in primate retina: comparison of lamellar plexus formation in monkey and human. *Invest Ophthalmol Vis Sci* **35**, 3442-3455 (1994).
- 284 Provis, J. M., Diaz, C. M. & Dreher, B. Ontogeny of the primate fovea: a central issue in retinal development. *Prog Neurobiol* **54**, 549-580 (1998). [https://doi.org/10.1016/s0301-0082\(97\)00079-8](https://doi.org/10.1016/s0301-0082(97)00079-8)
- 285 Engerman, R. L. Development of the macular circulation. *Invest Ophthalmol* **15**, 835-840 (1976).
- 286 Hendrickson, A. E. & Yuodelis, C. The morphological development of the human fovea. *Ophthalmology* **91**, 603-612 (1984). [https://doi.org/10.1016/s0161-6420\(84\)34247-6](https://doi.org/10.1016/s0161-6420(84)34247-6)

- 287 Alder, V. A., Ben-Nun, J. & Cringle, S. J. PO₂ profiles and oxygen consumption in cat retina with an occluded retinal circulation. *Invest Ophthalmol Vis Sci* **31**, 1029-1034 (1990).
- 288 Ahmed, J., Braun, R. D., Dunn, R., Jr. & Linsenmeier, R. A. Oxygen distribution in the macaque retina. *Invest Ophthalmol Vis Sci* **34**, 516-521 (1993).
- 289 Chase, J. The evolution of retinal vascularization in mammals. A comparison of vascular and avascular retinæ. *Ophthalmology* **89**, 1518-1525 (1982).
[https://doi.org/10.1016/s0161-6420\(82\)34608-4](https://doi.org/10.1016/s0161-6420(82)34608-4)
- 290 Buttery, R. G., Haight, J. R. & Bell, K. Vascular and avascular retinæ in mammals. A fundusoscopic and fluorescein angiographic study. *Brain Behav Evol* **35**, 156-175 (1990). <https://doi.org/10.1159/000115864>
- 291 Provis, J. M., Penfold, P. L., Cornish, E. E., Sandercoe, T. M. & Madigan, M. C. Anatomy and development of the macula: specialisation and the vulnerability to macular degeneration. *Clin Exp Optom* **88**, 269-281 (2005).
<https://doi.org/10.1111/j.1444-0938.2005.tb06711.x>
- 292 Gariano, R. F., Sage, E. H., Kaplan, H. J. & Hendrickson, A. E. Development of astrocytes and their relation to blood vessels in fetal monkey retina. *Invest Ophthalmol Vis Sci* **37**, 2367-2375 (1996).
- 293 Provis, J. M., Sandercoe, T. & Hendrickson, A. E. Astrocytes and blood vessels define the foveal rim during primate retinal development. *Invest Ophthalmol Vis Sci* **41**, 2827-2836 (2000).
- 294 Kurihara, T. *et al.* von Hippel-Lindau protein regulates transition from the fetal to the adult circulatory system in retina. *Development* **137**, 1563-1571 (2010).
<https://doi.org/10.1242/dev.049015>
- 295 Perelli, R. M., O'Sullivan, M. L., Zarnick, S. & Kay, J. N. Environmental oxygen regulates astrocyte proliferation to guide angiogenesis during retinal development. *Development* **148** (2021). <https://doi.org/10.1242/dev.199418>
- 296 Provis, J. M. & Hendrickson, A. E. The foveal avascular region of developing human retina. *Arch Ophthalmol* **126**, 507-511 (2008).
<https://doi.org/10.1001/archophth.126.4.507>
- 297 Kozulin, P., Natoli, R., O'Brien, K. M., Madigan, M. C. & Provis, J. M. Differential expression of anti-angiogenic factors and guidance genes in the developing macula. *Mol Vis* **15**, 45-59 (2009).
- 298 Kozulin, P., Natoli, R., Bumsted O'Brien, K. M., Madigan, M. C. & Provis, J. M. The cellular expression of antiangiogenic factors in fetal primate macula. *Invest Ophthalmol Vis Sci* **51**, 4298-4306 (2010). <https://doi.org/10.1167/iovs.09-4905>
- 299 Kozulin, P., Natoli, R., Madigan, M. C., O'Brien, K. M. & Provis, J. M. Gradients of Eph-A6 expression in primate retina suggest roles in both vascular and axon guidance. *Mol Vis* **15**, 2649-2662 (2009).
- 300 Hendrickson, A., Troilo, D., Possin, D. & Springer, A. Development of the neural retina and its vasculature in the marmoset *Callithrix jacchus*. *J Comp Neurol* **497**, 270-286 (2006). <https://doi.org/10.1002/cne.20996>

- 301 Dubis, A. M. *et al.* Relationship between the foveal avascular zone and foveal pit morphology. *Invest Ophthalmol Vis Sci* **53**, 1628-1636 (2012). <https://doi.org/10.1167/iovs.11-8488>
- 302 Chui, T. Y., Zhong, Z., Song, H. & Burns, S. A. Foveal avascular zone and its relationship to foveal pit shape. *Optom Vis Sci* **89**, 602-610 (2012). <https://doi.org/10.1097/OPX.0b013e3182504227>
- 303 Yanni, S. E. *et al.* Foveal avascular zone and foveal pit formation after preterm birth. *Br J Ophthalmol* **96**, 961-966 (2012). <https://doi.org/10.1136/bjophthalmol-2012-301612>
- 304 Hellstrom, A., Smith, L. E. & Damman, O. Retinopathy of prematurity. *Lancet* **382**, 1445-1457 (2013). [https://doi.org/10.1016/S0140-6736\(13\)60178-6](https://doi.org/10.1016/S0140-6736(13)60178-6)
- 305 Hammer, D. X. *et al.* Foveal fine structure in retinopathy of prematurity: an adaptive optics Fourier domain optical coherence tomography study. *Invest Ophthalmol Vis Sci* **49**, 2061-2070 (2008). <https://doi.org/10.1167/iovs.07-1228>
- 306 Springer, A. D. & Hendrickson, A. E. Development of the primate area of high acuity. 1. Use of finite element analysis models to identify mechanical variables affecting pit formation. *Vis Neurosci* **21**, 53-62 (2004). <https://doi.org/10.1017/s0952523804041057>
- 307 Linderman, R. E. *et al.* Preservation of the Foveal Avascular Zone in Achromatopsia Despite the Absence of a Fully Formed Pit. *Invest Ophthalmol Vis Sci* **61**, 52 (2020). <https://doi.org/10.1167/iovs.61.10.52>
- 308 Yuodelis, C. & Hendrickson, A. A qualitative and quantitative analysis of the human fovea during development. *Vision Res* **26**, 847-855 (1986). [https://doi.org/10.1016/0042-6989\(86\)90143-4](https://doi.org/10.1016/0042-6989(86)90143-4)
- 309 Hendrickson, A., Possin, D., Vajzovic, L. & Toth, C. A. Histologic development of the human fovea from midgestation to maturity. *Am J Ophthalmol* **154**, 767-778 e762 (2012). <https://doi.org/10.1016/j.ajo.2012.05.007>
- 310 Hendrickson, A. A morphological comparison of foveal development in man and monkey. *Eye (Lond)* **6 (Pt 2)**, 136-144 (1992). <https://doi.org/10.1038/eye.1992.29>
- 311 Robinson, S. R. & Hendrickson, A. Shifting relationships between photoreceptors and pigment epithelial cells in monkey retina: implications for the development of retinal topography. *Vis Neurosci* **12**, 767-778 (1995). <https://doi.org/10.1017/s0952523800009020>
- 312 Preising, M., Op de Laak, J. P. & Lorenz, B. Deletion in the OA1 gene in a family with congenital X linked nystagmus. *Br J Ophthalmol* **85**, 1098-1103 (2001). <https://doi.org/10.1136/bjo.85.9.1098>
- 313 Zhang, Y. *et al.* Genetic mapping of the Kallmann syndrome and X linked ocular albinism gene loci. *J Med Genet* **30**, 923-925 (1993). <https://doi.org/10.1136/jmg.30.11.923>
- 314 Hutton, S. M. & Spritz, R. A. A comprehensive genetic study of autosomal recessive ocular albinism in Caucasian patients. *Invest Ophthalmol Vis Sci* **49**, 868-872 (2008). <https://doi.org/10.1167/iovs.07-0791>

- 315 Elschmig, A. Anatomie des menschlichen Albinoauges. *Graefes Arch Ophthalmol* **84**, 401-419 (1913).
- 316 Bhansali, P., Rayport, I., Rebsam, A. & Mason, C. Delayed neurogenesis leads to altered specification of ventrotemporal retinal ganglion cells in albino mice. *Neural Dev* **9**, 11 (2014). <https://doi.org/10.1186/1749-8104-9-11>
- 317 Rebsam, A., Bhansali, P. & Mason, C. A. Eye-specific projections of retinogeniculate axons are altered in albino mice. *J Neurosci* **32**, 4821-4826 (2012). <https://doi.org/10.1523/JNEUROSCI.5050-11.2012>
- 318 Slavi, N. *et al.* CyclinD2-mediated regulation of neurogenic output from the retinal ciliary margin is perturbed in albinism. *Neuron* **111**, 49-64 e45 (2023). <https://doi.org/10.1016/j.neuron.2022.10.025>
- 319 Roffler-Tarlov, S., Liu, J. H., Naumova, E. N., Bernal-Ayala, M. M. & Mason, C. A. L-Dopa and the albino riddle: content of L-Dopa in the developing retina of pigmented and albino mice. *PLoS One* **8**, e57184 (2013). <https://doi.org/10.1371/journal.pone.0057184>
- 320 Kubrusly, R. C. *et al.* L-DOPA supply to the neuro retina activates dopaminergic communication at the early stages of embryonic development. *J Neurochem* **86**, 45-54 (2003). <https://doi.org/10.1046/j.1471-4159.2003.01813.x>
- 321 Tibber, M. S., Whitmore, A. V. & Jeffery, G. Cell division and cleavage orientation in the developing retina are regulated by L-DOPA. *J Comp Neurol* **496**, 369-381 (2006). <https://doi.org/10.1002/cne.20920>
- 322 Wilk, M. A. *et al.* Relationship between foveal cone specialization and pit morphology in albinism. *Invest Ophthalmol Vis Sci* **55**, 4186-4198 (2014). <https://doi.org/10.1167/iovs.13-13217>
- 323 Al-Araimi, M. *et al.* A new recessively inherited disorder composed of foveal hypoplasia, optic nerve decussation defects and anterior segment dysgenesis maps to chromosome 16q23.3-24.1. *Mol Vis* **19**, 2165-2172 (2013).
- 324 Kuht, H. J. *et al.* SLC38A8 mutations result in arrested retinal development with loss of cone photoreceptor specialization. *Hum Mol Genet* **29**, 2989-3002 (2020). <https://doi.org/10.1093/hmg/ddaa166>
- 325 Lauderdale, J. D., Wilensky, J. S., Oliver, E. R., Walton, D. S. & Glaser, T. 3' deletions cause aniridia by preventing PAX6 gene expression. *Proc Natl Acad Sci U S A* **97**, 13755-13759 (2000). <https://doi.org/10.1073/pnas.240398797>
- 326 Glaser, T., Walton, D. S. & Maas, R. L. Genomic structure, evolutionary conservation and aniridia mutations in the human PAX6 gene. *Nat Genet* **2**, 232-239 (1992). <https://doi.org/10.1038/ng1192-232>
- 327 Azuma, N., Nishina, S., Yanagisawa, H., Okuyama, T. & Yamada, M. PAX6 missense mutation in isolated foveal hypoplasia. *Nat Genet* **13**, 141-142 (1996). <https://doi.org/10.1038/ng0696-141>
- 328 Vincent, M. C. *et al.* Variable phenotype related to a novel PAX 6 mutation (IVS4+5G>C) in a family presenting congenital nystagmus and foveal hypoplasia. *Am J Ophthalmol* **138**, 1016-1021 (2004). <https://doi.org/10.1016/j.ajo.2004.08.003>

- 329 Shaham, O., Menuchin, Y., Farhy, C. & Ashery-Padan, R. Pax6: a multi-level regulator of ocular development. *Prog Retin Eye Res* **31**, 351-376 (2012). <https://doi.org/10.1016/j.preteyeres.2012.04.002>
- 330 Hingorani, M., Williamson, K. A., Moore, A. T. & van Heyningen, V. Detailed ophthalmologic evaluation of 43 individuals with PAX6 mutations. *Invest Ophthalmol Vis Sci* **50**, 2581-2590 (2009). <https://doi.org/10.1167/iovs.08-2827>
- 331 Sannan, N. S. *et al.* Correlation of novel PAX6 gene abnormalities in aniridia and clinical presentation. *Can J Ophthalmol* **52**, 570-577 (2017). <https://doi.org/10.1016/j.cjco.2017.04.006>
- 332 Azuma, N. *et al.* The Pax6 isoform bearing an alternative spliced exon promotes the development of the neural retinal structure. *Hum Mol Genet* **14**, 735-745 (2005). <https://doi.org/10.1093/hmg/ddi069>
- 333 Dowling, J. E. The retina: an approachable part of the brain. *Harvard University Press* (1987).
- 334 Kolb, H. in *Webvision: The Organization of the Retina and Visual System* (eds H. Kolb, E. Fernandez, & R. Nelson) (1995).
- 335 Rapaport, D. H., Wong, L. L., Wood, E. D., Yasumura, D. & LaVail, M. M. Timing and topography of cell genesis in the rat retina. *J Comp Neurol* **474**, 304-324 (2004). <https://doi.org/10.1002/cne.20134>
- 336 Viets, K., Eldred, K. & Johnston, R. J., Jr. Mechanisms of Photoreceptor Patterning in Vertebrates and Invertebrates. *Trends Genet* **32**, 638-659 (2016). <https://doi.org/10.1016/j.tig.2016.07.004>
- 337 Kolb, H., Nelson, R. F., Ahnelt, P. K., Ortuno-Lizaran, I. & Cuenca, N. in *Webvision: The Organization of the Retina and Visual System* (eds H. Kolb, E. Fernandez, & R. Nelson) (1995).
- 338 Gariano, R. F., Provis, J. M. & Hendrickson, A. E. Development of the foveal avascular zone. *Ophthalmology* **107**, 1026 (2000). [https://doi.org/10.1016/s0161-6420\(00\)00050-6](https://doi.org/10.1016/s0161-6420(00)00050-6)
- 339 Sannan, N. S., Shan, X., Gregory-Evans, K., Kusumi, K. & Gregory-Evans, C. Y. *Anolis carolinensis* as a model to understand the molecular and cellular basis of foveal development. *Exp Eye Res* **173**, 138-147 (2018). <https://doi.org/10.1016/j.exer.2018.05.012>
- 340 Rasys, A. M. *et al.* Ocular elongation and retraction in foveated reptiles. *Dev Dyn* **250**, 1584-1599 (2021). <https://doi.org/10.1002/dvdy.348>
- 341 Roll, B. Retina of Bouton's skink (Reptilia, Scincidae): visual cells, fovea, and ecological constraints. *J Comp Neurol* **436**, 487-496 (2001). <https://doi.org/10.1002/cne.1082>
- 342 Picaud, S. *et al.* The primate model for understanding and restoring vision. *Proc Natl Acad Sci U S A* **116**, 26280-26287 (2019). <https://doi.org/10.1073/pnas.1902292116>
- 343 Tarantal, A. F. Ultrasound Imaging in Rhesus (*Macaca mulatta*) and Long-Tailed (*Macaca fascicularis*) Macaques. . *The Laboratory Primate Ch. 20. City (Cambridge): Elsevier Academic Press*, 315-317 (2005).

- 344 Tarantal, A. F. in *Laboratory Primate Ch. 20* (ed Wolfe-Coote S.) 315-317
(Elsevier Academic Press, 2005).
- 345 Buenaventura, D. F., Corseri, A. & Emerson, M. M. Identification of Genes With
Enriched Expression in Early Developing Mouse Cone Photoreceptors. *Invest*
Ophthalmol Vis Sci **60**, 2787-2799 (2019). <https://doi.org/10.1167/iovs.19-26951>
- 346 Vazquez-Chona, F. R., Clark, A. M. & Levine, E. M. Rlbp1 promoter drives robust
Muller glial GFP expression in transgenic mice. *Invest Ophthalmol Vis Sci* **50**,
3996-4003 (2009). <https://doi.org/10.1167/iovs.08-3189>
- 347 Amamoto, R. *et al.* Probe-Seq enables transcriptional profiling of specific cell
types from heterogeneous tissue by RNA-based isolation. *Elife* **8** (2019).
<https://doi.org/10.7554/eLife.51452>
- 348 Yamagata, M., Yan, W. & Sanes, J. R. A cell atlas of the chick retina based on
single-cell transcriptomics. *Elife* **10** (2021). <https://doi.org/10.7554/eLife.63907>
- 349 Lee, D. A. *et al.* Genetic and neuronal regulation of sleep by neuropeptide VF.
Elife **6** (2017). <https://doi.org/10.7554/eLife.25727>
- 350 Yi, W. *et al.* A single-cell transcriptome atlas of the aging human and macaque
retina. *Natl Sci Rev* **8**, nwa179 (2021). <https://doi.org/10.1093/nsr/nwaa179>
- 351 Okada, M., Erickson, A. & Hendrickson, A. Light and electron microscopic
analysis of synaptic development in Macaca monkey retina as detected by
immunocytochemical labeling for the synaptic vesicle protein, SV2. *J Comp*
Neurol **339**, 535-558 (1994). <https://doi.org/10.1002/cne.903390406>
- 352 Cornish, E. E. *et al.* Gradients of cone differentiation and FGF expression during
development of the foveal depression in macaque retina. *Vis Neurosci* **22**, 447-
459 (2005). <https://doi.org/10.1017/S0952523805224069>
- 353 Wikler, K. C. & Rakic, P. Relation of an array of early-differentiating cones to the
photoreceptor mosaic in the primate retina. *Nature* **351**, 397-400 (1991).
<https://doi.org/10.1038/351397a0>
- 354 Finkbeiner, C. *et al.* Single-cell ATAC-seq of fetal human retina and stem-cell-
derived retinal organoids shows changing chromatin landscapes during cell fate
acquisition. *Cell Rep* **38**, 110294 (2022).
<https://doi.org/10.1016/j.celrep.2021.110294>
- 355 Thomas, E. D. *et al.* Cell-specific cis-regulatory elements and mechanisms of
non-coding genetic disease in human retina and retinal organoids. *Dev Cell* **57**,
820-836 e826 (2022). <https://doi.org/10.1016/j.devcel.2022.02.018>
- 356 Bringmann, A. *et al.* The primate fovea: Structure, function and development.
Prog Retin Eye Res **66**, 49-84 (2018).
<https://doi.org/10.1016/j.preteyeres.2018.03.006>
- 357 Rakic, P. & Riley, K. P. Overproduction and elimination of retinal axons in the
fetal rhesus monkey. *Science* **219**, 1441-1444 (1983).
<https://doi.org/10.1126/science.6828871>
- 358 Marsh-Armstrong, N., McCaffery, P., Gilbert, W., Dowling, J. E. & Drager, U. C.
Retinoic acid is necessary for development of the ventral retina in zebrafish. *Proc*
Natl Acad Sci U S A **91**, 7286-7290 (1994).
<https://doi.org/10.1073/pnas.91.15.7286>

- 359 Yamada, E. Some structural features of the fovea centralis in the human retina. *Arch Ophthalmol* **82**, 151-159 (1969).
<https://doi.org/10.1001/archophth.1969.00990020153002>
- 360 Gass, J. D. Muller cell cone, an overlooked part of the anatomy of the fovea centralis: hypotheses concerning its role in the pathogenesis of macular hole and foveomacular retinoschisis. *Arch Ophthalmol* **117**, 821-823 (1999).
<https://doi.org/10.1001/archophth.117.6.821>
- 361 Delaunay, K. *et al.* Glial cells of the human fovea. *Mol Vis* **26**, 235-245 (2020).
- 362 Voigt, A. P. *et al.* Molecular characterization of foveal versus peripheral human retina by single-cell RNA sequencing. *Exp Eye Res* **184**, 234-242 (2019).
<https://doi.org/10.1016/j.exer.2019.05.001>
- 363 Szel, A., Rohlich, P., Caffè, A. R. & van Veen, T. Distribution of cone photoreceptors in the mammalian retina. *Microsc Res Tech* **35**, 445-462 (1996).
[https://doi.org/10.1002/\(SICI\)1097-0029\(19961215\)35:6<445::AID-JEMT4>3.0.CO;2-H](https://doi.org/10.1002/(SICI)1097-0029(19961215)35:6<445::AID-JEMT4>3.0.CO;2-H)
- 364 Bruhn, S. L. & Cepko, C. L. Development of the pattern of photoreceptors in the chick retina. *J Neurosci* **16**, 1430-1439 (1996).
- 365 Fadool, J. M. Development of a rod photoreceptor mosaic revealed in transgenic zebrafish. *Dev Biol* **258**, 277-290 (2003). [https://doi.org/10.1016/s0012-1606\(03\)00125-8](https://doi.org/10.1016/s0012-1606(03)00125-8)
- 366 Raymond, P. A., Barthel, L. K. & Curran, G. A. Developmental patterning of rod and cone photoreceptors in embryonic zebrafish. *J Comp Neurol* **359**, 537-550 (1995). <https://doi.org/10.1002/cne.903590403>
- 367 Carter-Dawson, L. D. & LaVail, M. M. Rods and cones in the mouse retina. I. Structural analysis using light and electron microscopy. *J Comp Neurol* **188**, 245-262 (1979). <https://doi.org/10.1002/cne.901880204>
- 368 Bumsted O'Brien, K. M. *et al.* Expression of photoreceptor-specific nuclear receptor NR2E3 in rod photoreceptors of fetal human retina. *Invest Ophthalmol Vis Sci* **45**, 2807-2812 (2004). <https://doi.org/10.1167/iovs.03-1317>
- 369 Springer, A. D. & Hendrickson, A. E. Development of the primate area of high acuity, 3: temporal relationships between pit formation, retinal elongation and cone packing. *Vis Neurosci* **22**, 171-185 (2005).
<https://doi.org/10.1017/S095252380522206X>
- 370 Provis, J. M., Dubis, A. M., Maddess, T. & Carroll, J. Adaptation of the central retina for high acuity vision: cones, the fovea and the avascular zone. *Prog Retin Eye Res* **35**, 63-81 (2013). <https://doi.org/10.1016/j.preteyeres.2013.01.005>
- 371 Dubis, A. M. *et al.* Evaluation of normal human foveal development using optical coherence tomography and histologic examination. *Arch Ophthalmol* **130**, 1291-1300 (2012). <https://doi.org/10.1001/archophthalmol.2012.2270>
- 372 Wong, W. L. *et al.* Global prevalence of age-related macular degeneration and disease burden projection for 2020 and 2040: a systematic review and meta-analysis. *Lancet Glob Health* **2**, e106-116 (2014). [https://doi.org/10.1016/S2214-109X\(13\)70145-1](https://doi.org/10.1016/S2214-109X(13)70145-1)

- 373 Friedman, D. S. *et al.* Prevalence of age-related macular degeneration in the United States. *Arch Ophthalmol* **122**, 564-572 (2004).
<https://doi.org/10.1001/archophth.122.4.564>
- 374 Sidman, R. L. *Histogenesis of mouse retina studied with thymidine-H3*. (Academic Press, New York (NY), 1961).
- 375 Watanabe, T. & Raff, M. C. Rod photoreceptor development in vitro: intrinsic properties of proliferating neuroepithelial cells change as development proceeds in the rat retina. *Neuron* **4**, 461-467 (1990). [https://doi.org/10.1016/0896-6273\(90\)90058-n](https://doi.org/10.1016/0896-6273(90)90058-n)
- 376 Clark, B. S. *et al.* Single-Cell RNA-Seq Analysis of Retinal Development Identifies NFI Factors as Regulating Mitotic Exit and Late-Born Cell Specification. *Neuron* **102**, 1111-1126.e1115 (2019).
<https://doi.org/10.1016/j.neuron.2019.04.010>
- 377 Baek, D. *et al.* The impact of microRNAs on protein output. *Nature* **455**, 64-71 (2008). <https://doi.org/10.1038/nature07242>
- 378 Selbach, M. *et al.* Widespread changes in protein synthesis induced by microRNAs. *Nature* **455**, 58-63 (2008). <https://doi.org/10.1038/nature07228>
- 379 Saurat, N., Andersson, T., Vasistha, N. A., Molnar, Z. & Livesey, F. J. Dicer is required for neural stem cell multipotency and lineage progression during cerebral cortex development. *Neural Dev* **8**, 14 (2013).
<https://doi.org/10.1186/1749-8104-8-14>
- 380 Wohl, S. G., Hooper, M. J. & Reh, T. A. MicroRNAs miR-25, let-7 and miR-124 regulate the neurogenic potential of Muller glia in mice. *Development* **146** (2019).
<https://doi.org/10.1242/dev.179556>
- 381 Patterson, M. *et al.* let-7 miRNAs can act through notch to regulate human gliogenesis. *Stem Cell Reports* **3**, 758-773 (2014).
<https://doi.org/10.1016/j.stemcr.2014.08.015>
- 382 Andersson, T. *et al.* Reversible block of mouse neural stem cell differentiation in the absence of dicer and microRNAs. *PLoS One* **5**, e13453 (2010).
<https://doi.org/10.1371/journal.pone.0013453>
- 383 Nowakowski, T. J. *et al.* MicroRNA-92b regulates the development of intermediate cortical progenitors in embryonic mouse brain. *Proc Natl Acad Sci U S A* **110**, 7056-7061 (2013). <https://doi.org/10.1073/pnas.1219385110>
- 384 Bian, S. *et al.* MicroRNA cluster miR-17-92 regulates neural stem cell expansion and transition to intermediate progenitors in the developing mouse neocortex. *Cell Rep* **3**, 1398-1406 (2013). <https://doi.org/10.1016/j.celrep.2013.03.037>
- 385 Wohl, S. G. & Reh, T. A. miR-124-9-9* potentiates Ascl1-induced reprogramming of cultured Muller glia. *Glia* **64**, 743-762 (2016).
<https://doi.org/10.1002/glia.22958>
- 386 Louvi, A. & Artavanis-Tsakonas, S. Notch signalling in vertebrate neural development. *Nat Rev Neurosci* **7**, 93-102 (2006).
<https://doi.org/10.1038/nrn1847>

- 387 Perron, M. & Harris, W. A. Determination of vertebrate retinal progenitor cell fate by the Notch pathway and basic helix-loop-helix transcription factors. *Cell Mol Life Sci* **57**, 215-223 (2000). <https://doi.org/10.1007/PL00000685>
- 388 Maurer, K. A., Riesenberger, A. N. & Brown, N. L. Notch signaling differentially regulates Atoh7 and Neurog2 in the distal mouse retina. *Development* **141**, 3243-3254 (2014). <https://doi.org/10.1242/dev.106245>
- 389 Pan, L., Deng, M., Xie, X. & Gan, L. ISL1 and BRN3B co-regulate the differentiation of murine retinal ganglion cells. *Development* **135**, 1981-1990 (2008). <https://doi.org/10.1242/dev.010751>
- 390 Mu, X., Fu, X., Beremand, P. D., Thomas, T. L. & Klein, W. H. Gene regulation logic in retinal ganglion cell development: Isl1 defines a critical branch distinct from but overlapping with Pou4f2. *Proc Natl Acad Sci U S A* **105**, 6942-6947 (2008). <https://doi.org/10.1073/pnas.0802627105>
- 391 Jiang, Y. *et al.* Transcription factors SOX4 and SOX11 function redundantly to regulate the development of mouse retinal ganglion cells. *J Biol Chem* **288**, 18429-18438 (2013). <https://doi.org/10.1074/jbc.M113.478503>
- 392 Fotaki, V., Smith, R., Pratt, T. & Price, D. J. Foxg1 is required to limit the formation of ciliary margin tissue and Wnt/beta-catenin signalling in the developing nasal retina of the mouse. *Dev Biol* **380**, 299-313 (2013). <https://doi.org/10.1016/j.ydbio.2013.04.017>
- 393 Smith, R. *et al.* The Transcription Factor Foxg1 Promotes Optic Fissure Closure in the Mouse by Suppressing Wnt8b in the Nasal Optic Stalk. *J Neurosci* **37**, 7975-7993 (2017). <https://doi.org/10.1523/JNEUROSCI.0286-17.2017>
- 394 Zhao, X. F., Suh, C. S., Prat, C. R., Ellingsen, S. & Fjose, A. Distinct expression of two foxg1 paralogues in zebrafish. *Gene Expr Patterns* **9**, 266-272 (2009). <https://doi.org/10.1016/j.gep.2009.04.001>
- 395 Shintani, T. *et al.* Large-scale identification and characterization of genes with asymmetric expression patterns in the developing chick retina. *J Neurobiol* **59**, 34-47 (2004). <https://doi.org/10.1002/neu.10338>
- 396 da Silva, S. & Cepko, C. L. Fgf8 Expression and Degradation of Retinoic Acid Are Required for Patterning a High-Acuity Area in the Retina. *Dev Cell* **42**, 68-81.e66 (2017). <https://doi.org/10.1016/j.devcel.2017.05.024>
- 397 Xiang, L. *et al.* miR-183/96 plays a pivotal regulatory role in mouse photoreceptor maturation and maintenance. *Proc Natl Acad Sci U S A* **114**, 6376-6381 (2017). <https://doi.org/10.1073/pnas.1618757114>
- 398 Sass, S. *et al.* MicroRNAs coordinately regulate protein complexes. *BMC Syst Biol* **5**, 136 (2011). <https://doi.org/10.1186/1752-0509-5-136>
- 399 Licursi, V., Conte, F., Fisco, G. & Paci, P. MIENTURNET: an interactive web tool for microRNA-target enrichment and network-based analysis. *BMC Bioinformatics* **20**, 545 (2019). <https://doi.org/10.1186/s12859-019-3105-x>
- 400 Wu, Y., Wei, B., Liu, H., Li, T. & Rayner, S. MiRPara: a SVM-based software tool for prediction of most probable microRNA coding regions in genome scale sequences. *BMC Bioinformatics* **12**, 107 (2011). <https://doi.org/10.1186/1471-2105-12-107>

- 401 Hendrickson, A. *et al.* Rod photoreceptor differentiation in fetal and infant human retina. *Exp Eye Res* **87**, 415-426 (2008).
<https://doi.org/10.1016/j.exer.2008.07.016>
- 402 Cornish, E. E., Hendrickson, A. E. & Provis, J. M. Distribution of short-wavelength-sensitive cones in human fetal and postnatal retina: early development of spatial order and density profiles. *Vision Res* **44**, 2019-2026 (2004). <https://doi.org/10.1016/j.visres.2004.03.030>
- 403 Cornish, E. E., Xiao, M., Yang, Z., Provis, J. M. & Hendrickson, A. E. The role of opsin expression and apoptosis in determination of cone types in human retina. *Exp Eye Res* **78**, 1143-1154 (2004). <https://doi.org/10.1016/j.exer.2004.01.004>
- 404 Ledford, H. US scientist fear new restrictions on fetal-tissue research. *Nature* (2017).
- 405 Picaud, S. *et al.* The primate model for understanding and restoring vision. *Proc Natl Acad Sci U S A* (2019). <https://doi.org/10.1073/pnas.1902292116>
- 406 Roska, B. & Sahel, J. A. Restoring vision. *Nature* **557**, 359-367 (2018).
<https://doi.org/10.1038/s41586-018-0076-4>
- 407 Francis, P. J. *et al.* Rhesus monkeys and humans share common susceptibility genes for age-related macular disease. *Hum Mol Genet* **17**, 2673-2680 (2008).
<https://doi.org/10.1093/hmg/ddn167>
- 408 Pahl, L. *et al.* Characterization of the 10q26-orthologue in rhesus monkeys corroborates a functional connection between ARMS2 and HTRA1. *Exp Eye Res* **98**, 75-78 (2012). <https://doi.org/10.1016/j.exer.2012.03.007>
- 409 Yiu, G. *et al.* In Vivo Multimodal Imaging of Drusenoid Lesions in Rhesus Macaques. *Sci Rep* **7**, 15013 (2017). <https://doi.org/10.1038/s41598-017-14715-z>
- 410 Moshiri, A. *et al.* A nonhuman primate model of inherited retinal disease. *J Clin Invest* **129**, 863-874 (2019). <https://doi.org/10.1172/JCI123980>
- 411 Finlay, B. L. & Darlington, R. B. Linked regularities in the development and evolution of mammalian brains. *Science* **268**, 1578-1584 (1995).
<https://doi.org/10.1126/science.7777856>
- 412 Clancy, B., Darlington, R. B. & Finlay, B. L. Translating developmental time across mammalian species. *Neuroscience* **105**, 7-17 (2001).
[https://doi.org/10.1016/s0306-4522\(01\)00171-3](https://doi.org/10.1016/s0306-4522(01)00171-3)
- 413 Workman, A. D., Charvet, C. J., Clancy, B., Darlington, R. B. & Finlay, B. L. Modeling transformations of neurodevelopmental sequences across mammalian species. *J Neurosci* **33**, 7368-7383 (2013).
<https://doi.org/10.1523/JNEUROSCI.5746-12.2013>
- 414 Hendrickson, A. & Zhang, C. Development of cone photoreceptors and their synapses in the human and monkey fovea. *J Comp Neurol* **527**, 38-51 (2019).
<https://doi.org/10.1002/cne.24170>
- 415 Busskamp, V. *et al.* miRNAs 182 and 183 are necessary to maintain adult cone photoreceptor outer segments and visual function. *Neuron* **83**, 586-600 (2014).
<https://doi.org/10.1016/j.neuron.2014.06.020>

- 416 Zuzic, M., Rojo Arias, J. E., Wohl, S. G. & Busskamp, V. Retinal miRNA Functions in Health and Disease. *Genes (Basel)* **10** (2019).
<https://doi.org/10.3390/genes10050377>
- 417 Cimmino, A. *et al.* miR-15 and miR-16 induce apoptosis by targeting BCL2. *Proc Natl Acad Sci U S A* **102**, 13944-13949 (2005).
<https://doi.org/10.1073/pnas.0506654102>
- 418 Gao, F. *et al.* miR-342-5p Regulates Neural Stem Cell Proliferation and Differentiation Downstream to Notch Signaling in Mice. *Stem Cell Reports* **8**, 1032-1045 (2017). <https://doi.org/10.1016/j.stemcr.2017.02.017>
- 419 Fairchild, C. L. *et al.* RBX2 maintains final retinal cell position in a DAB1-dependent and -independent fashion. *Development* **145** (2018).
<https://doi.org/10.1242/dev.155283>
- 420 Fairchild, C. L. *et al.* RBX2 maintains final retinal cell position in a DAB1-dependent and -independent fashion. *Development* **145** (2018).
<https://doi.org/10.1242/dev.155283>
- 421 Leger, H., Santana, E., Beltran, W. A. & Luca, F. C. Preparation of Mouse Retinal Cryo-sections for Immunohistochemistry. *J Vis Exp* (2019).
<https://doi.org/10.3791/59683>
- 422 Fischer, A. H., Jacobson, K. A., Rose, J. & Zeller, R. Hematoxylin and eosin staining of tissue and cell sections. *CSH Protoc* **2008**, pdb prot4986 (2008).
<https://doi.org/10.1101/pdb.prot4986>
- 423 Kapranov, P. *et al.* Large-scale transcriptional activity in chromosomes 21 and 22. *Science* **296**, 916-919 (2002). <https://doi.org/10.1126/science.1068597>
- 424 Carninci, P. *et al.* The transcriptional landscape of the mammalian genome. *Science* **309**, 1559-1563 (2005). <https://doi.org/10.1126/science.1112014>
- 425 Mattick, J. S. & Makunin, I. V. Non-coding RNA. *Hum Mol Genet* **15 Spec No 1**, R17-29 (2006). <https://doi.org/10.1093/hmg/ddl046>
- 426 Birney, E. *et al.* Identification and analysis of functional elements in 1% of the human genome by the ENCODE pilot project. *Nature* **447**, 799-816 (2007).
<https://doi.org/10.1038/nature05874>
- 427 Hangauer, M. J., Vaughn, I. W. & McManus, M. T. Pervasive transcription of the human genome produces thousands of previously unidentified long intergenic noncoding RNAs. *PLoS Genet* **9**, e1003569 (2013).
<https://doi.org/10.1371/journal.pgen.1003569>
- 428 Mercer, T. R. & Mattick, J. S. Understanding the regulatory and transcriptional complexity of the genome through structure. *Genome Res* **23**, 1081-1088 (2013).
<https://doi.org/10.1101/gr.156612.113>
- 429 Bushati, N. & Cohen, S. M. microRNA functions. *Annu Rev Cell Dev Biol* **23**, 175-205 (2007). <https://doi.org/10.1146/annurev.cellbio.23.090506.123406>
- 430 Bartel, D. P. MicroRNAs: target recognition and regulatory functions. *Cell* **136**, 215-233 (2009). <https://doi.org/10.1016/j.cell.2009.01.002>
- 431 Chekulaeva, M. & Filipowicz, W. Mechanisms of miRNA-mediated post-transcriptional regulation in animal cells. *Curr Opin Cell Biol* **21**, 452-460 (2009).
<https://doi.org/10.1016/j.ceb.2009.04.009>

- 432 Lee, R. C., Feinbaum, R. L. & Ambros, V. The *C. elegans* heterochronic gene *lin-4* encodes small RNAs with antisense complementarity to *lin-14*. *Cell* **75**, 843-854 (1993).
- 433 Dexheimer, P. J. & Cochella, L. MicroRNAs: From Mechanism to Organism. *Front Cell Dev Biol* **8**, 409 (2020). <https://doi.org/10.3389/fcell.2020.00409>
- 434 Kozomara, A. & Griffiths-Jones, S. miRBase: integrating microRNA annotation and deep-sequencing data. *Nucleic Acids Res* **39**, D152-157 (2011). <https://doi.org/10.1093/nar/gkq1027>
- 435 Xu, S., Witmer, P. D., Lumayag, S., Kovacs, B. & Valle, D. MicroRNA (miRNA) transcriptome of mouse retina and identification of a sensory organ-specific miRNA cluster. *J Biol Chem* **282**, 25053-25066 (2007). <https://doi.org/10.1074/jbc.M700501200>
- 436 Loscher, C. J. *et al.* Altered retinal microRNA expression profile in a mouse model of retinitis pigmentosa. *Genome Biol* **8**, R248 (2007). <https://doi.org/10.1186/gb-2007-8-11-r248>
- 437 Bak, M. *et al.* MicroRNA expression in the adult mouse central nervous system. *RNA* **14**, 432-444 (2008). <https://doi.org/10.1261/rna.783108>
- 438 Hackler, L., Jr., Wan, J., Swaroop, A., Qian, J. & Zack, D. J. MicroRNA profile of the developing mouse retina. *Invest Ophthalmol Vis Sci* **51**, 1823-1831 (2010). <https://doi.org/10.1167/iovs.09-4657>
- 439 Karali, M. *et al.* miRNeye: a microRNA expression atlas of the mouse eye. *BMC Genomics* **11**, 715 (2010). <https://doi.org/10.1186/1471-2164-11-715>
- 440 Karali, M. *et al.* High-resolution analysis of the human retina miRNome reveals isomiR variations and novel microRNAs. *Nucleic Acids Res* **44**, 1525-1540 (2016). <https://doi.org/10.1093/nar/gkw039>
- 441 Lewis, B. P., Shih, I. H., Jones-Rhoades, M. W., Bartel, D. P. & Burge, C. B. Prediction of mammalian microRNA targets. *Cell* **115**, 787-798 (2003). [https://doi.org/10.1016/s0092-8674\(03\)01018-3](https://doi.org/10.1016/s0092-8674(03)01018-3)
- 442 Ohana, R. *et al.* MicroRNAs are essential for differentiation of the retinal pigmented epithelium and maturation of adjacent photoreceptors. *Development* **142**, 2487-2498 (2015). <https://doi.org/10.1242/dev.121533>
- 443 Wohl, S. G. & Reh, T. A. The microRNA expression profile of mouse Muller glia in vivo and in vitro. *Sci Rep* **6**, 35423 (2016). <https://doi.org/10.1038/srep35423>
- 444 Decembrini, S., Andreazzoli, M., Barsacchi, G. & Cremisi, F. Dicer inactivation causes heterochronic retinogenesis in *Xenopus laevis*. *Int J Dev Biol* **52**, 1099-1103 (2008). <https://doi.org/10.1387/ijdb.082646sd>
- 445 Pinter, R. & Hindges, R. Perturbations of microRNA function in mouse dicer mutants produce retinal defects and lead to aberrant axon pathfinding at the optic chiasm. *PLoS One* **5**, e10021 (2010). <https://doi.org/10.1371/journal.pone.0010021>
- 446 Iida, A., Shinoue, T., Baba, Y., Mano, H. & Watanabe, S. Dicer plays essential roles for retinal development by regulation of survival and differentiation. *Invest Ophthalmol Vis Sci* **52**, 3008-3017 (2011). <https://doi.org/10.1167/iovs.10-6428>

- 447 Davis, N., Mor, E. & Ashery-Padan, R. Roles for Dicer1 in the patterning and differentiation of the optic cup neuroepithelium. *Development* **138**, 127-138 (2011). <https://doi.org/10.1242/dev.053637>
- 448 Sundermeier, T. R. *et al.* MicroRNA-processing Enzymes Are Essential for Survival and Function of Mature Retinal Pigmented Epithelial Cells in Mice. *J Biol Chem* **292**, 3366-3378 (2017). <https://doi.org/10.1074/jbc.M116.770024>
- 449 Barbato, S. *et al.* MiR-211 is essential for adult cone photoreceptor maintenance and visual function. *Sci Rep* **7**, 17004 (2017). <https://doi.org/10.1038/s41598-017-17331-z>
- 450 Decembrini, S. *et al.* MicroRNAs couple cell fate and developmental timing in retina. *Proc Natl Acad Sci U S A* **106**, 21179-21184 (2009). <https://doi.org/10.1073/pnas.0909167106>
- 451 Taylor, S. M., Giuffre, E., Moseley, P. & Hitchcock, P. F. The MicroRNA, miR-18a, Regulates NeuroD and Photoreceptor Differentiation in the Retina of Zebrafish. *Dev Neurobiol* **79**, 202-219 (2019). <https://doi.org/10.1002/dneu.22666>
- 452 Borenstein, E. & Ruppin, E. Direct evolution of genetic robustness in microRNA. *Proc Natl Acad Sci U S A* **103**, 6593-6598 (2006). <https://doi.org/10.1073/pnas.0510600103>
- 453 Sangoram, A. M. *et al.* Mammalian circadian autoregulatory loop: a timeless ortholog and mPer1 interact and negatively regulate CLOCK-BMAL1-induced transcription. *Neuron* **21**, 1101-1113 (1998). [https://doi.org/10.1016/s0896-6273\(00\)80627-3](https://doi.org/10.1016/s0896-6273(00)80627-3)
- 454 Zylka, M. J. *et al.* Molecular analysis of mammalian timeless. *Neuron* **21**, 1115-1122 (1998). [https://doi.org/10.1016/s0896-6273\(00\)80628-5](https://doi.org/10.1016/s0896-6273(00)80628-5)
- 455 Lowrey, P. L. & Takahashi, J. S. Mammalian circadian biology: elucidating genome-wide levels of temporal organization. *Annu Rev Genomics Hum Genet* **5**, 407-441 (2004). <https://doi.org/10.1146/annurev.genom.5.061903.175925>
- 456 Besharse, J. C. & Iuvone, P. M. Circadian clock in *Xenopus* eye controlling retinal serotonin N-acetyltransferase. *Nature* **305**, 133-135 (1983). <https://doi.org/10.1038/305133a0>
- 457 Tosini, G., Pozdeyev, N., Sakamoto, K. & Iuvone, P. M. The circadian clock system in the mammalian retina. *Bioessays* **30**, 624-633 (2008). <https://doi.org/10.1002/bies.20777>
- 458 LaVail, M. M. & Ward, P. A. Studies on the hormonal control of circadian outer segment disc shedding in the rat retina. *Invest Ophthalmol Vis Sci* **17**, 1189-1183 (1978).
- 459 Doyle, S. E., Grace, M. S., McIvor, W. & Menaker, M. Circadian rhythms of dopamine in mouse retina: the role of melatonin. *Vis Neurosci* **19**, 593-601 (2002). <https://doi.org/10.1017/s0952523802195058>
- 460 Storch, K. F. *et al.* Intrinsic circadian clock of the mammalian retina: importance for retinal processing of visual information. *Cell* **130**, 730-741 (2007). <https://doi.org/10.1016/j.cell.2007.06.045>

- 461 Maeda, A. *et al.* Circadian intraocular pressure rhythm is generated by clock genes. *Invest Ophthalmol Vis Sci* **47**, 4050-4052 (2006). <https://doi.org/10.1167/iovs.06-0183>
- 462 Ko, G. Y. Circadian regulation in the retina: From molecules to network. *Eur J Neurosci* **51**, 194-216 (2020). <https://doi.org/10.1111/ejn.14185>
- 463 Wuarin, J. *et al.* The role of the transcriptional activator protein DBP in circadian liver gene expression. *J Cell Sci Suppl* **16**, 123-127 (1992). https://doi.org/10.1242/jcs.1992.supplement_16.15
- 464 Mauvoisin, D. *et al.* Circadian clock-dependent and -independent rhythmic proteomes implement distinct diurnal functions in mouse liver. *Proc Natl Acad Sci U S A* **111**, 167-172 (2014). <https://doi.org/10.1073/pnas.1314066111>
- 465 Cheng, H. Y. *et al.* microRNA modulation of circadian-clock period and entrainment. *Neuron* **54**, 813-829 (2007). <https://doi.org/10.1016/j.neuron.2007.05.017>
- 466 Yan, Y. *et al.* Dicer expression exhibits a tissue-specific diurnal pattern that is lost during aging and in diabetes. *PLoS One* **8**, e80029 (2013). <https://doi.org/10.1371/journal.pone.0080029>
- 467 Xu, S., Witmer, P. D., Lumayag, S., Kovacs, B. & Valle, D. MicroRNA (miRNA) transcriptome of mouse retina and identification of a sensory organ-specific miRNA cluster. *J Biol Chem* **282**, 25053-25066 (2007). <https://doi.org/10.1074/jbc.M700501200>
- 468 Yang, M., Lee, J. E., Padgett, R. W. & Edery, I. Circadian regulation of a limited set of conserved microRNAs in *Drosophila*. *BMC Genomics* **9**, 83 (2008). <https://doi.org/10.1186/1471-2164-9-83>
- 469 Krol, J. *et al.* Characterizing light-regulated retinal microRNAs reveals rapid turnover as a common property of neuronal microRNAs. *Cell* **141**, 618-631 (2010). <https://doi.org/10.1016/j.cell.2010.03.039>
- 470 Lagos-Quintana, M. *et al.* Identification of tissue-specific microRNAs from mouse. *Curr Biol* **12**, 735-739 (2002). [https://doi.org/10.1016/s0960-9822\(02\)00809-6](https://doi.org/10.1016/s0960-9822(02)00809-6)
- 471 Weston, M. D., Pierce, M. L., Rocha-Sanchez, S., Beisel, K. W. & Soukup, G. A. MicroRNA gene expression in the mouse inner ear. *Brain Res* **1111**, 95-104 (2006). <https://doi.org/10.1016/j.brainres.2006.07.006>
- 472 Loscher, C. J. *et al.* Altered retinal microRNA expression profile in a mouse model of retinitis pigmentosa. *Genome Biol* **8**, R248 (2007). <https://doi.org/10.1186/gb-2007-8-11-r248>
- 473 Peskova, L. *et al.* miR-183/96/182 cluster is an important morphogenetic factor targeting PAX6 expression in differentiating human retinal organoids. *Stem Cells* (2020). <https://doi.org/10.1002/stem.3272>
- 474 Davis, E. S. *et al.* The rax homeobox gene is mutated in the eyeless axolotl, *Ambystoma mexicanum*. *Dev Dyn* **250**, 807-821 (2021). <https://doi.org/10.1002/dvdy.246>
- 475 Glaser, T. *et al.* PAX6 gene dosage effect in a family with congenital cataracts, aniridia, anophthalmia and central nervous system defects. *Nat Genet* **7**, 463-471 (1994). <https://doi.org/10.1038/ng0894-463>

- 476 Saus, E. *et al.* Genetic variants and abnormal processing of pre-miR-182, a circadian clock modulator, in major depression patients with late insomnia. *Hum Mol Genet* **19**, 4017-4025 (2010). <https://doi.org/10.1093/hmg/ddq316>
- 477 Bhattacharyya, S. N., Habermacher, R., Martine, U., Closs, E. I. & Filipowicz, W. Stress-induced reversal of microRNA repression and mRNA P-body localization in human cells. *Cold Spring Harb Symp Quant Biol* **71**, 513-521 (2006). <https://doi.org/10.1101/sqb.2006.71.038>
- 478 Hwang, H. W., Wentzel, E. A. & Mendell, J. T. A hexanucleotide element directs microRNA nuclear import. *Science* **315**, 97-100 (2007). <https://doi.org/10.1126/science.1136235>
- 479 Zhou, L. *et al.* A genome-wide microRNA screen identifies the microRNA-183/96/182 cluster as a modulator of circadian rhythms. *Proc Natl Acad Sci U S A* **118** (2021). <https://doi.org/10.1073/pnas.2020454118>
- 480 Ben-Moshe, Z. *et al.* The light-induced transcriptome of the zebrafish pineal gland reveals complex regulation of the circadian clockwork by light. *Nucleic Acids Res* **42**, 3750-3767 (2014). <https://doi.org/10.1093/nar/gkt1359>
- 481 Ait-Hmyed, O. *et al.* Mice lacking Period 1 and Period 2 circadian clock genes exhibit blue cone photoreceptor defects. *Eur J Neurosci* **37**, 1048-1060 (2013). <https://doi.org/10.1111/ejn.12103>
- 482 Baba, K. *et al.* Removal of clock gene Bmal1 from the retina affects retinal development and accelerates cone photoreceptor degeneration during aging. *Proc Natl Acad Sci U S A* **115**, 13099-13104 (2018). <https://doi.org/10.1073/pnas.1808137115>
- 483 Ambros, V. microRNAs: tiny regulators with great potential. *Cell* **107**, 823-826 (2001). [https://doi.org/10.1016/s0092-8674\(01\)00616-x](https://doi.org/10.1016/s0092-8674(01)00616-x)
- 484 Lee, R. C. & Ambros, V. An extensive class of small RNAs in *Caenorhabditis elegans*. *Science* **294**, 862-864 (2001). <https://doi.org/10.1126/science.1065329>
- 485 Ambros, V. & Horvitz, H. R. Heterochronic mutants of the nematode *Caenorhabditis elegans*. *Science* **226**, 409-416 (1984). <https://doi.org/10.1126/science.6494891>
- 486 Moss, E. G., Lee, R. C. & Ambros, V. The cold shock domain protein LIN-28 controls developmental timing in *C. elegans* and is regulated by the lin-4 RNA. *Cell* **88**, 637-646 (1997). [https://doi.org/10.1016/s0092-8674\(00\)81906-6](https://doi.org/10.1016/s0092-8674(00)81906-6)
- 487 Johnson, S. M. *et al.* RAS is regulated by the let-7 microRNA family. *Cell* **120**, 635-647 (2005). <https://doi.org/10.1016/j.cell.2005.01.014>
- 488 Zhao, C. *et al.* MicroRNA let-7b regulates neural stem cell proliferation and differentiation by targeting nuclear receptor TLX signaling. *Proc Natl Acad Sci U S A* **107**, 1876-1881 (2010). <https://doi.org/10.1073/pnas.0908750107>
- 489 Sampson, V. B. *et al.* MicroRNA let-7a down-regulates MYC and reverts MYC-induced growth in Burkitt lymphoma cells. *Cancer Res* **67**, 9762-9770 (2007). <https://doi.org/10.1158/0008-5472.CAN-07-2462>
- 490 Pasquinelli, A. E. *et al.* Conservation of the sequence and temporal expression of let-7 heterochronic regulatory RNA. *Nature* **408**, 86-89 (2000). <https://doi.org/10.1038/35040556>

- 491 Reinhart, B. J. *et al.* The 21-nucleotide let-7 RNA regulates developmental timing in *Caenorhabditis elegans*. *Nature* **403**, 901-906 (2000).
<https://doi.org/10.1038/35002607>
- 492 Xia, X. & Ahmad, I. let-7 microRNA regulates neurogliogenesis in the mammalian retina through Hmga2. *Dev Biol* **410**, 70-85 (2016).
<https://doi.org/10.1016/j.ydbio.2015.12.010>
- 493 Ramachandran, R., Fausett, B. V. & Goldman, D. Ascl1a regulates Muller glia dedifferentiation and retinal regeneration through a Lin-28-dependent, let-7 microRNA signalling pathway. *Nat Cell Biol* **12**, 1101-1107 (2010).
<https://doi.org/10.1038/ncb2115>
- 494 Wu, Y. C., Chen, C. H., Mercer, A. & Sokol, N. S. Let-7-complex microRNAs regulate the temporal identity of *Drosophila* mushroom body neurons via chinmo. *Dev Cell* **23**, 202-209 (2012). <https://doi.org/10.1016/j.devcel.2012.05.013>
- 495 Arora, A., McKay, G. J. & Simpson, D. A. Prediction and verification of miRNA expression in human and rat retinas. *Invest Ophthalmol Vis Sci* **48**, 3962-3967 (2007). <https://doi.org/10.1167/iovs.06-1221>
- 496 Alexiades, M. R. & Cepko, C. Quantitative analysis of proliferation and cell cycle length during development of the rat retina. *Dev Dyn* **205**, 293-307 (1996).
[https://doi.org/10.1002/\(SICI\)1097-0177\(199603\)205:3<293::AID-AJA9>3.0.CO;2-D](https://doi.org/10.1002/(SICI)1097-0177(199603)205:3<293::AID-AJA9>3.0.CO;2-D)
- 497 Bueno, M. J. & Malumbres, M. MicroRNAs and the cell cycle. *Biochim Biophys Acta* **1812**, 592-601 (2011). <https://doi.org/10.1016/j.bbadis.2011.02.002>
- 498 Lee, Y. S. & Dutta, A. The tumor suppressor microRNA let-7 represses the HMGA2 oncogene. *Genes Dev* **21**, 1025-1030 (2007).
<https://doi.org/10.1101/gad.1540407>
- 499 Sauer, F. C. Mitosis in the neural tube. *Journal of Comparative Neurology* **62**, 377-405 (1935).
- 500 Miyata, T. Development of three-dimensional architecture of the neuroepithelium: role of pseudostratification and cellular 'community'. *Dev Growth Differ* **50 Suppl 1**, S105-112 (2008). <https://doi.org/10.1111/j.1440-169X.2007.00980.x>
- 501 Gerard, C., Lemaigre, F. & Gonze, D. Modeling the Dynamics of Let-7-Coupled Gene Regulatory Networks Linking Cell Proliferation to Malignant Transformation. *Front Physiol* **10**, 848 (2019).
<https://doi.org/10.3389/fphys.2019.00848>
- 502 Yu, Z. *et al.* Cyclin D1 induction of Dicer governs microRNA processing and expression in breast cancer. *Nat Commun* **4**, 2812 (2013).
<https://doi.org/10.1038/ncomms3812>
- 503 Liu, Q., Novak, M. K., Pepin, R. M., Eich, T. & Hu, W. microRNA-mediated regulation of microRNA machinery controls cell fate decisions. *Elife* **10** (2021).
<https://doi.org/10.7554/eLife.72289>
- 504 Dorsky, R. I., Rapaport, D. H. & Harris, W. A. Xotch inhibits cell differentiation in the *Xenopus* retina. *Neuron* **14**, 487-496 (1995). [https://doi.org/10.1016/0896-6273\(95\)90305-4](https://doi.org/10.1016/0896-6273(95)90305-4)

- 505 Jadhav, A. P., Cho, S. H. & Cepko, C. L. Notch activity permits retinal cells to progress through multiple progenitor states and acquire a stem cell property. *Proc Natl Acad Sci U S A* **103**, 18998-19003 (2006). <https://doi.org/10.1073/pnas.0608155103>
- 506 Tomita, K. *et al.* Mammalian hairy and Enhancer of split homolog 1 regulates differentiation of retinal neurons and is essential for eye morphogenesis. *Neuron* **16**, 723-734 (1996). [https://doi.org/10.1016/s0896-6273\(00\)80093-8](https://doi.org/10.1016/s0896-6273(00)80093-8)
- 507 Kaufman, M. L. *et al.* Transcriptional profiling of murine retinas undergoing semi-synchronous cone photoreceptor differentiation. *Dev Biol* **453**, 155-167 (2019). <https://doi.org/10.1016/j.ydbio.2019.05.016>
- 508 Bosze, B., Moon, M. S., Kageyama, R. & Brown, N. L. Simultaneous Requirements for Hes1 in Retinal Neurogenesis and Optic Cup-Stalk Boundary Maintenance. *J Neurosci* **40**, 1501-1513 (2020). <https://doi.org/10.1523/JNEUROSCI.2327-19.2020>
- 509 Baek, J. H., Hatakeyama, J., Sakamoto, S., Ohtsuka, T. & Kageyama, R. Persistent and high levels of Hes1 expression regulate boundary formation in the developing central nervous system. *Development* **133**, 2467-2476 (2006). <https://doi.org/10.1242/dev.02403>
- 510 Riesenberger, A. N., Liu, Z., Kopan, R. & Brown, N. L. Rbpj cell autonomous regulation of retinal ganglion cell and cone photoreceptor fates in the mouse retina. *J Neurosci* **29**, 12865-12877 (2009). <https://doi.org/10.1523/JNEUROSCI.3382-09.2009>
- 511 Chen, X. & Emerson, M. M. Notch signaling represses cone photoreceptor formation through the regulation of retinal progenitor cell states. *Sci Rep* **11**, 14525 (2021). <https://doi.org/10.1038/s41598-021-93692-w>
- 512 Furukawa, T., Mukherjee, S., Bao, Z. Z., Morrow, E. M. & Cepko, C. L. rax, Hes1, and notch1 promote the formation of Muller glia by postnatal retinal progenitor cells. *Neuron* **26**, 383-394 (2000). [https://doi.org/10.1016/s0896-6273\(00\)81171-x](https://doi.org/10.1016/s0896-6273(00)81171-x)
- 513 Bernardos, R. L., Lentz, S. I., Wolfe, M. S. & Raymond, P. A. Notch-Delta signaling is required for spatial patterning and Muller glia differentiation in the zebrafish retina. *Dev Biol* **278**, 381-395 (2005). <https://doi.org/10.1016/j.ydbio.2004.11.018>
- 514 Nelson, B. R. *et al.* Genome-wide analysis of Muller glial differentiation reveals a requirement for Notch signaling in postmitotic cells to maintain the glial fate. *PLoS One* **6**, e22817 (2011). <https://doi.org/10.1371/journal.pone.0022817>
- 515 Conner, C., Ackerman, K. M., Lahne, M., Hobgood, J. S. & Hyde, D. R. Repressing notch signaling and expressing TNFalpha are sufficient to mimic retinal regeneration by inducing Muller glial proliferation to generate committed progenitor cells. *J Neurosci* **34**, 14403-14419 (2014). <https://doi.org/10.1523/JNEUROSCI.0498-14.2014>
- 516 Sahu, A., Devi, S., Jui, J. & Goldman, D. Notch signaling via Hey1 and Id2b regulates Muller glia's regenerative response to retinal injury. *Glia* **69**, 2882-2898 (2021). <https://doi.org/10.1002/glia.24075>

- 517 Dexter, J. S. The analysis of a case of continuous variation in *Drosophila* by a study of its linkage relations. *The American Naturalist* **48**, 712-758 (1914).
- 518 Bray, S. J. Notch signalling in context. *Nat Rev Mol Cell Biol* **17**, 722-735 (2016). <https://doi.org/10.1038/nrm.2016.94>
- 519 Pierfelice, T., Alberi, L. & Gaiano, N. Notch in the vertebrate nervous system: an old dog with new tricks. *Neuron* **69**, 840-855 (2011). <https://doi.org/10.1016/j.neuron.2011.02.031>
- 520 Ohtsuka, T. *et al.* Hes1 and Hes5 as notch effectors in mammalian neuronal differentiation. *EMBO J* **18**, 2196-2207 (1999). <https://doi.org/10.1093/emboj/18.8.2196>
- 521 Dennis, D. J., Han, S. & Schuurmans, C. bHLH transcription factors in neural development, disease, and reprogramming. *Brain Res* **1705**, 48-65 (2019). <https://doi.org/10.1016/j.brainres.2018.03.013>
- 522 Taylor, S. M. *et al.* The bHLH Transcription Factor NeuroD Governs Photoreceptor Genesis and Regeneration Through Delta-Notch Signaling. *Invest Ophthalmol Vis Sci* **56**, 7496-7515 (2015). <https://doi.org/10.1167/iovs.15-17616>
- 523 Jarriault, S. *et al.* Signalling downstream of activated mammalian Notch. *Nature* **377**, 355-358 (1995). <https://doi.org/10.1038/377355a0>
- 524 Masamizu, Y. *et al.* Real-time imaging of the somite segmentation clock: revelation of unstable oscillators in the individual presomitic mesoderm cells. *Proc Natl Acad Sci U S A* **103**, 1313-1318 (2006). <https://doi.org/10.1073/pnas.0508658103>
- 525 Shimojo, H., Ohtsuka, T. & Kageyama, R. Oscillations in notch signaling regulate maintenance of neural progenitors. *Neuron* **58**, 52-64 (2008). <https://doi.org/10.1016/j.neuron.2008.02.014>
- 526 Imayoshi, I. *et al.* Oscillatory control of factors determining multipotency and fate in mouse neural progenitors. *Science* **342**, 1203-1208 (2013). <https://doi.org/10.1126/science.1242366>
- 527 Hirata, H. *et al.* Oscillatory expression of the bHLH factor Hes1 regulated by a negative feedback loop. *Science* **298**, 840-843 (2002). <https://doi.org/10.1126/science.1074560>
- 528 Shimojo, H. *et al.* Oscillatory control of Delta-like1 in cell interactions regulates dynamic gene expression and tissue morphogenesis. *Genes Dev* **30**, 102-116 (2016). <https://doi.org/10.1101/gad.270785.115>
- 529 Cepko, C. Intrinsically different retinal progenitor cells produce specific types of progeny. *Nat Rev Neurosci* **15**, 615-627 (2014). <https://doi.org/10.1038/nrn3767>
- 530 Dixit, R. *et al.* Gene expression is dynamically regulated in retinal progenitor cells prior to and during overt cellular differentiation. *Gene Expr Patterns* **14**, 42-54 (2014). <https://doi.org/10.1016/j.gep.2013.10.003>
- 531 Inui, M., Martello, G. & Piccolo, S. MicroRNA control of signal transduction. *Nat Rev Mol Cell Biol* **11**, 252-263 (2010). <https://doi.org/10.1038/nrm2868>
- 532 Roese-Koerner, B. *et al.* Reciprocal Regulation between Bifunctional miR-9/9(*) and its Transcriptional Modulator Notch in Human Neural Stem Cell Self-

- Renewal and Differentiation. *Stem Cell Reports* **7**, 207-219 (2016).
<https://doi.org/10.1016/j.stemcr.2016.06.008>
- 533 Tan, S. L., Ohtsuka, T., Gonzalez, A. & Kageyama, R. MicroRNA9 regulates neural stem cell differentiation by controlling Hes1 expression dynamics in the developing brain. *Genes Cells* **17**, 952-961 (2012).
<https://doi.org/10.1111/gtc.12009>
- 534 Roese-Koerner, B., Stappert, L. & Brustle, O. Notch/Hes signaling and miR-9 engage in complex feedback interactions controlling neural progenitor cell proliferation and differentiation. *Neurogenesis (Austin)* **4**, e1313647 (2017).
<https://doi.org/10.1080/23262133.2017.1313647>
- 535 Leucht, C. *et al.* MicroRNA-9 directs late organizer activity of the midbrain-hindbrain boundary. *Nat Neurosci* **11**, 641-648 (2008).
<https://doi.org/10.1038/nn.2115>
- 536 Bonev, B., Pisco, A. & Papalopulu, N. MicroRNA-9 reveals regional diversity of neural progenitors along the anterior-posterior axis. *Dev Cell* **20**, 19-32 (2011).
<https://doi.org/10.1016/j.devcel.2010.11.018>
- 537 Bonev, B., Stanley, P. & Papalopulu, N. MicroRNA-9 Modulates Hes1 ultradian oscillations by forming a double-negative feedback loop. *Cell Rep* **2**, 10-18 (2012). <https://doi.org/10.1016/j.celrep.2012.05.017>
- 538 Goodfellow, M., Phillips, N. E., Manning, C., Galla, T. & Papalopulu, N. microRNA input into a neural ultradian oscillator controls emergence and timing of alternative cell states. *Nat Commun* **5**, 3399 (2014).
<https://doi.org/10.1038/ncomms4399>
- 539 Wohl, S. G., Jorstad, N. L., Levine, E. M. & Reh, T. A. Muller glial microRNAs are required for the maintenance of glial homeostasis and retinal architecture. *Nat Commun* **8**, 1603 (2017). <https://doi.org/10.1038/s41467-017-01624-y>
- 540 Thomas, E. D. *et al.* Multi-omic Analysis of Developing Human Retina and Organoids Reveals Cell-Specific Cis-Regulatory Elements and Mechanisms of Non-Coding Genetic Disease Risk. *bioRxiv*, 2021.2007.2031.454254 (2021).
<https://doi.org/10.1101/2021.07.31.454254>
- 541 Hackler, L., Jr., Wan, J., Swaroop, A., Qian, J. & Zack, D. J. MicroRNA profile of the developing mouse retina. *Invest Ophthalmol Vis Sci* **51**, 1823-1831 (2010).
<https://doi.org/10.1167/iovs.09-4657>
- 542 Ramachandran, R., Zhao, X. F. & Goldman, D. Ascl1a/Dkk/beta-catenin signaling pathway is necessary and glycogen synthase kinase-3beta inhibition is sufficient for zebrafish retina regeneration. *Proc Natl Acad Sci U S A* **108**, 15858-15863 (2011). <https://doi.org/10.1073/pnas.1107220108>
- 543 Mu, G. *et al.* Correlation of overexpression of HMGA1 and HMGA2 with poor tumor differentiation, invasion, and proliferation associated with let-7 down-regulation in retinoblastomas. *Hum Pathol* **41**, 493-502 (2010).
<https://doi.org/10.1016/j.humpath.2009.08.022>
- 544 Makarev, E., Spence, J. R., Del Rio-Tsonis, K. & Tsonis, P. A. Identification of microRNAs and other small RNAs from the adult newt eye. *Mol Vis* **12**, 1386-1391 (2006).

- 545 Smit-McBride, Z. *et al.* Unique molecular signatures of microRNAs in ocular fluids and plasma in diabetic retinopathy. *PLoS One* **15**, e0235541 (2020).
<https://doi.org/10.1371/journal.pone.0235541>
- 546 Ertekin, S. *et al.* Evaluation of circulating miRNAs in wet age-related macular degeneration. *Mol Vis* **20**, 1057-1066 (2014).
- 547 Ryan, D. G., Oliveira-Fernandes, M. & Lavker, R. M. MicroRNAs of the mammalian eye display distinct and overlapping tissue specificity. *Mol Vis* **12**, 1175-1184 (2006).
- 548 Deo, M., Yu, J. Y., Chung, K. H., Tippens, M. & Turner, D. L. Detection of mammalian microRNA expression by in situ hybridization with RNA oligonucleotides. *Dev Dyn* **235**, 2538-2548 (2006).
<https://doi.org/10.1002/dvdy.20847>
- 549 Qiu, R. *et al.* The role of miR-124a in early development of the *Xenopus* eye. *Mech Dev* **126**, 804-816 (2009). <https://doi.org/10.1016/j.mod.2009.08.002>
- 550 Karali, M. *et al.* MicroRNA-restricted transgene expression in the retina. *PLoS One* **6**, e22166 (2011). <https://doi.org/10.1371/journal.pone.0022166>
- 551 Chu-Tan, J. A. *et al.* MicroRNA-124 Dysregulation is Associated With Retinal Inflammation and Photoreceptor Death in the Degenerating Retina. *Invest Ophthalmol Vis Sci* **59**, 4094-4105 (2018). <https://doi.org/10.1167/iovs.18-24623>
- 552 Berber, P., Grassmann, F., Kiel, C. & Weber, B. H. An Eye on Age-Related Macular Degeneration: The Role of MicroRNAs in Disease Pathology. *Mol Diagn Ther* **21**, 31-43 (2017). <https://doi.org/10.1007/s40291-016-0234-z>
- 553 Yang, Y. & Mei, Q. miRNA signature identification of retinoblastoma and the correlations between differentially expressed miRNAs during retinoblastoma progression. *Mol Vis* **21**, 1307-1317 (2015).
- 554 Wang, Q. *et al.* Dual Anti-Inflammatory and Anti-Angiogenic Action of miR-15a in Diabetic Retinopathy. *EBioMedicine* **11**, 138-150 (2016).
<https://doi.org/10.1016/j.ebiom.2016.08.013>
- 555 Gao, Q., Zhou, L., Yang, S. Y. & Cao, J. M. A novel role of microRNA 17-5p in the modulation of circadian rhythm. *Sci Rep* **6**, 30070 (2016).
<https://doi.org/10.1038/srep30070>
- 556 Sage, J. & Ventura, A. miR than meets the eye. *Genes Dev* **25**, 1663-1667 (2011). <https://doi.org/10.1101/gad.17454011>
- 557 Indrieri, A. *et al.* miR-181a/b downregulation exerts a protective action on mitochondrial disease models. *EMBO Mol Med* **11** (2019).
<https://doi.org/10.15252/emmm.201708734>
- 558 Wienholds, E. *et al.* MicroRNA expression in zebrafish embryonic development. *Science* **309**, 310-311 (2005). <https://doi.org/10.1126/science.1114519>
- 559 Lagos-Quintana, M., Rauhut, R., Meyer, J., Borkhardt, A. & Tuschl, T. New microRNAs from mouse and human. *RNA* **9**, 175-179 (2003).
<https://doi.org/10.1261/rna.2146903>
- 560 Fairchild, C. L. A. *et al.* Author Correction: Let-7 regulates cell cycle dynamics in the developing cerebral cortex and retina. *Sci Rep* **11**, 2872 (2021).
<https://doi.org/10.1038/s41598-021-82224-1>

- 561 Intartaglia, D., Giamundo, G. & Conte, I. The Impact of miRNAs in Health and Disease of Retinal Pigment Epithelium. *Front Cell Dev Biol* **8**, 589985 (2020). <https://doi.org/10.3389/fcell.2020.589985>
- 562 Gao, L., Jiang, B. O., Lei, D., Zhou, X. & Yuan, H. Expression profiling of microRNAs in optineurin (E50K) mutant transgenic mice. *Biomed Rep* **4**, 193-196 (2016). <https://doi.org/10.3892/br.2015.565>
- 563 Dantas da Costa, E. S. M. E. *et al.* Plasma levels of miR-29b and miR-200b in type 2 diabetic retinopathy. *J Cell Mol Med* **23**, 1280-1287 (2019). <https://doi.org/10.1111/jcmm.14030>
- 564 Conte, I. *et al.* miR-204 is required for lens and retinal development via Meis2 targeting. *Proc Natl Acad Sci U S A* **107**, 15491-15496 (2010). <https://doi.org/10.1073/pnas.0914785107>
- 565 Villarreal, G., Jr., Oh, D. J., Kang, M. H. & Rhee, D. J. Coordinated regulation of extracellular matrix synthesis by the microRNA-29 family in the trabecular meshwork. *Invest Ophthalmol Vis Sci* **52**, 3391-3397 (2011). <https://doi.org/10.1167/iovs.10-6165>
- 566 Walker, J. C. & Harland, R. M. microRNA-24a is required to repress apoptosis in the developing neural retina. *Genes Dev* **23**, 1046-1051 (2009). <https://doi.org/10.1101/gad.1777709>
- 567 Kapsimali, M. *et al.* MicroRNAs show a wide diversity of expression profiles in the developing and mature central nervous system. *Genome Biol* **8**, R173 (2007). <https://doi.org/10.1186/gb-2007-8-8-r173>
- 568 Smith, J. L. & Schoenwolf, G. C. Neurulation: coming to closure. *Trends Neurosci* **20**, 510-517 (1997). [https://doi.org/10.1016/s0166-2236\(97\)01121-1](https://doi.org/10.1016/s0166-2236(97)01121-1)
- 569 Gao, P. *et al.* Deterministic progenitor behavior and unitary production of neurons in the neocortex. *Cell* **159**, 775-788 (2014). <https://doi.org/10.1016/j.cell.2014.10.027>
- 570 Hoshino, M. Neuronal subtype specification in the cerebellum and dorsal hindbrain. *Dev Growth Differ* **54**, 317-326 (2012). <https://doi.org/10.1111/j.1440-169X.2012.01330.x>
- 571 Malatesta, P., Hartfuss, E. & Gotz, M. Isolation of radial glial cells by fluorescent-activated cell sorting reveals a neuronal lineage. *Development* **127**, 5253-5263 (2000). <https://doi.org/10.1242/dev.127.24.5253>
- 572 Noctor, S. C., Flint, A. C., Weissman, T. A., Dammerman, R. S. & Kriegstein, A. R. Neurons derived from radial glial cells establish radial units in neocortex. *Nature* **409**, 714-720 (2001). <https://doi.org/10.1038/35055553>
- 573 Xu, H. T. *et al.* Distinct lineage-dependent structural and functional organization of the hippocampus. *Cell* **157**, 1552-1564 (2014). <https://doi.org/10.1016/j.cell.2014.03.067>
- 574 Lee, H. O. & Norden, C. Mechanisms controlling arrangements and movements of nuclei in pseudostratified epithelia. *Trends Cell Biol* **23**, 141-150 (2013). <https://doi.org/10.1016/j.tcb.2012.11.001>

- 575 Seymour, R. M. & Berry, M. Scanning and transmission electron microscope studies of interkinetic nuclear migration in the cerebral vesicles of the rat. *J Comp Neurol* **160**, 105-125 (1975). <https://doi.org/10.1002/cne.901600107>
- 576 Strzyz, P. J. *et al.* Interkinetic nuclear migration is centrosome independent and ensures apical cell division to maintain tissue integrity. *Dev Cell* **32**, 203-219 (2015). <https://doi.org/10.1016/j.devcel.2014.12.001>
- 577 Haubensak, W., Attardo, A., Denk, W. & Huttner, W. B. Neurons arise in the basal neuroepithelium of the early mammalian telencephalon: a major site of neurogenesis. *Proc Natl Acad Sci U S A* **101**, 3196-3201 (2004). <https://doi.org/10.1073/pnas.0308600100>
- 578 Miyata, T. *et al.* Asymmetric production of surface-dividing and non-surface-dividing cortical progenitor cells. *Development* **131**, 3133-3145 (2004). <https://doi.org/10.1242/dev.01173>
- 579 Noctor, S. C., Martinez-Cerdeno, V., Ivic, L. & Kriegstein, A. R. Cortical neurons arise in symmetric and asymmetric division zones and migrate through specific phases. *Nat Neurosci* **7**, 136-144 (2004). <https://doi.org/10.1038/nn1172>
- 580 Bian, S. *et al.* MicroRNA cluster miR-17-92 regulates neural stem cell expansion and transition to intermediate progenitors in the developing mouse neocortex. *Cell Rep* **3**, 1398-1406 (2013). <https://doi.org/10.1016/j.celrep.2013.03.037>
- 581 Ramón y Cajal, S. *Textura del sistema nervioso del hombre y vertebrados. Moya: Madrid* (1899).
- 582 Rakic, P. Mode of cell migration to the superficial layers of fetal monkey neocortex. *J Comp Neurol* **145**, 61-83 (1972). <https://doi.org/10.1002/cne.901450105>
- 583 Rallu, M., Corbin, J. G. & Fishell, G. Parsing the prosencephalon. *Nat Rev Neurosci* **3**, 943-951 (2002). <https://doi.org/10.1038/nrn989>
- 584 Wilson, S. W. & Rubenstein, J. L. Induction and dorsoventral patterning of the telencephalon. *Neuron* **28**, 641-651 (2000). [https://doi.org/10.1016/s0896-6273\(00\)00171-9](https://doi.org/10.1016/s0896-6273(00)00171-9)
- 585 Hebert, J. M. & Fishell, G. The genetics of early telencephalon patterning: some assembly required. *Nat Rev Neurosci* **9**, 678-685 (2008). <https://doi.org/10.1038/nrn2463>
- 586 Sidman, R. L. & Rakic, P. Neuronal migration, with special reference to developing human brain: a review. *Brain Res* **62**, 1-35 (1973). [https://doi.org/10.1016/0006-8993\(73\)90617-3](https://doi.org/10.1016/0006-8993(73)90617-3)
- 587 Villalba, A., Gotz, M. & Borrell, V. The regulation of cortical neurogenesis. *Curr Top Dev Biol* **142**, 1-66 (2021). <https://doi.org/10.1016/bs.ctdb.2020.10.003>
- 588 Frantz, G. D. & McConnell, S. K. Restriction of late cerebral cortical progenitors to an upper-layer fate. *Neuron* **17**, 55-61 (1996). [https://doi.org/10.1016/s0896-6273\(00\)80280-9](https://doi.org/10.1016/s0896-6273(00)80280-9)
- 589 Walsh, C. & Cepko, C. L. Clonally related cortical cells show several migration patterns. *Science* **241**, 1342-1345 (1988). <https://doi.org/10.1126/science.3137660>

- 590 Luskin, M. B., Pearlman, A. L. & Sanes, J. R. Cell lineage in the cerebral cortex
of the mouse studied in vivo and in vitro with a recombinant retrovirus. *Neuron* **1**,
635-647 (1988). [https://doi.org/10.1016/0896-6273\(88\)90163-8](https://doi.org/10.1016/0896-6273(88)90163-8)
- 591 Reid, C. B., Liang, I. & Walsh, C. Systematic widespread clonal organization in
cerebral cortex. *Neuron* **15**, 299-310 (1995). [https://doi.org/10.1016/0896-6273\(95\)90035-7](https://doi.org/10.1016/0896-6273(95)90035-7)
- 592 Artavanis-Tsakonas, S., Rand, M. D. & Lake, R. J. Notch signaling: cell fate
control and signal integration in development. *Science* **284**, 770-776 (1999).
<https://doi.org/10.1126/science.284.5415.770>
- 593 Yoon, K. & Gaiano, N. Notch signaling in the mammalian central nervous system:
insights from mouse mutants. *Nat Neurosci* **8**, 709-715 (2005).
<https://doi.org/10.1038/nn1475>
- 594 Irvine, K. D. Fringe, Notch, and making developmental boundaries. *Curr Opin
Genet Dev* **9**, 434-441 (1999). [https://doi.org/10.1016/S0959-437X\(99\)80066-5](https://doi.org/10.1016/S0959-437X(99)80066-5)
- 595 Schroeter, E. H., Kisslinger, J. A. & Kopan, R. Notch-1 signalling requires ligand-
induced proteolytic release of intracellular domain. *Nature* **393**, 382-386 (1998).
<https://doi.org/10.1038/30756>
- 596 Fortini, M. E. & Artavanis-Tsakonas, S. The suppressor of hairless protein
participates in notch receptor signaling. *Cell* **79**, 273-282 (1994).
[https://doi.org/10.1016/0092-8674\(94\)90196-1](https://doi.org/10.1016/0092-8674(94)90196-1)
- 597 Smoller, D. *et al.* The Drosophila neurogenic locus mastermind encodes a
nuclear protein unusually rich in amino acid homopolymers. *Genes Dev* **4**, 1688-
1700 (1990). <https://doi.org/10.1101/gad.4.10.1688>
- 598 Ohtsuka, T. & Kageyama, R. Hes1 overexpression leads to expansion of
embryonic neural stem cell pool and stem cell reservoir in the postnatal brain.
Development **148** (2021). <https://doi.org/10.1242/dev.189191>
- 599 Bansod, S., Kageyama, R. & Ohtsuka, T. Hes5 regulates the transition timing of
neurogenesis and gliogenesis in mammalian neocortical development.
Development **144**, 3156-3167 (2017). <https://doi.org/10.1242/dev.147256>
- 600 Singh, S. N., Malik, M. Z. & Singh, R. K. B. Molecular crosstalk: Notch can
manipulate Hes1 and miR-9 behavior. *J Theor Biol* **504**, 110404 (2020).
<https://doi.org/10.1016/j.jtbi.2020.110404>
- 601 Murtaugh, L. C., Stanger, B. Z., Kwan, K. M. & Melton, D. A. Notch signaling
controls multiple steps of pancreatic differentiation. *Proc Natl Acad Sci U S A*
100, 14920-14925 (2003). <https://doi.org/10.1073/pnas.2436557100>
- 602 Gorski, J. A. *et al.* Cortical excitatory neurons and glia, but not GABAergic
neurons, are produced in the Emx1-expressing lineage. *J Neurosci* **22**, 6309-
6314 (2002). <https://doi.org/20026564>
- 603 Tu, L. *et al.* Notch signaling is an important regulator of type 2 immunity. *J Exp
Med* **202**, 1037-1042 (2005). <https://doi.org/10.1084/jem.20050923>
- 604 Britanova, O. *et al.* Satb2 is a postmitotic determinant for upper-layer neuron
specification in the neocortex. *Neuron* **57**, 378-392 (2008).
<https://doi.org/10.1016/j.neuron.2007.12.028>

- 605 Dobрева, G. *et al.* SATB2 is a multifunctional determinant of craniofacial patterning and osteoblast differentiation. *Cell* **125**, 971-986 (2006). <https://doi.org/10.1016/j.cell.2006.05.012>
- 606 Alcamo, E. A. *et al.* Satb2 regulates callosal projection neuron identity in the developing cerebral cortex. *Neuron* **57**, 364-377 (2008). <https://doi.org/10.1016/j.neuron.2007.12.012>
- 607 Srivatsa, S. *et al.* Unc5C and DCC act downstream of Ctip2 and Satb2 and contribute to corpus callosum formation. *Nat Commun* **5**, 3708 (2014). <https://doi.org/10.1038/ncomms4708>
- 608 Ozaki, H. S. & Wahlsten, D. Timing and origin of the first cortical axons to project through the corpus callosum and the subsequent emergence of callosal projection cells in mouse. *J Comp Neurol* **400**, 197-206 (1998). [https://doi.org/10.1002/\(sici\)1096-9861\(19981019\)400:2<197::aid-cne3>3.0.co;2-4](https://doi.org/10.1002/(sici)1096-9861(19981019)400:2<197::aid-cne3>3.0.co;2-4)
- 609 Khalaf-Nazzal, R. & Francis, F. Hippocampal development - old and new findings. *Neuroscience* **248**, 225-242 (2013). <https://doi.org/10.1016/j.neuroscience.2013.05.061>
- 610 Han, J. S. *et al.* CRL5-dependent regulation of the small GTPases ARL4C and ARF6 controls hippocampal morphogenesis. *Proc Natl Acad Sci U S A* **117**, 23073-23084 (2020). <https://doi.org/10.1073/pnas.2002749117>
- 611 Subramanian, L. & Tole, S. Mechanisms underlying the specification, positional regulation, and function of the cortical hem. *Cereb Cortex* **19 Suppl 1**, i90-95 (2009). <https://doi.org/10.1093/cercor/bhp031>
- 612 Imayoshi, I., Shimogori, T., Ohtsuka, T. & Kageyama, R. Hes genes and neurogenin regulate non-neural versus neural fate specification in the dorsal telencephalic midline. *Development* **135**, 2531-2541 (2008). <https://doi.org/10.1242/dev.021535>
- 613 Soriano, E. & Del Rio, J. A. The cells of cajal-retzius: still a mystery one century after. *Neuron* **46**, 389-394 (2005). <https://doi.org/10.1016/j.neuron.2005.04.019>
- 614 Sekine, K., Honda, T., Kawachi, T., Kubo, K. & Nakajima, K. The outermost region of the developing cortical plate is crucial for both the switch of the radial migration mode and the Dab1-dependent "inside-out" lamination in the neocortex. *J Neurosci* **31**, 9426-9439 (2011). <https://doi.org/10.1523/JNEUROSCI.0650-11.2011>
- 615 Borrell, V. *et al.* Reelin and mDab1 regulate the development of hippocampal connections. *Mol Cell Neurosci* **36**, 158-173 (2007). <https://doi.org/10.1016/j.mcn.2007.06.006>
- 616 Reyes, R. V. *et al.* The E3 Ubiquitin Ligase CRL5 Regulates Dentate Gyrus Morphogenesis, Adult Neurogenesis, and Animal Behavior. *Front Neurosci* **16**, 908719 (2022). <https://doi.org/10.3389/fnins.2022.908719>
- 617 Simo, S. & Cooper, J. A. Rbx2 regulates neuronal migration through different cullin 5-RING ligase adaptors. *Dev Cell* **27**, 399-411 (2013). <https://doi.org/10.1016/j.devcel.2013.09.022>

- 618 Simo, S., Jossin, Y. & Cooper, J. A. Cullin 5 regulates cortical layering by modulating the speed and duration of Dab1-dependent neuronal migration. *J Neurosci* **30**, 5668-5676 (2010). <https://doi.org/10.1523/JNEUROSCI.0035-10.2010>
- 619 Gonzalez-Billault, C. *et al.* A role of MAP1B in Reelin-dependent neuronal migration. *Cereb Cortex* **15**, 1134-1145 (2005). <https://doi.org/10.1093/cercor/bhh213>
- 620 Hevner, R. F., Neogi, T., Englund, C., Daza, R. A. & Fink, A. Cajal-Retzius cells in the mouse: transcription factors, neurotransmitters, and birthdays suggest a pallial origin. *Brain Res Dev Brain Res* **141**, 39-53 (2003). [https://doi.org/10.1016/s0165-3806\(02\)00641-7](https://doi.org/10.1016/s0165-3806(02)00641-7)
- 621 Sekar, A. *et al.* RapID Cell Counter: Semi-Automated and Mid-Throughput Estimation of Cell Density within Diverse Cortical Layers. *eNeuro* **8** (2021). <https://doi.org/10.1523/ENEURO.0185-21.2021>
- 622 Zema, S. *et al.* A Dynamic Role of Mastermind-Like 1: A Journey Through the Main (Path)ways Between Development and Cancer. *Front Cell Dev Biol* **8**, 613557 (2020). <https://doi.org/10.3389/fcell.2020.613557>
- 623 Alves-Guerra, M. C., Ronchini, C. & Capobianco, A. J. Mastermind-like 1 Is a specific coactivator of beta-catenin transcription activation and is essential for colon carcinoma cell survival. *Cancer Res* **67**, 8690-8698 (2007). <https://doi.org/10.1158/0008-5472.CAN-07-1720>
- 624 Quaranta, R. *et al.* Maml1 acts cooperatively with Gli proteins to regulate sonic hedgehog signaling pathway. *Cell Death Dis* **8**, e2942 (2017). <https://doi.org/10.1038/cddis.2017.326>
- 625 Kim, J. *et al.* MAML1/2 promote YAP/TAZ nuclear localization and tumorigenesis. *Proc Natl Acad Sci U S A* **117**, 13529-13540 (2020). <https://doi.org/10.1073/pnas.1917969117>
- 626 Yang, X. *et al.* Notch activation induces apoptosis in neural progenitor cells through a p53-dependent pathway. *Dev Biol* **269**, 81-94 (2004). <https://doi.org/10.1016/j.ydbio.2004.01.014>
- 627 Son, A. I. *et al.* Dual Role of Rbpj in the Maintenance of Neural Progenitor Cells and Neuronal Migration in Cortical Development. *Cereb Cortex* **30**, 6444-6457 (2020). <https://doi.org/10.1093/cercor/bhaa206>
- 628 Kageyama, R., Ohtsuka, T., Shimojo, H. & Imayoshi, I. Dynamic regulation of Notch signaling in neural progenitor cells. *Curr Opin Cell Biol* **21**, 733-740 (2009). <https://doi.org/10.1016/j.ceb.2009.08.009>
- 629 Huang, C., Chan, J. A. & Schuurmans, C. Proneural bHLH genes in development and disease. *Curr Top Dev Biol* **110**, 75-127 (2014). <https://doi.org/10.1016/B978-0-12-405943-6.00002-6>
- 630 Imayoshi, I., Sakamoto, M., Yamaguchi, M., Mori, K. & Kageyama, R. Essential roles of Notch signaling in maintenance of neural stem cells in developing and adult brains. *J Neurosci* **30**, 3489-3498 (2010). <https://doi.org/10.1523/JNEUROSCI.4987-09.2010>

- 631 Nieto, M., Schuurmans, C., Britz, O. & Guillemot, F. Neural bHLH genes control the neuronal versus glial fate decision in cortical progenitors. *Neuron* **29**, 401-413 (2001). [https://doi.org/10.1016/s0896-6273\(01\)00214-8](https://doi.org/10.1016/s0896-6273(01)00214-8)
- 632 Del Bene, F., Wehman, A. M., Link, B. A. & Baier, H. Regulation of neurogenesis by interkinetic nuclear migration through an apical-basal notch gradient. *Cell* **134**, 1055-1065 (2008). <https://doi.org/10.1016/j.cell.2008.07.017>
- 633 Austin, C. P., Feldman, D. E., Ida, J. A., Jr. & Cepko, C. L. Vertebrate retinal ganglion cells are selected from competent progenitors by the action of Notch. *Development* **121**, 3637-3650 (1995). <https://doi.org/10.1242/dev.121.11.3637>
- 634 Harris, L., Zalucki, O. & Piper, M. BrdU/EdU dual labeling to determine the cell-cycle dynamics of defined cellular subpopulations. *J Mol Histol* **49**, 229-234 (2018). <https://doi.org/10.1007/s10735-018-9761-8>
- 635 Govindan, S., Oberst, P. & Jabaudon, D. In vivo pulse labeling of isochronic cohorts of cells in the central nervous system using FlashTag. *Nat Protoc* **13**, 2297-2311 (2018). <https://doi.org/10.1038/s41596-018-0038-1>
- 636 Barta, T., Peskova, L. & Hampl, A. miRNAsong: a web-based tool for generation and testing of miRNA sponge constructs in silico. *Sci Rep* **6**, 36625 (2016). <https://doi.org/10.1038/srep36625>
- 637 Sestan, N., Artavanis-Tsakonas, S. & Rakic, P. Contact-dependent inhibition of cortical neurite growth mediated by notch signaling. *Science* **286**, 741-746 (1999). <https://doi.org/10.1126/science.286.5440.741>
- 638 Hashimoto-Torii, K. *et al.* Interaction between Reelin and Notch signaling regulates neuronal migration in the cerebral cortex. *Neuron* **60**, 273-284 (2008). <https://doi.org/10.1016/j.neuron.2008.09.026>
- 639 Del-Valle-Anton, L. & Borrell, V. Folding brains: from development to disease modeling. *Physiol Rev* **102**, 511-550 (2022). <https://doi.org/10.1152/physrev.00016.2021>
- 640 Han, S. *et al.* Proneural genes define ground-state rules to regulate neurogenic patterning and cortical folding. *Neuron* **109**, 2847-2863 e2811 (2021). <https://doi.org/10.1016/j.neuron.2021.07.007>
- 641 Koester, S. E. & O'Leary, D. D. Axons of early generated neurons in cingulate cortex pioneer the corpus callosum. *J Neurosci* **14**, 6608-6620 (1994).
- 642 Hunter, G. L. *et al.* Coordinated control of Notch/Delta signalling and cell cycle progression drives lateral inhibition-mediated tissue patterning. *Development* **143**, 2305-2310 (2016). <https://doi.org/10.1242/dev.134213>
- 643 Prasov, L. & Glaser, T. Dynamic expression of ganglion cell markers in retinal progenitors during the terminal cell cycle. *Mol Cell Neurosci* **50**, 160-168 (2012). <https://doi.org/10.1016/j.mcn.2012.05.002>
- 644 Maurer, K. A. K., A.; Shoja-Taheri, F.; Brown, L.N. Integral bHLH factor regulation of cell cycle exit and RGC differentiation. *Dev Dyn* **247**, 965-975 (2018). <https://doi.org/https://doi.org/10.1002/dvdy.24638>
- 645 Nguyen, L., Besson, A., Roberts, J. M. & Guillemot, F. Coupling cell cycle exit, neuronal differentiation and migration in cortical neurogenesis. *Cell Cycle* **5**, 2314-2318 (2006). <https://doi.org/10.4161/cc.5.20.3381>

- 646 Castro, D. S. *et al.* A novel function of the proneural factor *Ascl1* in progenitor proliferation identified by genome-wide characterization of its targets. *Genes Dev* **25**, 930-945 (2011). <https://doi.org/10.1101/gad.627811>
- 647 Toma, K., Kumamoto, T. & Hanashima, C. The timing of upper-layer neurogenesis is conferred by sequential derepression and negative feedback from deep-layer neurons. *J Neurosci* **34**, 13259-13276 (2014). <https://doi.org/10.1523/JNEUROSCI.2334-14.2014>
- 648 Srinivasan, K. *et al.* A network of genetic repression and derepression specifies projection fates in the developing neocortex. *Proc Natl Acad Sci U S A* **109**, 19071-19078 (2012). <https://doi.org/10.1073/pnas.1216793109>
- 649 Tsyporin, J. *et al.* Transcriptional repression by FEZF2 restricts alternative identities of cortical projection neurons. *Cell Rep* **35**, 109269 (2021). <https://doi.org/10.1016/j.celrep.2021.109269>
- 650 Fernandez, V. *et al.* Repression of *Irs2* by let-7 miRNAs is essential for homeostasis of the telencephalic neuroepithelium. *EMBO J* **39**, e105479 (2020). <https://doi.org/10.15252/embj.2020105479>
- 651 Emmrich, S. *et al.* miR-99a/100~125b tricistrons regulate hematopoietic stem and progenitor cell homeostasis by shifting the balance between TGFbeta and Wnt signaling. *Genes Dev* **28**, 858-874 (2014). <https://doi.org/10.1101/gad.233791.113>
- 652 Akshoomoff, N., Mattson, S. N. & Grossfeld, P. D. Evidence for autism spectrum disorder in Jacobsen syndrome: identification of a candidate gene in distal 11q. *Genet Med* **17**, 143-148 (2015). <https://doi.org/10.1038/gim.2014.86>
- 653 Favier, R., Akshoomoff, N., Mattson, S. & Grossfeld, P. Jacobsen syndrome: Advances in our knowledge of phenotype and genotype. *Am J Med Genet C Semin Med Genet* **169**, 239-250 (2015). <https://doi.org/10.1002/ajmg.c.31448>
- 654 Guerin, A. *et al.* Interstitial deletion of 11q-implicating the KIRREL3 gene in the neurocognitive delay associated with Jacobsen syndrome. *Am J Med Genet A* **158A**, 2551-2556 (2012). <https://doi.org/10.1002/ajmg.a.35621>
- 655 Beneteau, C. *et al.* Microtriplication of 11q24.1: a highly recognisable phenotype with short stature, distinctive facial features, keratoconus, overweight, and intellectual disability. *J Med Genet* **48**, 635-639 (2011). <https://doi.org/10.1136/jmedgenet-2011-100008>
- 656 Kumar, M. S. *et al.* Suppression of non-small cell lung tumor development by the let-7 microRNA family. *Proc Natl Acad Sci U S A* **105**, 3903-3908 (2008). <https://doi.org/10.1073/pnas.0712321105>
- 657 Chaudhuri, A. A. *et al.* Oncomir miR-125b regulates hematopoiesis by targeting the gene *Lin28A*. *Proc Natl Acad Sci U S A* **109**, 4233-4238 (2012). <https://doi.org/10.1073/pnas.1200677109>
- 658 Kim, S. *et al.* Generation, transcriptome profiling, and functional validation of cone-rich human retinal organoids. *Proc Natl Acad Sci U S A* **116**, 10824-10833 (2019). <https://doi.org/10.1073/pnas.1901572116>

- 659 Hadyniak, S. E. *et al.* Retinoic acid signaling regulates spatiotemporal specification of human green and red cones. *PLoS Biol* **22**, e3002464 (2024). <https://doi.org/10.1371/journal.pbio.3002464>
- 660 Kaya, K. D. *et al.* Transcriptome-based molecular staging of human stem cell-derived retinal organoids uncovers accelerated photoreceptor differentiation by 9-cis retinal. *Mol Vis* **25**, 663-678 (2019).
- 661 Chichagova, V. *et al.* Differentiation of Retinal Organoids from Human Pluripotent Stem Cells. *Curr Protoc Stem Cell Biol* **50**, e95 (2019). <https://doi.org/10.1002/cpsc.95>
- 662 Li, G. *et al.* Generation of Retinal Organoids with Mature Rods and Cones from Urine-Derived Human Induced Pluripotent Stem Cells. *Stem Cells Int* **2018**, 4968658 (2018). <https://doi.org/10.1155/2018/4968658>
- 663 Zhang, Y., Wang, Z. & Gemeinhart, R. A. Progress in microRNA delivery. *J Control Release* **172**, 962-974 (2013). <https://doi.org/10.1016/j.jconrel.2013.09.015>
- 664 Xin, Y. *et al.* Nano-based delivery of RNAi in cancer therapy. *Mol Cancer* **16**, 134 (2017). <https://doi.org/10.1186/s12943-017-0683-y>
- 665 Calegari, F. & Huttner, W. B. An inhibition of cyclin-dependent kinases that lengthens, but does not arrest, neuroepithelial cell cycle induces premature neurogenesis. *J Cell Sci* **116**, 4947-4955 (2003). <https://doi.org/10.1242/jcs.00825>
- 666 Ohnuma, S., Philpott, A., Wang, K., Holt, C. E. & Harris, W. A. p27^{Xic1}, a Cdk inhibitor, promotes the determination of glial cells in *Xenopus* retina. *Cell* **99**, 499-510 (1999). [https://doi.org/10.1016/s0092-8674\(00\)81538-x](https://doi.org/10.1016/s0092-8674(00)81538-x)
- 667 McConnell, S. K. & Kaznowski, C. E. Cell cycle dependence of laminar determination in developing neocortex. *Science* **254**, 282-285 (1991). <https://doi.org/10.1126/science.254.5029.282>
- 668 Lehman, D. A. *et al.* Cis-regulatory elements of the mitotic regulator, string/Cdc25. *Development* **126**, 1793-1803 (1999). <https://doi.org/10.1242/dev.126.9.1793>
- 669 Huard, J. M., Forster, C. C., Carter, M. L., Sicinski, P. & Ross, M. E. Cerebellar histogenesis is disturbed in mice lacking cyclin D2. *Development* **126**, 1927-1935 (1999). <https://doi.org/10.1242/dev.126.9.1927>
- 670 Yang, A. *et al.* p73-deficient mice have neurological, pheromonal and inflammatory defects but lack spontaneous tumours. *Nature* **404**, 99-103 (2000). <https://doi.org/10.1038/35003607>
- 671 Dyer, M. A. & Cepko, C. L. p57(Kip2) regulates progenitor cell proliferation and amacrine interneuron development in the mouse retina. *Development* **127**, 3593-3605 (2000). <https://doi.org/10.1242/dev.127.16.3593>
- 672 Dobashi, Y., Shoji, M., Kitagawa, M., Noguchi, T. & Kameya, T. Simultaneous suppression of cdc2 and cdk2 activities induces neuronal differentiation of PC12 cells. *J Biol Chem* **275**, 12572-12580 (2000). <https://doi.org/10.1074/jbc.275.17.12572>

- 673 Hardcastle, Z. & Papalopulu, N. Distinct effects of XBF-1 in regulating the cell cycle inhibitor p27(XIC1) and imparting a neural fate. *Development* **127**, 1303-1314 (2000). <https://doi.org/10.1242/dev.127.6.1303>
- 674 Li, L. & Vaessin, H. Pan-neural Prospero terminates cell proliferation during Drosophila neurogenesis. *Genes Dev* **14**, 147-151 (2000).
- 675 Farah, M. H. *et al.* Generation of neurons by transient expression of neural bHLH proteins in mammalian cells. *Development* **127**, 693-702 (2000). <https://doi.org/10.1242/dev.127.4.693>
- 676 Lv, X., Jiang, H., Liu, Y., Lei, X. & Jiao, J. MicroRNA-15b promotes neurogenesis and inhibits neural progenitor proliferation by directly repressing TET3 during early neocortical development. *EMBO Rep* **15**, 1305-1314 (2014). <https://doi.org/10.15252/embr.201438923>
- 677 Rago, L., Beattie, R., Taylor, V. & Winter, J. miR379-410 cluster miRNAs regulate neurogenesis and neuronal migration by fine-tuning N-cadherin. *EMBO J* **33**, 906-920 (2014). <https://doi.org/10.1002/emboj.201386591>
- 678 Khandelwal, N., Dey, S. K., Chakravarty, S. & Kumar, A. miR-30 Family miRNAs Mediate the Effect of Chronic Social Defeat Stress on Hippocampal Neurogenesis in Mouse Depression Model. *Front Mol Neurosci* **12**, 188 (2019). <https://doi.org/10.3389/fnmol.2019.00188>
- 679 Meza-Sosa, K. F., Pedraza-Alva, G. & Perez-Martinez, L. microRNAs: key triggers of neuronal cell fate. *Front Cell Neurosci* **8**, 175 (2014). <https://doi.org/10.3389/fncel.2014.00175>
- 680 Sawant, O. B. *et al.* The Circadian Clock Gene Bmal1 Controls Thyroid Hormone-Mediated Spectral Identity and Cone Photoreceptor Function. *Cell Rep* **21**, 692-706 (2017). <https://doi.org/10.1016/j.celrep.2017.09.069>
- 681 Elliott, J., Jolicoeur, C., Ramamurthy, V. & Cayouette, M. Ikaros confers early temporal competence to mouse retinal progenitor cells. *Neuron* **60**, 26-39 (2008). <https://doi.org/10.1016/j.neuron.2008.08.008>
- 682 Mattar, P., Stevanovic, M., Nad, I. & Cayouette, M. Casz1 controls higher-order nuclear organization in rod photoreceptors. *Proc Natl Acad Sci U S A* **115**, E7987-E7996 (2018). <https://doi.org/10.1073/pnas.1803069115>
- 683 Cepko, C. L. The Determination of Rod and Cone Photoreceptor Fate. *Annu Rev Vis Sci* **1**, 211-234 (2015). <https://doi.org/10.1146/annurev-vision-090814-121657>
- 684 Kallman, A. *et al.* Investigating cone photoreceptor development using patient-derived NRL null retinal organoids. *Commun Biol* **3**, 82 (2020). <https://doi.org/10.1038/s42003-020-0808-5>
- 685 Le Douarin, N. [Details of the interphase nucleus in Japanese quail (*Coturnix coturnix japonica*)]. *Bull Biol Fr Belg* **103**, 435-452 (1969).
- 686 Ribatti, D. Nicole Le Douarin and the use of quail-chick chimeras to study the developmental fate of neural crest and hematopoietic cells. *Mech Dev* **158**, 103557 (2019). <https://doi.org/10.1016/j.mod.2019.103557>
- 687 Le Douarin, N. M. A Feulgen-positive nucleolus. *Exp Cell Res* **77**, 459-468 (1973). [https://doi.org/10.1016/0014-4827\(73\)90600-9](https://doi.org/10.1016/0014-4827(73)90600-9)